Defining the roles of hnRNP family members in Acute Myeloid Leukaemia, with a focus on hnRNPA0 and hnRNPA3

Maryam Alanazi

A thesis submitted for the degree of

Doctor of Philosophy in Medicine

Cardiff University

December 2025

Wadha, my mother, your love, sacrifices, prayers, and unwavering faith in me have been my greatest source of strength. Everything I am, and everything I have achieved, is rooted in you.

Acknowlege

I would like to truly thank my supervisors, Alex Tonks and Richard Darley, for their continuous support, patience, and expert guidance throughout this study. Their generosity with their time, constructive feedback, and constant encouragement have greatly shaped both this work and my growth as a researcher. I would also like to thank Professor Steven Knapper for his valuable clinical insight, support, and guidance, which greatly enriched the translational and clinical perspective of this work.

I would also like to thank Mrs Amanda Gilkes, Michelle Lazenby, and Zulfa Yoosuf for their excellent technical support and assistance in the laboratory, with special thanks to Amanda for her outstanding teaching and guidance.

Above all, I thank my family from the bottom of my heart. Your unconditional love, patience, and constant faith in me sustained me through every obstacle of this journey. Near or far, your presence was always felt, and in my hardest moments, your support gave me the strength to continue. Everything I have achieved stands on the foundation you built for me.

I would like to express my sincere gratitude to my friend, Abdullah Al-Qahtani, whose unwavering support meant more than words can express. During the most challenging moments of this journey, he was always present offering encouragement, strength, and reassurance precisely when I needed them most. His constant belief in me, especially during moments of doubt and exhaustion, made a profound difference. His presence, support, and quiet confidence in my abilities gave me the strength to persevere and continue moving forward.

I would like to thank Shaqra University for their granting me this scholarship and funding this project.

Finally, I would like to thank every member of the Cancer and Genetics department for their support, collegiality, and encouragement throughout my PhD.

Abstract

Acute myeloid leukaemia (AML) is a biologically heterogeneous malignancy characterised by genetic, epigenetic, transcriptional, and clinical diversity. Patients with AML have variable treatment responses and high relapse rates and therefore have a significant unmet clinical need regarding the availability of targeted therapies for all AML subtypes. While recurrent transcription factor alterations and oncogenic signalling pathways have been extensively studied, the contribution of post transcriptional gene regulation to AML pathobiology remains less well defined.

RNA binding proteins, including members of the heterogeneous nuclear ribonucleoprotein (hnRNP) family, play central roles in coordinating mRNA stability, processing, and translation, enabling dynamic adaptation to cellular stress and differentiation cues. Here, analysis of nuclear proteomic data revealed a coordinated reduction in multiple heterogeneous nuclear ribonucleoproteins (hnRNP) in AML blasts, key regulators of mRNA processing, transport, and stability. Using publicly available mRNA data sets, this study examined the expression of hnRNPs family members during normal haematopoiesis and in AML patient blasts.

hnRNPA0 and hnRNPA3 were prioritised for functional investigation. Functional studies using shRNA and CRISPR-Cas9 to reduce hnRNPA3 expression did not significantly impair the growth or survival of THP1 AML cells. In contrast, reduced hnRNPA0 expression in KG1a cells resulted in a marked reduction in cell growth and viability, as assessed by flow cytometry. This growth impairment was accompanied by a redistribution of the cell cycle, with an increased proportion of cells accumulating in the G_2/M phase.

Further, an increase in apoptosis was observed using flow cytometry and Appotracker. To define the molecular programmes governed by hnRNPA0 to allow AML cells to survive RNA sequencing was performed in KG1a cells where hnRNPA0 was knocked down. Using a combination of gene ontology, KEGG and GSEA analysis, several pathways characterised by coordinated suppression of proliferative networks, including E2F regulated and G2/M checkpoint programmes were changed. In addition, an enrichment of stress responsive and apoptotic pathways were identified. Among the most prominently upregulated transcripts was the pro apoptotic effector *BCL2L11 (BIM)*, suggesting hnRNPA0 knockdown may mediate AML cell survival by suppressing BIM expression. To support this data in an AML cell line, analysis of mRNA AML patient blasts demonstrated an inverse relationship between *hnRNPA0* and *BCL2L11* expression, supporting the relevance of hnRNPA0 dependent transcriptional programmes beyond *in vitro* models.

In conclusion, this work positions hnRNPA0 as a post transcriptional regulator that sustains AML cell survival by maintaining proliferative and stress adaptive gene expression programmes. Rather than acting as a classical oncogenic driver, hnRNPA0 appears to modulate apoptosis.

Publications and presentations

Oral presentation:

2021-2025 Haematology Department Seminar Series, Cardiff University, UK

2022-2023 Division of Cancer and Genetics PGR Symposium, Cardiff University, UK

Poster presentation

- 2022 Division of Cancer and Genetics PGR Symposium, Cardiff University, UK
- 2023 Cancer Awayday, Cardiff University, UK
- 2025 Wales cancer research, Cardiff University, UK
- 2025 British Society of Haematology, Glasgow, UK

Knockdown of hnRNPA0 Induces G2/M Arrest and reduces cell growth in acute myeloid leukaemia.

Alanazi MO, Halawi M, Hughes, OM, Rizzo, S, Gilkes AF, Yoosuf Aly, Z, Alruwaili AM, Knapper S, Darley RL, and Tonks A.

- 2025 Yong EHA (British Society of Haematology), Glasgow, UK

Knockdown of hnRNPA0 Induces G2/M Arrest and reduces cell growth in acute myeloid leukaemia.

Alanazi MO, Halawi M, Hughes, OM, Rizzo, S, Gilkes AF, Yoosuf Aly, Z, Alruwaili AM, Knapper S,[7] Darley RL, and Tonks A.

Awarded

2nd Place in best poster in Cancer Awayday, Cardiff University, UK

List of Abbreviations

Abbreviation	Full term
AGM	Aorta gonad mesonephros
AML	Acute myeloid leukaemia
ANGPT1	Angiopoietin-1
APL	Acute promyelocytic leukaemia
ATRA	All-trans retinoic acid
BM	Bone marrow
CBF	Core-binding factor
CD	Cluster of differentiation
CHIP	Clonal haematopoiesis of indeterminate potential
CMP	Common myeloid progenitor
CMML	Chronic myelomonocytic leukaemia
CRISPR	Clustered regularly interspaced short palindromic repeats
CXCL12	C-X-C motif chemokine ligand 12
DFS	Disease-free survival
DNA	Deoxyribonucleic acid
EHT	Endothelial to haematopoietic transition
ELN	European Leukaemia Net
EPO	Erythropoietin
FACS	Fluorescence activated cell sorting
FDR	False discovery rate
FISH	Fluorescence in situ hybridisation
FLT3-ITD	FMS-like tyrosine kinase 3 internal tandem duplication
GM CSF	Granulocyte macrophage colony-stimulating factor
GMP	Granulocyte macrophage progenitor
GO	Gene ontology
G-CSF	Granulocyte colony stimulating factor
HLA-DR	Human leukocyte antigen-DR
hnRNP	Heterogeneous nuclear ribonucleoprotein
HSC	Haematopoietic stem cell
HSPC	Haematopoietic stem and progenitor cell

ICC	International Consensus Classification
IDH	Isocitrate dehydrogenase
IL	Interleukin
JAK	Janus kinase
KEGG	Kyoto Encyclopedia of Genes and Genomes
KH	K-homology
LT-HSC	Long-term haematopoietic stem cell
MEP	Megakaryocyte-erythroid progenitor
MDS	Myelodysplastic syndrome
MPL	Myeloproliferative leukemia virus oncogene
mRNA	Messenger ribonucleic acid
MRD	Measurable residual disease
MPP	Multipotent progenitor
NGS	Next-generation sequencing
NES	Nuclear export signal
NF-κB	Nuclear factor kappa-B
NLS	Nuclear localisation signal
OS	Overall survival
PB	Peripheral blood
PCA	Principal component analysis
RAS	Rat sarcoma viral oncogene homolog
RBP	RNA-binding protein
RNA	Ribonucleic acid
RNA seq	RNA sequencing
RRM	RNA recognition motif
SCF	Stem cell factor
sAML	Secondary acute myeloid leukaemia
STAT	Signal transducer and activator of transcription
ST-HSC	Short term haematopoietic stem cell
TGF-β	Transforming growth factor beta
SD	Standard deviation
NS	Not significant

TPO	Thrombopoietin
t-AML	Therapy related acute myeloid leukaemia
WHO	World Health Organization
CO_2	Carbon dioxide
RBPs	RNA binding proteins
RNP	Ribonucleoprotein
OS	Overall survival
DFS	Disease-free survival
MS	Mass spectrometry
iTRAQ	Isobaric tags for relative and absolute quantitation
RNAi	RNA interference
TCGA	The cancer genome atlas
DepMap	Dependency map (Broad institute's cancer dependency map portal)
TPM	Transcripts per million
m6A	N6-Methyladenosine
qPCR	Quantitative polymerase chain reaction
ANOVA	Analysis of variance
CI	Confidence interval
LQ	Lower quartile
UQ	Upper quartile
KO	Knockout
KD	Knocdown
lncRNA	Long non coding RNA
GADD45α	Growth Arrest and DNA Damage inducible alpha
ARE	AU-rich element
PI	Propidium iodide
shRNA	Short hairpin RNA
sgRNA	Single guide RNA
WB	Western blot

Summary of Figures

Summary of Tables

Contents

1 Introduction

1.1 Haematopoiesis

1.1.1 Haematopoietic origins and sites of blood formation

Haematopoiesis is sustained by a rare population of haematopoietic stem cells (HSCs), defined by their ability to self renew and generate all mature blood lineages. The functional identity of HSCs was established when a single bone marrow derived cell fully reconstituted haematopoiesis in irradiated mice (Till 1961). Long term HSCs (LT-HSCs) give rise to short term HSCs (ST-HSCs), which retain limited self-renewal but preserve multipotency. ST-HSCs differentiate into multipotent progenitors (MPPs), which progressively segregate into lineage-restricted progenitors. Human prospective isolation studies demonstrated LT-HSC, ST-HSC and MPP relationships (Baum et al. 1992; Majeti et al. 2007). Within the myeloid branch, MPPs produce common myeloid progenitors (CMPs), which diverge into granulocyte macrophage progenitors (GMPs) (Akashi et al. 2000) and megakaryocyte erythroid progenitors (MEPs) committed to erythroid and megakaryocytic fates (Mori et al. 2015). This tiered organisation defines the classical hierarchical model of haematopoiesis.

More recent single cell studies propose a continuum model in which lineage priming emerges gradually across a spectrum of transcriptional states rather than at discrete branching points. This model (Mori et al. 2015) complements the hierarchical view by highlighting the fluidity of HSC fate decisions and the presence of intermediate transcriptional states during commitment. During embryogenesis, haematopoiesis arises in two sequential waves. The primitive wave originates in the yolk sac and generates early erythroid and myeloid precursors (Palis et al. 1999). The definitive programme emerges in the aorta gonad mesonephros (AGM), where endothelial to haematopoietic transition (EHT) gives rise to the first long term HSCs (Boisset et al. 2010). These nascent HSCs subsequently migrate through transient sites, including the foetal liver, before colonising the bone marrow as the lifelong site of adult haematopoiesis (Dzierzak and Speck 2008).These concepts are summarised in (**Figure 1-1)**

1.1.2 Aorta gonad mesonephros region definitive HSC emergence

Definitive haematopoiesis first arises in the aorta gonad mesonephros (AGM) region. Early functional studies in mouse embryos showed that the AGM can autonomously generate haematopoietic stem cells (HSCs) independent of the yolk sac or foetal liver (Medvinsky and Dzierzak 1996)**.**

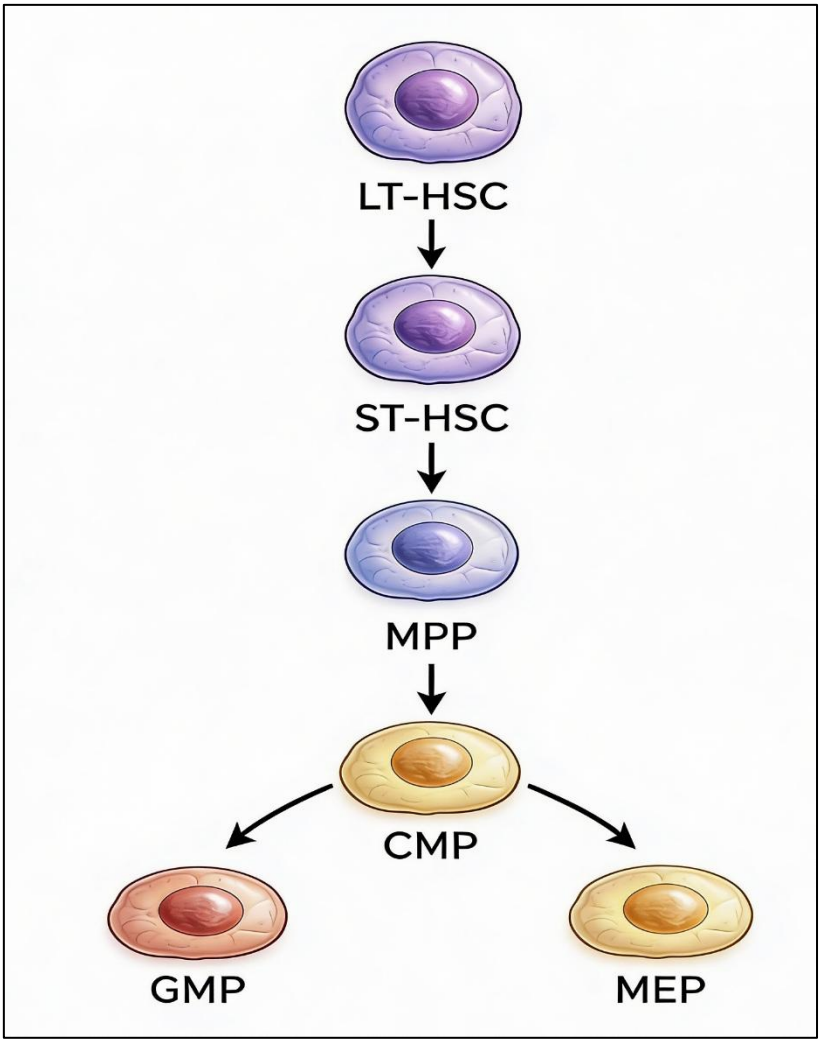

Figure 1-1 Classical hierarchical model of haematopoiesis

Schematic showing the stepwise differentiation of long-term haematopoietic stem cells (LT-HSCs) into short-term HSCs (ST-HSCs), multipotent progenitors (MPPs), and lineage restricted progenitors, including common myeloid progenitors (CMPs) that give rise to granulocyte macrophage progenitors (GMPs) and megakaryocyte erythroid progenitors (MEPs).

Within the dorsal aorta, specialised endothelial cells undergo an endothelial to haematopoietic transition (EHT) that produces the first long term HSCs (Boisset et al. 2010). Additional embryonic tissues, including the placenta, also contribute to the early HSC pool (Ottersbach and Dzierzak 2005). Once generated, nascent HSCs briefly expand and then enter the embryonic circulation before seeding the foetal liver (Taoudi et al. 2005). This positions the AGM as the first anatomical site capable of producing self-renewing, multipotent HSCs.

1.1.3 Foetal liver colonisation and expansion (E11.5-E15)

Following their emergence in the AGM, newly formed HSCs migrate to the foetal liver, which becomes the primary site of haematopoiesis between E11.5 and E15. The hepatic environment provides abundant growth factors, including SCF, TPO and IL-3, that support survival and rapid expansion (Higuchi et al. 2002). Interactions between hepatoblasts, endothelial cells and macrophage like nurse cells stabilise HSC retention and maturation (Kobayashi et al. 2010). During this developmental window, HSCs proliferate at rates not observed in adulthood (Mikkola and Orkin 2006). As haematopoietic activity declines after E15, maturing HSCs exit the liver and migrate towards the developing bone marrow (Zovein et al. 2008).

1.1.4 Bone marrow and post natal haematopoiesis (E18 Adult)

As embryonic development progresses, HSCs relocate from the liver to the forming bone marrow (BM), which becomes the definitive lifelong site of haematopoiesis. Within the BM, HSCs are maintained in distinct microenvironments. Endosteal regions promote quiescence through osteoblast derived signals (Calvi et al. 2003), while perivascular niches support self-renewal and early differentiation (Arai et al. 2004). Stromal and endothelial cells regulate HSC behaviour through CXCL12, SCF, ANGPT1 and TGF-β signalling pathways (Sugiyama et al. 2006). Under steady-state conditions, only a small proportion of HSCs enter circulation, but this increases during infection or cytokine stimulation such as G-CSF (Morrison and Scadden 2014). After birth, BM fully replaces the foetal liver, providing a stable environment that sustains haematopoiesis throughout life (Comazzetto et al. 2021b). These developmental stages are summarised in (**Figure 1-2)**.

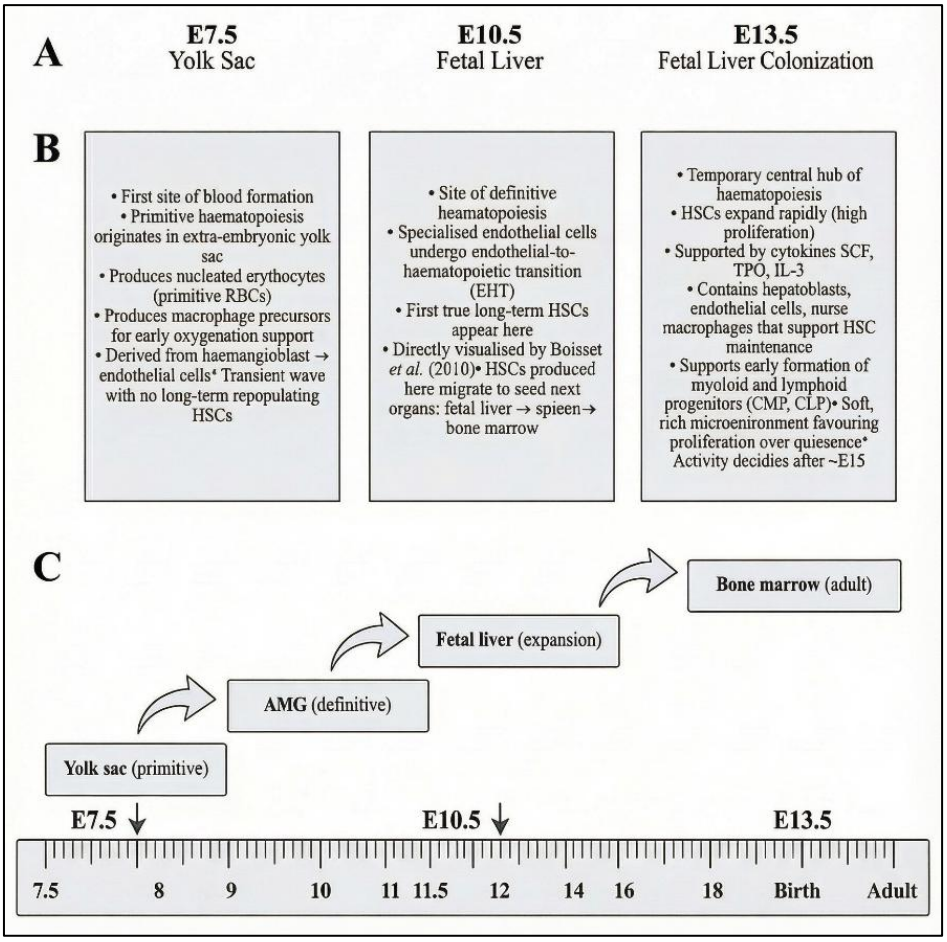

Figure 1-2 Developmental origins and anatomical progression of haematopoiesis

A Illustration of the major embryonic sites that support the transition from early primitive blood formation to the emergence of definitive HSCs, beginning in extra embryonic tissues and progressing into intra embryonic organs. **B** Summary of the functional characteristics of each haematopoietic site described in section **1.1**. **C** Developmental timeline showing the temporal contribution of each anatomical site to blood formation, from E7.5 through birth and into adulthood. Created with https://www.biorender.com/

1.2 Haematopoietic regulation

1.2.1 Transcriptional regulation of haematopoiesis

The development and maintenance of haematopoiesis rely on a network of transcription factors that work together to decide whether HSCs remain quiescent, self-renew, or begin differentiation (Orkin and Zon 2008; Laurenti and Göttgens 2018). At the earliest stages of blood formation, a core group of regulators *RUNX1*, *GATA2, TAL1* (SCL) and *LMO2* establishes and maintains the transcriptional programmes that define emerging HSCs. *RUNX1* is particularly important for enabling the EHT and for stabilising definitive HSC identity, while GATA2 supports stem-cell survival and prevents premature lineage restriction (Orkin and Zon 2008; Laurenti and Göttgens 2018). Disruption of either factor results in defective HSC emergence and has been linked to leukaemias in which differentiation is blocked (Iwasaki and Akashi 2007). TAL1 and LMO2 interact with these upstream factors to activate early haematopoietic genes such as c-KIT and GFI1B, creating a transcriptional framework that supports multipotent progenitors.

As cells begin to lose multipotency and approach lineage commitment, the balance between lineage defining transcription factors becomes critical. Within the myeloid programme, SPI1 and C/EBPα work together to promote myeloid differentiation while suppressing alternative fates (Laslo et al. 2006; Rosenbauer and Tenen 2007). The relative levels of these two regulators help determine the direction of differentiation: increased PU.1 activity favours macrophage and B-cell programmes, whereas higher C/EBPα supports granulocytic maturation through the opening and priming of myeloid-specific enhancers (Ikizler et al. 2020). When CEBPA is mutated or epigenetically impaired, this balance collapses, and progenitors become trapped in an immature state a characteristic feature of CEBPA-mutated AML (Pabst and Mueller 2007). In contrast, lymphoid commitment depends on the coordinated actions of IKAROS (IKZF1), E2A (TCF3) and GATA3, which restrain myeloid programmes and activate RAG, IL7R and NOTCH1-driven transcriptional circuits (Iwasaki and Akashi 2007).

Recent single cell transcriptomic studies have refined these classical models by showing that transcription factors do not operate as simple binary switches. Instead, their expression levels fluctuate dynamically, creating transient intermediate states that link stemness with lineage bias (Wilson et al. 2015; Tusi et al. 2018). Balanced activity of factors such as PU.1 and GATA2 helps maintain a poised multipotent state, while shifts in their relative dosage commit cells irreversibly to either the erythroid megakaryocytic or myeloid pathways (Laurenti and Göttgens 2018; Comazzetto et al. 2021a). These transcriptional adjustments are particularly

sensitive to stress and inflammatory signals, which can temporarily reshape lineage priorities by altering transcription-factor phosphorylation, stability or chromatin accessibility (Essers et al. 2009; Yamashita et al. 2016; Pietras 2017).

Together, these interconnected transcriptional circuits illustrate that haematopoietic differentiation is not a set of discrete steps, but a continuum shaped by cooperative and antagonistic interactions. When these networks are perturbed through mutation, abnormal signalling, or disrupted chromatin structure the balance between self-renewal and differentiation is lost. Such disturbances underpin the failure of normal maturation seen in AML, where altered transcription-factor dosage and activity help sustain uncontrolled, self-renewing leukaemic clones. The core organisation of these transcriptional hierarchies is summarised in (**Figure 1-3**).

1.2.2 Growth factor and cytokine mediated regulation of haematopoiesis

1.2.2.1 Haematopoietic growth factors

Blood formation relies on a steady exchange of signals between HSCs and the surrounding BM environment. Much of this communication is carried by soluble growth factors and cytokines released by stromal, endothelial and immune cells (Comazzetto et al. 2021b). These signals act both as sensors of physiological demand and as regulators that determine whether an HSC remains quiescent, undergoes self renewal, or begins lineage commitment. Among the best-studied factors are SCF, TPO, IL-3, GM-CSF and erythropoietin (EPO), each contributing to a slightly different aspect of early haematopoietic control (Metcalf 2008; Camacho et al. 2017; Sezaki et al. 2020; Mann et al. 2022).

SCF signals primarily through its receptor c-KIT on HSCs and progenitor cells, where it promotes survival and protects against oxidative stress (Lennartsson and Ronnstrand 2012). TPO, acting through MPL, has a complementary role: it helps maintain long term HSCs in a quiescent state by activating JAK STAT and related pathways (Qian et al. 2007; Yoshihara et al. 2007). IL-3 and GM-CSF, which share a common β-chain receptor, are more closely associated with early myeloid expansion. They increase the responsiveness of progenitors to inflammatory cues and enhance the production of monocytes and granulocytes when physiological demand rises (Hercus et al. 2009; Broughton et al. 2012).

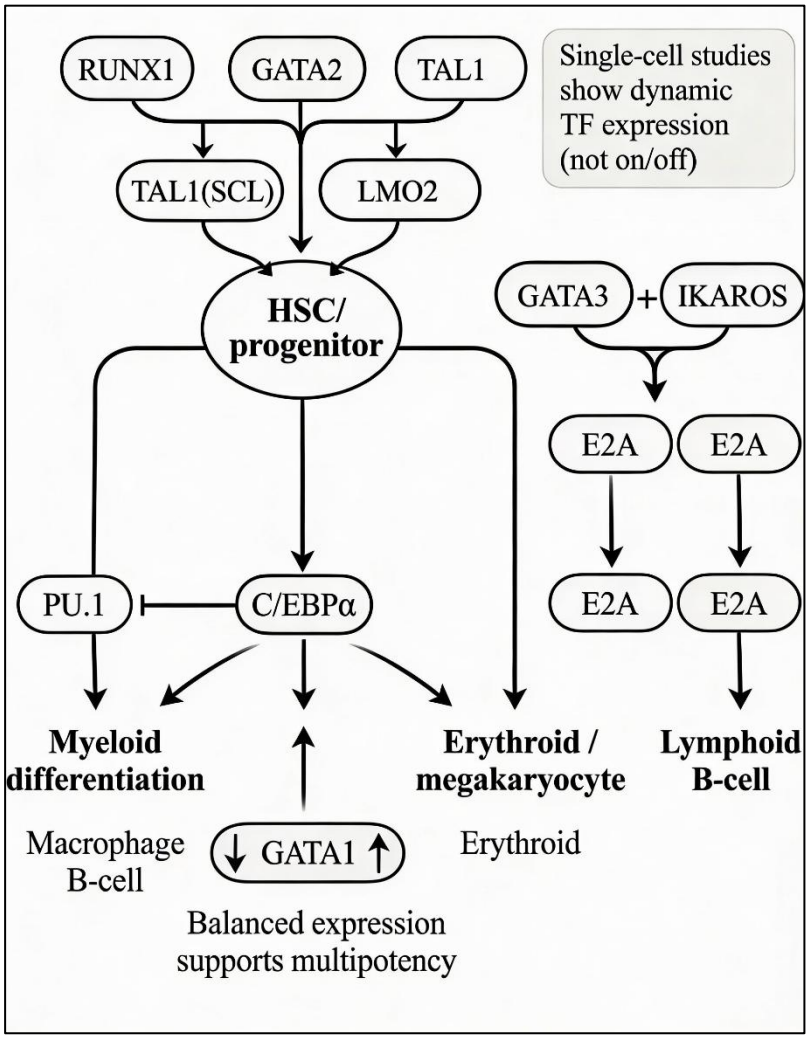

Figure 1-3 Transcription factor hierarchies regulating haematopoietic stem cell

A simplified schematic showing how core transcription factor networks maintain stem/progenitor identity and direct lineage commitment. Upstream regulators support HSC stability, while interacting downstream factors shift cells toward myeloid, erythroid/ megakaryocytic, or lymphoid pathways. The diagram highlights the graded and dynamic nature of transcription factor activity that shapes these early choices. Arrows reflect functional dominance and inhibitory balance between transcription factors, not direct activation**.** Created with https://www.biorender.com/

EPO acts later in the differentiation sequence, targeting erythroid precursors and supporting their survival through JAK2–STAT5-mediated induction of anti-apoptotic proteins such as BCL-xL (Koury and Ponka 2004; Richmond et al. 2005).

Although each growth factor has its own receptor and downstream pathway, their biological effects overlap considerably. Together, they create a flexible regulatory network that adjusts blood cell output to match the needs of the organism. During periods of increased stress or tissue demand, these signals allow haematopoiesis to accelerate; once homeostasis is restored, they help return HSC activity to a balanced state. This coordinated system of growth-factor signalling forms the foundation upon which additional cytokine and inflammatory cues build, linking environmental signals with the intrinsic transcriptional machinery that governs haematopoietic fate decisions.

1.2.2.2 Cytokine control of lineage commitment and stress haematopoiesis

Cytokines influence haematopoiesis in ways that extend beyond maintaining stem-cell survival. Several act as direct instructors of lineage choice, a concept confirmed by single-cell assays that traced individual differentiation events in real time. Macrophage colony stimulating factor (M-CSF), for example, raises PU.1 levels and guides early progenitors towards macrophage identity (Mossadegh-Keller et al. 2013). Granulocyte colony stimulating factor (G-CSF) has a complementary role: by increasing C/EBPα activity, it promotes granulocytic differentiation (Keeshan et al. 2003). In contrast, interleukin-7 (IL-7) maintains lymphoid potential by sustaining E2A and GATA3, two transcription factors that support lymphoid specification and suppress inappropriate myeloid drift (Dias et al. 2008). These observations established that cytokines are not passive supporters of differentiation but active signals that shape lineage trajectories by modulating transcription factor balance within progenitors (Rieger et al. 2009).

Beyond steady-state regulation, cytokine signalling has a distinct role during physiological stress. Inflammation triggers an “emergency” mode of haematopoiesis in which haematopoietic stem and progenitor cells (HSPC) produce large numbers of myeloid cells at short notice. Key inflammatory mediators including IL-1β, IL-6, TNF-α and interferons push HSCs out of quiescence and bias their output towards the myeloid lineage (Baldridge et al. 2011). These cytokines operate through pathways such as NF-κB, STAT1/3 and p38 MAPK, which transiently enhance proliferation and accelerate the commitment of progenitors towards

innate-immune fates (King and Goodell 2011; Pietras et al. 2016). This response is beneficial when brief, enabling rapid replacement of neutrophils and monocytes during infection or tissue injury.

Problems arise when inflammatory signalling persists. Chronic exposure to IL-1β, TNF-α or interferons gradually erodes stem cell maintenance, increases cycling, and shifts differentiation away from balanced output towards a sustained myeloid bias (Pietras et al. 2016). Over time, these pressures reduce the pool of long term HSCs and alter the composition of progenitor populations, creating a BM environment that is less resilient and more sensitive to further stress. The cumulative effect is a system in which haematopoietic behaviour becomes increasingly shaped by external cues rather than intrinsic regulatory circuits.

Together, these findings show that cytokines form a link between environmental state and intrinsic transcriptional machinery. By integrating steady state growth factor signalling with stress-induced pathways, they help determine whether haematopoiesis remains balanced or shifts towards emergency output. This framework sets the stage for understanding how the bone marrow microenvironment orchestrates these signals in vivo, a topic explored in the following section.

1.2.3 The bone marrow microenvironment

The endosteal surface, located along the inner bone lining, has long been associated with the residence of the most quiescent HSCs. Early studies showed that experimentally increasing osteoblast activity expanded the number of stem cells retained in this region, highlighting the role of osteolineage cells in maintaining a slow cycling HSC pool (Calvi et al. 2003). Although the signals involved are relatively modest largely adhesive interactions and locally produced supportive factors, they provide a protective environment that limits unnecessary proliferation and helps preserve long term stem cell function. More recent work places the endosteal niche within a broader network of stromal and vascular elements, indicating that osteoblasts contribute to, but do not exclusively control, HSC maintenance (Wei and Frenette 2018).

Blood vessels form a second major regulatory domain within the bone marrow, encompassing both arteriolar and sinusoidal niches. This environment supports both HSCs and early progenitors and enables more dynamic transitions between quiescence and activation in response to physiological demand (Acar et al. 2015). Together, the arteriolar and sinusoidal niches provide complementary modes of regulation, balancing stability with responsiveness.

Immune cells also contribute directly to the regulation of HSCs, a specialised subset of $CD169^+$ macrophages resides near stromal cells and sinusoidal vessels, where they promote the production of CXCL12 and other supportive factors (Chow et al. 2011). Their presence helps retain HSCs within the BM and prevents premature mobilisation. Although these macrophages do not instruct lineage commitment, they stabilise the surrounding microenvironment and are essential for maintaining stem-cell retention during steady-state haematopoiesis. Sympathetic nerve fibres extend along marrow vasculature and interact with local stromal populations. Fluctuations in sympathetic activity modulate CXCL12 expression, creating circadian patterns in HSC localisation and release (Méndez-Ferrer et al. 2008). Neural input therefore acts as an additional layer of control, linking systemic physiological rhythms to the timing of stem cell mobilisation without directly driving proliferation or differentiation.

Together, the endosteal, vascular, immune and neural elements form a coordinated microenvironment that protects HSCs while enabling rapid adjustment to physiological needs such as infection, repair or ageing. These regulatory layers ensure that stem cells can switch between quiescence and activation in a controlled manner, maintaining a stable but adaptable system of blood production. Understanding how the healthy niche is organised provides the foundation for examining how pathological conditions disrupt these regulatory networks, a topic addressed in the following section.

1.3 Acute myeloid leukaemia

1.3.1 Overview of AML

Acute myeloid leukaemia (AML) is an aggressive haematological malignancy arising from the myeloid lineage, characterised by impaired differentiation, accumulation of immature myeloid blasts, and disruption of normal haematopoiesis in the bone marrow and peripheral blood. According to the World Health Organization (WHO) classification, AML is defined by distinct genetic, cytogenetic, and molecular abnormalities that underpin disease heterogeneity and clinical behaviour (Alaggio et al. 2022). AML predominantly affects older adults, with a median age at diagnosis of approximately 65-70 years, and an incidence of 3-5 cases per 100,000 individuals per year. Despite therapeutic advances, long term outcomes remain poor, with 5 year overall survival rates of around 25-30%, declining sharply with increasing age (Döhner et al. 2024) (DiNardo et al. 2020). Large scale genomic sequencing studies have fundamentally reshaped the understanding of AML pathogenesis. What was once considered a relatively uniform disease is now recognised as a collection of biologically distinct subtypes defined by cooperating genetic lesions affecting signalling pathways, epigenetic regulation,

transcriptional control, and DNA repair. Papaemmanuil *et al*. demonstrated that most patients harbour multiple somatic mutations rather than a single dominant driver, with mutation combinations strongly influencing prognosis, therapeutic response, and relapse risk (Papaemmanuil et al. 2016). Importantly, this paradigm accommodates recognised exceptions, including acute promyelocytic leukaemia (APL), which is driven primarily by the PML RARA fusion resulting from t(15;17), and subsets of normal karyotype AML, where pathogenic mutations may be cryptic at the cytogenetic level (Tallman et al. 2002). Increasing evidence suggests that AML frequently originates from long lived haematopoietic stem cells (HSCs) that acquire early, pre leukaemic mutations while retaining near normal functional behaviour. These pre leukaemic clones can persist during chemotherapy, accumulate additional genetic hits, and ultimately evolve into overt AML. Studies by Shlush *et al*. provided direct evidence that relapse often arises from such therapy resistant founding clones rather than from newly acquired disease (Shlush et al. 2014). This concept overlaps with clonal haematopoiesis of indeterminate potential (CHIP), which represents an age associated reservoir of pre-malignant mutations that can predispose to AML development. Together, these biological principles highlight AML as a disease defined by blocked differentiation, clonal evolution, and profound genetic heterogeneity. These features form the framework for understanding AML risk factors, genetic drivers, and its interaction with the bone marrow microenvironment, which are explored in detail in the following sections.

1.3.2 Aetiology of AML

AML can arise through several converging routes that disrupt the stability of the haematopoietic system. Ageing is one of the strongest contributors, as HSC gradually accumulate somatic mutations over time. (Jaiswal et al. 2014). While most of these early lesions are clinically silent, a subset gives rise to clonal haematopoiesis, in which mutant stem-cell clones expand disproportionately. Although clonal haematopoiesis is not malignant in itself, it creates a genetic substrate in which additional cooperating mutations can promote progression to AML. Large population studies have shown that age related clonal haematopoiesis is common and confers a measurable increase in the long term risk of myeloid malignancy (Jaiswal et al. 2014). A second pathway involves prior exposure to cytotoxic chemotherapy or radiotherapy. Therapy related AML (t-AML) arises when treatment-induced DNA damage selects for clones carrying mutations associated with impaired DNA repair or genomic integrity. These cases frequently harbour TP53 mutations and display a characteristic mutational signature that distinguishes them from *de novo* disease. Work by Lindsley and

colleagues demonstrated that prior therapy shapes the evolutionary trajectory of the leukaemic clone and is associated with distinct clinical outcomes (Lindsley et al. 2015). Environmental mutagens provide an additional source of genotoxic stress, although individual level risk is more difficult to quantify. Benzene remains the most clearly established example: large multicentre studies have shown a dose dependent increase in myeloid neoplasms, including AML, with cumulative occupational exposure (Linet et al. 2019).

Inherited predisposition has become increasingly recognised as a contributor to AML aetiology. Advances in germline sequencing have revealed pathogenic variants in genes such as *RUNX1*, *GATA2, DDX41*, *ANKRD26* and *ETV6* in a proportion of patients previously thought to have sporadic disease (Guidugli et al. 2017; Tawana et al. 2022). These syndromes present with considerable clinical heterogeneity, some individuals manifest in childhood, others in adulthood, and many lack an obvious family history at diagnosis. Identifying germline predisposition has direct clinical implications, including donor selection for transplantation, counselling of at-risk relatives and anticipating treatment related toxicity.

Chronic inflammatory signalling has emerged as an additional driver of early myeloid transformation. Pro-inflammatory cytokines particularly IL-1β, TNF-α and interferons can force normally quiescent HSCs into repeated cycles of proliferation as part of emergency myelopoiesis. While adaptive in the short term, sustained exposure leads to exhaustion of wild type HSCs and creates a selective environment in which mutant clones gain a fitness advantage. Experimental studies show that HSCs carrying mutations such as TET2 or DNMT3A resist inflammatory attrition and expand preferentially under chronic cytokine signalling (Baldridge et al. 2011; King and Goodell 2011; Pronk et al. 2011; Pietras 2017; Hormaechea-Agulla et al. 2021). These pressures also reshape the BM microenvironment by altering stromal support, reducing CXCL12 expression and increasing oxidative stress, thereby further favouring the persistence of pre leukaemic clones.

Environmental and lifestyle exposures, including benzene and chronic metabolic inflammation, further modulate these processes by increasing genotoxic and inflammatory stress, thereby accelerating clonal selection rather than acting as independent initiating events (McHale et al. 2011). (Fuster et al. 2017; Bick et al. 2020). Together, these findings indicate that AML does not arise from a single initiating event but from an interplay of age-related mutational drift, therapy induced damage, environmental exposures, germline predisposition

and chronic inflammatory stress. These processes collectively shape the mutational landscape and clonal dynamics that underpin AML pathogenesis.

1.3.3 Genetic landscape of AML

AML is characterised by marked genetic heterogeneity, reflecting the accumulation of cooperating mutations that disrupt normal haematopoietic regulation. Rather than arising from a single transforming event, the disease develops through stepwise acquisition of lesions affecting stem cell self-renewal, myeloid differentiation and proliferative signalling.

At diagnosis, several recurrent genetic alterations are consistently observed and form the backbone of modern molecular classification. These include mutations in epigenetic regulators (*DNMT3A, TET2, IDH1/2*), transcription factors (*CEBPA, RUNX1*), tumour suppressors (*TP53*), signalling pathway genes (*FLT3-ITD/TKD, NRAS, KRAS, KIT*), and spliceosome components (*SRSF2, U2AF1, SF3B1*). *NPM1* mutations are among the most frequent lesions in AML and often co-occur with *FLT3* or epigenetic mutations. Recurrent cytogenetic abnormalities such as t(8;21), inv(16), and t(15;17), which generates the PML-RARA fusion, define additional biologically distinct subtypes with characteristic clinical behaviour. Collectively, these alterations influence disease phenotype, therapeutic response and prognostic risk classification (Papaemmanuil et al. 2016; Dohner et al. 2022).

Next generation sequencing (NGS) has been central to defining this molecular complexity, revealing that most patients harbour multiple cooperating mutations rather than a single dominant driver. Large genomic analyses demonstrated that patterns of co-occurring mutations cluster into reproducible molecular subgroups that correlate strongly with clinical behaviour and outcome (Papaemmanuil et al. 2016). These findings have shifted AML classification towards molecularly defined disease entities and now underpin contemporary risk stratification models (Dohner et al. 2022).

Genomic studies have also demonstrated that many AML-associated mutations originate years before overt disease develops. Work by Shlush et al. showed that AML may arise from long-lived haematopoietic stem cells carrying early founder mutations, with additional lesions acquired during clonal evolution (Shlush et al. 2014). Population-based analyses further support this model, showing that clonal haematopoiesis is common in ageing individuals and that AML-associated mutations may be detectable in peripheral blood years before diagnosis (Genovese et al. 2014; Desai et al. 2018).

Together, these findings demonstrate that AML represents a genetically diverse and evolutionarily dynamic malignancy. Integrating molecular profiling into routine diagnostic practice has therefore become essential for accurate classification, prognostic assessment and therapeutic decision making.

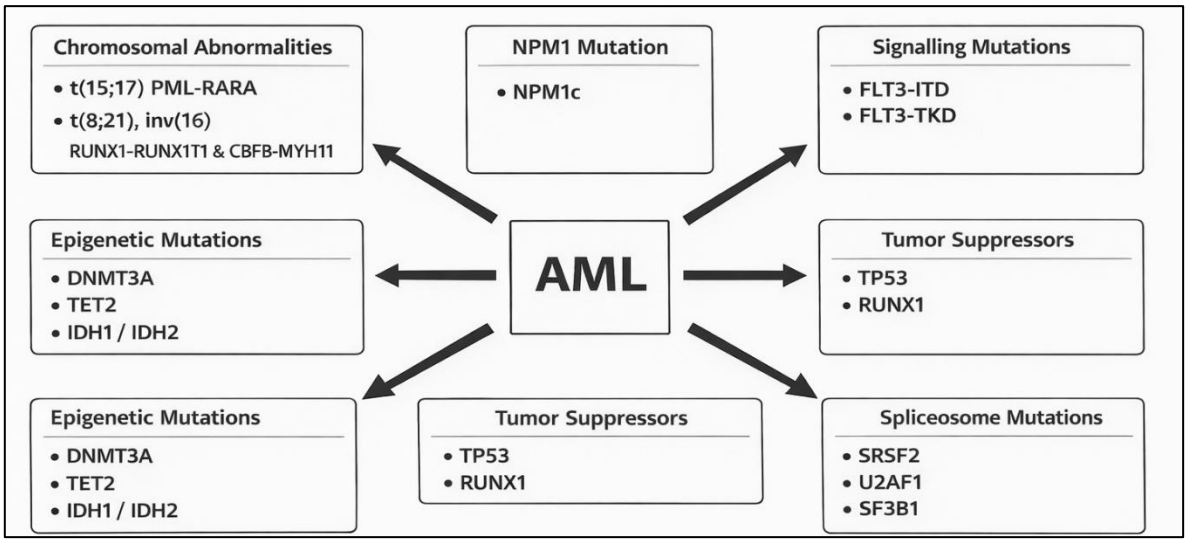

Figure 1-4 . Common genetic alterations in AML

AML arises from cooperating mutations affecting chromosomal integrity, epigenetic regulation, signalling pathways, tumour suppression and RNA splicing, forming the molecular foundation of modern classification systems.

1.3.4 Classification of AML

The classification of AML has undergone substantial revision over the past decade, reflecting increasing recognition that the disease is more accurately defined by its molecular architecture than by morphology alone. Large scale genomic studies demonstrated that AML clusters into reproducible molecular subgroups rather than arising from random assortments of mutations. These analyses identified biologically coherent entities defined by recurrent mutational constellations, many of which strongly correlate with clinical behaviour and outcome (Papaemmanuil et al. 2016). Representative groups include NPM1-mutated AML, AML with chromatin or spliceosome gene mutations, and subtypes dominated by kinase-activating lesions, collectively explaining much of the observed clinical heterogeneity.

Earlier classification frameworks, including the 2016 WHO revision (Arber et al. 2016), relied heavily on blast morphology and lineage assignment, with selected cytogenetic and molecular abnormalities incorporated for specific diagnostic entities. The WHO 2022 update places genetic features at the centre of disease definition, recognising several molecular subtypes even when blast counts fall below the traditional 20% threshold (Alaggio et al. 2022).

Historically, the French American British (FAB) classification grouped AML into subtypes (M0–M7) based on blast morphology and cytochemical staining patterns. Although FAB has largely been superseded by molecular systems, its terminology remains descriptively relevant in some clinical settings and is referenced later in this thesis when discussing morphology-based AML subtypes. Contemporary WHO and ICC systems, however, prioritise recurrent genetic abnormalities because these more accurately capture disease biology and guide modern risk stratification and treatment.

In parallel, the International Consensus Classification (ICC) has sought to harmonise and refine disease groupings. The ICC introduces categories that were previously less clearly delineated, including AML with mutated TP53, and more explicitly separates AML with MDS-related gene mutations from other molecularly defined entities (Thiele et al. 2023). Despite structural differences, both WHO 2022 and ICC share the same conceptual foundation: AML represents a collection of biologically distinct entities unified by overlapping clinical features yet driven by different genetic pathways. These refinements align closely with the European LeukemiaNet (ELN) 2022 risk stratification framework, which assigns patients to favourable, intermediate or adverse risk groups based on defined cytogenetic and molecular criteria (Dohner et al. 2022).

The clinical relevance of these systems emerges when molecular subgroups are linked to outcome. The ELN 2022 framework formalises this relationship by basing risk assignment on specific combinations of mutations and cytogenetic abnormalities present at diagnosis (Dohner et al. 2022). For example, NPM1-mutated AML without FLT3-ITD is typically associated with favourable prognosis, whereas TP53 mutations or complex karyotypes consistently confer adverse risk. Importantly, patterns of co-occurring mutations often provide stronger prognostic value than isolated lesions (Papaemmanuil et al. 2016).

Together, the WHO, ICC and ELN frameworks establish an integrated classification system that combines cytogenetic, molecular and clinical information into a unified structure. This approach enhances diagnostic precision and supports risk-adapted therapeutic decision-making from the earliest stage of patient evaluation. The key features and distinctions between these systems are summarised in (**Table 1-1)**

Table 1-1 Modern classification systems for AML

A descriptive summary comparing the main AML classification systems, showing how each system organises AML into diagnostic categories based on morphology, cytogenetics, molecular features and risk groups.

Classifications	Key Features	How AML Is Defined	Examples / Notes
WHO 2016	Morphology-first	Based mainly on blast percentage, lineage, and selected cytogenetic abnormalities	Genetics used only for specific subtypes (e.g., t(8;21), inv(16), APL)
WHO 2022	Genetics at the centre	AML entities defined by recurrent mutations, even when blasts <20%	NPM1-mutated AML; CEBPA-mutated AML; AML with MDS-related gene mutations
ICC 2022	Molecular refinement & clearer grouping	Distinguishes AML with mutated *TP53* as a separate entity; separates MDS-related gene mutations more clearly	TP53-mutated AML (new ICC entity); AML with MDS-related mutations (ASXL1, SRSF2, RUNX1, U2AF1…)
Molecularly Defined AML Entities (WHO 2022 + ICC)	Mutation-defined subtypes	AML is classified based on recurrent genomic patterns rather than morphology	NPM1-mutated AML; CEBPA (biallelic); TP53-mutated; AML with kinase lesions (FLT3, RAS…); AML with recurrent cytogenetic abnormalities
ELN 2022 Risk Groups	Integrates cytogenetics + mutations	Groups AML into *Favourable, Intermediate, Adverse* based on mutation combinations	**Favourable:** NPM1-mutated without FLT3-ITD, core-binding factor AML. **Intermediate:** NPM1-mutated + FLT3-ITD. **Adverse:** TP53-mutated; complex karyotype; MDS-related gene cluster.

1.3.5 Diagnosis of AML

The diagnostic assessment of suspected AML begins with routine clinical and laboratory evaluation. Patients typically present with features of BM failure, most commonly fatigue, infection or bleeding. Initial blood tests often reveal anaemia and thrombocytopenia, with the white-cell count showing either marked leucocytosis with circulating blasts or, less frequently, profound cytopenias. Examination of the peripheral blood film frequently raises the first suspicion of AML by demonstrating blasts or striking abnormalities in the appearance of maturing myeloid cells. A definitive diagnosis requires direct examination of the BM. Aspirate smears and trephine biopsies allow assessment of blast percentage, maturation pattern and lineage features. According to the WHO classification, the diagnosis of AML is no longer based solely on a fixed blast percentage threshold. While a blast count of ≥20% in blood or bone marrow remains relevant for many cases, the WHO 2022 classification recognises several genetically defined AML entities that can be diagnosed irrespective of blast percentage. These include AML with defining genetic abnormalities, reflecting the shift towards molecularly driven disease definition rather than morphology alone (Alaggio et al. 2022) Morphological assessment therefore remains an important initial step, but it is now integrated with cytogenetic and molecular features to establish a definitive diagnosis. In parallel, the European LeukemiaNet (ELN) framework uses cytogenetic and molecular abnormalities to stratify patients into prognostic risk groups, guiding therapeutic decision-making rather than defining disease diagnosis itself (Dohner et al. 2022).

Cytogenetic analysis remains central to diagnostic evaluation and has guided risk assessment for more than three decades. Conventional karyotyping is still the primary method because it detects both balanced chromosomal rearrangements and numerical abnormalities with major clinical significance. Recurrent lesions such as t(8;21), inv(16)/t(16;16) and t(15;17) define well-established biological subgroups and carry specific diagnostic and prognostic implications (Arber et al. 2016). Fluorescence in situ hybridisation (FISH) is frequently used alongside karyotyping particularly when metaphase yields are poor or when rapid confirmation of a suspected translocation, such as PML-RARA, is required.

The relevance of these cytogenetic findings has been underscored by large genomic studies, which demonstrated that characteristic chromosomal patterns form the structural framework of distinct molecular classes of AML (Papaemmanuil et al. 2016). Consequently, cytogenetic information is now embedded within ELN classification systems, directing patients into favourable, intermediate or adverse-risk groups at diagnosis (Dohner et al. 2022). This

stratification continues to guide early therapeutic decisions even in the era of comprehensive molecular testing.

Molecular profiling is now regarded as an essential component of AML diagnosis and treatment. Rapid tests for mutations in NPM1, FLT3-ITD/TKD, CEBPA and IDH1/2 are routinely performed because of their immediate implications for treatment selection (Dohner et al. 2022). Broader NGS panels further expand this assessment by evaluating multiple genes simultaneously, providing a more complete picture of the mutational combinations that shape disease biology. Flow cytometry adds a complementary layer to the diagnostic process by analysing antigen-expression patterns including MPO, CD13, CD33, CD117 and HLA-DR. Flow cytometry of AML blasts can confirm myeloid lineage and identify abnormal blast populations even when morphology is limited by hypocellular or poor-quality samples (Arber et al. 2016). Certain subtypes also show characteristic immunophenotypes. APL for example, commonly displays HLA-DR expression with bright CD33 expression and is absent for $CD34^{+}$ expression (Arber et al. 2016),features that often raise suspicion before cytogenetic confirmation. Flow cytometry is now integral not only at diagnosis but also later in measurable residual disease (MRD) assessment, a role emphasised in current ELN recommendations (Dohner et al. 2022). Together, morphology, cytogenetics, molecular profiling and immunophenotyping provide a multidimensional diagnostic framework. This integrated approach ensures accurate classification from the outset and supports precise risk stratification and treatment planning.

1.3.6 Prognosis and risk stratification

Clinical outcome in AML is shaped by a combination of patient related factors, disease biology, and early treatment response. Age remains one of the strongest clinical determinants in the western world. Older (or less fit) adults typically present with more chemotherapy resistant disease, a higher burden of adverse genetic features, and reduced tolerance for intensive induction, all of which contribute to poorer survival outcomes (Dohner et al. 2022). Baseline functional status is equally important, often assessed using performance status (e.g., ECOG) or frailty and comorbidity indices; limitations often limit the use of curative-intent therapy, and responses to lower-intensity regimens such as venetoclax azacitidine are generally less durable in this setting (Döhner et al. 2024). The disease origin also carries prognostic weight. Therapy related AML and cases arising from antecedent MDS or CMML frequently display complex genetic architecture and demonstrate more aggressive clinical trajectories than de novo disease

(Bazinet et al. 2022). Additional presentation features including marked leukocytosis, rapidly expanding disease, or early coagulopathy may further indicate more unstable disease biology. Finally, the depth and speed of initial treatment response, particularly the achievement of measurable residual disease MRD negativity, provide powerful prognostic insight and frequently influence decisions regarding allogeneic stem cell transplantation (Dohner et al. 2022).

Genetic profiling has now become the principal tool for risk assessment, with the ELN 2022 framework serving as the standard for clinical practice. This system integrates cytogenetic findings with recurrent gene mutations to categorise patients into favourable, intermediate or adverse risk groups (Dohner et al. 2022). Favourable risk disease includes core binding factor AML and NPM1-mutated AML without FLT3-ITD, whereas intermediate risk disease comprises cases lacking clear favourable or adverse features. The adverse-risk group is the broadest and includes TP53 mutated AML, complex karyotypes, inv(3)/t(3;3), and AML with MDS related gene mutations. These classifications reflect consistent observations from large scale genomic studies showing that mutational combinations, rather than isolated lesions, largely dictate disease biology and treatment response (Papaemmanuil et al. 2016).

Several co mutation patterns recur across the AML landscape and hold strong prognostic relevance. TP53 mutations form one of the clearest adverse subgroups, characterised by complex cytogenetics, genomic instability and profound resistance to both intensive chemotherapy and venetoclax based regimens (Testa et al. 2023; Thiele et al. 2023). In contrast, NPM1 mutated AML often demonstrates more favourable behaviour unless accompanied by FLT3-ITD or high-risk secondary mutations. Mutations in IDH1/2 generally position patients within the intermediate risk range and provide opportunities for targeted therapy. Conversely, RAS pathway mutations including NRAS and KRAS are increasingly recognised as markers of reduced venetoclax sensitivity and inferior outcomes in the non-intensive treatment setting (Lachowiez et al. 2023). Recent analyses in older adults receiving venetoclax–azacitidine have shown that co-mutations in TP53, FLT3-ITD, NRAS and KRAS identify a subgroup with particularly poor survival, underscoring the importance of integrated genetic profiling at diagnosis (Döhner et al. 2024).

The limitations of traditional prognostic models have become more apparent in the venetoclax era. Real-world data demonstrate that ELN 2017 and ELN 2022 risk groups do not reliably discriminate outcomes among older patients treated with venetoclax azacitidine (Döhner et al.

2024). To address this gap, a streamlined prognostic model has been proposed, focusing specifically on four high impact mutations TP53, FLT3-ITD, NRAS and KRAS which appear to provide more accurate stratification in this population. For patients within these high risk molecular groups, therapeutic alternatives remain limited and commonly include enrolment in clinical trials, consideration of allogeneic stem-cell transplantation in selected fit individuals, or supportive approaches where durable responses are unlikely. These observations highlight how prognostic tools may need to adapt to contemporary treatment strategies and reinforce the notion that risk stratification is increasingly context dependent.

1.3.7 Treatment of AML

The therapeutic management of AML has undergone substantial over the past four decades, yet the central principle remains the same: induction followed by consolidation to prevent relapse (Dohner et al. 2022). For medically fit adults, the long-standing standard of care continues to be the "7+3'' induction regimen, which refers to 7 days of continuous cytarabine combined with 3 days of an anthracycline such as daunorubicin. Despite being more than four decades old, this regimen remains highly effective in younger patients particularly those with favourable risk disease and still forms the basis on which contemporary therapies are built (Dohner et al. 2022). In patients who achieve remission, consolidation typically involves high-dose cytarabine or, for those with intermediate or adverse risk features, allogeneic stem-cell transplantation. These decisions increasingly depend on ELN 2022 genetic risk groups and MRD status.

A major refinement of traditional induction has been the incorporation of targeted agents into genetically defined subgroups. Acute promyelocytic leukaemia remains the 'gold standard' example of successful biology driven therapy. Treatment targets the PML:RARA fusion directly using all trans retinoic acid (ATRA) and arsenic trioxide, which induce terminal differentiation rather than relying on cytotoxic chemotherapy (Dohner et al. 2022). This targeted approach has transformed APL from a frequently fatal diagnosis into one of the most curable forms of AML. Chemotherapy is now reserved only for high risk presentations with substantial leukocytosis, and outcomes remain excellent with modern protocols. APL serves as a proof-of-concept for the power of precise molecularly targeted treatment.

In terms of mutations, FLT3 inhibitors represent the earliest and most widely adopted targeted example. The addition of midostaurin to standard 7+3 therapy in newly diagnosed FLT3

mutated AML has been shown to improve overall survival and is now incorporated into standard of care regimens for fit adults (Perl et al. 2019). Post remission maintenance and relapse treatment have also been reshaped by the availability of the more potent FLT3 inhibitor gilteritinib particularly in relapsed or refractory disease. Throughout the intensive treatment pathway, therapy selection is increasingly guided by genetic profiling and MRD response (Dohner et al. 2022). Parallel progress in IDH mutated AML has introduced the IDH1 and IDH2 inhibitors ivosidenib and enasidenib. These agents promote differentiation rather than cytotoxicity and have shown clinically meaningful activity in relapsed disease and in older patients unsuitable for intensive therapy (Lachowiez et al. 2023). Together, these developments illustrate how genetic context increasingly dictates therapeutic strategy in younger, medically fit individuals.

A substantial proportion of patients with AML are older or have significant comorbidities that preclude intensive chemotherapy. Treatment in this population has changed dramatically over the past decade, largely driven by the introduction of venetoclax-based regimens. The combination of venetoclax with azacitidine is now the standard first-line therapy for unfit adults, producing high remission rates without the toxicity associated with 7+3 (Dohner et al. 2022). However, responses vary markedly by genotype. Deep and durable remissions are most often seen in NPM1 mutated and IDH-mutated AML, whereas TP53 mutated disease and RAS pathway mutations (NRAS/KRAS) are consistently associated with poor or short lived responses (Testa et al. 2023; Döhner et al. 2024). These patterns reinforce the central role of mutation profiling in tailoring therapy for older patients.

Measurable residual disease has become one of the strongest predictors of long term outcome in AML. ELN 2022 guidelines recommend MRD testing at defined milestones after induction and consolidation, as MRD negative patients consistently experience lower relapse rates and improved survival across genetic subgroups (Dohner et al. 2022). MRD results now commonly influence decisions regarding the need for allogeneic transplantation, particularly among patients in intermediate-risk categories see **1.3.4**. Recent analyses in patients receiving venetoclax azacitidine show that MRD negativity remains achievable, even in older populations, and correlates strongly with prolonged remission and improved survival (Döhner et al. 2024). However, certain molecular groups particularly TP53 mutated and RAS mutated AML rarely achieve deep remissions, limiting the predictive value of MRD in these settings. Emerging work from Strati and colleagues suggests that MRD may soon transition from a

purely prognostic marker to a tool for pre-emptive therapeutic interventions, such as early transplant referral or treatment intensification in patients with detectable disease.

1.3.8 Relapse, clonal evolution and high risk AML

In the UK, acute myeloid leukaemia (AML) continues to represent a substantial clinical burden, with approximately 2,900 new cases and around 2,700 deaths recorded each year (2017-2019) (CRUK, 2019). Despite therapeutic advances, relapse remains the principal cause of treatment failure.

Although many patients achieve remission with initial therapy, longitudinal sequencing studies have shown that relapse rarely represents a simple reemergence of the diagnostic clone. Instead, most relapses arise from minor subclones already present at diagnosis that possess intrinsic resistance to chemotherapy. Deep sequencing analyses demonstrate that small baseline populations, undetectable by standard methods, expand under treatment pressure and dominate the disease at relapse (Wienecke et al. 2024). Founder mutations such as DNMT3A or NPM1 typically persist throughout the disease course, whereas mutations associated with resistance, including FLT3-ITD, NRAS, KRAS and TP53, either newly emerge or become more prominent at relapse (Qureshi et al. 2025). These patterns illustrate that AML evolves dynamically during therapy, and that relapse reflects clonal selection rather than simple regrowth.

Increasingly sensitive measurable residual disease NGS-MRD techniques now allow early detection of these resistant subclones. Their expansion during or after induction strongly correlates with relapse risk and inferior survival, emphasising the clinical relevance of clonal evolution in AML (Maher 2025). As a result, MRD guided decision making is becoming a central element of modern risk assessment.

Secondary AML (sAML) and therapy-related AML (t-AML) represent prototypical high-risk forms of the disease and often exemplify this evolutionary process. These subtypes are characterised by adverse cytogenetic features, complex karyotypes and an accumulation of age-related mutations, all contributing to low remission rates and high early mortality. Contemporary registry analyses, including the PETHEMA cohort, show markedly poorer outcomes in patients aged 60–75 years with AML transformed from prior MDS or chemotherapy exposure, with both complete remission rates and overall survival substantially lower than in de novo AML (Martínez-Cuadrón et al. 2024). Similar findings from the SEER

Medicare cohort highlight that transformation from MDS is most lethal when accompanied by high-risk disease features, transfusion dependence or significant comorbidity (Batra et al. 2025). These observations underscore the aggressive biology of sAML and t-AML and explain why treatment responses are typically short lived.

Together, these data demonstrate that AML is not a static disorder but one that adapts to therapeutic pressure through selective outgrowth of resistant clones. This evolutionary behaviour underpins relapse, shapes prognosis and defines the therapeutic challenges associated with high-risk disease.

1.4 Heterogeneous Nuclear Ribonucleoprotein (hnRNP)

1.4.1 Overview of hnRNPs

RNA binding proteins (RBPs) form one of the most diverse and functionally versatile groups of gene regulatory molecules in mammalian cells. They operate across the entire lifespan of mRNA from transcription and co-transcriptional splicing to nuclear export, localisation, translation and decay allowing them to act as sensitive integrators of metabolic, developmental and stress-related cues. Because of their position at these regulatory checkpoints, changes in RBP activity can have broad consequences for cell fate, survival and adaptation (Mancarella et al. 2024; Jungfleisch and Gebauer 2025).

Among these RBPs, the heterogeneous nuclear ribonucleoproteins (hnRNPs) represent one of the best characterised families. First identified through biochemical fractionation studies more than three decades ago (Swanson and Dreyfuss 1988; Dreyfuss et al. 1993), hnRNPs were initially defined as proteins that assemble with nascent RNA to form nuclear ribonucleoprotein particles. Subsequent structural analyses have expanded this concept substantially, showing that the family contains more than twenty members, typically designated hnRNPA–U, each distinguished by specific combinations of RNA binding domains and low complexity regions (Geuens et al. 2016; Xie et al. 2021). These features underpin a wide functional repertoire, enabling hnRNPs to regulate alternative splicing, stabilise or remodel nascent transcripts, and prepare mature mRNAs for export.

Once mRNAs enter the cytoplasm, several hnRNPs continue to exert regulatory control by modulating translational efficiency or determining the timing of mRNA turnover. Others are selectively recruited into stress granules or participate in DNA damage signalling, reflecting the importance of their prion like domains in organising transient ribonucleoprotein assemblies

during cellular challenge (Wang et al. 2020; Aitken et al. 2022). Although these functions are shared across the family, each hnRNP maintains a distinctive interaction profile. hnRNPA1, for instance, couples dual RNA recognition motifs (RRMs) with efficient nucleocytoplasmic shuttling to influence splicing and telomere maintenance, whereas hnRNPK integrates K-homology (KH) domain mediated RNA binding with broad transcriptional and translational effects (Aitken et al. 2022).

Over the last decade, disruptions to hnRNP biology have been increasingly linked to malignant transformation. Several members show altered abundance or mislocalisation in solid tumours and haematological malignancies, where aberrant hnRNP activity has been shown to drive inappropriate RNA processing and enhance cellular survival pathways. Mechanistic studies provide direct evidence for this link; for example, hnRNPK is phosphorylated in an ATM dependent manner following DNA damage and acts as a critical co factor for p53 mediated transcription, thereby modulating apoptotic responses independently of p53 mutational status (Moumen et al. 2013). Dysregulation of this axis can therefore promote resistance to apoptosis and sustained proliferative signalling (David et al. 2010), with broader alterations across the hnRNP network summarised in recent reviews (Vembuli et al. 2024).

In haematopoietic cells specifically, hnRNPs contribute to the fine tuning of lineage specification by regulating the processing and stability of transcripts that define stem cell identity (Hodson et al. 2019; Aguilar-Garrido et al. 2022). Experimental perturbation of individual hnRNPs has demonstrated that this regulation is functionally critical: for example, loss or mislocalisation of hnRNPK disrupts p53 dependent transcriptional programmes and apoptotic control, while altered hnRNPA1 activity affects splicing decisions linked to proliferation and differentiation (David et al. 2010; Moumen et al. 2013). Perturbation of these RNA regulatory pathways compromises progenitor fitness and creates a permissive context for clonal selection and leukaemic evolution. Although the family is broad, two members hnRNPA0 and hnRNPA3 are of particular interest in the context of this thesis. These proteins were identified in Chapter 3 as part of a global analysis of hnRNP dysregulation in AML (See Chapter 3). Both proteins participate in stress response and mRNA stability pathways that intersect with cell cycle control and checkpoint integrity, yet their precise contribution to AML biology remains unclear. This gap in knowledge provides the foundation for the experimental work that follows.

1.4.2 hnRNP structure and function

The structural organisation of hnRNP underpins their capacity to regulate a wide spectrum of post transcriptional events. The hnRNP family comprises at least twenty distinct members in mammals (hnRNPA1–hnRNPU) and displays considerable functional diversity; however, most proteins share a modular domain architecture that governs how and where they engage with RNA and associated regulatory factors (Tilliole et al. 2024). These domains do not act in isolation but instead function cooperatively to shape the behaviour of individual hnRNPs within both the nuclear and cytoplasmic compartments. At the core of many hnRNPs are one or more RNA recognition motifs (RRMs), which provide the primary interface for binding short RNA sequences. The modular organisation of key hnRNP domains is summarised in (**Figure 1-6**), which provide the primary interface for binding short RNA sequences. Despite being highly conserved at the structural level, RNA recognition motifs (RRMs) allow each hnRNP to exhibit subtle preferences for distinct RNA sequences or secondary transcript structures, a property that underpins their central role in alternative splicing decisions and transcript maturation through differential RNA binding affinity and context-dependent exon recognition (Clery et al. 2008), (Maris et al. 2005), (Geuens et al. 2016).

Alongside RRMs, several hnRNPs also contain arginine glycine glycine (RGG) or RGG like motifs, which preferentially interact with structured or G rich RNA elements and facilitate multivalent RNA protein and protein-protein interactions. These motifs are particularly important for dynamic ribonucleoprotein assembly and remodelling during cellular stress, contributing to the formation and regulation of stress granules and other RNA rich condensates (Thandapani et al. 2013) (Kwon et al. 2013) (Jain et al. 2016).

In contrast to the RRM dominant hnRNPs described above, a second group of hnRNPs, including hnRNPK and members of the E family, relies more heavily on K-homology (KH) domains as their principal RNA binding modules. KH domains provide a highly selective mode of RNA recognition and often position these proteins at the interface between transcriptional and translational control. As a result, KH containing hnRNPs frequently act as molecular scaffolds that integrate RNA targets with signalling pathways involved in cell growth, survival and stress adaptation (Valverde et al. 2008), (Bomsztyk et al. 2004).

Several hnRNP family members further contain low complexity or prion-like regions, which promote liquid-liquid phase separation and enable the rapid and reversible formation of stress granules or other RNA rich condensates in response to metabolic or genotoxic challenge. This phase-separation capacity is increasingly recognised as a key mechanism by which hnRNPs

coordinate RNA metabolism when cells are pushed outside steady-state conditions, as summarised in (**Figure 1-5**), and **(Figure 1-6)** (Banani et al. 2017) (Alberti et al. 2019) (Hennig et al. 2015).

Nuclear localisation and export signals further refine the behaviour of individual hnRNPs. Some, such as hnRNPA1, shuttle efficiently between nucleus and cytoplasm, allowing them to couple early splicing decisions with later effects on mRNA export, stability or translation (Dreyfuss et al. 2002) (Jean-Philippe et al. 2013). Others including hnRNPU (also known as SAF-A), remain largely nuclear and contribute to higher order chromatin organisation as well as transcriptional regulation through dynamic RNA chromatin interactions (Marenda et al. 2022) These differences in intracellular distribution add an additional layer of specificity to how each hnRNP shapes gene expression.

Together, these structural features explain why hnRNPs occupy such a broad functional space. Because haematopoietic cells rely on rapid shifts in RNA metabolism during lineage commitment and stress responses, this modular architecture places hnRNPs in a position of considerable regulatory influence a theme that becomes even more apparent when their roles in normal haematopoiesis and AML are considered in the following sections.

1.4.3 The role of hnRNPs in normal haematopoiesis

Normal blood formation depends on a sequence of tightly timed RNA processing events as haematopoietic stem and progenitor cells (HSPCs) move from dormancy into lineage commitment. Throughout this transition, RNA binding proteins play a decisive role, and several hnRNP family members act as key intermediaries that translate environmental cues including cytokine signalling, metabolic shifts and inflammatory stress into precise adjustments in splicing, mRNA stability and translational control (Hodson et al. 2019; Clarke et al. 2021).

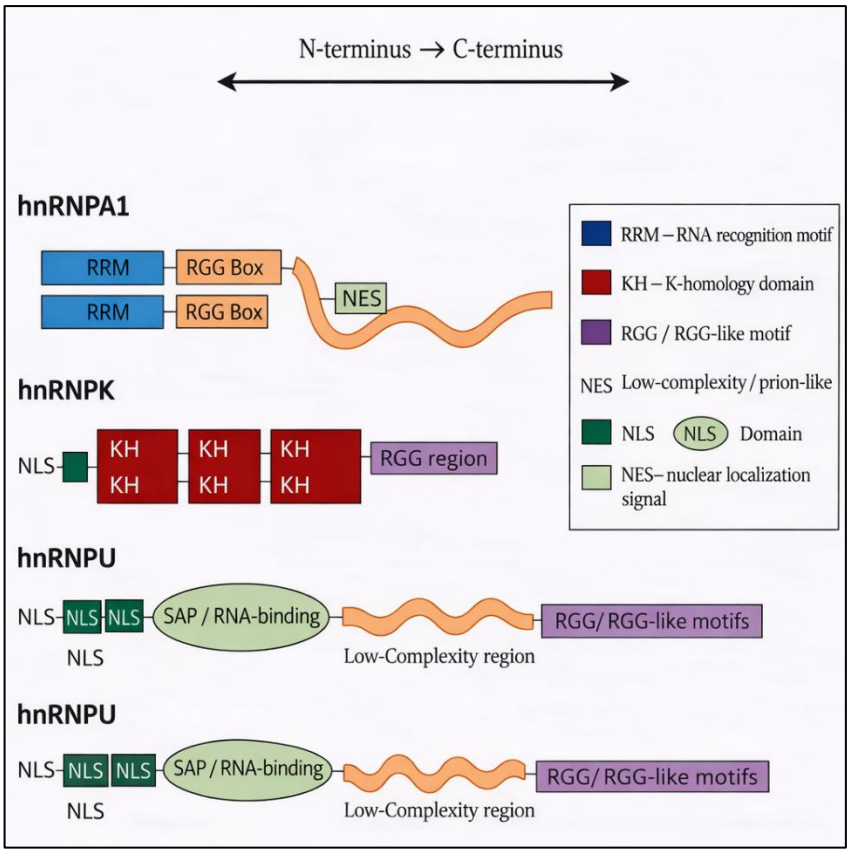

Figure 1-5 Modular domain architecture of key hnRNP family members

Linear schematics showing the domain organisation of selected hnRNP proteins from N-terminus to C-terminus, highlighting RNA recognition motifs (RRM), K-homology (KH) domains, RGG/RGG-like motifs, low-complexity/prion-like regions, and nuclear localisation (NLS) and export (NES) signals. Created with https://www.biorender.com/.

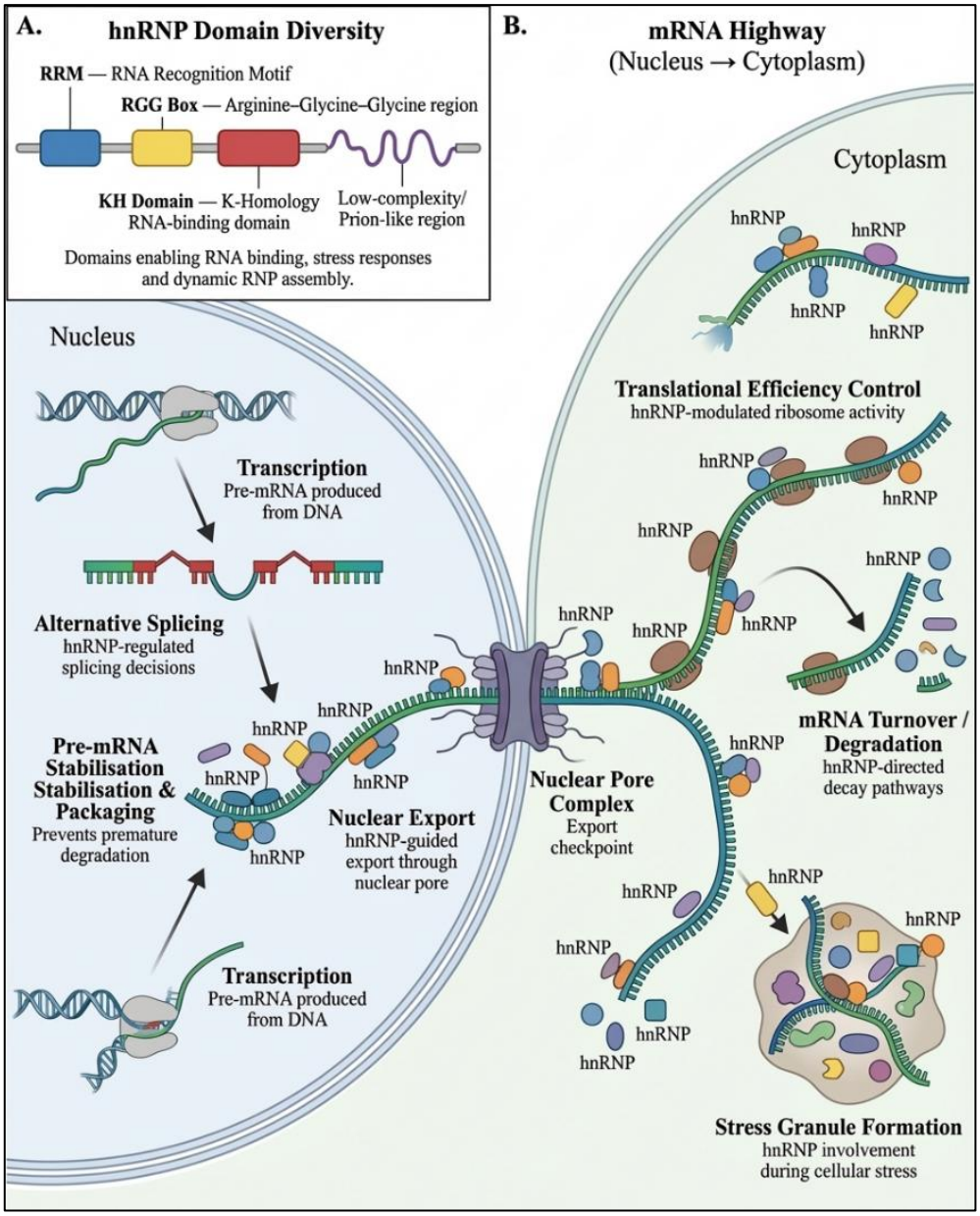

Figure 1-6 Structural diversity of hnRNPs and their regulatory roles across the mRNA cycle

A Domain organisation of hnRNP family proteins, illustrating the major motifs that underpin RNA binding and ribonucleoprotein assembly. **B** Overview of hnRNP activity during the journey of an mRNA from nucleus to cytoplasm. Created with https://www.biorender.com/

Transcriptomic profiling has consistently shown that many hnRNPs are highly expressed within early HSPCs. In this context, they participate in the selective splicing of transcripts that influence cell fate decisions. Small alterations in exon inclusion within transcription-factor or signalling mRNAs can tip the balance between erythroid, myeloid or lymphoid specification, and hnRNPs provide much of the regulatory flexibility required for these transitions (Clarke et al. 2021). Perturbation of RNA-binding proteins, including members of the hnRNP family, has been shown to disrupt post-transcriptional control mechanisms in haematopoietic systems, frequently resulting in impaired differentiation and aberrant progenitor behaviour. These findings highlight the dependence of progenitor populations on tightly regulated splicing and RNA-processing programmes (Aguilar-Garrido et al. 2022).

Beyond splicing, specific hnRNP-associated RNA-binding proteins, including ZFP36L1 and ZFP36L2, contribute to the maintenance of progenitor identity by regulating mRNA stability. These factors stabilise transcripts required for quiescence and survival while promoting the turnover of mRNAs associated with premature differentiation, thereby preventing inappropriate lineage commitment prior to the appropriate developmental cues (Hodson et al. 2019).

Their role in nuclear export adds an additional layer of regulation. By directing cytokine responsive transcripts into the cytoplasm, hnRNPs ensure that HSPCs can respond rapidly to environmental challenges such as infection, inflammatory stress or metabolic perturbation (Geuens et al. 2016). At the translational level, hnRNP K has been shown to extend its regulatory influence through interactions with translation initiation complexes and by modulating ribosome access to target mRNAs. Through these mechanisms, hnRNPK adjusts protein synthesis during phases of proliferation or lineage priming, acting as a secondary regulatory checkpoint that enables progenitor cells to fine-tune their behaviour without requiring large-scale rewiring of upstream transcriptional networks (Wang et al. 2020).

The importance of hnRNPs in haematopoiesis is most clearly demonstrated by what happens when they are disrupted. Loss of function and mechanistic studies demonstrate that disruption of hnRNP A2/B1, particularly through altered expression of its alternatively spliced isoforms, compromises splicing fidelity, RNA localisation and mRNA trafficking, thereby perturbing post-transcriptional regulation at both nuclear and cytoplasmic levels (Han et al. 2010b). In parallel, depletion of hnRNP M has been shown to impair splice-site selection and circRNA biogenesis, leading to widespread transcriptome instability and reduced cellular fitness in

cancer models (Ho et al. 2021). Together, these findings place hnRNP A2/B1 and hnRNP M as critical regulators of RNA processing whose dysregulation disrupts cellular homeostasis and gene regulatory precision.

1.4.4 The Role of hnRNPs in AML

The involvement of hnRNPs in AML is increasingly recognised, although the field remains far less developed than for transcription factors or signalling pathways. Much of what is currently known comes from studies examining how altered splicing, disrupted mRNA stability and deregulated stress response pathways contribute to leukemogenesis three cellular processes in which hnRNPs play central regulatory roles (Gallardo et al. 2016; Zhang et al. 2016; Dlamini et al. 2020).

Early studies highlighted that abnormal splicing programmes shaped by hnRNP activity can promote leukaemic transformation. Work by Dlamini and colleagues demonstrated that perturbations in BCL2-associated regulatory pathways alter the function of specific hnRNP family members, including hnRNPA1, hnRNPA2/B1 and hnRNPK, generating inappropriate splice variants and destabilised transcripts. These changes collectively favour survival of pre-leukaemic clones and acquisition of oncogenic phenotypes (Dlamini et al. 2020).

These findings emphasise that post-transcriptional regulation mediated by defined hnRNPs, rather than gene mutation alone, contributes meaningfully to AML biology. Other hnRNPs appear to influence chemotherapy response. Zhang *et al.* showed that dysregulated hnRNPK expression enhances autophagy-dependent survival pathways in AML cells exposed to adriamycin, thereby promoting chemoresistance (Zhang et al. 2016). This work positioned hnRNPK as a potential modifier of treatment response and raised the possibility that interruption of its signalling network may help restore drug sensitivity. In contrast, several groups have identified tumour-suppressive functions for hnRNPK under specific biological conditions. Using conditional knockout mouse models, Gallardo *et al.* reported that loss of hnRNPK disrupts genome stability pathways, increases mutational burden and ultimately promotes highly penetrant, transplantable myeloid malignancies (Gallardo et al. 2016). Together, these studies underscore the context-dependent roles of individual hnRNPs in AML, where the same protein may support chemoresistance in some settings while restraining malignant transformation in others.

Beyond hnRNPK, broader work on hnRNP biology suggests that the family as a whole contributes to key malignant behaviours observed in AML, including dysregulated apoptosis, aberrant cytokine responsiveness and altered proliferation dynamics through coordinated effects on RNA splicing, transcript stability and stress-adaptive signalling pathways (Zhang et al. 2016; Dlamini et al. 2020). In these studies, perturbation of hnRNP regulated RNA networks altered survival signalling thresholds and proliferative capacity, supporting a broader role for hnRNPs as modulators of leukaemic cell fitness rather than isolated gene specific regulators.

Despite this emerging evidence, the contribution of individual family members remains unevenly explored. Two proteins of particular interest hnRNPA0 and hnRNPA3 are known to participate in regulatory pathways involving mRNA stability, checkpoint signalling and stress adaptation. Early reports indicate that both A0 and A3 show altered expression in leukaemic settings, yet their mechanistic roles, downstream targets and relevance to disease progression are still poorly defined (Hodson et al. 2019; Aguilar-Garrido et al. 2022). This gap in knowledge forms the foundation for the work undertaken in Chapters 4 and 5, which aims to define the functional contribution of hnRNPA0 and hnRNPA3 and to determine whether their dysregulation creates vulnerabilities that could be exploited therapeutically summarised in (**Figure 1-7**)

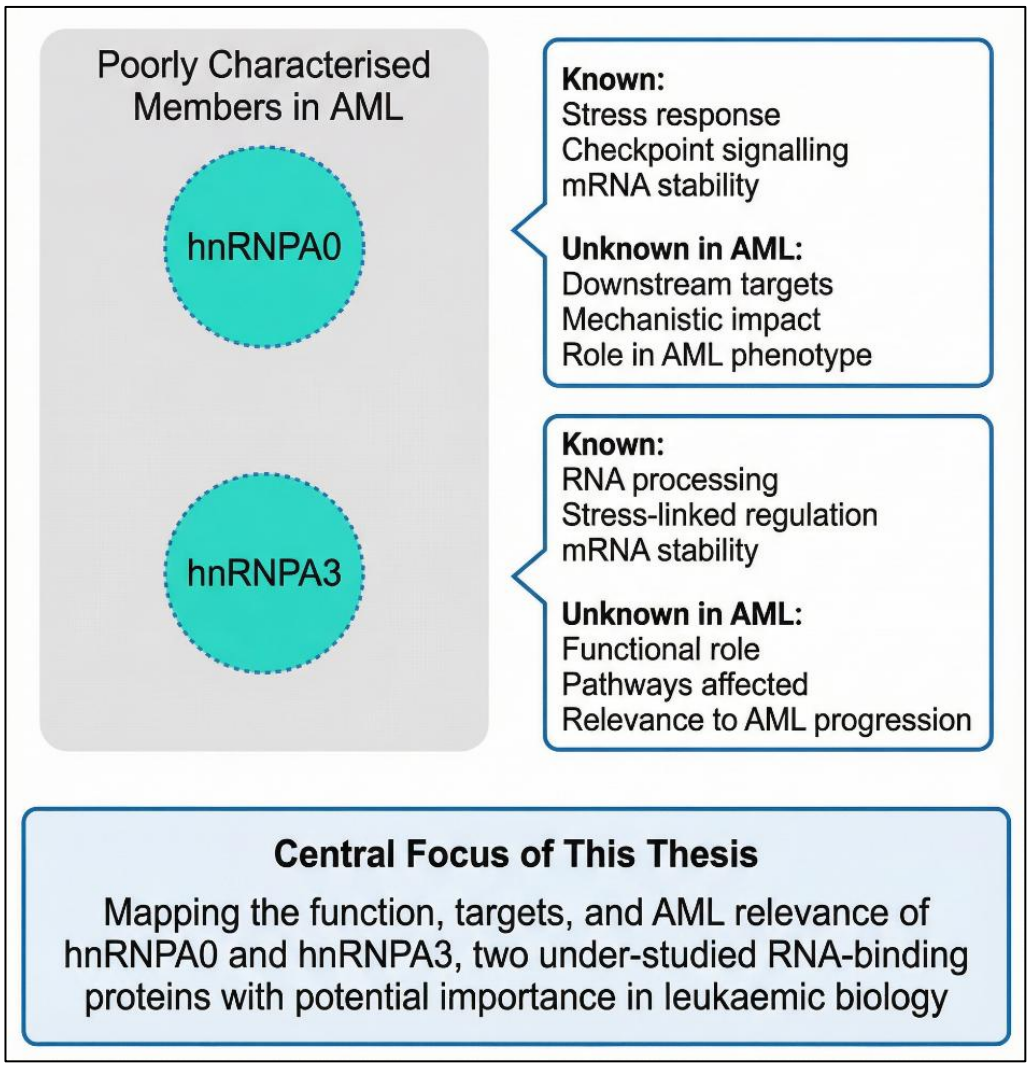

Figure 1-7 Knowledge gaps surrounding hnRNPA0 and hnRNPA3 in AML

A schematic illustration summarising current knowledge of hnRNPA0 and hnRNPA3 in general RNA biology and highlighting the major unresolved questions regarding their downstream targets, mechanistic impact and relevance to AML progression. The diagram outlines the rationale for focusing on these under-studied RNA-binding proteins as the central theme of this thesis. Created with https://www.biorender.com/

1.5 Aims and objective

AML is an aggressive bone marrow disorder driven by genetic and molecular abnormalities that disrupt normal haematopoietic development. Despite advances in genetic profiling and targeted therapy, outcomes for many patients remain poor, particularly in older adults and in those with high-risk molecular features. There is therefore a continued need to identify disease associated vulnerabilities that may inform new therapeutic strategies.

The overall aim of this research is to investigate the role of heterogeneous nuclear ribonucleoproteins in AML, and to determine whether dysregulation of one or more of these proteins contributes to altered AML cell growth and survival.

Hypothesis

It is hypothesised that dysregulation of specific hnRNP family members, particularly hnRNPA0 and/or hnRNPA3, contributes to AML cell survival by altering post transcriptional regulatory pathways, thereby influencing cell growth and apoptotic responses.

To achieve the above goal, the following objectives will be undertaken:

I. To identify the critical nuclear hnRNP genes/proteins for further study by examining the extent of and clinical significance of dysregulated expression of these genes in primary AML blasts. Thirteen hnRNP were identified in a proteomic (mass spectrometry) screen. Dysregulation of the most significant proteins and mRNA expression and clinical outcome will be performed and confirmed by western blot in primary AML patient blasts. Candidate targets will be selected for further study. This aims forms the work outlined in Chapter3.

II. To test the effect of a candidate target hnRNP (A0 or A3 identified from objective I) on AML cell growth and survival by modulating their expression (over-expression and knock down) in AML cell lines and using flow cytometry to measure growth and survival. This work forms the basis of Chapter 4.

III. To identify the changes in mRNA expression arising from dysregulated hnRNP to gain mechanistic understanding of any phenotype observed in Aim II. Understanding such mechanisms, or how haematopoietic development is disrupted, may potentially springboard new scientific approaches for therapeutic intervention in AML.

2 Materials and methods

2.1 Plasmid DNA and generation of virus

2.1.1 Plasmids used in the study

Lentiviral and retroviral plasmid constructs were used to achieve stable genetic modulation of hnRNPA0 and hnRNPA3 in AML cell lines. Gene manipulation strategies included short hairpin RNA (shRNA) mediated knockdown, CRISPR-Cas9 mediated knockout, and cDNA overexpression. All plasmids used in this study were obtained as sequence-verified DNA from VectorBuilder (Chicago, USA), with the exception of the PINCO hnRNPA0 overexpression construct, which was generated By Alex Tonks group (Cardiff 2024). A summary of all plasmids used in this study is provided in (**Table 2-1)** and representative plasmid maps are shown **in (Figure 2-1, Figure 2-2 and Figure 2-3).**

2.1.1.1 Background to CRISPR Cas 9 genome editing

CRISPR Cas 9 is a programmable genome editing system that introduces a targeted double strand break at a user-defined genomic locus using a single guide RNA (gRNA) and the Cas9 nuclease. Following DSB formation, cells repair the break predominantly via non-homologous end joining an error prone pathway that frequently generates small insertions/deletions (indels). Indels occurring within coding regions can shift the reading frame and create premature stop codons, thereby producing functional gene knockout. In this study, CRISPR Cas9 was used to generate stable hnRNPA3 knockout populations via lentiviral delivery of Cas9 and gene specific gRNAs, followed by antibiotic selection to enrich successfully transduced cells.

2.1.1.2 CRISPR Cas9 constructs and strategy used in this

For CRISPR Cas9 mediated knockout, lentiviral plasmids encoding hCas9 and hnRNPA3 targeting gRNAs were used (**Table 2-1**). A non targeting scrambled gRNA construct was included as a negative control. Viral particles were generated in HEK293T packaging cells, and AML cell lines were transduced as described in Section **2.1.7** and the transduction section below. Successfully transduced cells were enriched using puromycin selection, and knockout efficiency was subsequently assessed at the protein level by western blotting (Section **2.5**)

2.1.2 Bacterial cell growth and plasmid DNA isolation

Transformation of *Stbl*3 chemically competent *Escherichia coli* cells (Invitrogen, UK) with the PINCO hnRNPA0 plasmid was performed using a standard heat shock protocol. Briefly, 6 µL of plasmid DNA was added to competent cells and incubated on ice for 30 minutes. Cells were

heat shocked at 42°C for exactly 30 seconds, followed by incubation on ice for 2 minutes. Subsequently, 250 µL of pre warmed sterile SOC medium was added, and cells were incubated at 37°C with shaking at 225 rpm for 1 hour to allow recovery. Following recovery, 50 µL and 200 µL of the transformed cells were plated onto Luria Bertani agar plates supplemented with ampicillin (100 µg/mL) and incubated overnight at 37°C. Single colonies were selected the following day for glycerol stock preparation(**2.1.3**), plasmid DNA extraction(2.1.6), and downstream assays.

2.1.3 Preparation and thawing of glycerol stocks

To generate glycerol stocks for long-term storage, 150 µL of sterile glycerol was added to 850 µL of bacterial culture grown in LB broth supplemented with ampicillin (100 µg/mL). The suspension was mixed thoroughly and transferred to labelled cryovials, which were stored at -80°C. For recovery, glycerol stocks were maintained on dry ice, and a small amount of frozen culture was streaked onto selective LB agar plates using a sterile inoculation loop and incubated overnight at 37 °C.

Table 2-1 list of plasmid and constructs used in this study

Plasmid Number	Gene	Studies	Vector name	Target sequence	Markers	Source
576	**hnRNPA3**	CH4 (KD)	pLV[shRNA]-EGFP:T2A:Puro-U6>hHNRNPA3 [shRNA#6]	GATGGTGGATATAATGGATTT	Ampicillin; EGFP; Puromycin	vectorBuilder
581		CH4 (KD)	pLV[shRNA]-EGFP:T2A:Puro-U6>hHNRNPA3 (shRNA#1)	ATGACTGGTTGGCTCTATTTA	Ampicillin; EGFP; Puromycin	vectorBuilder
610		CH4 (KO)	pLV[CRISPR]-hCas9:T2A:Puro-U6>hHNRNPA3[gRNA#519]	TTGTAGGATTCTGTAAAGCC	Puromycin	vectorBuilder
611		CH4 (KO)	pLV[CRISPR]-hCas9:T2A:Puro-U6>hHNRNPA3[gRNA#561]	CTTGCCTGTATTAAAGGTCG	Puromycin	vectorBuilder
613		CH4 (OE)	pLV[Exp]-EGFP:T2A:Puro-EF1A	hHNRNPA3 (NM_001330249.2) full-length ORF	EGFP, Puromycin	vectorBuilder
600	**hnRNPA0**	CH4 (KD)	pLV[shRNA]-EGFP:T2A:Puro-U6>hHNRNPA0[shRNA#1]	GCCAAGGTTAAGAAGCTCTTT	EGFP, Puromycin	vectorBuilder
605		CH4 (KD)	pLV[shRNA]-EGFP:T2A:Puro-U6>hHNRNPA0[shRNA#4]	CGACAAGCAGTCCGGCAAGAA	EGFP, Puromycin	vectorBuilder
490		CH4 (OE)	PincoGFP-hnRNPA0	Full-length hnRNPA0 cDNA	EGFP, Puromycin	vectorBuilder
99	**Controls**	CH4 (OE)	overexpression	Full-length cDNA, Control	EGFP, Puromycin	vectorBuilder
497		CH4(KD)	pLV[shRNA]-EGFP:T2A:Puro-U6-Scramble-shRNA	Scramble shRNA	EGFP, Puromycin	vectorBuilder
407		CH4 (OE)	pLV-EGFP-T2A-Puro-EF1A	Multiple cloning site	EGFP, Puromycin	
463		CH4 (KO)	pLV Scramble_gRNA-hCas9-T2A-Puro	Non-targeting scrambled gRNA	Puromycin	vectorBuilder
189			pMD.2G	envelope plasmid	Puromycin	vectorBuilder
158			psPAX2	packaging plasmid Gag, Pol, Tat and Rev	Puromycin	vectorBuilder

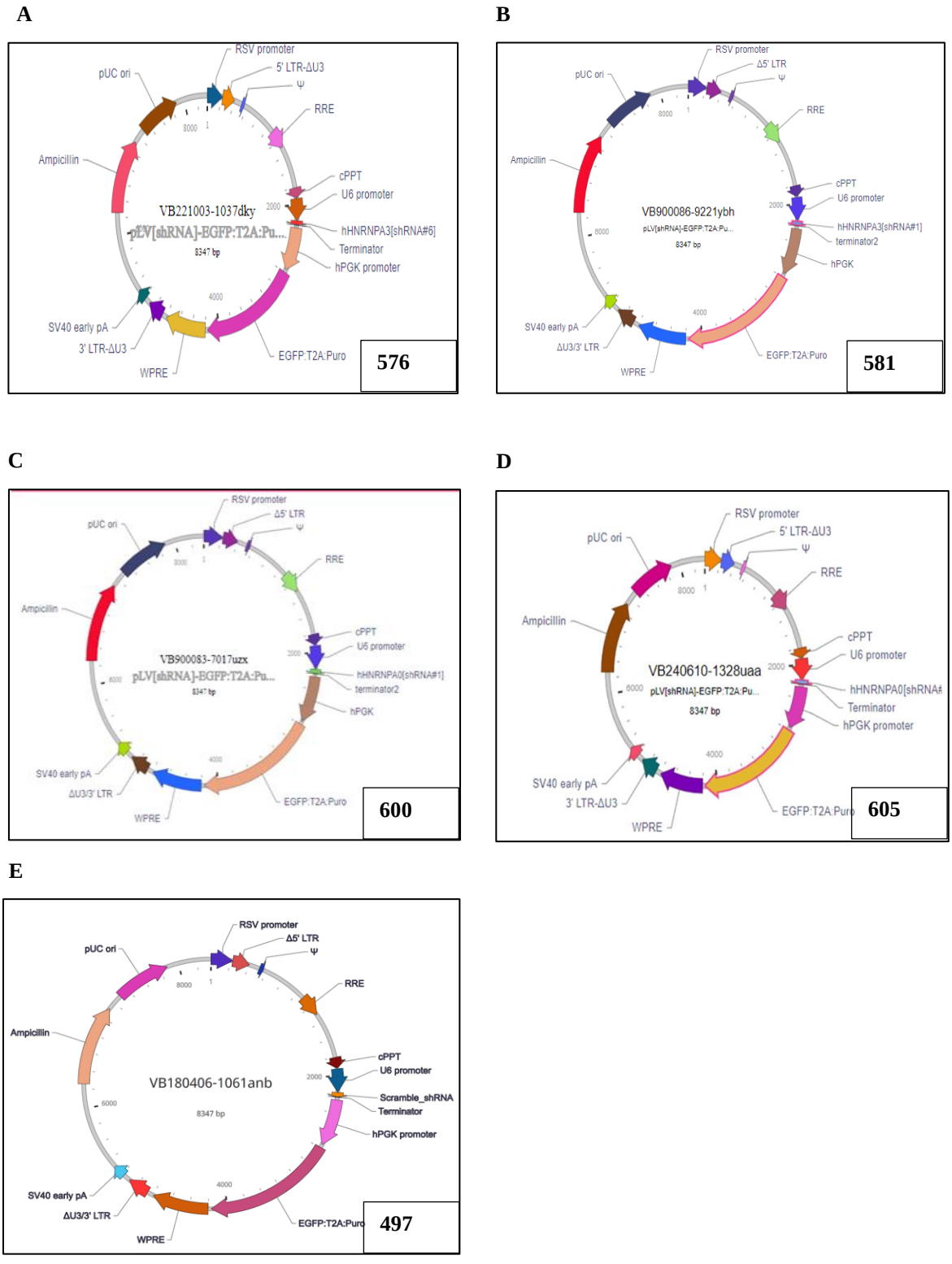

Figure 2-1 Plasmid constructs used for genetic modulation for KD

A shRNA targeting hnRNPA3 (construct 576), **B** shRNA targeting hnRNPA3 (construct 581), **C** shRNA targeting hnRNPA0 (construct 600), **D** shRNA targeting hnRNPA0 (construct 605), and **E** non targeting scrambled shRNA control. All constructs express EGFP to enable assessment of transduction efficiency.

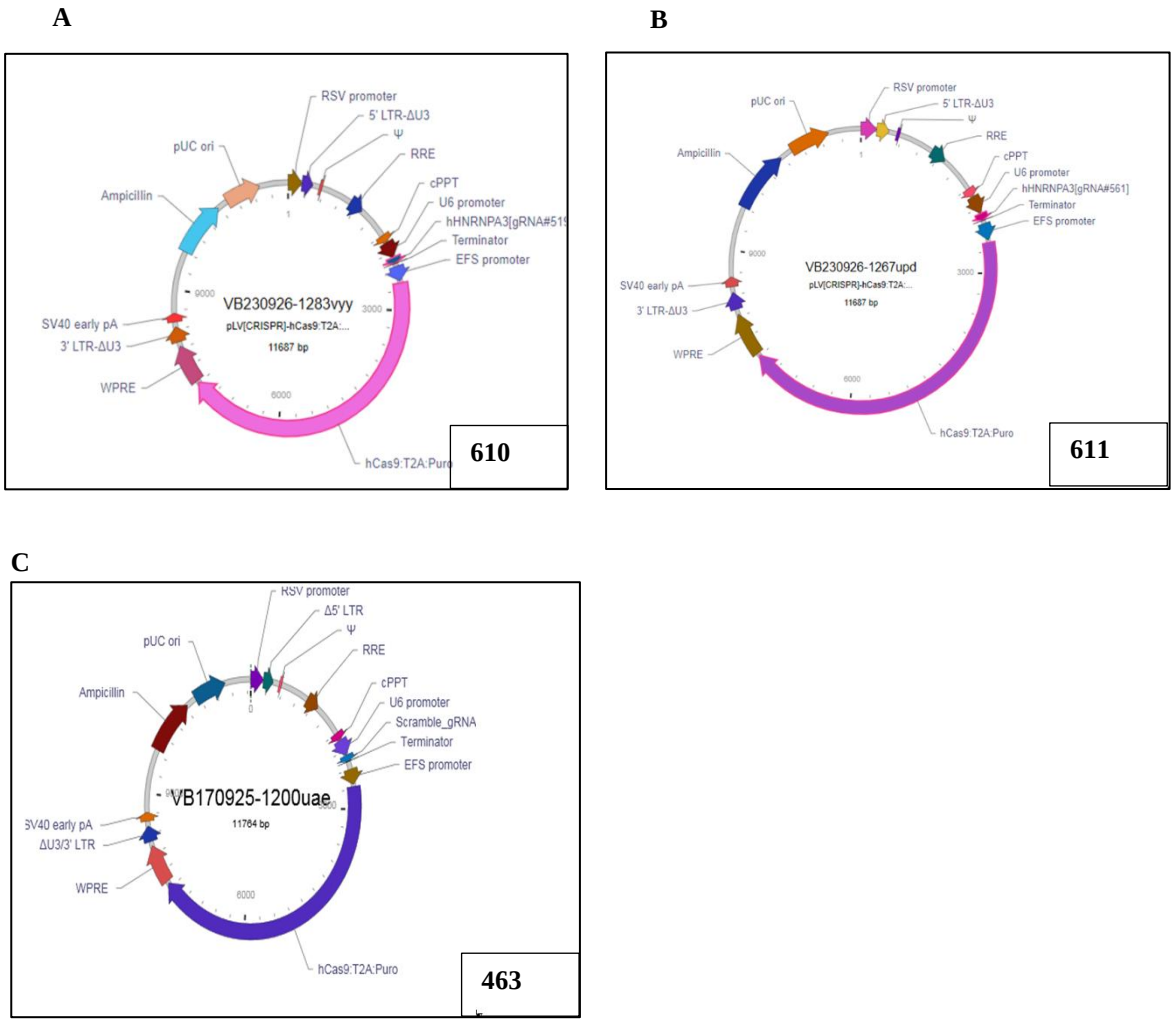

Figure 2-2Plasmid constructs used for genetic modulation for KO(CRISPR-Cas9)

A gRNA targeting hnRNPA3 (plasmid 610 **B** gRNA targeting hnRNPA3 (plasmid 611) **C** non targeting scrambled gRNA control. All constructs express Cas9 and a puromycin resistance cassette to enable selection of successfully transduced cells.

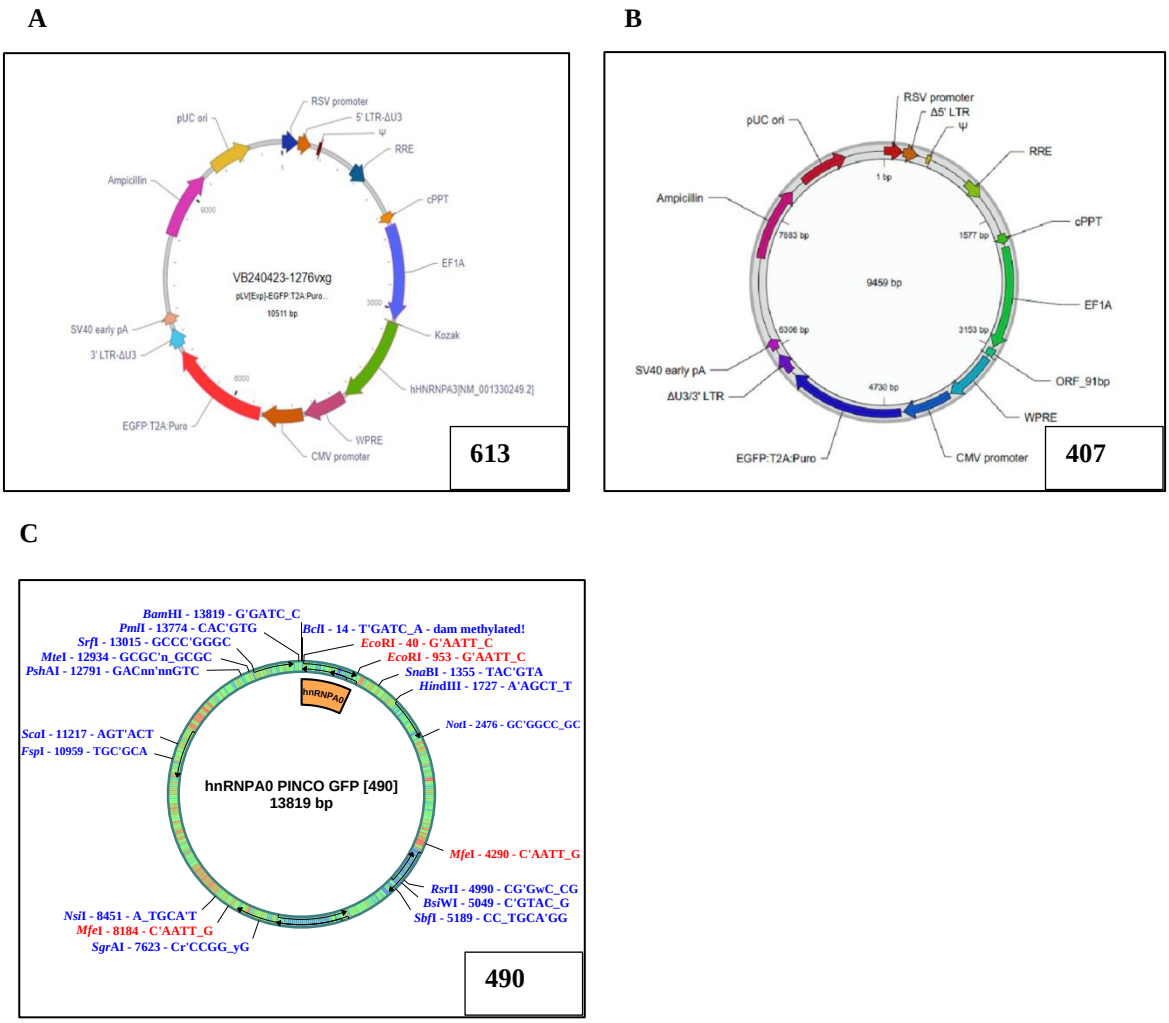

Figure 2-3 Plasmids for overexpression used in the study

A hnRNPA3 overexpression construct (plasmid 613) **B** empty vector control **C** hnRNPA0 overexpression construct (PINCO GFP-hnRNPA0; plasmid 490). All constructs express EGFP to enable identification of transduced cells and assessment of transduction efficiency.

2.1.4 Growth of bacteria for plasmid MiniPrep

Following overnight incubation, agar plates were inspected for well-isolated single colonies. Individual colonies were selected and used to inoculate 5 mL of sterile LB broth supplemented with ampicillin (100 µg/mL). Cultures were incubated at 37°C with shaking until sufficient bacterial growth was achieved. Where required, multiple starter cultures were established to allow selection of optimal clones for downstream plasmid amplification. These starter cultures served as the initial stage for both MiniPrep and MaxiPrep plasmid isolation.

2.1.5 Growth of bacteria for plasmid MaxiPrep

For large-scale plasmid DNA amplification required for viral production, bacterial cultures were expanded prior to plasmid MaxiPrep isolation. Starter cultures were expanded by transferring 150 µL of bacterial culture into 150 mL of LB broth supplemented with ampicillin (100 µg/mL) in sterile Erlenmeyer flasks. Cultures were incubated overnight at 37 °C with shaking at 225 rpm to allow high-density bacterial growth prior to plasmid isolation.

2.1.6 Plasmid DNA isolation using ZymoPURE Miniprep Kit

Plasmid DNA was isolated from bacterial cultures using the ZymoPURE Plasmid Miniprep Kit (Zymo Research, California, USA) according to the manufacturer's instructions. Briefly, bacterial cultures (0.5–5 mL) were harvested by centrifugation, and cell pellets were resuspended in ZymoPURE P1 buffer. Cells were lysed using alkaline lysis buffer (ZymoPURE P2), followed by neutralisation with ZymoPURE P3. Clarified lysates were obtained by centrifugation and combined with binding buffer prior to loading onto Zymo-Spin II-PX columns. Bound plasmid DNA was washed sequentially using the supplied wash buffers and eluted in sterile water. DNA concentration was determined using NanoDrop™ spectrophotometry, and purified plasmid DNA was stored at -20°C for downstream applications.

2.1.7 DNA transfection and viral harvest

Viral particles were generated using HEK293T packaging cells maintained under standard culture conditions. Cells were seeded one day prior to transfection to achieve optimal confluency at the time of DNA delivery. For retrovirus using Phoenix cell (Alpert and Chen 2017), briefly, cells were counted and initially seeded at $8x10^6$ cells *per* T75 flask. The following morning, media was replaced with 14 mL of fresh pre-warmed media. By the afternoon, tissue grade sterile water was mixed with 45 µg of plasmid DNA and 45 µL of CaCl2 (2.5M), followed by the dropwise addition of 450 µL of 2x HEPES-buffered saline (HBS; 50mM), whilst the solution was bubbled with a pipette. Following vortexing, the solution was

left to precipitate for 20 min at RT. Prior to the transfection, 15 µL of chloroquine (25 µM) was added to the cultures, followed by the dropwise addition of DNA to the medium. Cells were incubated 37˚C and 5% CO2 until the following day, by which growth media was changed, and cells were incubated at 33°C to maximise retroviral stability. Viral supernatant was harvested at 48 and 72 h post-transfection as previously described.

2.2 Tissue culture

2.2.1 Cell lines and culture media

All tissue culture work was performed under aseptic conditions in a Class II biological safety cabinet. Cells were maintained in a humidified incubator at 37°C with 5% CO_2 unless otherwise stated. Culture media and plasticware were equilibrated to 37°C prior to use and all plasticware was purchased from (ThermoFisher Scientific, UK). Cell cultures were regularly inspected to confirm appropriate growth characteristics and absence of bacterial/fungal contamination. Cell line identity and source were documented upon receipt according to supplier-provided authentication records (ATCC, ECACC, DSMZ), and cultures were routinely monitored for morphology and general cell health prior to experimental use. All cell lines used in this study are listed in (**Table 2-2)**.

Cells were maintained in the appropriate growth medium specified for each cell line (**Table 2-2**), supplemented with foetal bovine serum (FBS)(Biosera Europe, Nuaille, France) and 10 mL L-glutamine (Fisher Scientific, UK) and gentamicin 20 µg/mL (Fisher Scientific) to support cell growth and minimise the risk of bacterial contamination. Media were prepared using sterile technique and stored according to manufacturer recommendations. Suspension AML cell lines were maintained in logarithmic growth phase by regular monitoring of cell density and adjustment with fresh complete growth medium. Cells were passaged routinely to ensure cultures remained within the recommended working density range and to avoid overgrowth or nutrient limitation. Adherent cell lines (HEK293T and HeLa) were passaged upon reaching high confluence.

Cell culture medium was removed, and cells were washed briefly with phosphate-buffered saline (PBS) (Fisher Scientific). For adherent cells, cells were detached by incubation with prewarmed trypsin solution (Fisher Scientific) at room temperature for approximately 3 minutes until cells visibly detached from the flask surface. Trypsin activity was neutralised by the addition of an equal volume of complete growth medium. Detached cells were gently

resuspended to generate a single-cell suspension and transferred to a universal container. Cells were pelleted by centrifugation at approximately 270 × g for 10 minutes, after which the supernatant was discarded. Cell pellets were resuspended in fresh complete medium and either returned to culture flasks for routine maintenance or seeded at the required density for downstream experimental assays

2.2.1.1 Rationale for cell line selection and molecular characteristics

AML cell lines were selected to represent key biological and genetic subtypes of myeloid malignancy, covering immature/stem-like, monocytic, and signalling-driven models. Selection was guided by baseline hnRNPA0, and hnRNPA3 expression, differentiation status, and reported cytogenetic, mutational features to ensure findings were not restricted to a single AML context. A summary of the molecular characteristics and rationale for each cell line is provided in (**Table 2-3**)

2.2.2 Determination of cell density

Cell counts were performed using a Neubauer haemocytometer. Cell suspensions were gently mixed to ensure a homogeneous distribution before counting. A volume of 10 µL of cell suspension was loaded into the haemocytometer chamber and cells were counted under an inverted light microscope. Cells within the four large corner quadrants were counted, excluding cells touching the outer boundary lines, in accordance with standard haemocytometer counting conventions. Cell density was calculated using the following equation:

$10^4 \times \sum$ cells counted per quadrant⁄4= Cell density (cells/mL)

Where necessary, samples were diluted to ensure accurate counting within the optimal range of the haemocytometer. All counts were performed in duplicate, and the mean value was used for subsequent calculations. Only cultures displaying appropriate cell density and morphology were used for downstream experimental assays.

.

Table 2-2 list of cell lines used in this study

Abbreviations: **ATCC**: American Type Culture Collection, **ECACC**: European Collection of Authenticated Cell Cultures, **DSMZ:** German Collection of Microorganisms and Cell Cultures, **FBS:** foetal bovine serum, **DMEM**: Dulbecco′s Modified Eagle′s Medium, **IMDM:** Iscove's Modified Dulbecco's Medium **MEM:** Minimum Essential Medium Eagle

Line	Medium	Subculture	Normal working range (cells/mL)	Source
HEK293	DMEM + 10% FBS	Adherent; passaged at ~70–80% confluency	N/A	ATCC
HELA	DMEM + 10% FBS	Adherent; passaged at ~70–80% confluency	N/A	ATCC
THP-1	RPMI 1640 + 10% FBS	Suspension; passaged every 2–3 days	$2 \times 10^5 – 8 \times 10^5$	ECACC
HEL	RPMI 1640 + 10% FBS	Suspension; passaged every 2–3 days	$2 \times 10^5 – 1 \times 10^6$	ECACC
U937	RPMI 1640 + 10% FBS	Suspension; passaged every 2–3 days	$1 \times 10^5 – 1 \times 10^6$	ATCC
TF-1	RPMI 1640 + 10% FBS ± GM-CSF	Suspension; passaged every 2–3 days	$2 \times 10^5 – 1 \times 10^6$	ATCC
MV411	IMDM + 10% FBS	Suspension; passaged every 2–3 days	$2 \times 10^5 – 1 \times 10^6$	ATCC
OCIAML-2	MEM + 20% FBS	Suspension; passaged every 2–3 days	$2 \times 10^5 – 1 \times 10^6$	DSMZ
KG1	IMDM + 20% FBS	Suspension; passaged every 2–3 days	$2 \times 10^5 – 1 \times 10^6$	ATCC
SKNO-1	RPMI 1640 + 10% FBS	Suspension; passaged every 2–3 days	$2 \times 10^5 – 1 \times 10^6$	DSMZ
NOMO-1	RPMI 1640 + 10% FBS	Suspension; passaged every 2–3 days	$2 \times 10^5 – 1 \times 10^6$	DSMZ
MONO MAC 6	RPMI 1640 + 10% FBS	Suspension; passaged every 2–3 days	$2 \times 10^5 – 1 \times 10^6$	ATCC
ML-1	RPMI 1640 + 10% FBS	Suspension; passaged every 2–3 days	$2 \times 10^5 – 1 \times 10^6$	DSMZ
HL-60	RPMI 1640 + 10% FBS	Suspension; passaged every 2–3 days	$2 \times 10^5 – 1 \times 10^6$	ECACC
PLB	RPMI 1640 + 10% FBS	Suspension; passaged every 2–3 days	$2 \times 10^5 – 1 \times 10^6$	ATCC
KG1A	RPMI 1640 + 10% FBS	Suspension; passaged every 2–3 days	$2 \times 10^5 – 1 \times 10^6$	ATCC
K652	RPMI 1640 + 10% FBS	Suspension; passaged every 2–3 days	$2 \times 10^5 – 1 \times 10^6$	ATCC
Phoenix	DMEM + 10% FBS	Adherent; passaged at ~70–80% confluency	N/A	Prof Nolan, Stanford University

Table 2-3 Molecular characteristics and rationale

Summary of the disease subtype, defining molecular features, and justification for inclusion of each cell line used in functional and viral production experiments.

Cell lines	Disease	Key marker	Genetic features	Rationale for inclusion
KG1a	AML (immature/stem like)	$CD34^+$, primitive phenotype	Derived from KG1 (erythroleukaemia lineage); lacks recurrent defining fusion	Used as a high hnRNPA0-expressing, stem-like AML model to test dependency under endogenous expression conditions.
THP-1	AML M5 (monocytic)	Monocytic differentiation features	t (9;11) (p21; q23), KMT2A-MLLT3 (MLL-AF9)	Representative monocytic AML model; used for functional assays and to test context-dependency across AML subtypes.
U937	Monocytic lymphoma / AML-like	Monocyte like	t (10;11) (p12; q14) – MLLT10–PICALM	Used as a lower baseline expression background (suitable for overexpression / gain-of-function comparisons).
K562	CML blast crisis	Highly proliferative	t (9;22) (q34; q11) – BCR-ABL1	Used for viral titration/optimisation due to robust transduction and consistent growth.
HEK293T	Packaging line	High transfection efficiency	N/A	Used for lentiviral production due to high transfection efficiency and high viral yield.
Phoenix	Packaging line (retroviral)	High retroviral output	N/A	Used specifically for retroviral production.

2.2.3 Determination of cell viability

Cell viability was assessed using flow cytometry with TO-PRO™-3 iodide (Thermo Fisher Scientific), a membrane-impermeant nucleic acid dye that selectively stains non-viable cells (Van Hooijdonk et al. 1994). Cells were incubated with TO-PRO™-3 at a final concentration of 5 µM in PBS for 5 minutes at room temperature, protected from light. Following incubation, samples were analysed using an Accuri C6 Plus flow cytometer (BD Biosciences, UK). Data acquisition was performed without washing steps. Forward scatter (FSC) and side scatter (SSC) parameters were used to exclude debris and define the main cell population. Viable cells were identified as TO-PRO™-3-negative, while non-viable cells were identified based on positive far-red fluorescence. Representative gating strategies are shown in (**Figure 2-4)**

2.2.4 Cryopreservation and thawing of cell lines

For long term storage, cell lines were cryopreserved using standard laboratory procedures. Cells were harvested during logarithmic growth phase and transferred to a universal container, followed by centrifugation at 270 × g for 10 minutes. The supernatant was discarded, and cell pellets were gently resuspended in an appropriate volume of complete culture medium (**Table 2-2)**. An equal volume of freezing medium consisting of IMDM supplemented with 30% (*v/v*) FBS and 20% (*v/v*) dimethyl sulfoxide (DMSO) was added dropwise to the cell suspension while gently mixing to minimise osmotic shock.

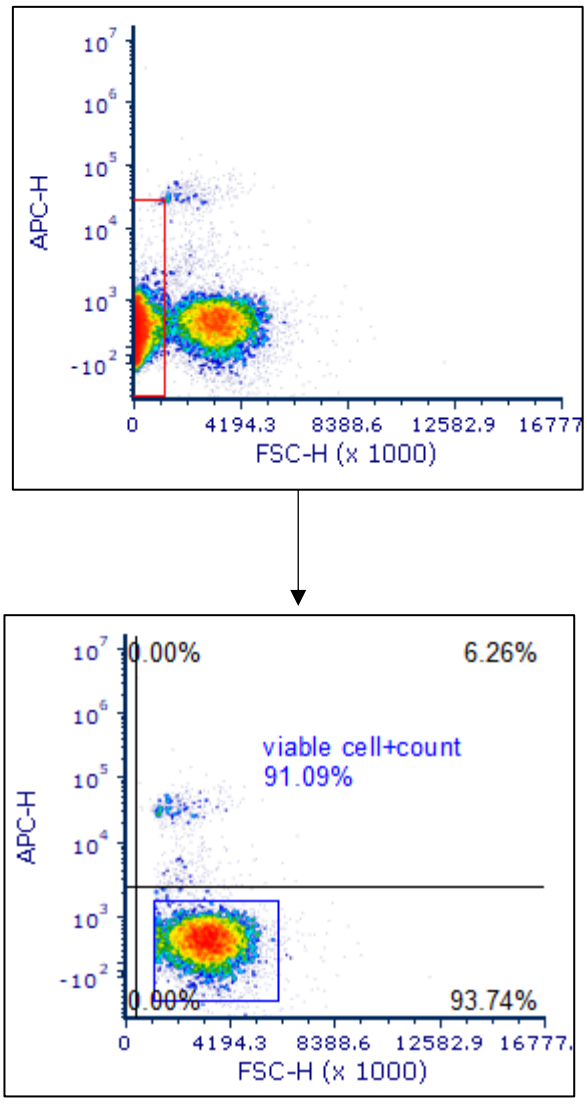

Figure 2-4 Gating strategy used for assessment of cell viability by flow cytometry

Representative flow cytometry plots illustrating the gating strategy used to assess cell viability using TO-PRO™-3 iodide (detected in the APC channel). **A** Cells were initially gated based on forward scatter height (FSC-H) to exclude debris and very small events using a lower FSC threshold (red exclusion gate). **B** The resulting gated population was subsequently analysed for viability by plotting FSC-H versus TO-PRO™-3 (APC). Viable cells were identified as TO-PRO™-3 negative, while non-viable cells were identified based on positive TO-PRO™-3 fluorescence. Percentages indicate the proportion of viable and non-viable cells within the gated population.

Cell suspensions were aliquoted into 1.8 mL cryovials, labelled accordingly, and placed in a controlled rate freezing container (CoolCell™) to ensure gradual cooling. Samples were stored overnight at -80 °C, allowing a controlled cooling rate of approximately -1°C per minute. For long-term storage, cryovials were subsequently transferred to liquid nitrogen.

For thawing, cryopreserved cells were rapidly warmed in a 37°C water bath until only a small ice crystal remained. Immediately after thawing, 1 mL of pre warmed FBS was added dropwise to the vial contents. Cells were then transferred to a universal container containing 5 mL of pre warmed complete culture medium (**Table 2-2**) and centrifuged at 270 × g for 5 minutes to remove residual DMSO. The supernatant was discarded, and the cell pellet was resuspended in fresh culture medium before transfer to an appropriate tissue culture flask. Cells were incubated overnight under standard culture conditions to allow recovery prior to any downstream experimental manipulation.Transduction of AML cell lines

For overexpression studies, using either retro- or lentiviral vectors, 12-well non-tissue culture plates were coated Retronectin® (30 μg/mL) and incubated at 4˚C overnight. The following day, Retronectin® was aspirated and replaced with 1% *v/v* BSA as previously described. The BSA was aspirated and replaced with 1 mL of retro- or lentiviral supernatant. The culture plate was centrifuged at 3000 xg for 120 minutes at Room temperature, following which the supernatant was removed from the wells and replaced with the appropriate number of cells ($4x10^5$ cells/mL), subsequently incubated at 37˚C overnight. Cells expressing GFP were assessed alongside parental cell cultures to measure transduction rates by flow cytometry (**2.3**).

For KD studies using shRNA constructs, pre-coating of cells was unnecessary given the higher titre virus generated from these constructs. Instead, cells were resuspended at $4x10^5$ cells/mL and seeded into a 12-well plate, and 1 mL of culture was added along with 0.5-1 mL of viral supernatant. Cells were assessed for GFP expression as previously described. Following successful cell transduction, cultures were subjected to antibiotic selection to enrich the culture for transduced cells and ensure a pure population. To this end, transduced cells were incubated with 10 μg/mL puromycin (Sigma-Aldrich; P8833), until parental non transduced cultures were no longer viable.

Accurate viral titration was performed to ensure consistent infection conditions across knockdown and overexpression experiments and to enable calculation of appropriate viral volumes for subsequent transduction assays. Estimation of viral titre allowed the determination of infection efficiency and ensured valid experimental comparisons between conditions. Viral

titre was assessed using K562 cells. Non tissue culture treated 96-well plates were coated with Retronectin® (30 µg/mL; Takara Bio) by adding 50 µL per well and incubating either for 2 h at room temperature or overnight at 4 °C. Following aspiration of Retronectin®, wells were blocked with 1% (v/v) BSA in PBS for 30 min at room temperature to minimise non-specific binding. After blocking, 100 µL of K562 cells (1×10^5 cells/mL in RPMI supplemented with 10% FCS) were added to each well, followed by 50 µL of viral supernatant. Mock control wells received an equivalent volume of complete medium in place of viral supernatant.

Cells were incubated for 48 h at 37 °C and 5% CO_2. On day 2, media were carefully aspirated to avoid disturbing the lightly adherent cells, and wells were gently washed with 150 µL of warm medium to remove residual viral particles. Cells were then harvested in 100 µL staining buffer (PBS supplemented with 1% BSA and 0.02% sodium azide).

GFP expression was quantified by flow cytometry using a BD Accuri™ C6 Plus flow cytometer, acquiring 5,000 events per sample at a high flow rate. Data were analysed using FCS Express software. Viral titres calculated from the proportion of GFP-positive cells were subsequently used to estimate the volume of viral supernatant required to achieve comparable transduction efficiencies in downstream experiments.

2.3 Flow cytometry assays

This study, flow cytometry was used to assess transduction efficiency, cell cycle distribution, and apoptosis related readouts following lentiviral gene modulation. Cells were prepared by washing in phosphate buffered saline (PBS) and resuspending at an appropriate concentration prior to acquisition. Data were acquired using a BD Accuri™ C6 Plus Flow Cytometer (BD Biosciences) located within the Cardiff University School of Medicine.

Instrument settings were optimised for each experiment and fluorescence compensation was performed using single-stained controls where appropriate. Data analysis was performed using FCS Express® software (De Novo Software, Pasadena, USA). A minimum of 10,000 events per sample were acquired for all analyses.

2.3.1 Cell growth assessment

Cell growth was assessed to determine the impact of hnRNPA0 and hnRNPA3 genetic modulation on the growth capacity of AML cell lines. Genetically modified cells and their

corresponding control populations were seeded at equal starting densities under standard culture conditions. At defined time points, 100 µL of cell suspension was taken directly from culture and mixed with 1 µL of TO-PRO™ viability dye immediately prior to acquisition. Live cells were identified as TO-PRO™ negative events following exclusion of debris based on forward and side scatter properties. Data were acquired using a BD Accuri™ C6 Plus Flow Cytometer (BD Biosciences), with a minimum of 10,000 events collected per sample. Viable cell counts were normalised to the initial seeding density or matched control populations, as indicated in the corresponding Results section.

2.3.2 Cell cycle analysis

Cell cycle distribution was analysed to assess the impact of hnRNPA0 and hnRNPA3 genetic modulation on cell cycle progression in AML cell lines. Genetically modified and corresponding control cells were harvested during logarithmic growth phase and prepared for DNA content analysis. Propidium iodide (PI, Sigma-Aldrich) was used to label intracellular DNA. For this analysis, 5 x 10^4 cells were transferred to a UC and washed with 20 mL of 1x PBS. Following centrifugation, supernatant was discarded, and cultures resuspended in 300 µL of PBS, following which cells were fixed for 30 min on ice by adding 700 µL absolute ethanol. After fixation, samples were stored at -20°C for an O/N incubation. The following day, cells were washed with 10 mL of 1x PBS and centrifuged at 270 xg for 10 min. Supernatant was discarded and cells were resuspended in 75 µL 1x PBS. Subsequently, cells were incubated with 25 µL staining solution, containing 40 µg/µL PI and 0.1 mg/mL RNase (Sigma-Aldrich) diluted in 1x PBS, at 37°C for 30 min. Samples were acquired within 20 min following incubation using the Accuri™C6 Plus cytometer. Cell cycle analysis was performed using FCS Express's Multicycle analysis tool plug in, according to the gating strategy outlined in **(Figure 2-5**).

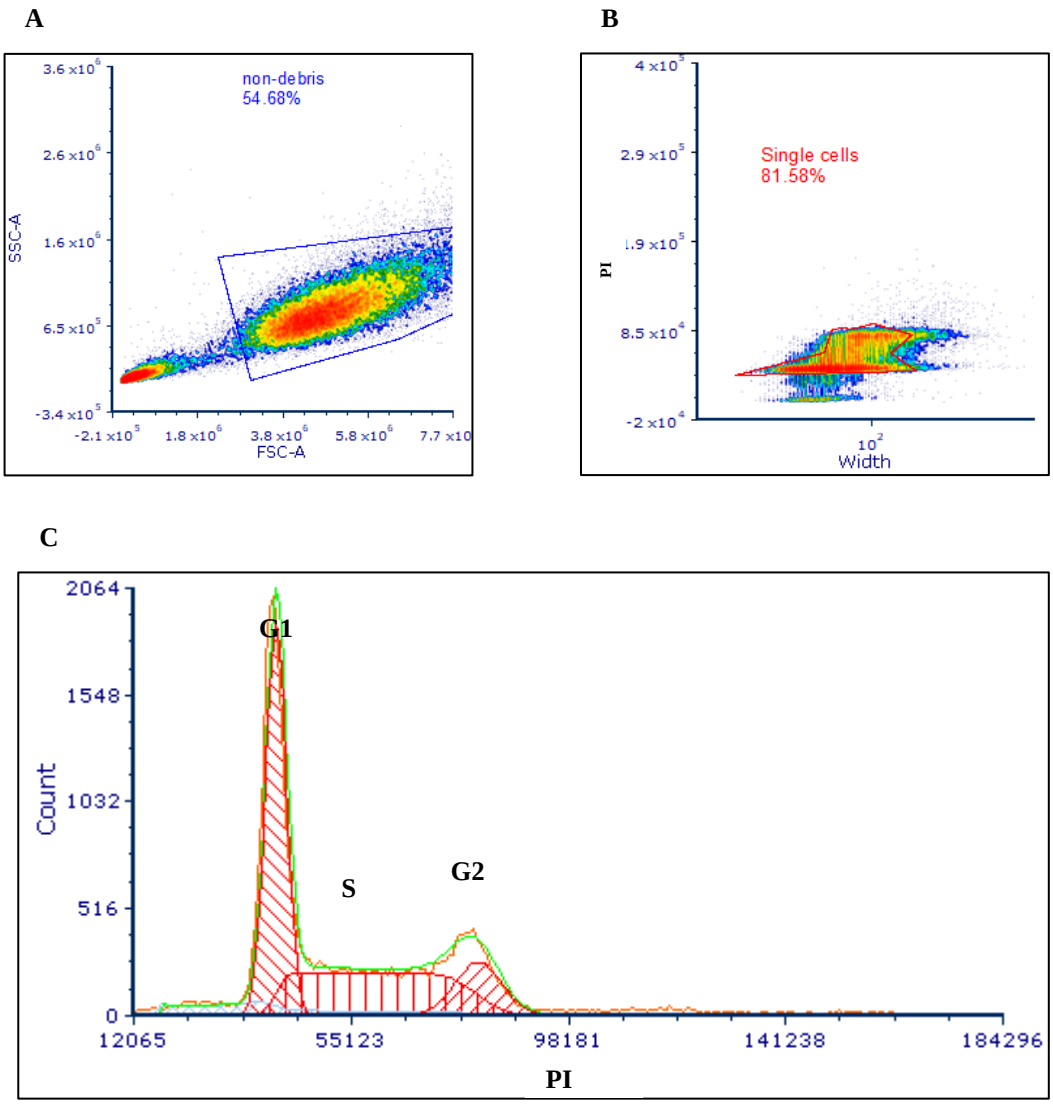

Figure 2-5 Gating strategy used to perform cell cycle analysis

A Gating strategy used to exclude cell debris based on FSC and SSC; **(B)** Gating strategy used to exclude doublet and cell aggregates. **C** Histogram showing DNA content analysis, and determination of the proportion of cells within the G1, S and G2 phases on cell cycle.

2.3.3 Apoptosis analysis

Apoptosis was assessed to determine the impact of hnRNPA0 and hnRNPA3 genetic modulation on cell survival in AML cell lines. Genetically modified cells and matched control populations were analysed under baseline culture conditions without additional treatment. Cells were harvested during logarithmic growth phase and resuspended in Cell Staining Buffer. For each sample, 1×10^6 cells were resuspended in 100 μL of buffer and stained using the ApoTracker™ Tetra staining system according to established laboratory protocols. Briefly, cells were incubated with the ApoTracker™ staining complex at room temperature in the dark to allow selective binding to apoptotic cells. Following staining, cells were washed to remove excess reagent and resuspended in cell staining buffer. Prior to acquisition, 7-AAD was added as a viability dye to enable discrimination of non-viable cells. Samples were analysed by flow cytometry using an Accuri C6 flow cytometer. Forward scatter (FSC) and side scatter (SSC) parameters were used to exclude debris, and appropriate gating strategies were applied to identify apoptotic and non-apoptotic cell populations. Data were analysed using FCS Express software, and apoptosis was quantified as the proportion of ApoTracker™ positive cells within the viable cell population. Results were compared between genetically modified and control cell lines to assess the effect of hnRNPA0 and hnRNPA3 modulation on apoptotic susceptibility summary in (**Figure 2-6**).

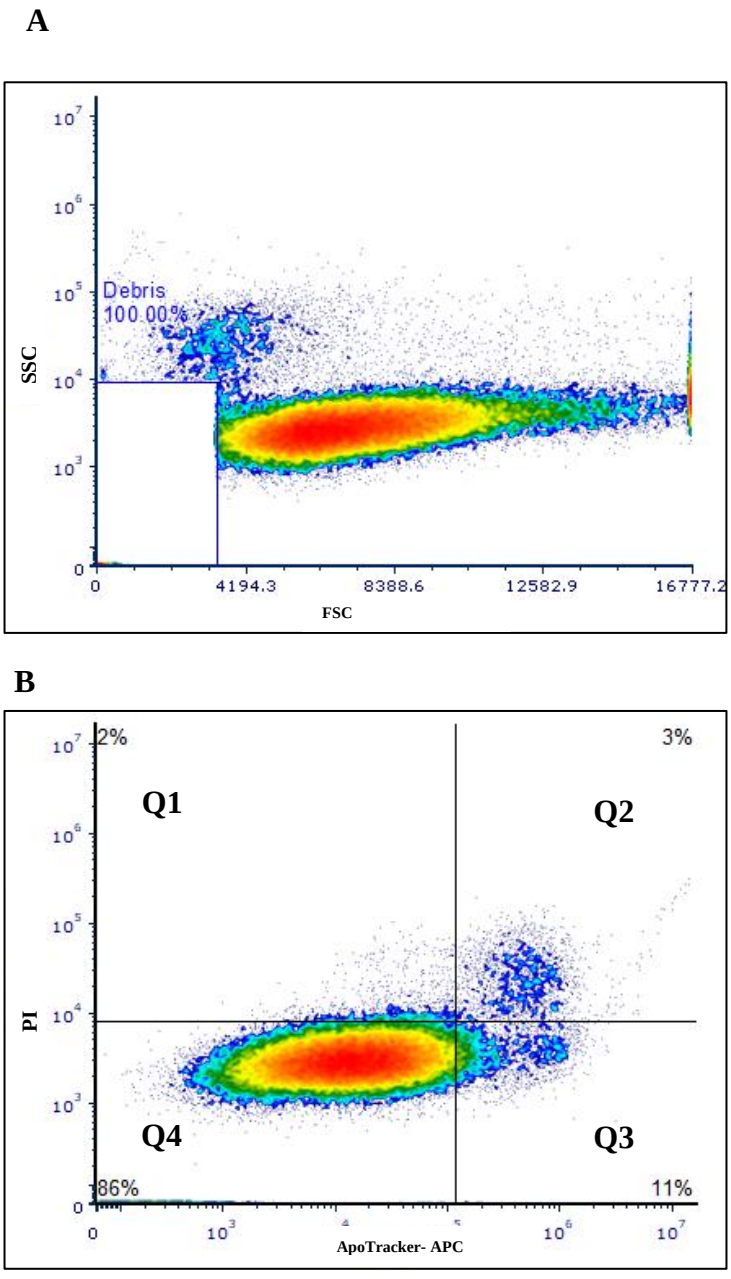

Figure 2-6 Gating strategy used to analyse apoptosis

A gating strategy used to identify cell debris and exclude them for further analysis, based on FSC and SSC; **B** quadrant gating used to determine viable (Q4), pre-apoptotic (Q3) and late apoptotic cells (Q2).

2.4 Protein extraction and Bradford protein assay

2.4.1 Protein extraction

Protein lysates were prepared from AML cell lines. For total extraction The TEAB lysis buffer was prepared freshly and contained 0.5 M triethylammonium bicarbonate (TEAB), 0.05% SDS, supplemented with protease inhibitor cocktail (Sigma-Aldrich) and phosphatase inhibitor cocktails (Sigma-Aldrich). Stock buffer was prepared by combining 5 mL of 1.0 M TEAB (pH 8.5), 50 µL of 10% SDS (Sigma), 100 µL protease inhibitor cocktail, 100 µL of each phosphatase inhibitor cocktail, and 4.7 mL tissue culture grade water to a final volume of 10 mL. Buffer was aliquoted and stored at -20 °C.

All steps were performed on ice where possible, and centrifugation steps were carried out at 4°C. Briefly, cell pellets corresponding to 2×10^6 cells per sample were used for protein extraction. Pellets were thawed gently using the warmth of the hand until just mobile, taking care not to allow warming beyond this point. Samples were then refrozen by placing tubes in the vapour phase of liquid nitrogen for 1 min, followed by thawing as described above. This freeze thaw cycle was repeated to a total of three cycles to facilitate efficient cell lysis. Following the final thaw, benzonase 2 µL (Merck, UK) was added directly to the pellet to reduce nucleic acid viscosity, and samples were gently mixed. Lysates were incubated on ice for 30 min with regular mixing; where residual viscosity was observed, incubation was extended up to 60 min. Cells were then lysed by addition of TEAB lysis buffer, followed by incubation on ice for a further 30 min with intermittent vortexing every 10 min. Lysates were clarified by centrifugation at 10,000 × g for 10 min at 4 °C, and the resulting supernatants containing soluble protein were transferred to fresh tubes

For separation of cytosolic and nuclear protein fractions, cells were harvested and fractionated using a detergent based differential extraction approach. Briefly, the appropriate number of cells were pelleted from culture medium and washed once with tris-buffered saline (TBS) (Starlab, UK) by centrifugation at 10000 g for 10 min, taking care not to disturb the cell pellet. Following complete removal of the supernatant, pellets were gently resuspended and transferred to pre-chilled microcentrifuge tubes.

Cells were resuspended in ice-cold Cytosol Extraction Buffer A (CEB-A) (Abcam, UK) supplemented with dithiothreitol (DTT) and protease inhibitors, using volumes adjusted according to cell type and number (0.2 mL, 5 million MV-4-11 cells, or 2 million K562, THP-1 or KG-1 cells). Samples were vortexed vigorously to ensure complete resuspension and

incubated on ice for 10 min to allow selective permeabilization of the plasma membrane. Ice-cold Cytosol Extraction Buffer B was then added, followed by brief vortexing and incubation on ice for 1 min.

Lysates were centrifuged at maximum speed (13,000 rpm) for 8 min at 4 °C, with tubes oriented consistently to allow accurate identification of the pellet. The resulting supernatant, representing the cytosolic protein fraction, was immediately transferred to a clean, pre-chilled tube and maintained on ice. Residual supernatant surrounding the pellet was carefully removed to minimise nuclear contamination. Pellets were washed once with TBS supplemented with $MgCl_2$ (ThermoFisher, UK), centrifuged, and snap-frozen in liquid nitrogen prior to nuclear protein extraction

Nuclear Extraction Buffer A (NEB) (Abcam, UK). All steps were performed on ice or at 4 °C, and centrifugation steps were carried out using a pre-cooled centrifuge. Nuclear pellets were subjected to three freeze thaw cycles by alternating between brief warming in the hand until mobile and refreezing in liquid nitrogen or on dry ice, to enhance nuclear membrane disruption.

Following the final thaw, benzonase 2 µL(2.5U/µL) (stock=25 U/µL) was added directly to the pellet to digest residual nucleic acids and reduce sample viscosity. Samples were incubated on ice for 30 min with regular mixing; incubation was extended up to 60 min where DNA aggregation persisted. Nuclear proteins were then extracted by addition of NEB supplemented with protease inhibitors and DTT, using 50 µL per 2 million tissue culture cells. Samples were vortexed vigorously for 15 s and returned to ice, with repeated vortexing every 10 min for a total extraction time of 40 min.

Extracts were clarified by centrifugation at 10,000 × g for 10 min at 4 °C, and the supernatant containing the nuclear protein fraction was transferred immediately to clean, pre-chilled tubes. Protein concentration was determined using a Bradford assay prior to downstream applications, and nuclear extracts were stored at -80 °C until use.

2.4.2 Determination of protein concentration by Bradford assay

Bradford protein assay prior to SDS-PAGE and western blotting to ensure equal protein loading across samples. The assay was performed according to standard laboratory protocols using BSA as a reference standard. Briefly, a BSA standard curve was prepared by diluting BSA in lysis buffer to generate concentrations of 0, 10, 40, 70, and 100 µg/mL. Bradford reagent was diluted 1:1 (*v/v*) with distilled water and allowed to equilibrate to room temperature prior to use. Protein samples were diluted 1:50 in distilled water to ensure measurements fell within

the linear range of the assay. Duplicate aliquots of 10 µL of each protein sample and BSA standard were transferred into a 96-well plate. Subsequently, 190 µL of diluted Bradford reagent (Merck,UK)was added to each well and mixed gently. Plates were incubated at room temperature for 10 minutes to allow colour development. Absorbance was measured at 590–595 nm using a plate reader. (Hidex Chameleon Microplate Reader, France) Protein concentrations of unknown samples were calculated by interpolation from the BSA standard curve using linear regression analysis. All measurements were performed in duplicate, and mean values were used for downstream applications.

2.5 Western blotting

2.5.1 Protein sample preparation

Using the NuPAGE® Bis–Tris system (ThermoFisher, UK). Samples were prepared using NuPAGE™ 4× lithium dodecyl sulfate (LDS) sample buffer (Thermo Fisher Scientific) and NuPAGE™ sample reducing agent (Thermo Fisher, UK). Where required, a diluent was prepared consisting of 10 µL NuPAGE™ 10× reducing agent, 25 µL 4× LDS sample buffer, and 65 µL sterile water. Appropriate volumes of LDS buffer, reducing agent, sterile water, and protein sample were determined. Reagents were added sequentially, beginning with LDS buffer, followed by reducing agent, sterile water, and finally the protein lysate. Samples were mixed thoroughly by vortexing and incubated at 70°C for 10 minutes to facilitate protein denaturation. Following incubation, samples were centrifuged briefly at 13,000 rpm for 5 minutes. The supernatant was transferred to clean, labelled microcentrifuge tubes and maintained on ice prior to electrophoresis or stored at −80 °C for longer term storage.

2.5.2 SDS–PAGE electrophoresis

Protein separation was carried out using pre-cast NuPAGE™ Bis–Tris polyacrylamide gels (4–12% or 10%, 10-, 12-, or 17-well formats) assembled in the XCell SureLock™ Mini-Cell electrophoresis system (Thermo Fisher, UK). Gels were removed from their packaging, rinsed with deionised water, and handled exclusively by their edges to minimise contamination. The comb was carefully removed to expose the sample wells, which were washed thoroughly with 1× MOPS SDS running buffer to eliminate trapped air bubbles. Electrophoresis was performed using 1× NuPAGE™ MOPS SDS running buffer prepared from 20× stock (ThermoFisher, UK) and supplemented with NuPAGE™ antioxidant (ThermoFisher) in the upper buffer chamber. The lower buffer chamber was filled with approximately 600 mL of running buffer to facilitate heat dissipation during electrophoresis. Molecular weight markers were prepared using MagicMarker™ XP (ThermoFisher) standards combined with LDS sample buffer and sterile

water. Protein samples were briefly centrifuged prior to loading, and aliquots were taken carefully from the meniscus to ensure homogeneity. Samples and ladder were loaded into the wells from left to right when viewed from the well side of the gel. Empty outer lanes were filled with LDS sample buffer where required to promote uniform electrophoretic migration. Electrophoresis was conducted at a constant voltage of 200 V for approximately 50 minutes using MOPS buffer. Expected current ranged from 100–125 mA per gel at the start of the run, decreasing to 60–80 mA per gel upon completion. During electrophoresis, transfer buffers and blotting materials were prepared in parallel for subsequent protein transfer.

2.5.3 Protein transfer (Transblotting)

Following electrophoresis, proteins were transferred from the polyacrylamide gels onto nitrocellulose (0.45 µm pore size) or Polyvinylidene Fluoride (PVDF) membranes using the Mini Gel tank blot module. Transfer buffer was prepared using 1× NuPAGE® 50mL transfer buffer supplemented with 100mL methanol and 1mL NuPAGE® antioxidant. Blotting pads, membranes, and filter papers were equilibrated thoroughly in transfer buffer prior to assembly. Gel cassettes were opened carefully using a gel knife, and gels were released without distortion. The stacking gel foot was removed before transfer. The transfer sandwich was assembled in the following order: blotting pads, filter paper, gel, membrane, filter paper, and additional blotting pads, ensuring that the gel was positioned closest to the cathode. All trapped air bubbles were removed by gently rolling a glass pipette over each layer. The blot module was assembled securely within the electrophoresis tank and filled with transfer buffer, while the outer chamber was filled with deionised water to dissipate heat. Protein transfer was carried out at a constant voltage of 30 V for 1 hour. Expected current values ranged from approximately 170 mA at initiation to 110 mA at completion. Following transfer, the blot module was dismantled, and membranes were immediately processed for immunodetection.

2.5.4 Immunodetection

Following transfer, membranes were washed twice for 5 minutes in sterile water to remove residual gel and buffer components. Membranes were optionally stained with Ponceau S solution (Sigma) for approximately 30 seconds to confirm efficient protein transfer and equal loading, followed by thorough washing with deionised water to remove residual stain. Membranes were blocked for 30 minutes at room temperature in 2.5% (*w/v*) Marvel milk solution prepared in TBS, with blocking conditions selected according to experimental requirements. Blocking was performed on a rotary shaker at approximately one revolution per second. Primary antibodies were diluted in blocking buffer and applied to the membranes,

which were incubated overnight at 4°C (**Table 2-4**). Following primary antibody incubation, membranes were washed in TBS-T (Merck) for 15 minutes, followed by three 5-minute washes. Secondary antibodies conjugated to horseradish peroxidase were diluted in blocking buffer and applied for 60 minutes at room temperature (**Table 2-4).** Membranes were subsequently washed extensively in TBS-T prior to chemiluminescent detection.

2.5.5 Chemiluminescent detection and imaging

Chemiluminescent detection was performed using Amersham™ ECL Advance detection reagents according to the manufacturer's instructions. Equal volumes of substrate solutions A and B were mixed immediately prior to use and allowed to equilibrate to room temperature. Membranes were incubated with substrate for 5 minutes, excess reagent was removed, and membranes were protected from drying. Protein signals were detected using the LAS-3000 imaging system. Initial exposures of 10-30 seconds were captured to detect weak signals, followed by longer exposures of up to 30 minutes as required. Multiple sequential images were acquired where necessary to optimise signal detection.

2.5.6 Fluorescent antibody detection and imaging (LI-COR)

Where fluorescent detection was required, membranes were processed following completion of chemiluminescent acquisition. Membranes were washed in TBS-T for 15 minutes, followed by three 5 minute washes to remove residual reagents. During washing, fluorescent secondary antibody solutions were prepared in 2.5% (*w/v*) Marvel milk blocking buffer (in TBS-T), according to experimental design. For PVDF membranes, 0.01% SDS was included in the antibody diluent as specified, and all subsequent steps were conducted under low light conditions with incubation containers protected from light (e.g., covered with foil or using a light protective box). Membranes were incubated with fluorescent secondary antibodies for 60 minutes at room temperature in a volume of 10 mL per full membrane. Following incubation, membranes were rinsed twice in TBS-T and washed for 15 minutes, followed by three additional 5-minute washes, protected from light. Membranes were then rinsed in 1× PBS prior to imaging. Fluorescent signals were captured using the LI-COR imaging system (LI-COR Biosciences, Nebraska, USA). As signal intensity is stable under fluorescent detection, short acquisition times (e.g., ~30 seconds) were sufficient for imaging, with channel selection dependent on fluorophore (e.g., 700 nm and/or 800 nm). For two-colour detection, compatible primary antibodies were selected and co-incubated on the same membrane, followed by simultaneous incubation with the appropriate fluorescent secondary antibodies. After imaging, membranes could be air-dried flat and stored dry at 4 °C in the dark for longer term retention.

All incubation trays, forceps, and imaging surfaces were cleaned prior to use to minimise residual dye/background and to maintain imaging consistency.

2.5.7 Densitometry and quantification of western blot signals

Band densitometry was performed on non-saturated images using ImageJ/Fiji software (NIH). Images were converted to 8-bit grayscale before analysis. Under the “Set Measurements” function, grey mean value was selected as the measurement parameter. For each protein of interest, a single rectangular region of interest (ROI) was defined based on the largest band within that row and consistently applied across all lanes to ensure uniform quantification. The same ROI dimensions were used for corresponding loading control bands. For each lane, grey mean values were recorded for both the protein band and an adjacent background region of identical size. To correct for background signal, pixel intensity values were inverted (255 - X) and background subtracted to obtain net band intensity values, as described in the ImageJ quantification protocol. Net protein signal was calculated as: Net band intensity = (Inverted band value − Inverted background value). Similarly, net loading control intensity was calculated for each lane. Target protein expression was then normalised to the corresponding loading control using the following ratio: Normalised expression = Net band intensity / Net loading control intensity. Where indicated, values were expressed relative to the matched control condition (set to 1.0). Quantified data are presented as mean ± standard deviation (SD) from independent biological replicates.

Table 2-4 All the antibodies used in this study

Primary Antibodies	Species	Dilution	Conjugate	Source
hnRNPA3	Rabbit	1:20000	-	Abcam, UK
hnRNPA0	Rabbit	1:10000	-	Abcam, UK
BCL2L11	Rabbit	1:1000	-	Proteintech, UK
Caspase 8	Rabbit	1:1000		Proteintech, UK
Caspase 9	Rabbit	1:1000		Proteintech, UK
Secondary Antibodies				
Anti-mouse	Donkey	1:5000	HRP	Amersham (GE Health Care)
Anti-rabbit	Donkey	1:5000	HRP	Amersham (GE Health Care)
Loading Controls				
GAPDH	Mouse	1:5000	Daylight 680	ThermoFisher, UK
Pan Histone	Mouse	1:5000	-	Merck, UK

2.6 RNA extraction and RNA sequencing

2.6.1 RNA extraction

Total RNA was isolated from AML cell lines following lentiviral-mediated gene modulation using the RNeasy® Plus Mini Kit (QIAGEN), according to the manufacturer's instructions. Briefly, 5×10^5 cells per sample were harvested under logarithmic growth conditions and lysed in Buffer RLT Plus supplemented with β-mercaptoethanol. Genomic DNA was removed using gDNA Eliminator spin columns prior to RNA purification on silica membrane based spin columns. Purified RNA was eluted in RNase free water. RNA concentration and purity were assessed spectrophotometrically using NanoDrop™, and only samples meeting quality requirements were used for downstream applications.

2.6.2 RNA quality control

RNA integrity was assessed using the Agilent 2100 Bioanalyzer (Agilent Technologies) with the Eukaryote Total RNA Nano assay, according to the manufacturer's instructions. This microfluidics based platform enables automated assessment of RNA size distribution, concentration, and integrity.

Electropherograms and gel like images were generated using 2100 Expert software, and RNA integrity was quantified as RNA Integrity Number (RIN) values. All RNA samples selected for sequencing exhibited high integrity (RIN = 10), with clearly resolved 18S and 28S rRNA peaks and minimal degradation. Only samples meeting these quality criteria were used for downstream library preparation and RNA sequencing.

2.6.3 Library preparation and RNA sequencing

Libraries were prepared using poly(A) selection with poly-T magnetic beads, followed by RNA fragmentation and cDNA synthesis according to the provider's standard workflow (Novogene, UK). Libraries underwent end repair, A-tailing, adapter ligation, size selection, PCR amplification and purification prior to sequencing.

2.6.4 Read processing and transcriptomic analysis

Sequencing RNA sequencing data processing and transcriptomic analysis were performed by Novogene using a standard mRNA seq bioinformatics pipeline. Raw sequencing data generated on the Illumina platform were converted to FASTQ files by base calling. Low quality reads and adapter contaminated sequences were removed to generate clean reads for downstream analysis. Clean reads were aligned to the human reference genome (GRCh38, Ensembl release 109) using the splice aware aligner HISAT2 with default parameters. Alignment statistics, including mapping efficiency and read distribution across genomic features, were assessed as part of quality control. Gene level read counts were generated from aligned reads, and transcript abundance was estimated using normalised expression metrics. Sample level quality and reproducibility were evaluated using expression distribution plots, correlation analysis, and principal component analysis. Differential gene expression analysis was performed using count based statistical models. Genes displaying significant expression changes were identified following multiple testing correction. Functional enrichment analysis of differentially expressed genes was subsequently conducted to identify over represented biological processes and pathways associated with hnRNPA0 knockdown. Reads were processed using established bioinformatic pipelines. Reads were aligned to the human reference genome, and gene level expression was quantified. Differential gene expression analysis was performed to identify transcripts significantly altered following hnRNPA0 modulation. Functional enrichment analyses were subsequently conducted to identify biological pathways and processes associated with observed transcriptional changes.

2.7 Data and statistical analysis

2.7.1 Publicly available databases and datasets

2.7.1.1 BloodSpot analysis

mRNA expression data for hnRNP family members were obtained using the BloodSpot database (https://servers.binf.ku.dk/bloodspot/), an online resource that enables interrogation of curated transcriptomic datasets across normal and malignant haematopoiesis (Bagger et al. 2019) Datasets representing normal human haematopoietic differentiation as well as AML patient cohorts, including the *Normal haematopoiesis with AML* dataset (GSE42519) were used(Rapin et al. 2014). Gene expression levels were assessed across defined stages of haematopoietic differentiation to examine dynamic expression trends and lineage specificity. For AML, *hnRNP* expression was compared across disease subtypes to identify genes displaying differential expression relative to normal haematopoietic populations. All expression data were analysed using default BloodSpot settings and corresponding probe sets where applicable.

2.7.1.2 TCGA AML dataset and cBioPortal analysis

hnRNP mRNA expression and associated clinical data from AML patients were further analysed using cBioPortal (https://www.cbioportal.org/), an interactive platform for the exploration of large-scale cancer genomics datasets(Cancer Genome Atlas Research et al. 2013). Analyses were performed using The Cancer Genome Atlas (TCGA) AML cohort which includes genomic and transcriptomic profiling of adult *de novo* AML cases. For survival analyses, patient samples were excluded if they were diagnosed with APL or had not received standard induction therapy. Remaining patients were stratified based on *hnRNP* mRNA expression levels, typically comparing high- and low-expression groups defined by quartile based thresholds. Overall survival and disease-free survival were assessed where applicable. Expression values within cBioPortal are presented as RNA seq RSEM normalised counts.

2.7.2 DepMap dependency analysis

Gene dependency data were interrogated using the Cancer Dependency Map (DepMap) portal (https://depmap.org/portal/), which integrates large scale CRISPR-Cas9 loss of function screening data across a wide panel of cancer cell lines (Dempster et al. 2021). Dependency scores for hnRNP family members were examined across AML cell lines to assess gene essentiality. DepMap dependency scores were interpreted using Chronos gene effect scores, a population dynamics based model that quantifies the impact of gene knockout on cellular fitness while correcting for copy number driven artefacts inherent to CRISPR screening data.

Within this framework, scores approximating zero indicate genes that are not required for cell survival, whereas increasingly negative scores indicate greater dependency, with scores around -1 representing the median dependency of pan-essential genes. Intermediate negative scores therefore reflect context dependent or selective gene essentiality rather than universal requirement. These analyses were used to support candidate selection by identifying hnRNP family members with potential functional relevance in AML cell survival and proliferation.

2.7.3 Statistical considerations

Statistical analysis was performed using a paired sample t-test, or one-way ANOVA with Bonferroni's multiple test correction, unless otherwise stated. Values of $p<0.05$ were considered statistically significant. Data are presented as mean ±1 standard deviation (SD), unless otherwise indicated. The value of *N* represents the number of independent biological replicates, with a minimum of N = 3 performed for all quantitative experiments unless explicitly stated otherwise**.** All statistical analyses were conducted using GraphPad Prism (ver. 9) (GraphPad Software, California, USA). Details regarding the statistical tests used are labelled in figure legends.

3 Expression of hnRNP family members in normal haematopoiesis and AML

3.1 Introduction

A block in haematopoietic differentiation is a hallmark of AML, which is thought to be caused by transcriptional dysregulation of myeloid development. To determine changes in protein expression that may mediate the development block in AML, the AML blast nuclear proteome was previously analysed using iTRAQ MS and compared to normal human cord blood-derived $CD34^+$ haematopoietic stem progenitor cells (Alanazi et al. 2020). Alanazi *et al*. identified 113 significantly changing nuclear proteins in AML. Amongst these were a family of altered proteins, including 13 heterogeneous nuclear ribonucleoproteins (hnRNPs; A0, A1, A2B1, A3, AB, C, D, DL, F, H1 M, R, and UL2).

hnRNPs are RBPs consisting of more than 20 members (Li et al. 2023). hnRNPs are found in the nucleus and play roles in pre-mRNA splicing, mRNA stability, and transcription and translation regulation (Beijer et al. 2021). Their role in diseases, such as cancer, has been previously reviewed by (Liu and Shi 2021). However, in AML, there are a paucity of studies linking the expression and or activity of this family of proteins to leukaemia development. For example, *HNRNPK* is one of six genes found in the minimally deleted region of the genome, which is thought to harbour a haploinsufficient tumour suppressor in patients with AML (Gallardo et al. 2015; Gallardo et al. 2016). Studies focussing on the role of *HNRNPK* in drug resistance in AML have shown that this protein helps form adriamycin resistance during autophagy (Zhang et al. 2016). The expression level of another family member, hnRNPH1, has previously been found to correlate with the progression of CML (Liu et al. 2021). Further, *in vivo* and *in vitro* experiments have shown that hnRNPH1 knockdown inhibits cell proliferation and promotes cellular apoptosis in CML cells (Liu et al. 2021). In terms of affecting haematopoietic differentiation, Young *et al*. examined hnRNPA0 expression in murine haematopoiesis. This protein is normally expressed at a higher level in HSC compared to its expression levels during subsequent stages of murine haematopoietic differentiation (Young et al. 2014). Further, using RNAi interference in primary murine cells, Young *et al*. showed that decreased hnRNPA0 expression causes a shift from monocytic to granulocytic differentiation (Young et al. 2014). However, little is known about the role of many of these *HNRNP* genes in normal haematopoiesis and haematological malignancies, particularly AML.

This chapter establishes the expression of *HNRNP* mRNA family members (identified above) during normal human and murine haematopoiesis. Further, I show whether *HNRNP* family mRNA expression are dysregulated in AML and associated with clinical outcome (OS/DFS). I have prioritised HNRNPs for further study in Chapter 4 based on data from this chapter.

3.1.1 Aim and Objectives

Given that little is known about hnRNP family member expression in normal haematopoiesis and haematological malignancies, especially AML, this Chapter will utilise pre-existing mRNA expression data to determine the expression of *HNRNP* during normal haematopoiesis, in AML, and association with clinical significance. These aims will be achieved through the following objectives:

- **Determine *HNRNP* mRNA expression level during normal haematopoiesis**
  Publicly available transcriptomic datasets will be analysed to determine the mRNA expression of thirteen *HNRNPs* (*A0, A1, A2B1, A3, AB, C, D, DL, F, H1, M, R,* and *UL2*) in normal human and murine myeloid haematopoiesis.

- **Determine which hnRNPs are frequently dysregulated in AML blasts compared to normal human haematopoietic CD34$^+$ cells**
  The most frequent and significantly changing hnRNPs proteins will be identified by reanalysing existing MS iTRAQ data derived by Alanazi *et al.*, 2020. This study compared nuclear proteins from fifteen AML blast samples to five normal human CD34$^+$ HSPC controls. Further, publicly available transcriptomic datasets will be analysed to determine the mRNA expression of thirteen *HNRNP (A0, A1, A2B1, A3, AB, C, D, DL, F, H1, M, R, and UL2*) in HSC compared to AML blasts.

- **Determine whether *HNRNP*s mRNA expression correlates with overall patient survival and other clinical attributes**
  TCGA data set will be analysed to determine the association of human *HNRNP* (*A0, A1, A2B1, A3, AB, C, D, DL, F, H1, M, R, and UL2*) mRNA expression level with patient OS, DFS, and other clinical attributes including WBC and cytogenetics.

- **Determination of hnRNP expression in AML cell lines and whether hnRNP expression is required for cell survival**

  The DepMap portal hosts publicy available data that will be used to analyse *HNRNP* mRNA and hnRNP protein expression levels in twenty-six AML cell lines. I will use this data set (CRISPR/RNAi synthetic lethality screen) to assess whether AML cell survival is enhanced or dependent on hnRNP expression.

3.2 Results

To prioritise which hnRNP proteins to take forward for further study, a series of analyses using pre-existing public data combined with a literature search was performed (**Figure 3-1**).

3.2.1 *HNRNP* expression is downregulated during normal human haematopoietic differentiation

The BloodSpot portal (Bagger et al. 2019) was used to determine the expression of *HNRNP* mRNA during normal haematopoietic development using the human dataset GSE24759 (Novershtern et al. 2011) together and murine dataset GSE6506 (Chambers et al. 2007). I examined 13 *HNRNPs* identified from our quantitative proteomic screen (Alanazi et al. 2020) (**Table 3-1**). In general, expression of each transcript is highest in phenotypically defined haematopoietic stem cells (HSCs) and early multipotent progenitor cells, then declines as differentiation proceeds and cells mature. For example, focussing on the top ranked hnrnp protein from MS (**Table 3-1**), *HNRNPD* mRNA expression in both the human and murine datasets remained statistically unchanged between HSCs and common/granulocyte–monocyte progenitors (CMPs/GMPs) **(Figure 3-2A)**. In the murine dataset, expression of *HNRNPD* rose transiently in GMPs and then declined by 4.3-fold in monocytes and 3-fold in granulocytes, returning to a level comparable with that in HSCs **(Figure 3-2B)**.

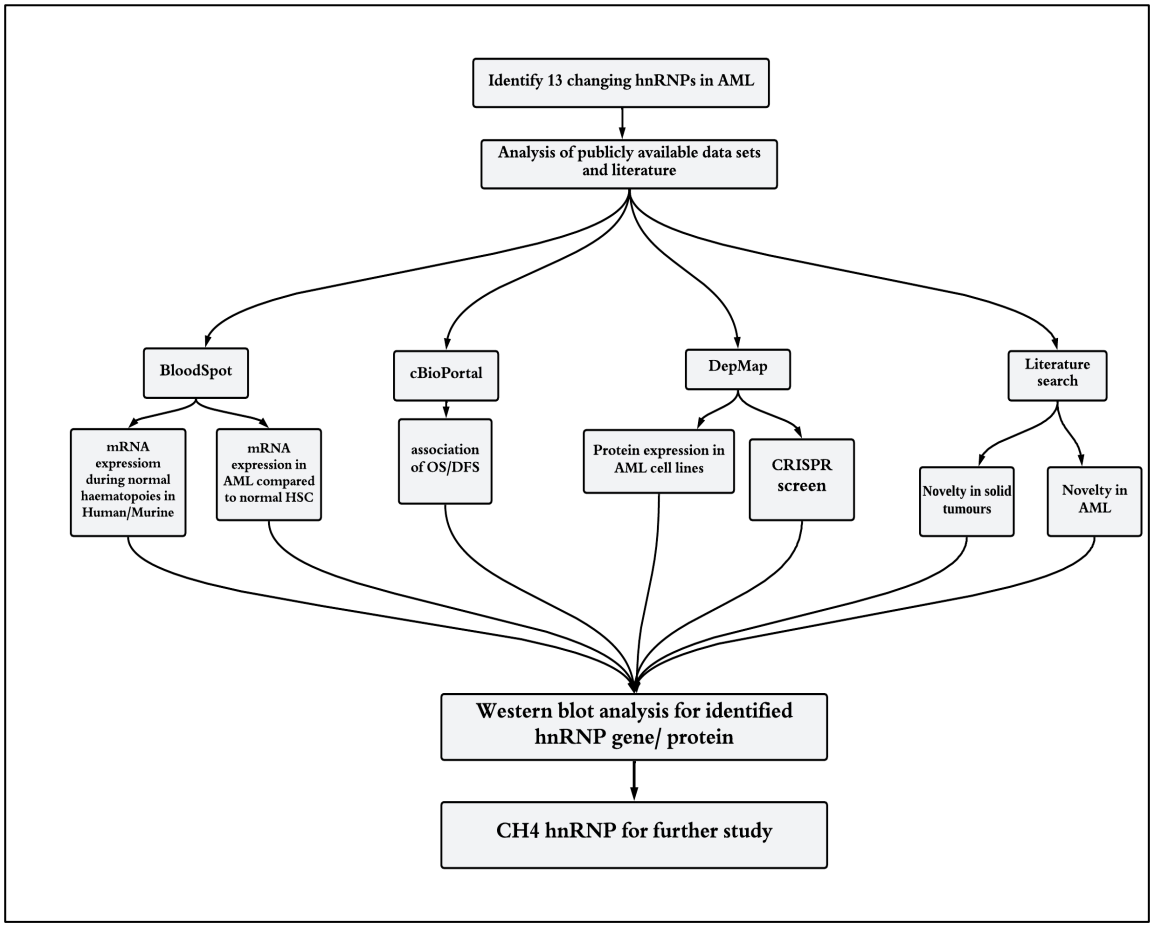

Figure 3-1: Summary workflow of hnRNP analysis

Thirteen significantly changing hnRNP nuclear proteins identified by (Alanazi et al. 2020) in AML compared to normal human $CD34^{+}$ HSPC were analysed according to this workflow (*HNRNPs; A0, A1, A2B1, A3, AB, C, D, DF, F, H1, M, R, and UL2*). Initially, analysis of publicly available mRNA and protein datasets via three analytical platforms (Bloodspot, cBioPortal, DepMap) was performed. Bloodspot was used to analyse the expression of *HNRNPs* mRNA in normal human and murine subsets and the expression of *HNRNPs* mRNA AML subtypes compared to normal HSC. cBioPortal was used in combination with the TCGA dataset to analyse disease-free survival (DFS) and overall survival (OS). DepMap portal was used to study the expression of HNRNPs (mRNA and protein) in AML cell lines using two data sets. It was also used to analyse the dependency of AML cell lines on hnRNP expression. Finally, novelty for further work was established through a literature review**.** Taken together, this approach led to the identification of hnRNPs for further study in Chapter **4**.

A

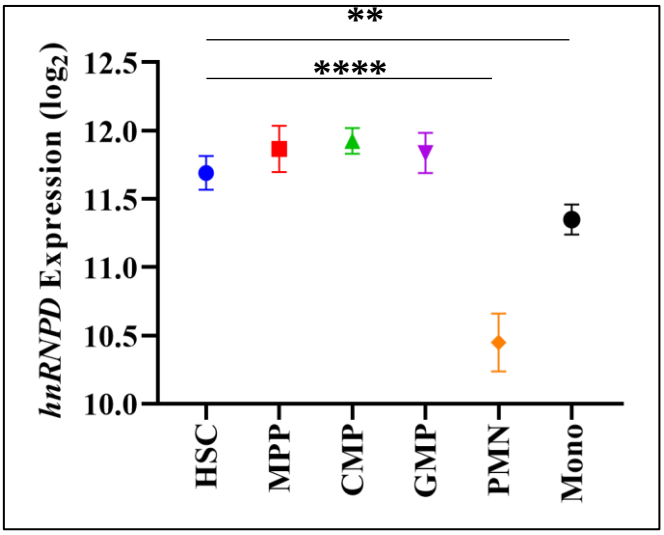

B

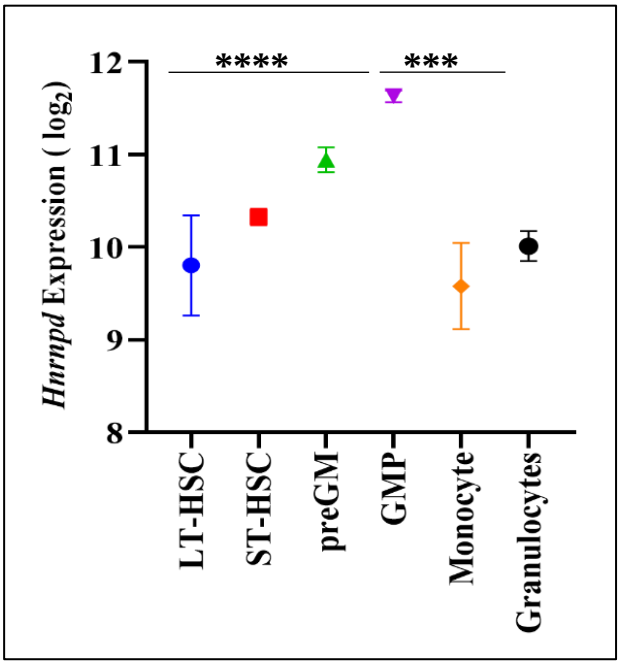

Figure 3-2: *HNRNPD* mRNA expression during normal haematopoietic development

A Microarray data (log_2) showing *HNRNPD* mRNA expression in normal human haematopoietic cells. Probeset (200073_s_at) from **GSE42519** (Rapin et al. 2014) (Svendsen et al. 2016) was used (n=252) (Rapin et al. 2014). **B** Microarray data (log_2) indicates *Hnrnpd* mRNA expression in mouse haematopoietic system cell types. Probeset (1425142_a_at) from **GSE14833** (Di Tullio et al. 2011) and **GSE6506** (Chambers et al. 2007) (Berg et al. 2011) (n=67) (Di Tullio et al. 2011) were used. Data represents mean ± 1SD. Statistical analysis was performed using one-way ANOVA with Tukey's multiple comparisons tests; ** denotes $p<0.01$; *** denotes $p<0.001$; **** denotes $p<0.0001$.

HSC-haematopoietic stem cell, **MPP**-Multipotential progenitors, **CMP**-Common myeloid progenitor cell, **GMP**-Granulocyte monocyte progenitors, **Mono**-Monocytes, **PMN** Polymorphonuclear cells. **LT-HSC**- Long term Haematopoietic stem cell, **ST-HSC**-Short term Haematopoietic stem cell, **Granulocytes**, **preGM**-pre-granulocyte monocyte

The second-ranked MS hit was hnRNPDL. However, due to the unavailability of this gene in the publicly available dataset (Bagger et al. 2019), I analysed the third highest ranked protein, HNRNPAB (**Table 3-2)**. In the human dataset, *HNRNPAB* mRNA expression showed a modest 0.3-fold increase between HSCs and GMPs, followed by a significant 3.7-fold reduction in granulocytes and a 1.3-fold reduction in monocytes compared with HSCs **(Figure 3-3A)**. With murine haematopoiesis, *Hnrnpab* expression showed no significant difference between HSCs and early progenitors, but expression declined upon differentiation, with 3.3-fold and 2.1-fold decreases in monocytes and granulocytes compared to GMPs **(Figure 3-3B)**.

The expression of the other twelve *HNRNP* family members was also assessed. Most genes displayed a similar profile to *HNRNPD,* being highest in stem and progenitor populations and decreasing with differentiation. The combined human and murine data are summarised in **(Table 3-1)** with detailed expression values across haematopoietic subtypes provided in **Appendix**. In both models, the most consistent trend was a progressive decrease in expression once cells committed to the monocyte or polymorphonuclear lineages. members displayed particularly pronounced reductions in expression during myeloid differentiation. For example, HNRNPA0 showed consistently high expression in HSCs and early progenitors, followed by a marked and progressive decline upon commitment to monocytic and polymorphonuclear lineages in both human and murine datasets. Similar trends were observed for other hnRNPs, including HNRNPA1 and HNRNPR, which demonstrated sharp reductions of approximately five- to ten-fold during terminal differentiation. Taken together, all hnRNPs analysed showed reduced expression as cells progressed into monocytic or polymorphonuclear populations, indicating that high hnRNP expression is a defining feature of stem and progenitor states, whereas reduced levels characterise terminally differentiated myeloid cells.

3.2.1 Expression of several hnRNPs are dysregulated in AML

Alanazi *et al.* identified 13 significantly changing hnRNP nuclear proteins in AML compared to normal human $CD34^+$ HSPC (Alanazi et al. 2020). To expand on this, I re-analysed the dataset to consider fold change and frequency of change amongst 15 AML patient blasts analysed compared to 5 normal human $CD34^+$ cells. As shown in (**Table 3-2**), all hnRNPs proteins were downregulated compared to normal human $CD34^+$ cells. The most frequent significant changes were observed in hnRNPD and hnRNPDL (10/15 and 11/15, respectively), while hnRNPF showed the lowest frequency of alteration (6/15). Median fold changes ranged from (2.8-fold) for hnRNPF to (4.0) for hnRNPAB

A

B

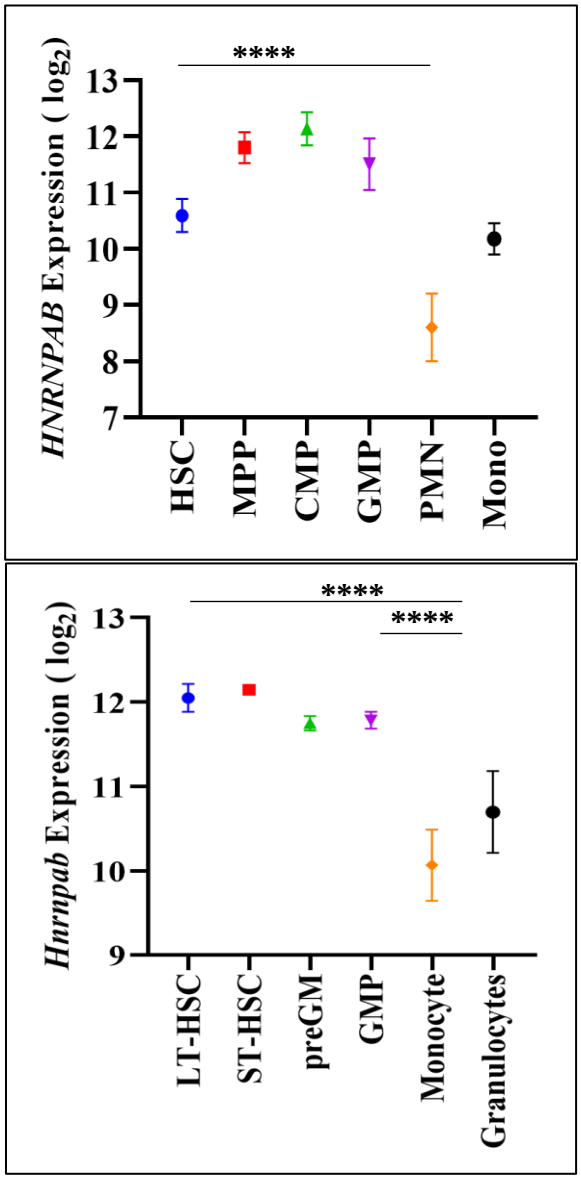

Figure 3-3 : *HNRNPAB* mRNA expression during normal haematopoietic development

A Microarray data (log_2) showing *HNRNPAB* mRNA expression in normal human haematopoietic cells. Probeset (201277_s_at) from **GSE42519** (Rapin et al. 2014) (Svendsen et al. 2016) was used (n=252) (Rapin et al. 2014). **B** Microarray data (log_2) indicates *Hnrnpab* mRNA expression in mouse haematopoietic system cell types. Probeset (1415914 _at) from **GSE14833** (Di Tullio et al. 2011) and **GSE6506** (Chambers et al. 2007) (Berg et al. 2011) (n=67) (Di Tullio et al. 2011) were used. Data represents mean ± 1SD. Statistical analysis was performed using one-way ANOVA with Tukey's multiple comparisons tests; ** denotes p<0.01; *** denotes p<0.001; **** denotes p<0.0001.

HSC-haematopoietic stem cell, **MPP**-Multipotential progenitors, **CMP**-Common myeloid progenitor cell, **GMP**-Granulocyte monocyte progenitors, **Mono**-Monocytes, **PMN** Polymorphonuclear cells. **LT-HSC**- Long term haematopoietic stem cell, **ST-HSC**-Short term haematopoietic stem cell, **Granulocytes**, **preGM**-pre-granulocyte monocyte.

	Human				Mouse							
	HSC vs Mono		HSC Vs PMN		LT-HSC vs Mono		LT-HSC vs Granulocyte		GMP vs Mono		GMP vs Granulocyte	
Gene¥	**Fold change†**	**P-Value**	**Fold change‡**	**P-Value**	**Fold change⁺**	**P-Value**	**Fold change‡**	**P-Value**	**Fold change˙**	**P-Value**	**Fold change˙**	**P-Value**
HNRNPA0	2.30	p<0.001	6.50	p<0.0001	3.25	p<0.0001	2.14	p<0.001	6.50	p<0.0001	4.29	p<0.0001
HNRNPA1	1.32	p<0.01	9.85	p<0.0001	4.59	p<0.0001	5.28	p<0.0001	2.30	p<0.001	2.64	p<0.001
HNRNPA2B1	1.07	NS	1.74	p<0.0001	2.64	p<0.0001	1.52	NS	2.64	p<0.0001	1.52	NS
HNRNPA3	2	p<0.001	2.30	p<0.001	2.46	NS	1.32	NS	4.59	p<0.0001	2.46	p<0.001
HNRNPAB	1.32	NS	3.73	p<0.0001	4	p<0.0001	2.64	p<0.001	3.25	p<0.0001	2.14	p<0.001
HNRNPC	1.07	NS	0.81	NS	1.15	NS	1.41	p<0.01	1.23	NS	1.52	p<0.01
HNRNPD	1.23	p<0.01	2.30	p<0.0001	1.23	NS	0.87	NS	4.29	p<0.001	3.03	p<0.001
HNRNPF	0.5	p<0.001	0.5	NS	1.52	NS	0.87	NS	0.38	NS	0.22	p<0.01
HNRNPH1	1.74	p<0.01	2.83	p<0.0001	2	NS	2.83	p<0.01	1.52	NS	2.14	NS
HNRNPM	1.52	NS	2.46	p<0.001	1.74	NS	0.87	NS	1.87	NS	0.93	NS
HNRNPR	1.74	p<0.01	5.28	p<0.0001	4	p<0.0001	3.23	p<0.0001	6.96	p<0.0001	5.62	p<0.0001
HNRNPUL2	1.41	NS	1.62	NS	0.93	NS	0.87	NS	1.15	NS	1.07	NS

Table 3-1: Changes in *HNRNP* mRNA expression in human and mouse haematopoietic cells as they differentiate into monocytes and PMNs

† Average fold change of *HNRNP* mRNA expression in human HSC versus terminally differentiated monocytes. ‡ Average fold change of *HNRNP* mRNA expression in human HSC versus terminally differentiated polymorphonuclear cells. ⁺ Average fold change of *Hnrnp* mRNA expression in mouse LT-HSC versus terminally differentiated monocytes. ‡ Average fold change of *Hnrnp* mRNA expression in mouse LT-HSC versus terminally differentiated granulocyte. ˙ Average fold change of *Hnrnp* mRNA expression in mouse GMP versus terminally differentiated in monocyte. ˙ Average fold change of *Hnrnp* mRNA expression in mouse GMP versus terminally differentiated granulocyte. Statistical analysis was performed using one-way ANOVA with Tukey's multiple comparisons tests; ** denotes p<0.01*;* *** denotes p<0.001,**** denotes p<0.0001. NS indicates not significant. ¥ Probeset ID for each gene can be found in (**Appendix**).

Protein	Frequency†	Fold Change‡	Ranking#
hnRNPD	66% (10/15)	-3.8	2.51
hnRNPDL	73% (11/15)	-3.3	2.41
hnRNPAB	60% (9/15)	-4.0	2.40
hnRNPR	60% (9/15)	-3.3	1.98
hnRNPA2B1	60% (9/15)	-3.1	1.86
hnRNPC	60% (9/15)	-3.1	1.86
hnRNPA1	53% (8/15)	-3.4	1.80
hnRNPA0	60% (9/15)	-3.0	1.80
hnRNPA3	53% (8/15)	-3.1	1.64
hnRNPUL2	53% (8/15)	-2.9	1.54
hnRNPH1	46% (7/15)	-2.9	1.33
hnRNPM	46% (7/15)	-2.9	1.33
hnRNPF	40% (6/15)	-2.8	1.12

Table 3-2: hnRNPs are downregulated in AML patient blasts compared to normal human CD34$^+$ cells

Proteomic MS data were obtained from (Alanazi et al. 2020). In this study, iTRAQ proteomics was used to quantify the relative changes in nuclear protein expression of hnRNP in 15 AML blast samples compared to 5 normal CD34$^+$ cord blood-derived HSPC. † Frequency represents the proportion of AML patient samples showing statistically significant downregulation (for example, 10 out of 15 samples = 0.66). ‡ Fold change was calculated by comparing the expression level in AML to normal human CD34$^+$ cells. The negative sign indicates downregulation in AML compared to normal. # A ranking score was calculated by multiplying the proportion of affected patient samples by the absolute fold-change. Proteins were ranked from highest to lowest based on this score.

.

Thus, hnRNPF displayed the smallest reduction, both in magnitude and in frequency, whereas hnRNPAB showed the strongest decrease compared to control. To prioritise these findings, proteins were ranked according to a combined score based on fold change and frequency. Using this approach, hnRNPD, hnRNPDL and hnRNPAB emerged as the three most consistently altered proteins, each with a product score exceeding 2.4 (**Table 3-2**).

To support the protein changes observed above (**Table 3-2**) I next determined the mRNA expression level of *HNRNPs* in AML compared to normal human HSC using publicly available transcriptomic datasets coupled with Bloodspot (Bagger et al. 2019). I initially analysed *HNRNPD and HNRNPAB* mRNA expression levels. The percentage of AML patients with lower *HNRNPD* and *AB* expression compared to HSC was 42% and 2%, respectively **(Figure 3-4** and **Figure 3-5** respectively**)**.

When stratified by cytogenetic subtype *HNRNPD* expression showed a broadly reduced expression level across most groups, with the strongest downregulation observed in complex karyotype and t(11q23)/KMT2A cases, and comparatively milder changes in inv(16) and t(15;17) **(Figure 3-4).** In contrast, *HNRNPAB* expression remained largely stable across subtypes, with only a minority of patients in the complex and t(11q23)/KMT2A groups showing values below the normal HSC range **(Figure 3-5)**. These findings suggest that while *HNRNPD* downregulation is a common feature across AML subtypes, *HNRNPAB* expression is largely preserved.

Notably, this mRNA expression pattern represents a direct contradiction to the proteomic data, in which HNRNPAB protein levels were among the most strongly reduced in AML patient blasts (**Table 3-2**). This discordance between mRNA and protein expression suggests that post transcriptional regulatory mechanisms may play an important role in regulating HNRNPAB protein abundance in AML, potentially involving altered translational efficiency, protein stability, or degradation.

A summary of downregulation across the *hnRNP* family at the mRNA level is presented in **(Table 3-5)**, which supports the overall conclusion that hnRNP expression is frequently decreased in AML compared with normal HSC, with the magnitude of change varying between family members and AML subtypes.

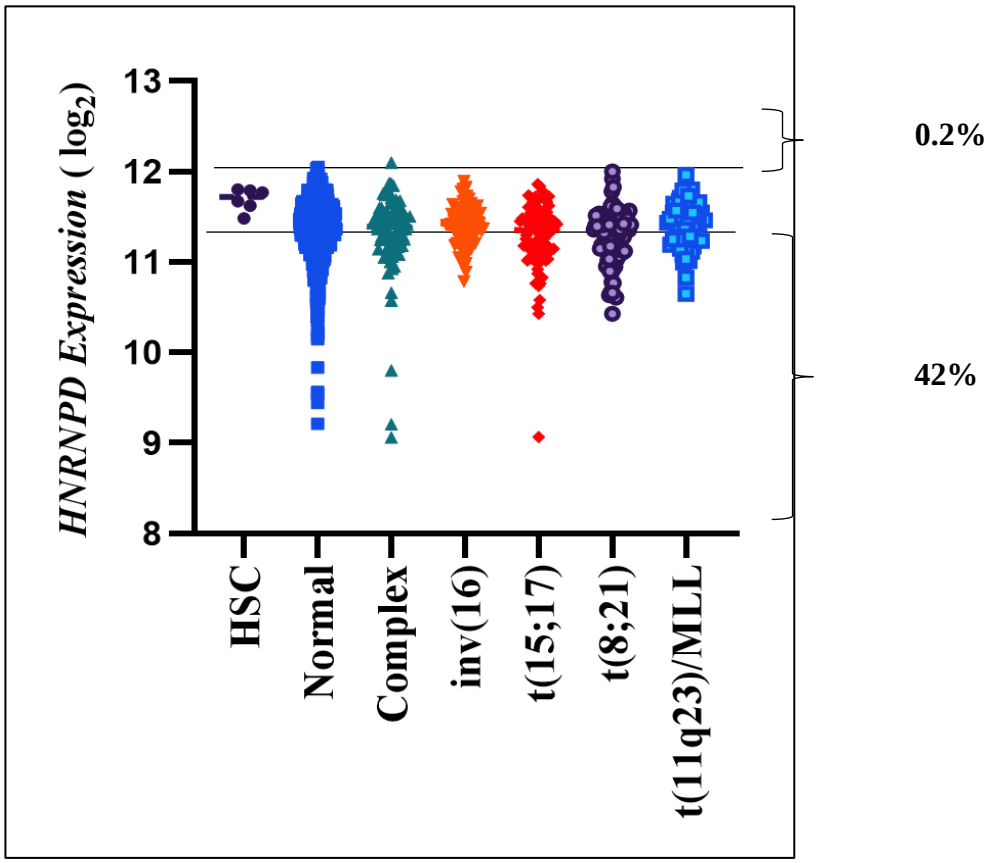

Figure 3-4: Expression of *HNRNPD* mRNA in AML compared to normal human HSC

Expression of *HNRNPD* mRNA in AML subtypes compared to normal human HSC. Probeset 200073_s_at was used for analysis from Human Normal Haematopoiesis (**GSE42519**) and AML blasts (**GSE13159**) (Kohlmann et al. 2008; Haferlach et al. 2010), (**GSE15434**) (Klein et al. 2009), (**GSE61804**) (Metzelder et al. 2015), GSE14468 (Wouters et al. 2009; Taskesen et al. 2011), The Cancer Genome Atlas (TCGA) (Bagger et al. 2019)(**n=251**) (Kohlmann et al. 2008). Data represents mean ± 2 SD. Statistical analysis was performed using one-way ANOVA with Tukey's multiple comparisons test to HSC. The horizontal line indicates the number of patients that fall outside the 95% confidence level (mean ± 2 SD) of the normal distribution in normal HSC. The percentage of patients down or up-regulated in AML compared to HSC is shown.

HSC = haematopoietic stem cell, **Normal** =AML with normal karyotype, **Complex** = AML with complex karyotype, **inv (16**) = AML with inv (16), **t (15;17)** = AML with t (15;17), **t (8;21)** AML with t(8;21), **t(11q23)/MLL (aka KMT2A)** = AML with t(11q23)/MLL.

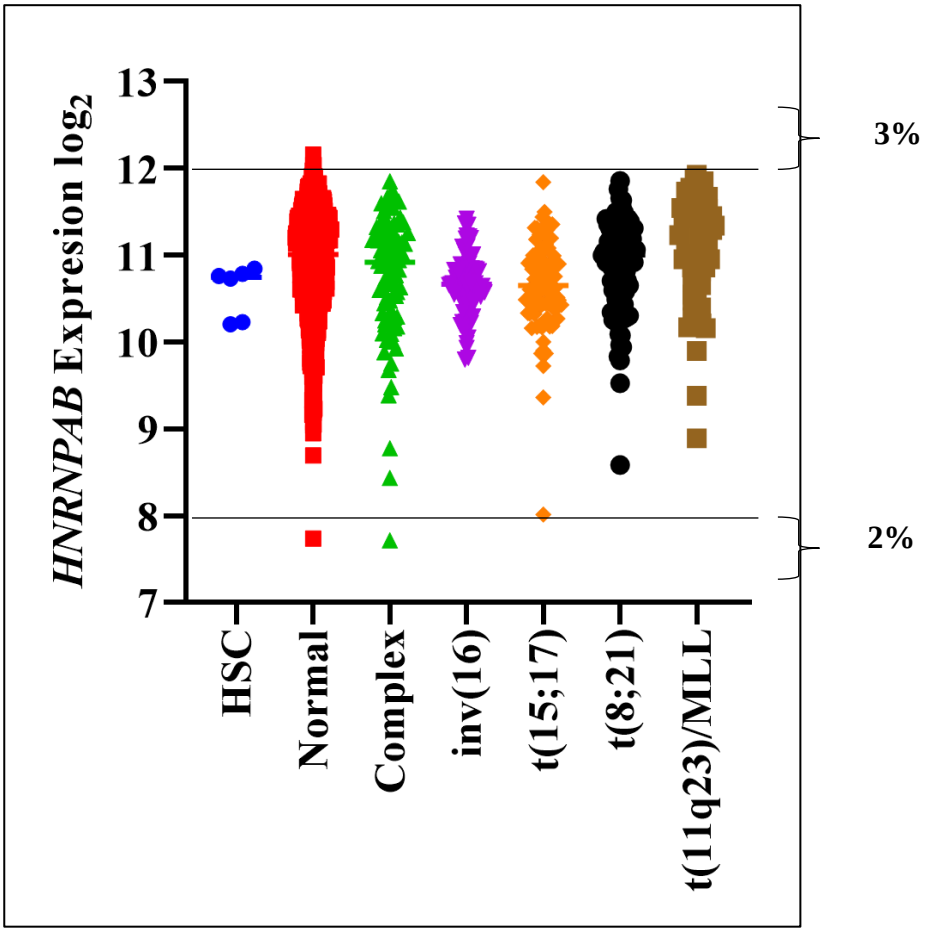

Figure 3-5: Expression of *HNRNPAB* in AML compared to normal human HSC

Expression of *HNRNPAB* mRNA in AML subtypes compared to normal human HSC. Probeset 201277_s_at was used for analysis from Human Normal Haematopoiesis (**GSE42519**) and AML blasts (**GSE13159**) (Kohlmann et al. 2008; Haferlach et al. 2010), (**GSE15434**) (Klein et al. 2009), (**GSE61804**) (Metzelder et al. 2015), GSE14468 (Wouters et al. 2009; Taskesen et al. 2011), The Cancer Genome Atlas (TCGA) (Bagger et al. 2019)(**n=251**) (Kohlmann et al. 2008). Data represents mean ± 2 SD. Statistical analysis was performed using one-way ANOVA with Tukey's multiple comparisons test to HSC. Horizontal lines indicate the normal HSC expression range defined as mean ± 2 SD, reflecting biological variability within the control population rather than a confidence interval of the mean. The percentage of AML patients with HNRNPAB expression falling above or below this normal HSC range is shown.

HSC = haematopoietic stem cell, **Normal** =AML with normal karyotype, **Complex** = AML with complex karyotype, **inv (16)** = AML with inv (16), **t (15;17)** = AML with t (15;17), **t(8;21)** AML with t(8;21), **t(11q23)/MLL** = AML with t(11q23)/MLL.

3.2.2 Higher levels of *HNRNPA2B1 or A3* mRNA expression are associated with poorer patient overall survival

To further explore the relationship between *HNRNPs* mRNA expression and clinical outcome in AML, I analysed the TCGA dataset using cBioPortal (Cerami et al. 2012) to generate Kaplan–Meier survival curves for patients using upper and lower quartiles of mRNA expression. Each group contained approximately 30–31 cases per gene Patients diagnosed with APL and those lacking complete clinical annotation were excluded from survival analysis. As shown in (**Figure 3-6** and **Figure 3-7)**, no significant associations were observed between *HNRNPD or HNRNPAB* mRNA expression with overall survival (OS) or disease-free survival (DFS). Similar results were obtained for the majority of other *HNRNPs* family members (*A0, A1, A2B1, A3, C, DL, F, H1, M, R,* and *UL2*).

In contrast, high expression of *HNRNPA2B1* and *HNRNPA3* was significantly associated with poor OS **(Figure 3-8** and **Figure 3-9** respectively**).** Patients in the high-expression quartile for either gene had a shorter median OS compared with the low-expression group, while DFS was not significantly affected. The survival difference approached one year in both cases, underscoring potential clinical relevance. Importantly, expression levels of *HNRNPA2B1* and *HNRNPA3* did not correlate with other clinical variables, including WBC, cytogenetic, molecular risk group, tumour histological subtype, fraction of altered genome, peripheral blood blast percentage, or age at diagnosis. This suggests that their adverse effect on OS may represent an independent prognostic feature rather than reflecting established risk categories.

3.2.3 mRNA and protein expression in AML cell lines

To investigate hnRNP expression in AML cell lines, I analysed publicly available transcriptomic and proteomic datasets from the DepMap portal. The mRNA compendium encompassed forty-four AML cell lines, while quantitative MS data were available for a subset of fourteen lines.

As shown in **Figure 3-10A** *HNRNP* mRNA was abundantly expressed across cell lines, with mean transcript values of 8.5, 8.2, and 7.5 TPM for *HNRNPD, HNRNPDL,* and *HNRNPAB,* respectively. Among all family members, *HNRNPA1* displayed the highest transcript levels, whereas *HNRNPA0 and* HNRNPUL2 were the lowest. Variability between cell lines was limited, suggesting relatively stable basal expression.

A

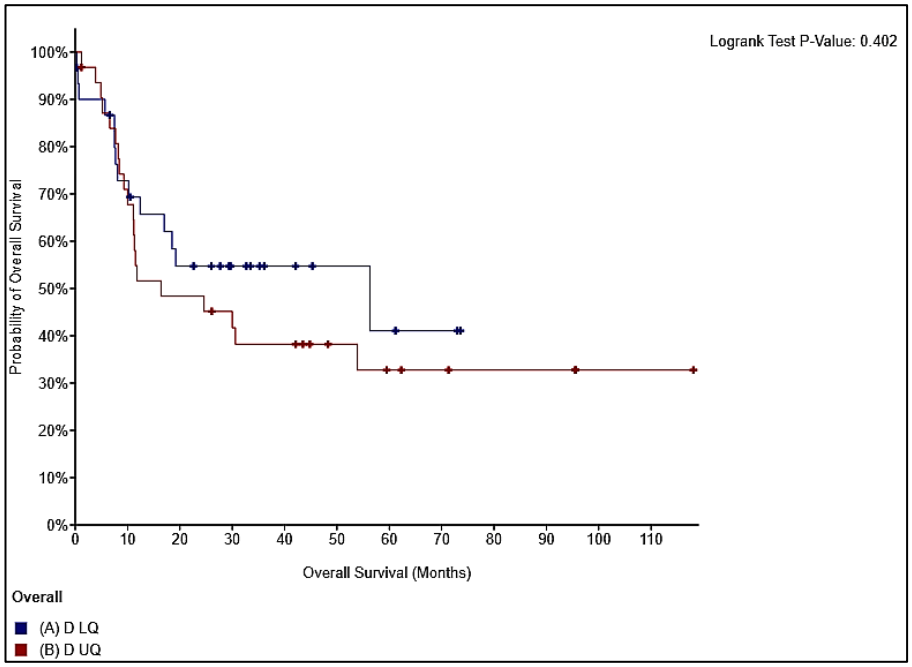

B

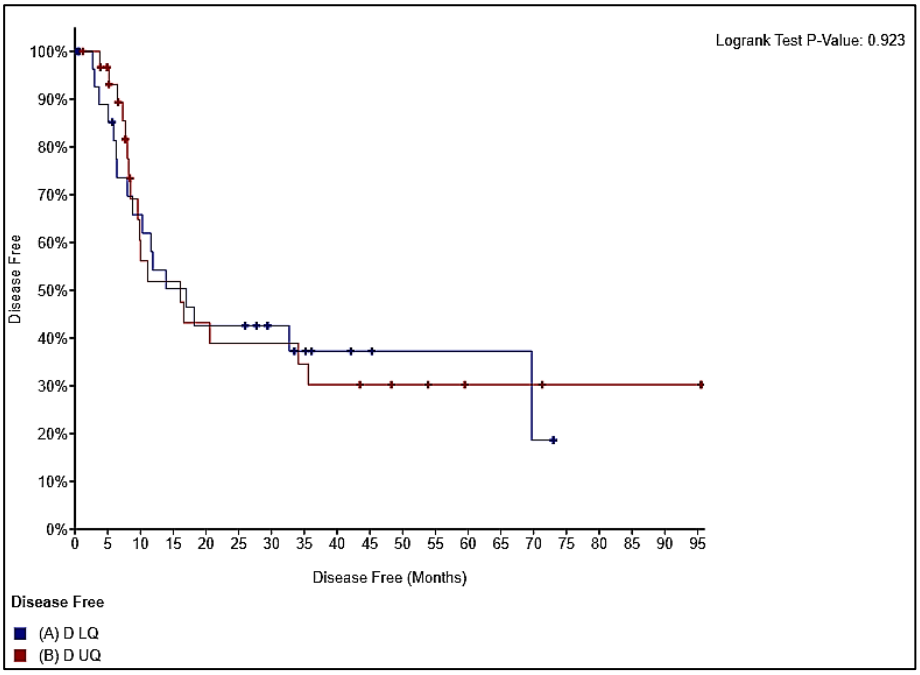

Figure 3-6: *HNRNPD* mRNA expression does not associate with OS and DFS

Kaplan-Meier survival curves for AML patients stratified according to upper quartile (UQ) and lower quartile (LQ) expression for *HNRNPD* mRNA expression. Data were obtained from TCGA (Cancer Genome Atlas Research et al. 2013) using cBioportal (www.cbioportal.org). LQ (**n=30**); and UQ (**n=31**) (**A)** Overall survival (**B)** Disease-free survival. Statistical significance for OS and DFS was calculated using the Log-Rank test. blue: LQ, Red: UQ.

A

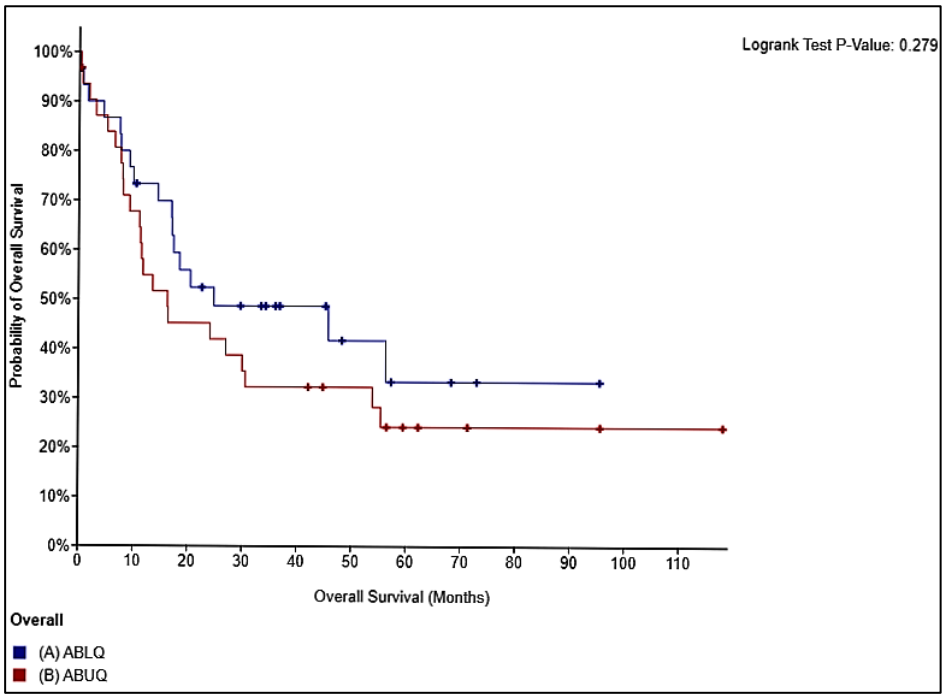

B

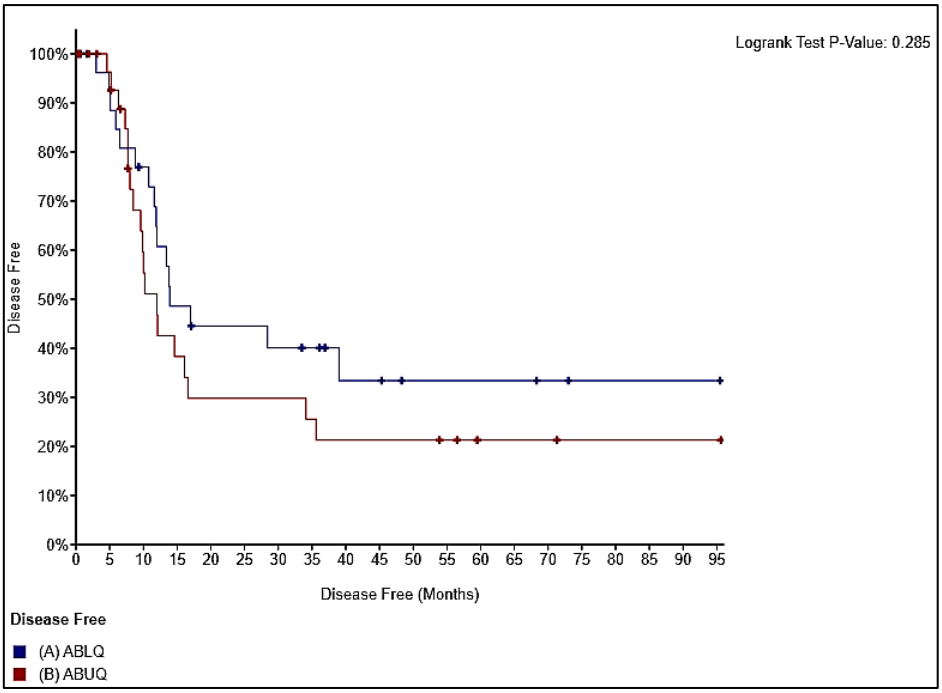

Figure 3-7: Low level of *HNRNPAB* is not associated with poor OS/ DFS

Kaplan-Meier survival curves for AML patients stratified according to upper quartile (UQ) and lower quartile (LQ) expression for *HNRNPAB* mRNA expression. Data were obtained from TCGA (Cancer Genome Atlas Research et al. 2013) using cBioportal (www.cbioportal.org). LQ (**n=30**); and UQ (**n=31**) (**A)** Overall survival (**B)** Disease-free survival. Statistical significance for OS and DFS was calculated using the Log-Rank test. blue: LQ, Red: UQ.

A

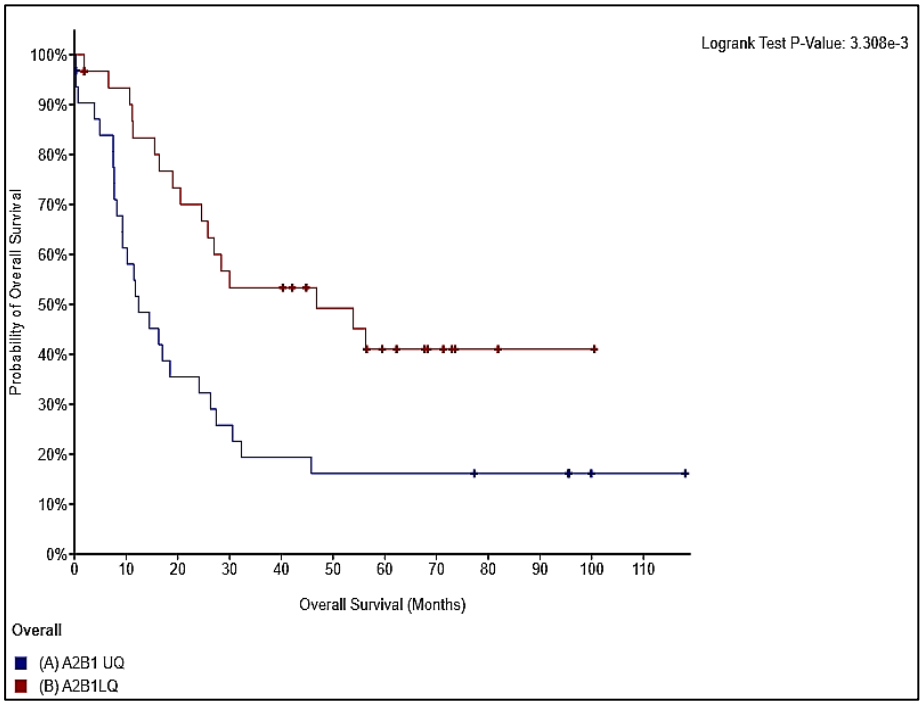

B

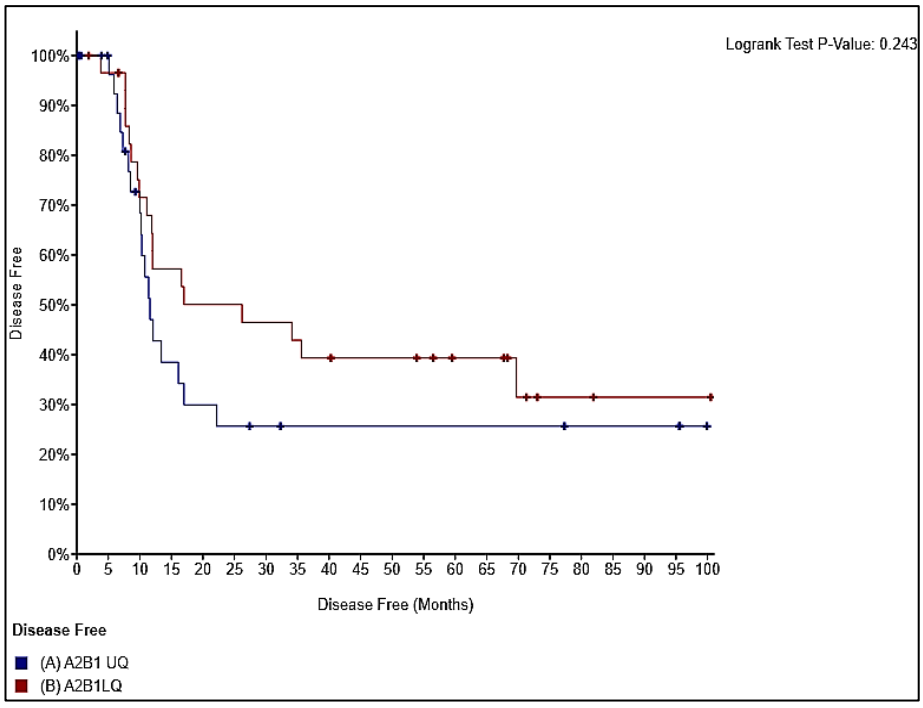

Figure 3-8: High level of *HNRNPA2B1* associated with poorer OS

Kaplan-Meier survival curves for AML patients stratified according to upper quartile (UQ) and lower quartile (LQ) expression for *HNRNPA2B1* mRNA expression. Data were obtained from TCGA (Cancer Genome Atlas Research et al. 2013) using cBioportal (www.cbioportal.org). LQ (**n=30**); and UQ (**n=31**) (**A)** Overall survival (**B)** Disease-free survival. Statistical significance for OS and DFS was calculated using the Log-Rank test. blue: LQ, Red: UQ.

A

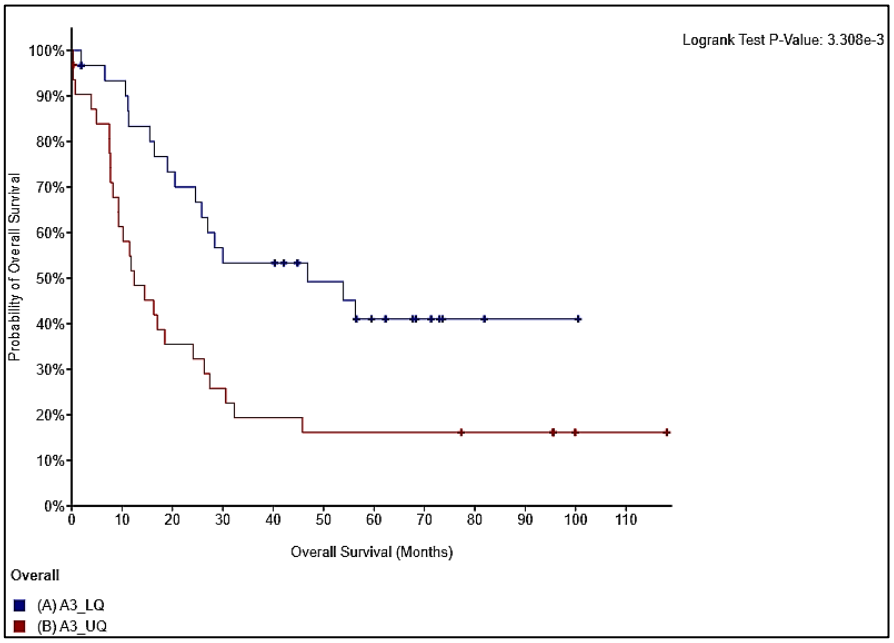

B

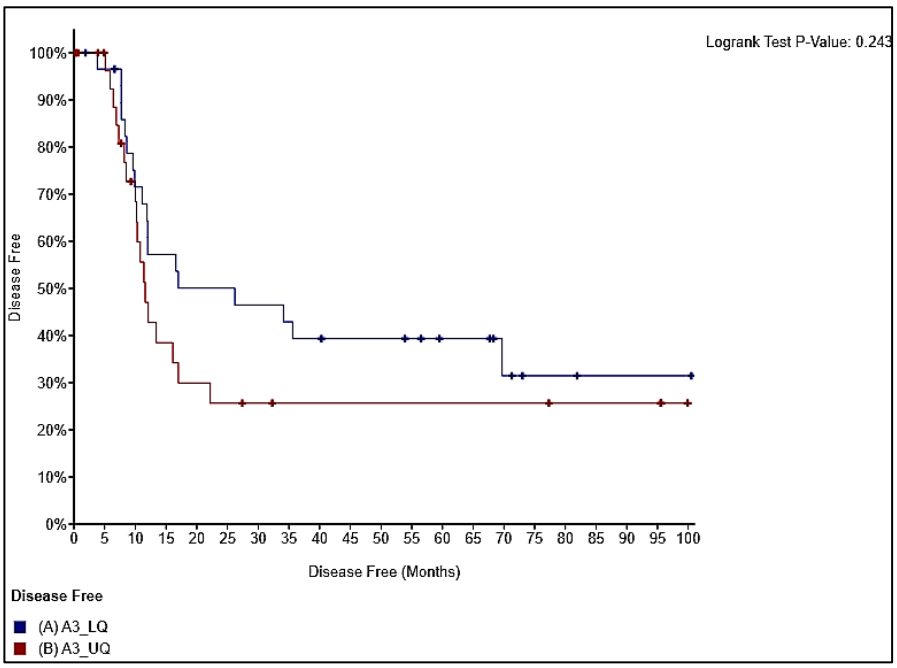

Figure 3-9: High level of *HNRNPA3* associated with poorer OS

Kaplan-Meier survival curves for AML patients stratified according to upper quartile (UQ) and lower quartile (LQ) expression for *HNRNPA3* mRNA expression. Data were obtained from TCGA (Cancer Genome Atlas Research et al. 2013) using cBioportal (www.cbioportal.org). LQ (**n=30**); and UQ (**n=31**) (**A)** Overall survival (**B)** Disease-free survival. Statistical significance for OS and DFS was calculated using the Log-Rank test. blue: LQ, Red: UQ.

.

Protein profiling by MS (**Figure 3-10B**) detected multiple hnRNP isoforms in AML cell lines. HNRNPD was detected as two isoforms, both showing moderate relative protein expression across models. HNRNPAB was expressed at lower levels, while HNRNPDL was comparatively the least abundant. Overall, protein expression profiles broadly mirrored mRNA patterns, although some divergence was observed, consistent with post-transcriptional regulation.

Taken together, these data indicate that hnRNP gene and protein expression is consistently detectable in AML cell lines, but the relative abundance differs between family members and isoforms. The presence of substantial HNRNPD and HNRNPAB transcripts and proteins across models suggests that these factors are well represented in AML biology, whereas HNRNPDL is comparatively less abundant at the protein level.

A

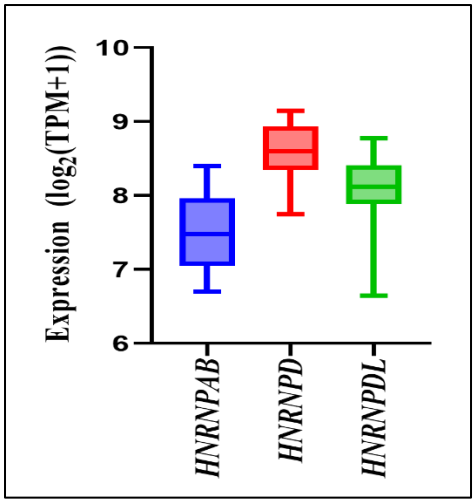

B

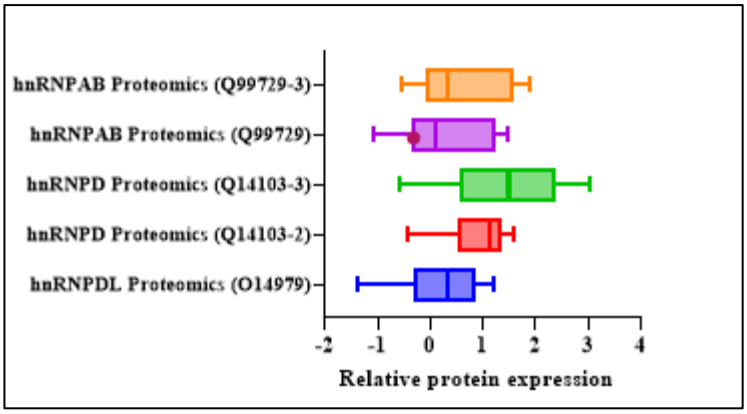

Figure 3-10: Expression of mRNA and protein for hnRNPs across AML cell lines

(A) mRNA expression of hnRNP genes in AML cell lines (n = 44), obtained from the Broad Institute's Cancer Dependency Map (DepMap, 22Q1 public dataset; https://depmap.org/portal) (Barretina et al. 2012). Expression values are presented as $\log_2$[transcripts per million (TPM) + 1]. and displayed as boxplots (median with interquartile range; whiskers represent minimum and maximum values**).**

(B) Relative protein expression of hnRNPs in AML cell lines (n = 14), determined by mass spectrometry through the DepMap proteomics dataset. Protein abundance values are log2-normalised and expressed relative to the median protein abundance across all analysed cell lines, where values above zero indicate higher than median expression and values below zero indicate lower than median expression.Data are displayed as boxplots (median with interquartile range; whiskers represent minimum and maximum values

3.2.4 AML cells do not require hnRNP expression for cell survival

CRISPR/Cas9-mediated viability screens provide a systematic means of identifying essential genes for cell survival in cancer cell lines (Collonnier et al. 2017). To determine whether AML cell lines depend on hnRNP expression for survival, I analysed genome-scale CRISPR screen data available through the DepMap portal (Dempster et al. 2021). Gene dependency is measured using the Chronos score, where a value of 0 indicates non-essentiality, –1 approximates the median of all pan-essential genes, and scores below –0.5 are considered to reflect a significant effect on viability.

As shown in (**Figure 3-11**), knockout of most hnRNPs analysed exerted little or no effect on the survival of 26 AML cell lines analysed. (**Table 3-3),** summarises the proportion of cell lines displaying dependency on each hnRNP. No gene displayed positive Chronos scores, indicating that hnRNP loss did not enhance survival in any model. Among the family members, hnRNPA0, hnRNPD, and hnRNPF fell below the –0.5 threshold in a minority of lines (≤20%), suggesting context-dependent vulnerability.

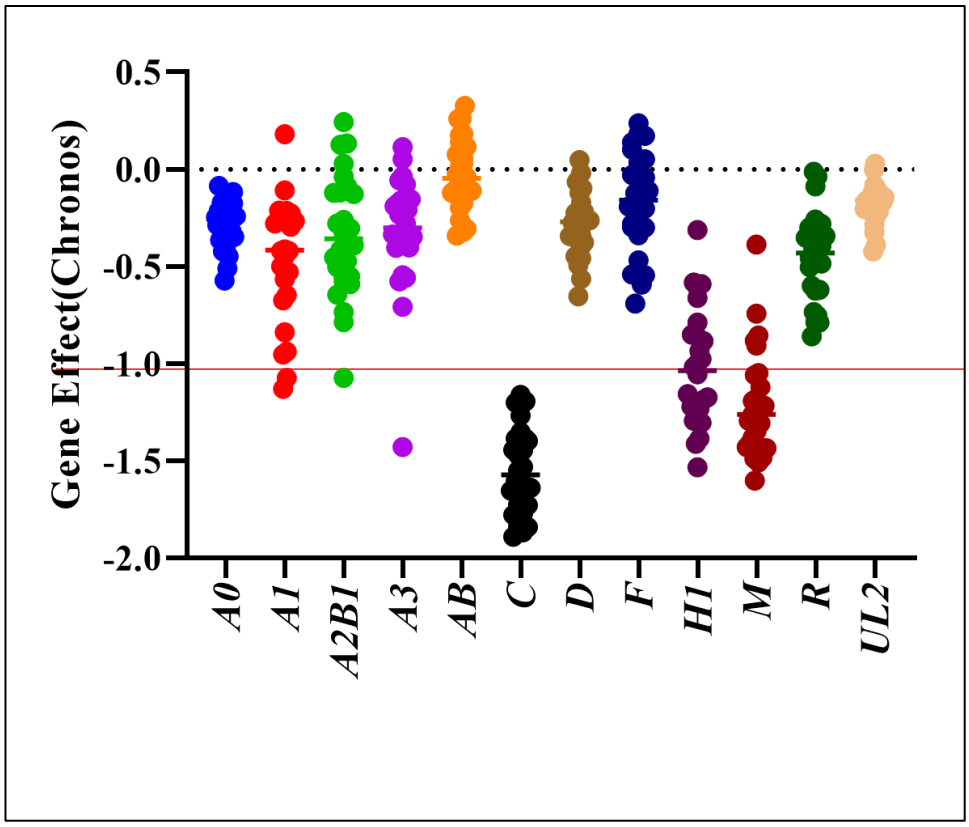

Figure 3-11: Lack of significant dependency of hnRNP expression in AML cell lines

CRISPRCas9 'dependency' data were analysed using the DepMap portal. Lower Chronos scores indicate greater dependency of the cell line on a given gene for survival. A score of **0** represents a non-essential gene, whereas a score of **–1** corresponds to the median of all common essential genes(Meyers et al. 2017) (McFarland et al. 2018).Each dot represents an individual AML cell line (n = 26).

	Gene effect (Chronos)		
Protein	**Poor survival (-0.5 to -1)**	**Poor survival (exceeded -1)**	**Enhanced survival**
HNRNPA0	(2/26) 7.7%	-	-
HNRNPA1	(8/26) 30.8%	(2/26) 7.7%	-
HNRNPA2B1	(8/26) 30.8%	(1/26) 3.8%	-
HNRNPA3	(4/26) 15.4%	(1/26) 3.8%	-
HNRNPAB	-	-	-
HNRNPC	-	(26/26) 100%	-
HNRNPD	(2/26) 7.7%	-	-
HNRNPDL	-	-	-
HNRNPF	(5/26) 19.2%	-	-
HNRNPH1	(11/26) 42.3%	(14/26) 53.8%	-
HNRNPM	(4/26) 15.4%	(21/26) 80.8%	-
HNRNPR	(9/26) 34.6%	-	-
HNRNPUL2	-	-	-

Table 3-3: Proportion of AML cell lines dependent on hnRNP gene expression for survival

The proportion of AML cell lines reliant on hnRNP expression was determined using the DepMap 22Q1 dataset (Barretina et al. 2012). CRISPRCas9 knockout screens in 26 AML lines were analysed, and dependency was classified by Chronos scores as follows: *moderate (–0.5 to –1), strong (< –1), or enhanced survival (> +0.5).* Percentages indicate the proportion of AML cell lines falling into each category.

The A/B subfamily (hnRNPA1, hnRNPA2B1, hnRNPA3) showed modest dependency in ~30% of models, but only a small fraction (<10%) exceeded the "–1" threshold, indicating partial redundancy. By contrast, three hnRNPs displayed stronger effects: hnRNPC knockout reduced viability across all AML cell lines (median Chronos ≈ –1.3), while hnRNPH1 and hnRNPM exceeded the –1 threshold in 54% and 81% of lines, respectively.

Taken together, these data suggest that while most hnRNPs are dispensable for AML cell line survival, hnRNPC, hnRNPH1, and hnRNPM represent stronger dependencies. Overall, suppression of hnRNPs does not appear to affect cell survival, but selected family members may play more critical roles.

3.2.5 Literature search: hnRNP role in AML or solid tumours

To clarify hnRNP involvement in AML and in solid tumours, I conducted a focused literature review. The findings, grouped by individual family members, are summarised in **Table 3-4**. Two consistent themes emerge:

1. hnRNP dosage is highly context-dependent, with individual paralogues acting as either oncogenes or tumour suppressors depending on tissue type and mutational background.
2. Aberrant splicing, RNA stabilisation, and RNA modifications such as m^6A methylation represent key mechanisms through which hnRNPs contribute to cancer biology.

hnRNPA0 is dynamically regulated during normal haematopoietic differentiation. Knockdown in murine BM promotes granulocytic maturation, whereas enforced expression blocks differentiation, highlighting a dosage-sensitive role in lineage specification. In AML, hnRNPA0 mRNA and protein are elevated in specific subclasses compared with normal $CD34^+$ stem/progenitor cells (Konig et al. 2016), However, the precise lineage context in which hnRNPA0 exerts these effects in AML remains incompletely defined. Notably, previous reports associating higher hnRNPA0 transcript levels with inferior overall survival in TCGA-LAML and Beat-AML cohorts contrast with the findings of the current analysis, in which hnRNPA0 expression is not uniformly elevated across AML subtypes. This apparent discrepancy highlights the context dependent nature of hnRNPA0 regulation and will be discussed in detail in the Discussion section.

Table 3-4: Summary literature search of hnRNP known role in cancer development

Protein	Literature in Blood cancer†	Literature in solid tumour cancer‡	Literature in AML‡	Reported roles in haematological malignancies †	References†
hnRNPA0	N	Y	Y	HNRNPA0 expression in haematopoietic stem cells is normally high and changes dynamically during differentiation. Discovered that decreased HNRNPA0 expression leads to a shift from monocytic to granulocytic differentiation using RNAi interference in primary murine cells and an experimental cell system.	(Young et al. 2014)
hnRNPA1	Y	Y	Y	qPCR was measured mRNA expression of 7 splicing factors belonging to the serine/arginine-rich (SR) protein family, HNRNPA1, in peripheral blood mononuclear cells of 26 patients with newly diagnosed AML and 26 healthy controls. The expression in SRSF7 and HNRNPA1 is higher in AML patients. Taken together, these results strongly suggest that the aberrant expression of factors SRSF1, HNRNPA1, and SRSF3 may be closely related to AML.	(Liu et al. 2012)
hnRNPA2B1	N	Y	Y	Functions as an m^6A reader regulating alternative splicing and miRNA maturation. Associated with adverse survival in selected AML datasets. Frequently described as oncogenic in solid tumours.	(Alarcón et al. 2015)
hnRNPA3	N	Y	Y	Mechanistically implicated in t(8;21) AML. Acts as an m^6A reader regulating ARUNX1::RUNX1T1 splicing	(Chen et al. 2025)
hnRNPAB	N	Y	N	Reported dysregulation in solid tumours; limited direct mechanistic evidence in AML.	-
hnRNPD	N	Y	N	Reported dysregulation in solid tumours; limited direct mechanistic evidence in AML.	-
hnRNPDL	N	Y	N	Reported dysregulation in solid tumours; limited direct mechanistic evidence in AML.	-
hnRNPC	Y	Y	N	Reported dysregulation in solid tumours; limited direct mechanistic evidence in AML.	-
hnRNPM	Y	Y	N	Reported dysregulation in solid tumours; limited direct mechanistic evidence in AML.	-
hnRNPF	N	Y	N	Reported dysregulation in solid tumours; limited direct mechanistic evidence in AML.	-
hnRNPR	N	N	N	N/A	-
hnRNPH1	Y	Y	N	Reported dysregulation in solid tumours; limited direct mechanistic evidence in AML.	-
hnRNPUL2	N	Y	N	Reported dysregulation in solid tumours; limited direct mechanistic evidence in AML.	-

The literature review was performed using the key terms “hnRNP”, “AML”, “leukaemia”, “blood cancer”, and “solid tumour”. Y indicates the presence of published evidence supporting a role for the indicated hnRNP in the specified cancer context, with further details provided either in the Notes column or in the accompanying text. N indicates no published evidence identified at the time of writing, and N/A indicates data not available

Although large scale studies in solid tumours are lacking, smaller studies indicate upregulation in hepatocellular carcinoma and colorectal cancer, where hnRNPA0 influences the splicing of cell cycle regulators (Belhadj et al. 2020)

hnRNPA1 is among the most abundant nuclear RNA-binding proteins and has been reported to be upregulated in approximately 70% of de novo AML cases (Liu et al. 2012). Elevated hnRNPA1 expression has also been described in several epithelial cancers, including hepatocellular carcinoma, gastric cancer, and lung cancer (Qin et al. 2018; Ryu et al. 2021; Cao et al. 2023). However, this reported upregulation contrasts with the protein expression patterns observed in the current study, where hnRNPA1 was not consistently elevated across AML samples. Furthermore, interrogation of BloodSpot mRNA datasets does not uniformly support widespread hnRNPA1 upregulation across normal haematopoiesis and AML. These discrepancies highlight the context-dependent regulation of hnRNPA1 and will be addressed in detail in the Discussion section. Collectively, these findings suggest that hnRNPA1 may have context-specific roles in both haematological and epithelial malignancies.

hnRNPA2B1 functions as an N^6-methyladenosine (m^6A) reader that recognises methylated pre-mRNAs and microRNAs, thereby influencing alternative splicing and miRNA maturation (Alarcón et al. 2015). It is increasingly recognised as an oncogenic driver in both AML and solid tumours.

hnRNPF and hnRNPR act as auxiliary splicing factors that promote exon inclusion. Loss-of-function screens suggest moderate essentiality in AML cell lines with FLT3-ITD mutations, likely reflecting hnRNPF's role in stabilising STAT5A and STAT5B transcripts (Dempster et al. 2021).

hnRNPH1 and hnRNPM regulate splice-site selection through binding G-runs near intronic splice silencers. CRISPR-Cas9 dropout datasets indicate conditional essentiality in 50–80% of AML cell lines, implicating them in splicing regulation of the MAPK pathway (Dempster et al. 2021).

In summary, although many of these hnRNPs (hnRNPA2B1, hnRNPA3, hnRNPAB, hnRNPD, hnRNPDL, hnRNPF, hnRNPR, hnRNPH1) have variable expression across solid tumours, their precise role in AML remains incompletely defined. Literature indicates that hnRNPs play roles in both AML and solid tumours with hnRNPA0 and hnRNPA1 implicated in AML, while

hnRNPAB, hnRNPD, hnRNPDL, and hnRNPA2B1 display cancer-type-specific alterations. These findings highlight hnRNPs as potential biomarkers and therapeutic targets.

3.2.6 Summary

Comprehensive multi-omic analysis of hnRNP family reveals consistent trends across normal haematopoiesis. BloodSpot profiling shows that all thirteen hnRNP transcripts have highest levels in HSCs and progressively decline as cells differentiate into granulocytic and monocytic lineages summarised in **(Table 3-5**). Proteomic data from normal BM progenitors support this observation, suggesting a correlation between transcript and protein abundance during normal differentiation. In AML, iTRAQ MS identified broad reductions in nuclear hnRNP protein levels compared with $CD34^+$ HSPC, with fold changes of up to fourfold for several family members. Public transcriptomic datasets, including TCGA and Beat -AML, confirmed similar reductions in hnRNP gene expression in leukaemic blasts. However, two members, *HNRNPA2B1* and *HNRNPA3*, display a distinct expression profile: while downregulation predominates across the cohort, a substantial subset of patients exhibits marked upregulation, highlighting pronounced heterogeneity in the regulation of these hnRNPs.

Kaplan-Meier survival analysis demonstrated that higher expression of *HNRNPA2B1* and *HNRNPA3* was significantly associated with poorer overall survival, independent of established risk factors such as age, cytogenetics, and molecular subtype. By contrast, no consistent associations with outcome were observed for the other *HNRNP*s.

DepMap analyses further highlighted functional diversity within the family. Across forty-four AML cell lines, transcript and protein levels were generally concordant, though exceptions were noted. For example, hnRNPDL showed high mRNA levels but low protein abundance, suggesting post-transcriptional regulation. CRISPR–Cas9 knockout screens indicated that most hnRNPs are dispensable for AML cell line survival. Only three *HNRNPC*, *HNRNPH1*and *HNRNPM* were essential for viability in more than half of the tested lines.

To prioritise candidates for further study, I integrated several criteria: consistent mRNA and protein dysregulation in AML compared with HSCs; prognostic impact on patient survival; functional dependency in CRISPR screens; and novelty in the literature. From this integrated analysis, hnRNPA3 emerged as the highest-priority candidate. It is downregulated in 81% of AML patients, with only 0.2% showing upregulation, and was one of the most significantly

changed hnRNP protein family member in AML. In parallel, hnRNPA0 is also an important candidate due to its dynamic regulation during normal hematopoietic differentiation, notable downregulation in AML, and previous research linking it to lineage specification (Young et al. 2014; Konig et al. 2016). Together, hnRNPA3 and hnRNPA0 are two noteworthy members of the hnRNP family whose functions in AML are explored in the following chapters.

Table 3-5: Summarising the overall data of hnRNPs

Integrated summary of transcriptomic, proteomic, dependency, and literature evidence for hnRNP family members in AML. BloodSpot values indicate the percentage of AML patients showing significant downregulation relative to normal HSC populations. The MS product score represents the combined magnitude and frequency of protein downregulation in AML patient blasts relative to $CD34^+$ HSPCs, calculated as the product of the proportion of affected patients and the absolute fold-change. DepMap dependency values represent the percentage of AML cell lines exhibiting gene dependency based on Chronos scores (Chronos < −1), while enhanced fitness values represent the percentage of AML cell lines showing improved viability upon gene loss (Chronos > +1). Literature evidence indicates whether at least one published study has directly linked the indicated hnRNP to AML biology. Proteins are not ordered by rank. N/A indicates data not available.

Protein	BloodSpot: % AML patients downregulated vs HSC	MS product score	DepMap dependency (Chronos score < −1)	DepMap enhanced fitness (Chronos score > +1)	Literature evidence in AML
hnRNPA3	81	1.64	19.2	0	No
hnRNPA0	81	1.80	7.7	0	Yes
hnRNPD	42	2.51	7.7	0	No
hnRNPUL2	30	1.54	0	0	No
hnRNPA2B1	15	1.86	34.6	0	No
hnRNPR	7	1.98	34.6	0	No
hnRNPM	21.6	1.33	96.2	0	No
hnRNPH1	18	1.33	96.2	0	No
hnRNPC	9	1.86	100	0	No
hnRNPA1	9	1.80	38.5	0	Yes
hnRNPAB	2	2.40	0	0	No
hnRNPF	0.3	1.12	19.2	0	No
hnRNPDL	N/A	2.41	0	0	No

3.3 Discussion

3.3.1 Overview

The findings presented in this chapter provide a broad survey of hnRNP expression during normal haematopoiesis and in AML. By integrating public resources including BloodSpot (Bagger et al. 2019), TCGA (Cancer Genome Atlas Research et al. 2013), and DepMap datasets (Barretina et al. 2012; Dempster et al. 2021) with our previous iTRAQ nuclear proteome study (Alanazi et al. 2020), we observed consistent downregulation of multiple hnRNP family members during myeloid differentiation and in AML blasts.

In contrast to this general pattern of reduced expression, members of the hnRNPA/B subfamily showed a different behaviour. While most AML patients exhibited downregulation similar to other hnRNPs, a distinct subset of patients showed marked upregulation of HNRNPA2B1 and HNRNPA3. This mixed pattern of downregulation in the majority and upregulation in a defined subset distinguishes the A/B subfamily from other hnRNP family members and was associated with poorer overall survival in TCGA AML cohorts. hnRNPA0 demonstrated dynamic regulation during haematopoietic differentiation and evidence of adverse prognostic association in publicly available AML patient cohorts (for example, TCGA and Beat-AML).

3.3.2 hnRNPs in normal haematopoiesis

RNA-binding proteins have long been recognised as central regulators of lineage fate, yet relatively few studies have examined the hnRNP family systematically in human haematopoiesis. Evidence from BloodSpot (Bagger et al. 2019) and the murine dataset GSE6506 (Chambers et al. 2007) shows that many hnRNP transcripts are highly expressed in stem and early progenitor compartments, then fall away as cells progress into granulocytic and monocytic fates. This points to a dosage requirement for these proteins in sustaining progenitor identity. Support for this view comes from functional work; when hnRNPA0 was knocked down in murine progenitors, granulocytic output increased, while sustained expression restricted differentiation (Young et al. 2014). This type of dosage-sensitive behaviour is not unique to hnRNPs; splicing regulators such as SRSF2 and RBM39 behave in a similar way, where reduced expression promotes lineage commitment (Beijer et al. 2021; Chen et al. 2022). Taken together, the available evidence indicates that hnRNP downregulation is unlikely to be a passive marker of differentiation. More likely, it forms part of the molecular machinery that permits progenitors to relinquish stem identity and commit to terminal myeloid fates.

3.3.3 Global dysregulation of hnRNPs in AML

Proteomic studies have shown that nuclear hnRNP levels are generally reduced in patient blasts when compared with $CD34^+$ HSPC (Alanazi et al. 2020), and this is now supported by mRNA transcript data from BloodSpot and TCGA (Cancer Genome Atlas Research et al. 2013; Bagger et al. 2019). Even so, the reduction is not consistent across the whole family analysed.For example, hnRNPC and hnRNPM show relatively consistent downregulation across AML patient samples, with limited inter-patient heterogeneity compared with other hnRNP family members. While this uniform expression pattern may initially suggest functional redundancy, RNAi/CRISPR dependency screens indicate that loss of hnRNPC and hnRNPM results in a strong fitness defect in AML cell lines, consistent with these proteins being among the most essential hnRNP family members rather than functionally redundant (Barretina et al. 2012; Dempster et al. 2021). These findings highlight that low expression heterogeneity does not equate to dispensability and emphasise the importance of integrating functional dependency data with expression analyses. In contrast, hnRNPA2B1 and hnRNPA3 behave differently. A proportion of patients show overexpression, of *HNRNPA2B1* or *HNRNPA3* and in both cases this has been associated with worse overall survival (Liu et al. 2012; Chen et al. 2022). Depending on the context, the same factor can act like a tumour suppressor or, instead, promote malignant growth. For this reason, it seems unwise to treat hnRNPs as a uniform group; each family member must be evaluated on its own expression pattern, functional dependency, and clinical association.

3.3.4 hnRNPA0: a dosage-sensitive regulator of lineage fate

Data from BloodSpot and murine models show that hnRNPA0 is strongly expressed in stem and early progenitor compartments but lower levels observed as cells move into granulocytic and monocytic lineages. In experimental systems, reducing hnRNPA0 levels in murine progenitors drove them more quickly towards granulocytes, while maintaining expression held cells back from committing (Young et al. 2014). The implication is that A0 levels actively influence lineage choice rather than being a passive marker. In AML, reports are less consistent, but some transcriptomic studies have found higher expression associated with worse overall survival (Konig et al. 2016). That raises the possibility that blasts retaining elevated A0 remain in an undifferentiated state, reinforcing the maturation block typical of AML. Mechanistically, hnRNPA0 has been linked to stabilising transcripts involved in cell-cycle progression and inflammatory pathways (Beijer et al. 2021; Liu and Shi 2021), which could

provide a route through which its mis-regulation contributes to leukaemic biology. Overall, the picture that emerges is of a dosage-sensitive factor: too much A0 may preserve stemness and obstruct differentiation, and too little can accelerate lineage commitment.

3.3.5 hnRNPA3 a context dependent candidate with dual behaviour

hnRNPA3 is much less explored in the context of AML than other A/B subfamily members, which makes it both challenging and intriguing. Across differentiation datasets, A3 tends to follow the general pattern of downregulation with maturation, and in patient blasts its expression is often reduced compared with normal progenitors. However, my analyses of TCGA data indicate high A3 expression, and this group has significantly worse overall survival. The biology behind this dual behaviour is not yet clear. In other cancers, particularly solid tumours, paralogues such as hnRNPA1 and hnRNPA2B1 are well recognised as oncogenic drivers, promoting proliferation, invasion, and altered splicing programmes (Liu et al. 2012; Qin et al. 2018; Ryu et al. 2021; Cao et al. 2023). It is therefore plausible that, under certain molecular conditions, hnRNPA3 deviates from its typical downregulation during differentiation and instead becomes aberrantly upregulated in specific AML contexts, where it may behave more like its oncogenic paralogues and enhance malignant potential.

A recent mechanistic study demonstrated that hnRNPA3 functions as an m^{6}A reader and regulates *RUNX1::RUNX1T1* splicing specifically in t(8;21) AML, with inhibition of hnRNPA3 promoting myeloid differentiation (Liu et al. 2024). These findings provide mechanistic evidence that hnRNPA3 can contribute to leukaemogenesis in defined molecular subtypes of AML. Taken together**,** hnRNPA3 emerges as a context-dependent candidate that is typically downregulated during normal haematopoietic differentiation and in the majority of AML cases analysed in this study, yet can act as an adverse factor when aberrantly upregulated in specific AML contexts, such as t(8;21) AML. This highlights the importance of molecular context in determining hnRNPA3 function and cautions against generalising its role across all AML subtypes.

3.3.6 Clinical implications

The dysregulation of hnRNPs raises the possibility that they could contribute to risk stratification or even represent therapeutic entry points. Published studies have reported that hnRNPA3 overexpression is associated with poor outcome in defined subsets of AML patients, suggesting a potential prognostic role in specific molecular contexts(Cancer Genome Atlas

Research et al. 2013). Given that these survival associations are derived from large, independent patient cohorts, they provide a stronger basis for clinical inference than the smaller datasets analysed in this study. Similarly, the persistence of hnRNPA0 expression observed in AML blasts in this study is consistent with a role in maintaining a stem-like transcriptional state, although this interpretation is limited by the use of bulk RNA-seq and proteomic data, which obscure cell-to-cell heterogeneity and may reflect contributions from residual normal progenitor populations.

Given that hnRNPA3 can function as an m^{6}A reader, previous studies have proposed targeting m^{6}A-dependent pathways as a therapeutic strategy, either by inhibiting reader proteins or modulating the methylation machinery itself (Lee et al. 2019). If the adverse effects of hnRNPA3 overexpression in AML are mediated through aberrant m^{6}A dependent RNA processing, these pathways may represent a rational therapeutic vulnerability in selected AML subtypes**.** In this context, hnRNPA3 would function as both a molecular marker of higher-risk disease and a potential mechanistic entry point for intervention.

Taken together, the parallel investigation of hnRNPA3 and hnRNPA0 in this study provides complementary insights into how mis-regulated hnRNPs may influence AML biology: hnRNPA3 through context dependent effects on RNA processing, and hnRNPA0 through dosage-sensitive regulation of progenitor cell state. These conclusions are primarily supported by integrative analysis of expression and functional datasets, with clinical implications inferred cautiously in light of existing literature.

3.3.7 Conclusion

Taken together, the data presented in this chapter indicate that hnRNP expression is dynamically regulated during normal haematopoiesis and is frequently altered in AML, with substantial variation between individual family members. Across multiple transcriptomic and proteomic datasets, most hnRNPs show highest expression in stem and progenitor populations, followed by progressive downregulation with differentiation and broad reduction in AML blasts.Within this overall trend, hnRNPA0 and hnRNPA3 exhibit distinct expression patterns that differentiate them from other family members. hnRNPA0 shows sustained expression across progenitor states and AML blasts, consistent with a potential role in maintaining immature transcriptional programmes. In contrast, hnRNPA3 is generally reduced but displays marked upregulation in defined AML subsets, where it is associated with adverse clinical features in published patient cohorts. These observations, derived from integrative analysis of public datasets, highlight hnRNPA0 and hnRNPA3 as informative candidates for further

functional investigation rather than establishing definitive mechanistic roles**.** Accordingly, the following chapter focuses on experimental perturbation of hnRNPA3 to directly test its contribution to AML-associated phenotypes, while hnRNPA0 is retained as a comparator to explore broader principles of dosage-sensitive regulation during myeloid differentiation.

4 hnRNPA0 expression is required for AML cell survival

4.1 Introduction

Heterogeneous nuclear ribonucleoproteins (hnRNPs) are widely recognised as central post-transcriptional regulators of gene expression (**1.4**). Most family members are known for their roles in splicing and RNA stability, and their influence also extends to mRNA transport, translation, DNA repair, and cellular stress responses (Han et al. 2010a; Geuens et al. 2016). Perturbation of hnRNP dosage can alter splicing decisions and stabilise transcripts that promote proliferation, giving cells a selective growth advantage (Chi et al. 2005; Jin et al. 2017; Kedzierska and Piekielko-Witkowska 2017). Much of this evidence derives from solid tumour studies, however their function in haematological malignancies such as AML remains less well understood.

In Chapter **3**, I systematically examined the expression of thirteen hnRNP family members across normal haematopoiesis and AML. These analyses showed that hnRNPs proteins are expressed in stem and early progenitor cells but decline as cells differentiate towards granulocytic and monocytic lineages. In AML, this developmental pattern was disrupted, with blasts showing widespread downregulation compared with $CD34^{+}$ HSPC (Alanazi et al. 2020). Based on criteria that combined degree of dysregulation, prognostic association, dependency of expression on survival, and novelty, hnRNPA3 and hnRNPA0 were prioritised for functional investigation.

Although hnRNPA3 was consistently downregulated in AML blasts, patients with higher expression paradoxically showed poorer overall survival (Chapter **3 Figure 3-9**). Unlike hnRNPA1 and hnRNPA2B1, which have been widely studied in AML and solid tumours, hnRNPA3 has received little attention in haematological malignancies. Studies in solid tumours such as hepatocellular and bladder show hnRNPA3 is upregulated compared with adjacent normal tissue, and patients with higher levels exhibit poorer outcomes. Experimental assays show enhanced proliferation and invasiveness when hnRNPA3 is raised (Ren et al. 2021) (Amano et al. 2021). Unlike hnRNPA3, hnRNPA0 has been investigated though not extensively. Mechanistic evidence supports a role in haematopoiesis where loss of hnRNPA0 in murine progenitors impaired normal differentiation, skewed output towards granulocytic lineages, and enhanced proliferation through stabilisation of AU-rich element (AREs) containing transcripts (Young et al. 2014). hnRNPA0 also stabilises checkpoint regulators such as GADD45α, linking it to G2/M control and stress responses in mice (Cannell et al. 2015a).

Despite these findings, hnRNPA0 has not been studied in human AML or human haematopoiesis.

4.1.1 Aim and Objectives

The overall goal is to determine whether hnRNPA3 or hnRNPA0 are essential for the growth and survival of human blood cells. Initially I focussed on hnRNPA3, given its prognostic association and novelty. hnRNPA0 was subsequently investigated, supported by prior evidence linking it to haematopoietic regulation. To accomplish this goal, the following objectives were established:

- **To determine protein expression of hnRNPA3 and hnRNPA0 in AML cell lines to establish models for subsequent investigation**

Protein expression will be analysed across a small cohort of AML lines by WB to identify which lines are most appropriate for genetic modifications and functional assays.

- **To explore the functional importance of hnRNPA3 and hnRNPA0 in AML**

Utilising knockdown, knockout, and overexpression approaches, I will assess whether altering hnRNPA3 or A0 levels affects cell growth, cell-cycle progression, and viability in AML cell lines.

4.2 Results

I first focused on hnRNPA3, given its prognostic association and novelty, and optimised conditions for detecting its protein expression.

4.2.1 hnRNPA3 protein is variably expressed in AML cell lines and AML blasts

4.2.1.1 Optimisation of hnRNPA3 protein detection by western blot

To assess hnRNPA3 protein expression in AML blasts and cell lines, it was first necessary to optimise detection conditions using WB. Two commercial monoclonal antibodies were compared: Abcam AB78000 and Fisher A305-815A-T, using HeLa cells as a positive control. Both antibodies detected hnRNPA3 at the expected molecular weight (42 kDa), but AB78000

produced a stronger signal-to-noise ratio and was selected for all subsequent experiments (**Figure 4-1**).

I next optimised transblotting conditions and blocking reagents. Signal to noise ratios were broadly similar when comparing membrane type (nitrocellulose vs PVDF) and 'milk' concentrations, although 2.5% (*w/v*) milk .However, PVDF membranes consistently produced a slightly higher signal to noise ratio under the conditions tested and were therefore adopted for subsequent experiments (**Figure 4-2**). Titration of the primary antibody demonstrated that dilutions as low as 1:40,000 yielded detection. A 1:20,000 dilution was selected as it combined sensitivity with cost efficiency (**Figure 4-4**).

To confirm antibody specificity, lysates from THP-1 cells transduced with shRNA constructs targeting hnRNPA3 were analysed by WB. More than 99% of cells were successfully transduced (as indicated by GFP positivity) and WB showed marked reduction of hnRNPA3 protein in knockdown clones 576 and 581 compared with controls. No additional non-specific bands were observed, further confirming antibody specificity (**Figure 4-4**).

In summary, AB78000 (Abcam) provided optimal detection of hnRNPA3 when used at 1:20,000 dilution with 2.5% milk blocking on nitrocellulose membranes. These optimised conditions were applied in all subsequent experiments to assess hnRNPA3 protein expression in AML cell lines (**Figure 4-5**).

4.2.1.2 hnRNPA3 protein expression is variable in AML patient blasts

Using the optimised conditions established above, cytosolic and nuclear protein fractions were prepared from AML blasts isolated from seven patients representing different FAB subtypes (samples provided by Dr Rizzo, Cardiff University, 2024). Western blot analysis revealed qualitative heterogeneity in hnRNPA3 protein detection between individual patient samples (**Figure 4-6**). Given the limited sample number and the absence of quantitative densitometric analysis, no statistical comparisons were performed and no conclusions regarding differential expression between FAB subtypes can be drawn. Notably, hnRNPA3 was detectable in both cytosolic and nuclear fractions across multiple samples, suggesting variability in subcellular distribution between patients. This observation is consistent with prior proteomic findings reported in Chapter **3** (**Table 3-5**) but should be interpreted as descriptive rather than comparative. These preliminary observations highlight inter patient variability and motivate future studies using larger, quantitatively analysed AML cohorts.

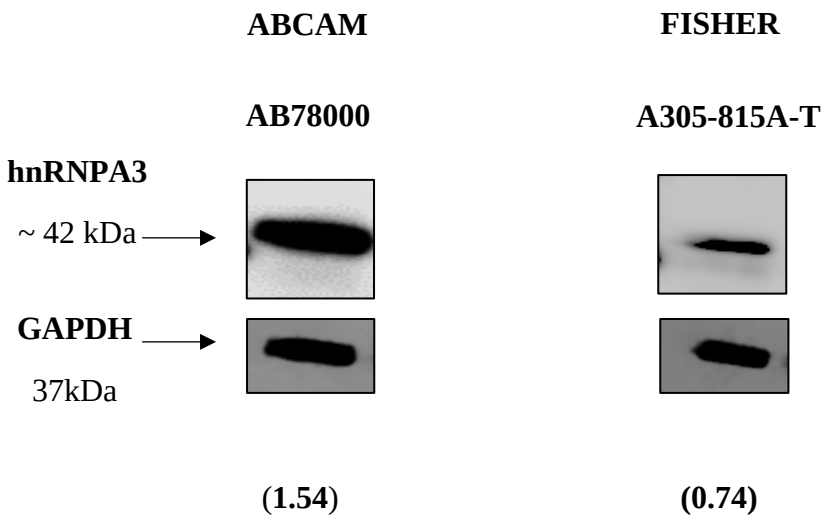

Figure 4-1: Optimisation of hnRNPA3 protein detection using different antibody clones

Western blot analysis of hnRNPA3 expression in HeLa cells (positive control). Two commercial monoclonal antibodies were compared: Abcam AB78000 and Fisher A305-815A-T. GAPDH (37 kDa) was used to verify protein loading and normalisation. Values in parentheses represent signal-to-noise ratios normalised to GAPDH using Image J. **(**N=1).

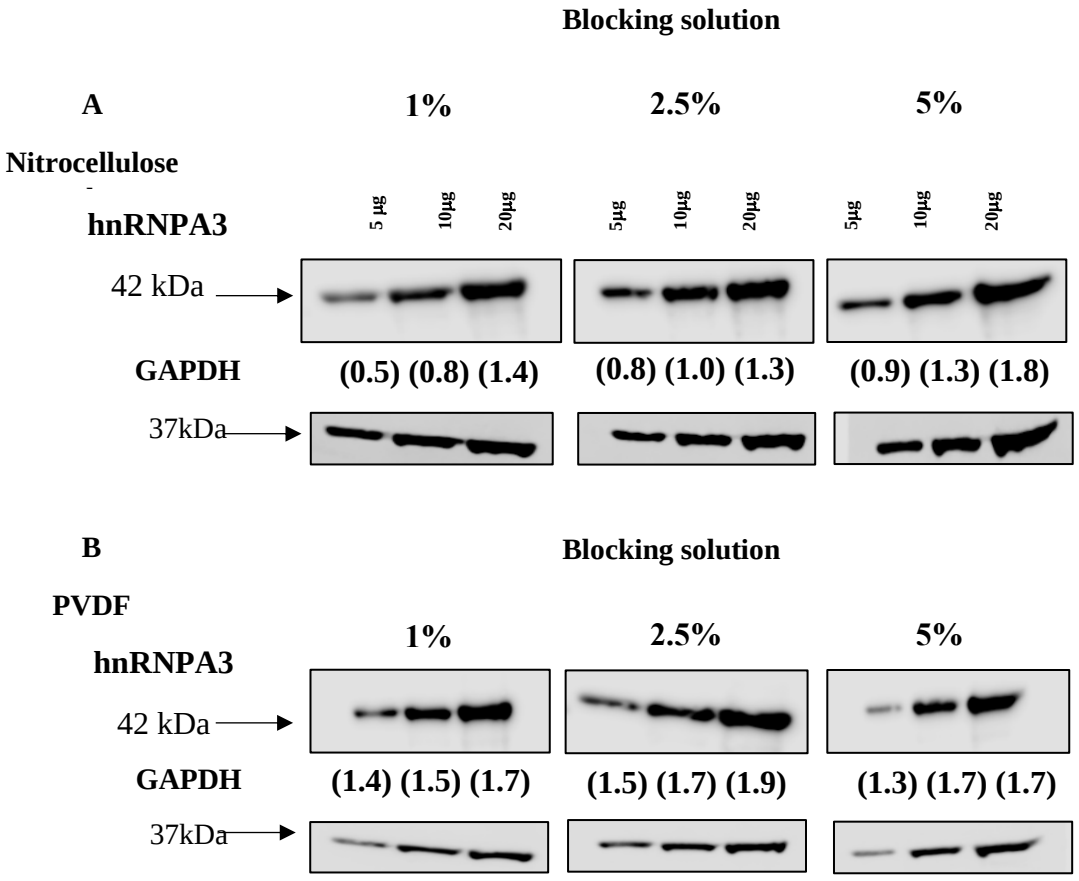

Figure 4-2: Optimisation of blocking solution and membrane for detection of hnRNPA3

Western blots showing optimisation of blocking solution and membrane support matrices to detect hnRNPA3 using Abcam monoclonal antibody AB78000. Each lane was loaded with the amount of protein indicated (using HeLa cell line). The dilutions are of blocking solutions are based on *w/v* of milk proteins. (N=1). Values in parentheses represent signal to noise ratio normalised to loading control (GAPDH) using Image J.

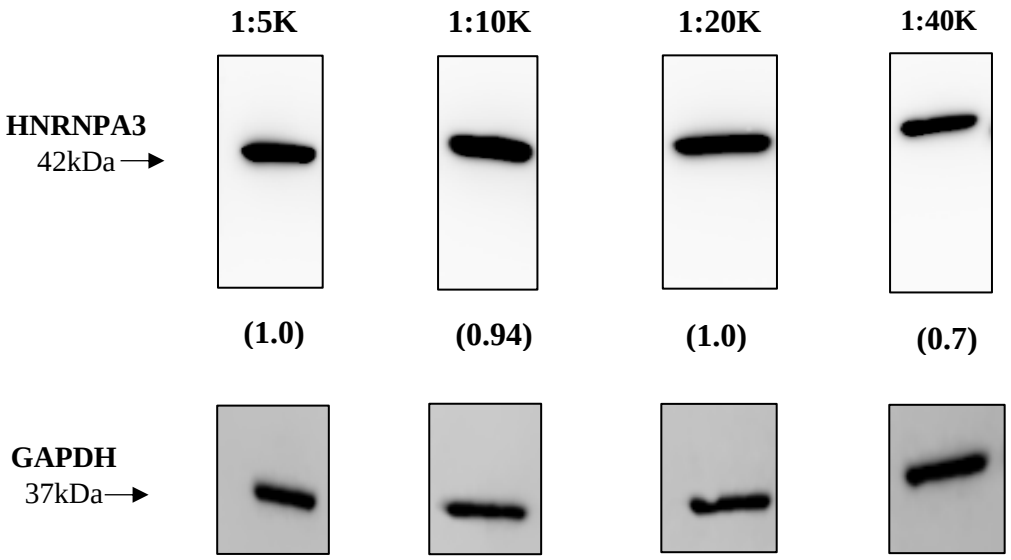

Figure 4-3: Optimisation of primary antibody dilution for hnRNPA3 detection by WB

Western blot analysis of hnRNPA3 protein in HeLa cells (positive control) using Abcam monoclonal antibody AB78000 at different primary antibody dilutions indicated. Conditions included 2.5% (*w/v*) Marvel milk blocking and nitrocellulose membranes. GAPDH (37 kDa) was used as a loading control and normalisation control. Values in parentheses represent signal to noise ratios normalised to GAPDH using Image J. (N=1).

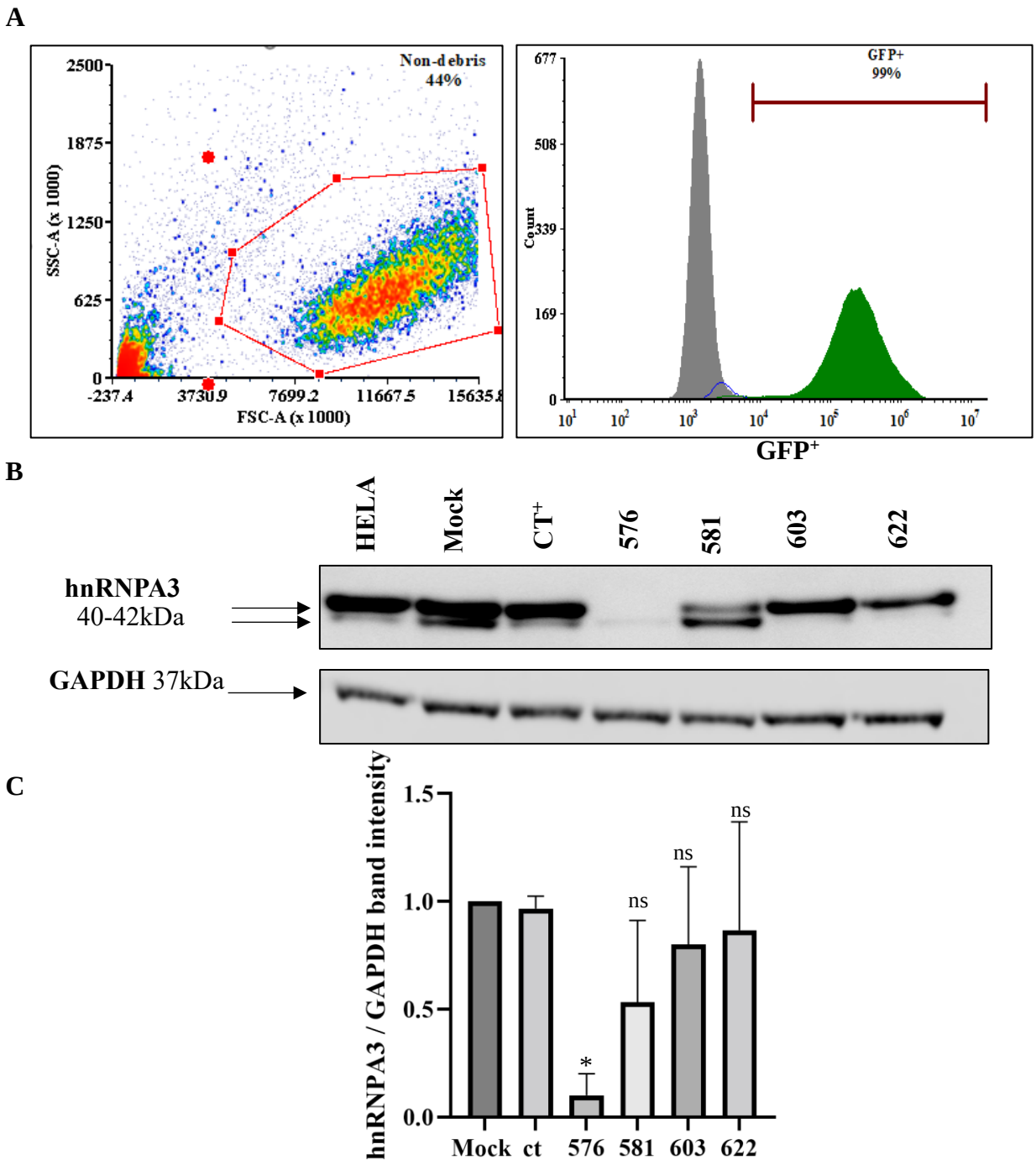

Figure 4-4: Expression of hnRNPA3 in THP-1 cells targeted with shRNA to hnRNPA3

A Flow cytometry plots showing forward scatter (FSC) vs side scatter (SSC) (left panel) exclude debris in gating. Right panel shows histogram of GFP^+ fluorescence. The grey overlay represents mock control (THP-1 cells exposed to transduction reagents without DNA), while the green histogram represents THP-1 cells transduced with the control vector expressing GFP^+ only. Background autofluorescence was based on mock cells. **B** WB analysis of hnRNPA3 protein expression in THP-1 cells following lentiviral transduction. Lanes: HeLa (positive control, PC), Mock (untraduced THP-1), Control (CT^+, construct 497, GFP-only), and four hnRNPA3 knockdown vectors (576, 581, 603, 622). hnRNPA3 protein was detected at 40 - 42 kDa and GAPDH at 37 kDa as a loading control. **C** Densitometric quantification of hnRNPA3 / GAPDH band intensity from three independent biological replicates (mean + 1SD, upper error bar only; N = 3) Statistical analysis was performed using one-way ANOVA followed by Dunnett's multiple comparisons test (each shRNA vs CT). * $p < 0.05$; ns, not significant.

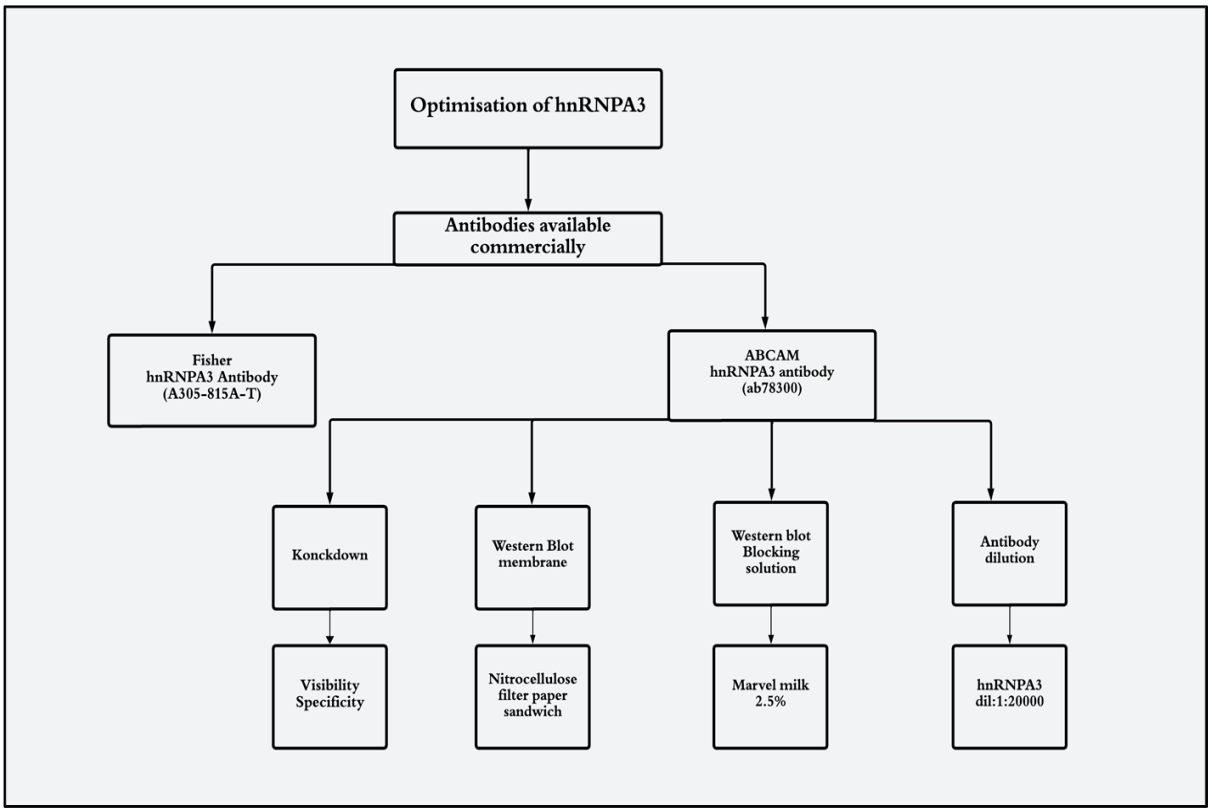

Figure 4-5: Summary workflow of hnRNPA3 optimisation

This schematic illustrates the optimisation workflow and establishes conditions for hnRNPA3 WB detection using commercially available antibodies. Two antibodies were assessed (Abcam AB78000 and Fisher A305-815A-T). The diagram provides an overview of the methods and conditions optimised, including antibody selection, membrane type, blocking solution, and antibody dilution, for effective hnRNPA3 detection in experimental setups. This schematic was created using Lucidchart (www.lucidchart.com).

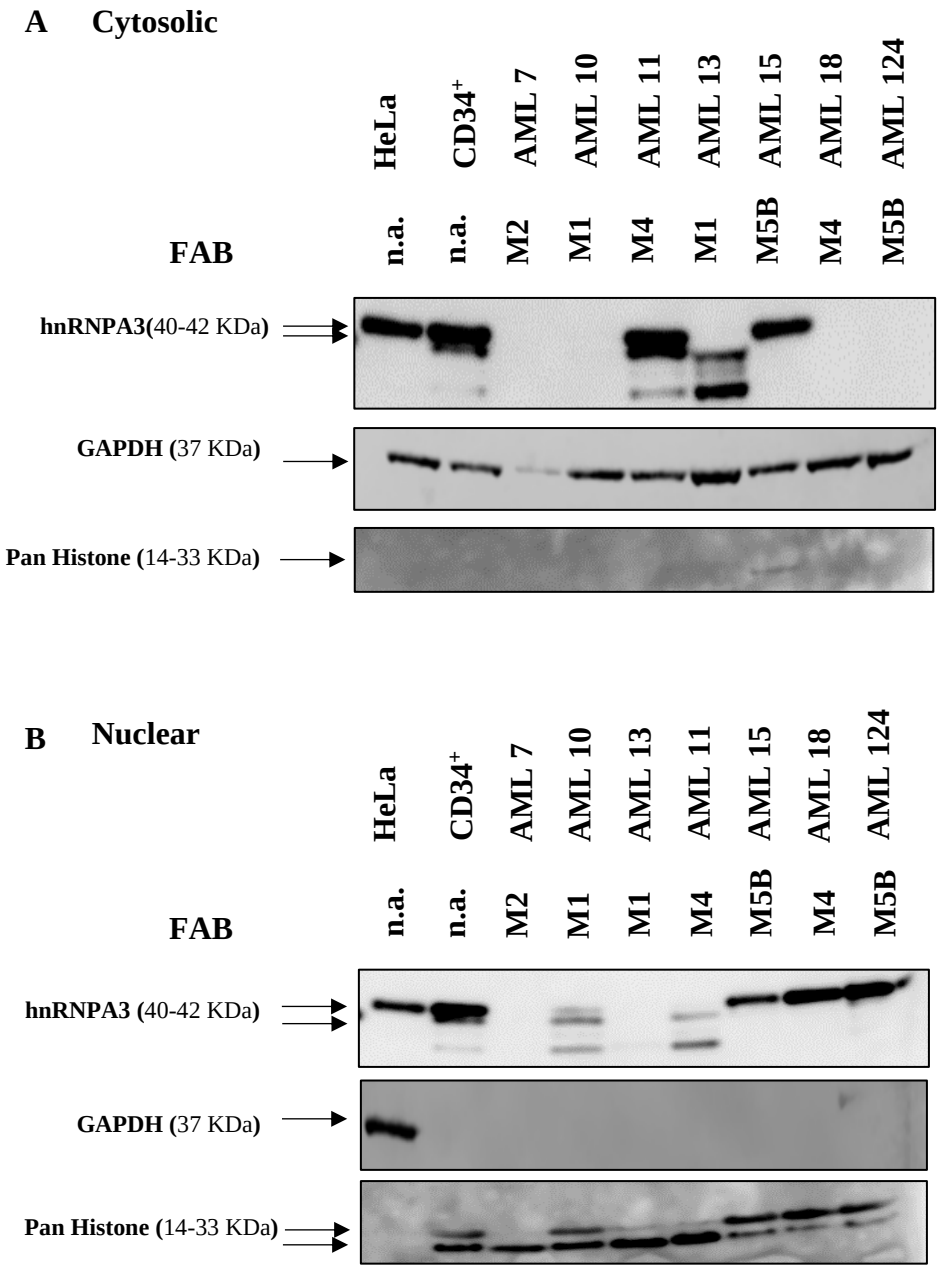

Figure 4-6: hnRNPA3 protein expression in AML patient blasts samples

WB analysis of hnRNPA3 protein in cytosolic and nuclear fractions isolated from AML patient blasts representing different FAB subtypes. GAPDH (37 kDa) was used as a loading control for cytosolic extracts, and Pan Histone (14–33 kDa) was used as a loading control for nuclear extracts. (N=1). n.a., not applicable; FAB, French American British classification.

An apparent difference in the relative cytosolic versus nuclear signal intensity was observed between samples; however, this was not quantified and is therefore noted descriptively only.

4.2.1.3 Expression of hnRNPA3 is observed in various AML cell lines

To evaluate hnRNPA3 protein expression in cell lines, WB analysis was performed on total protein extracts as well as on cytosolic and nuclear fractions. hnRNPA3 was detected as either a single or a double protein band at 40-42 kDa, consistent with the presence of isoforms or post-translational modifications. As shown in (**Figure 4-7**), hnRNPA3 protein was expressed in total extracts from THP-1, HEL, U937, TF-1, MV4-11, OCI-AML2, KG1, and SKNO-1. Subcellular fractionation revealed further heterogeneity. Cytosolic hnRNPA3 expression level was variable across the panel of cell lines tested (**Figure 4-8)**. In contrast, nuclear hnRNPA3 expression was variable but also not exclusively present in the nucleus of all cells lines **(Figure 4-9**): HEL, THP-1, OCI-AML2, and KG1 cells showed nuclear protein bands at 40 - 42 kDa, while TF-1, MM6, NOMO-1, and HL-60 had only weak or undetectable levels of the higher molecular weight form. ML-1 and PLB cells lacked detectable nuclear hnRNPA3 expression altogether.

Taken together, these findings indicate that hnRNPA3 protein is expressed in multiple AML cell lines, and the abundance and subcellular distribution of the protein vary between lines.

4.2.2 Knockdown of hnRNPA3 protein expression did not impact AML cell growth

To investigate the impact of hnRNPA3 knockdown (KD) on AML cell growth, THP-1, U937, and TF-1 cell lines were selected on the basis of detectable hnRNPA3 protein expression (0). Two lentiviral shRNA constructs were used, previously validated to reduce hnRNPA3 protein by approximately 90% (shRNA Ref. 576) and 60% (shRNA Ref. 581) in THP-1 cells (**Figure 4-4**). In THP-1 cells, WB confirmed that both shRNAs reduced hnRNPA3 protein at 42 kDa relative to GAPDH, with (shRNA Ref.576) showing the greatest depletion (**Figure 4-10**). Growth analysis by cumulative viable cell counts demonstrated that cells transduced with shRNA576 grew at levels indistinguishable from the control, with no significant difference at day 9 (fold change relative to control ≈0.88, ns).

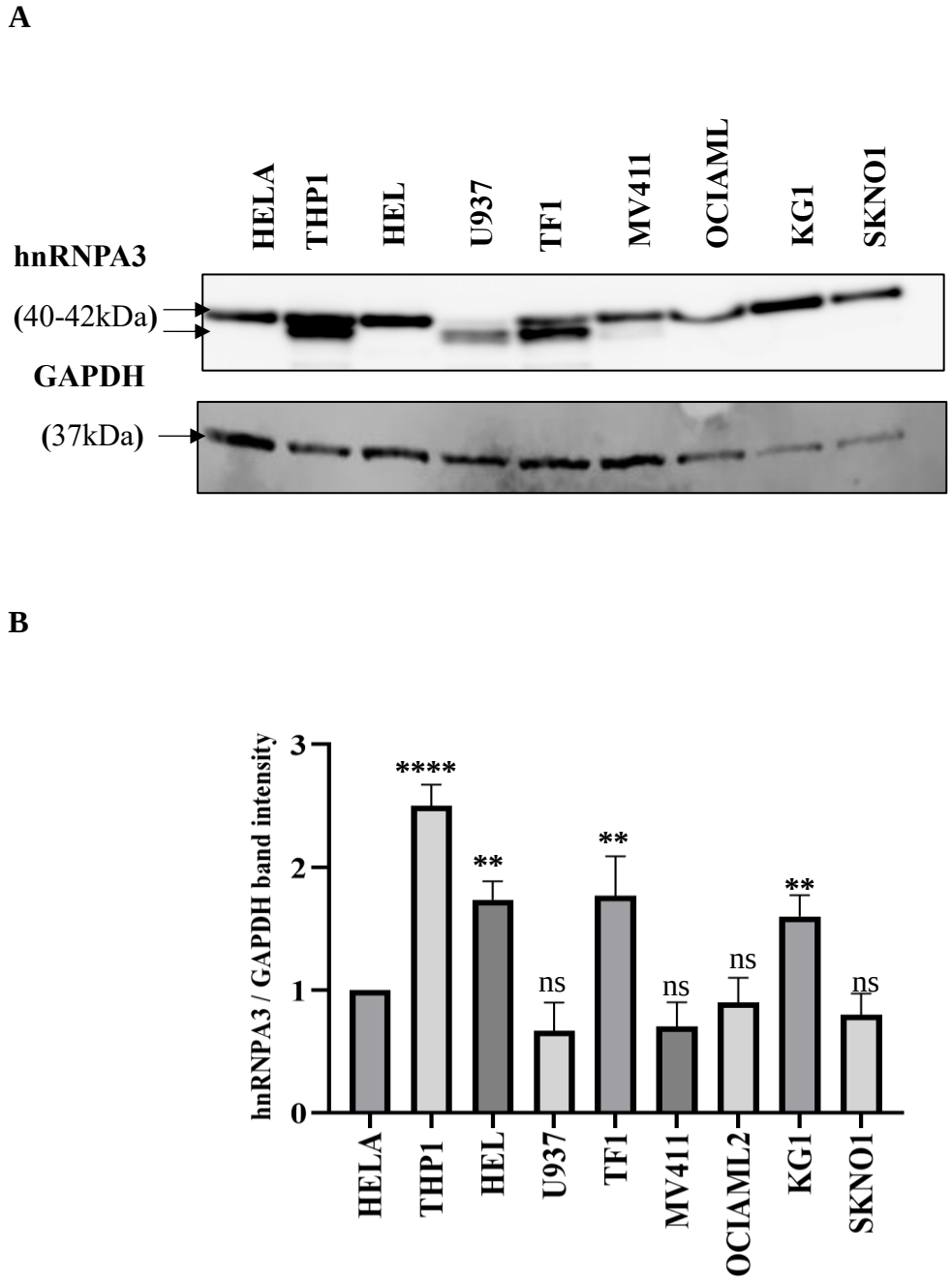

Figure 4-7 hnRNPA3 protein expression in leukaemia cell lines

A WB analysis showing hnRNPA3 protein expression in total protein extracts from a panel of leukaemia cell lines. HeLa cells were included as a positive control and GAPDH used as loading control. **B** Densitometric quantification of hnRNPA3 / GAPDH band intensity from three independent biological replicates (mean + 1SD, upper error bar only); (N = 3) Statistical analysis was performed using one-way ANOVA followed by Dunnett's multiple comparisons test (each AML cell line vs HeLa). **, $p < 0.01$; ****, $p < 0.0001$; ns, not significant.

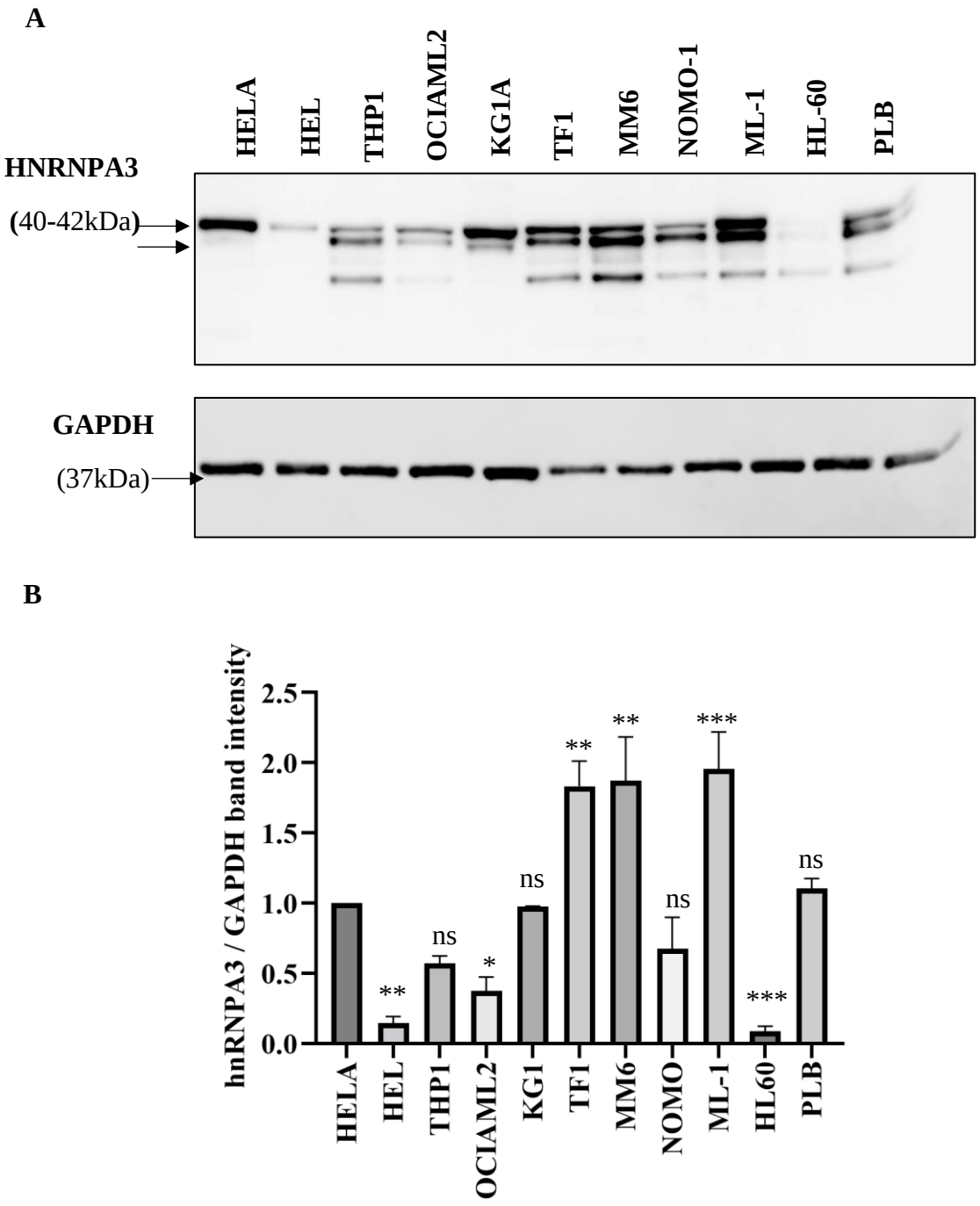

Figure 4-8: Cytosolic hnRNPA3 protein expression in AML cell lines

A Example WB showing cytosolic hnRNPA3 protein expression in AML cell lines. Hela was used as a positive control. GAPDH was used as a loading control for cytosolic fraction at 37kDa. **B** Densitometric quantification of hnRNPA3analysis using ImageJ normalised to GAPDH. Bars show mean with +1SD error bars (upper error bar only) ; N = 3 biological replicates). Statistics by one-way ANOVA with Dunnett's multiple comparisons test (each AML cell line vs HeLa): *, $p < 0.05$, ****** $p < 0.01$, *** $p < 0.001$, ns, not significant

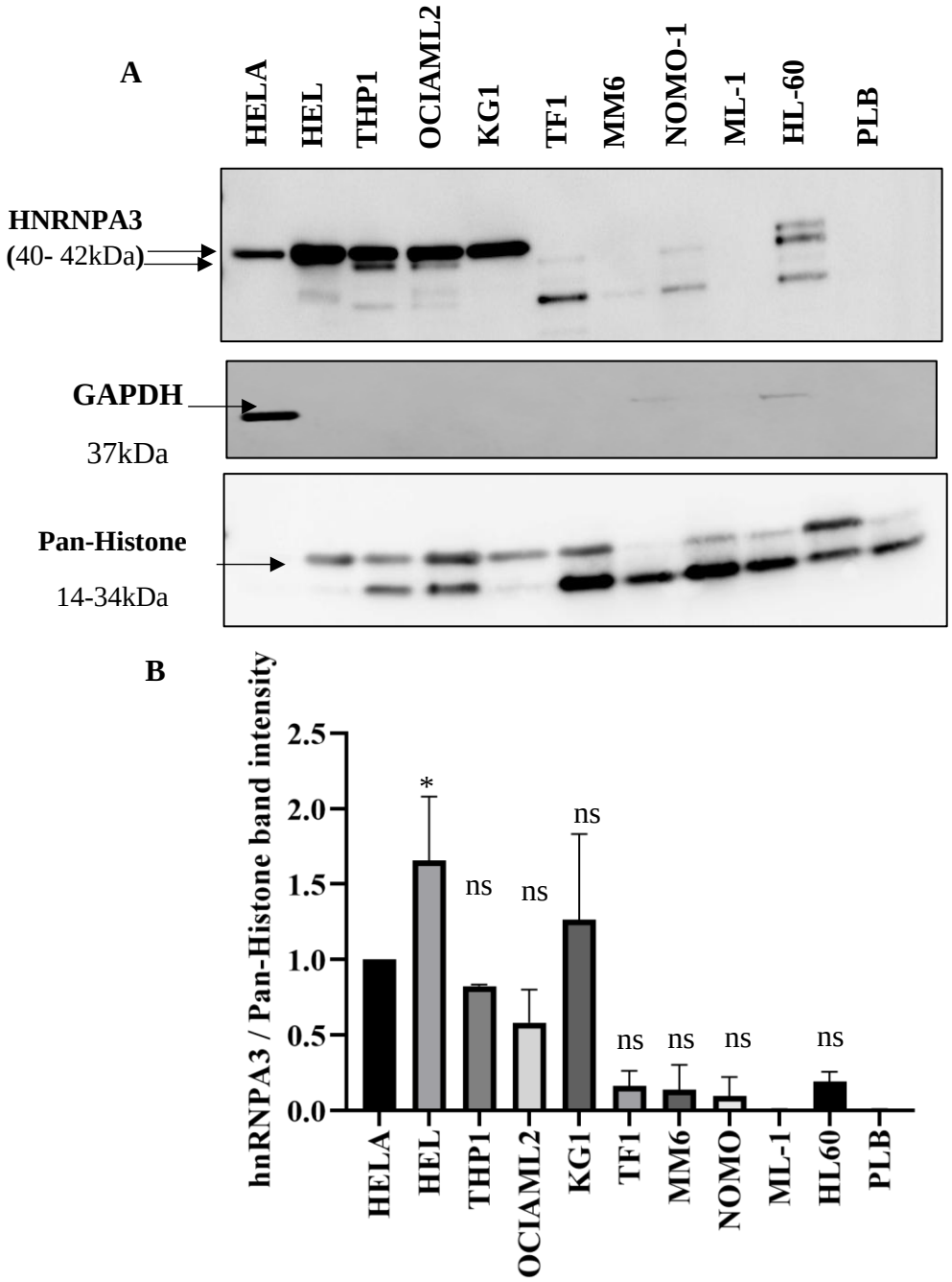

Figure 4-9: Expression of hnRNPA3 in the nuclear fraction of AML cell lines

A Example western blot showing nuclear hnRNPA3 protein expression in AML cell lines. Hela was used as a positive control Pan Histone was used as a control for nuclear fraction at 14-34kDa and GAPDH (37 kDa) was included to monitor possible cytoplasmic contamination. **B** Densitometric quantification of hnRNPA3analysis using ImageJ normalised to pan-histone. Bars show mean with +1SD error bars (upper error bar only); (N = 3 biological replicates). Statistics by one-way ANOVA with Dunnett's multiple comparisons test (each AML cell line vs HeLa); significance: * $p < 0.05$, ns, not significant.

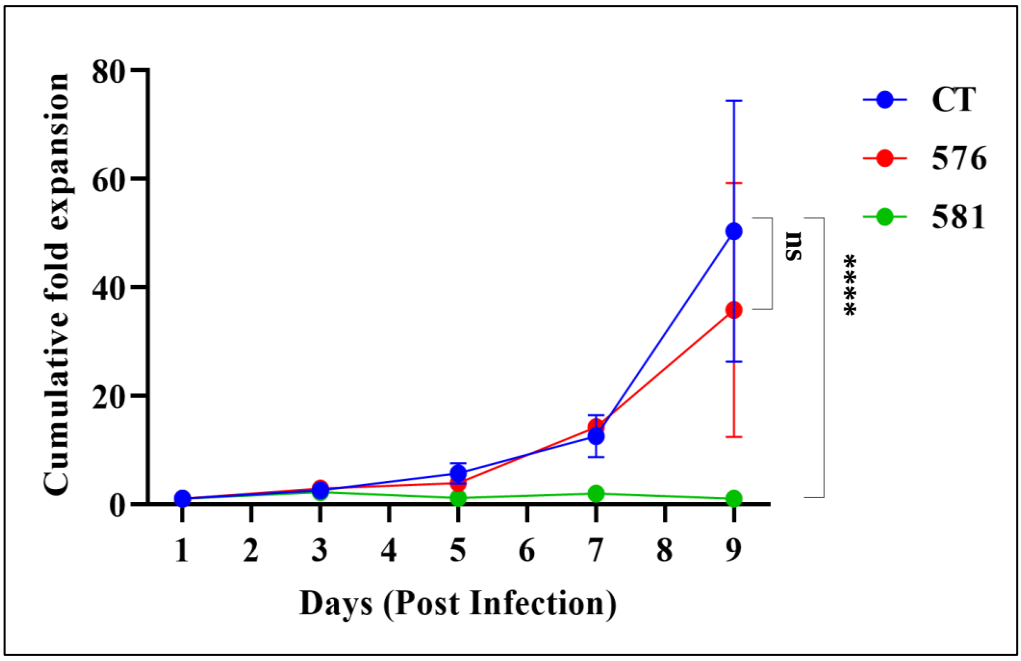

Figure 4-10: hnRNPA3 knockdown in the leukaemia monocytic cell line THP-1

Growth curves of THP-1 cells monitored for 9 days following lentiviral transduction with control (CT) and hnRNPA3 shRNA constructs (576 and 581). Data represent mean ± 1SD from three independent biological replicates (N = 3). Statistical analysis was performed using two-way ANOVA (time × growth) followed by Bonferroni's multiple-comparison test across all time points. **** $p < 0.0001$; ns = not significant.

By contrast, (shRNA Ref.581) markedly impaired growth, reducing cumulative expansion to ~9% compared to control levels at day 9.

Notably, this inverse relationship where the weaker knockdown produced a stronger growth phenotype was unexpected if growth inhibition were driven by on target hnRNPA3 loss. If hnRNPA3 were required for AML cell proliferation, the more efficient shRNA 576 would be expected to induce a more pronounced growth defect. Instead, this discordant pattern is characteristic of sequence dependent off target toxicity, a well recognised limitation of RNA interference approaches.

In U937 cells, the canonical hnRNPA3 band at ~42 kDa clearly visible in HeLa positive control was not detected. Instead, bands appeared between ~30-40 kDa (**Figure 4-11A**).These signals likely represent shorter hnRNPA3 isoforms or post-translationally modified variants, as reported previously in other cell systems (Ma et al. 2002).Therefore, knockdown efficiency in U937 should be interpreted cautiously. Growth assays nevertheless showed that shRNA 576 cells expanded comparably to control, while shRNA 581 produced a consistent growth deficit, with cumulative expansion at day 9 approximately 4-5 fold lower than control (**Figure 4-11B**).

In TF-1 cells, hnRNPA3 KD was confirmed by WB, with reduced protein levels evident for both shRNA576 and shRNA581 relative to GAPDH (**Figure 4-12A**). However, cumulative viable cell counts revealed no significant differences between either KD or the control population across the 9-day time course (**Figure 4-12B**).

Overall, hnRNPA3 protein KD was successfully achieved in all three AML cell lines. Despite robust depletion by shRNA576, no growth inhibition was observed, while shRNA581 reduced growth in THP-1 and U937 but not in TF-1 cells. These findings are inconclusive given the disparate effects of two shRNA constructs; one vector suggest that hnRNPA3 maybe dispensable for AML cell growth and a second shows an inhibitory growth phenotype associated with shRNA581. To provide additional evidence, CRISPR mediated knockout (KO) studies were subsequently performed **4.2.2.1**

4.2.2.1 Knockout of hnRNPA3 has no effect on cell growth

The shRNA-based KD experiments described in section (**4.2.2**) gave inconsistent results, with shRNA576 showing no effect and shRNA581 producing reduced proliferation. To exclude potential off-target effects, CRISPR-Cas9 KO was used as an independent approach.

A

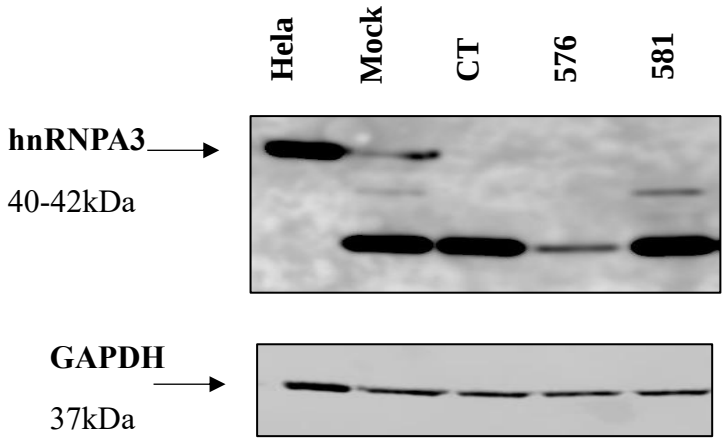

B

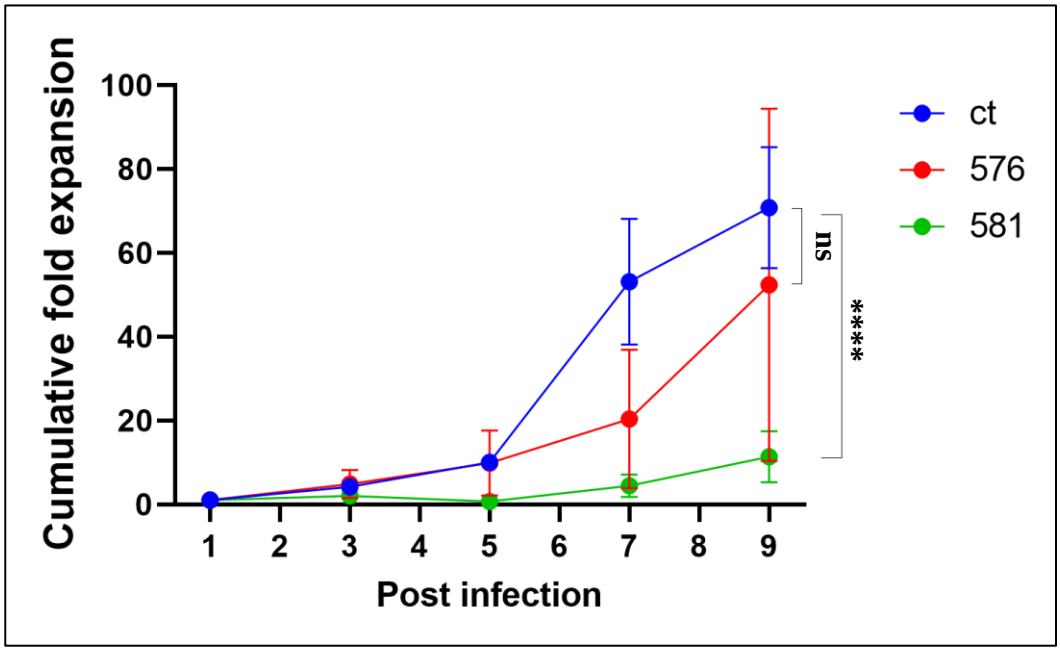

Figure 4-11: Effect of hnRNPA3 knockdown on growth of U937 cells showing no significant impact

A Western blot analysis of hnRNPA3 protein expression in U937 cells transduced with shRNA constructs (576 and 581). HeLa was used as a positive control (PC). CT refers to construct 497.U937 samples (Mock, CT, 576, 581) showed lower-molecular-weight bands between 30 and 40 kDa. GAPDH (37 kDa) was used as a loading control. **B** Growth curves of U937 cells monitored for 9 days following transduction with control and hnRNPA3 shRNA constructs. Data represent mean ±1 SD from three independent biological replicates (N = 3). Statistical significance was assessed using two-way ANOVA (time × growth) with Bonferroni's multiple-comparison test across all time points; **** $p < 0.0001$; ns = not significant.

A

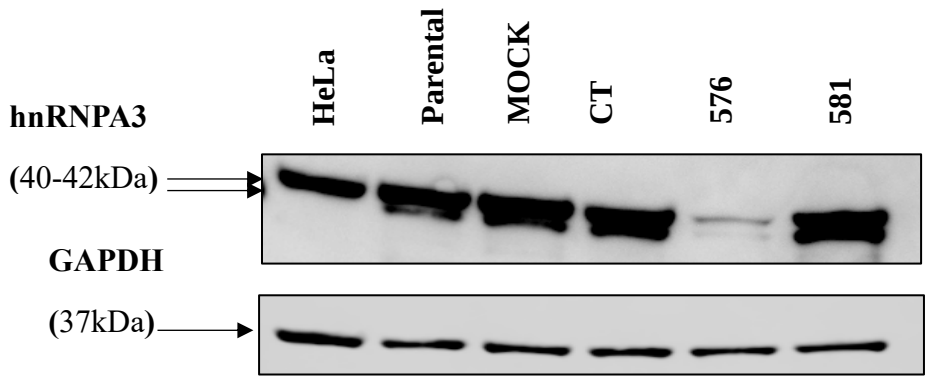

B

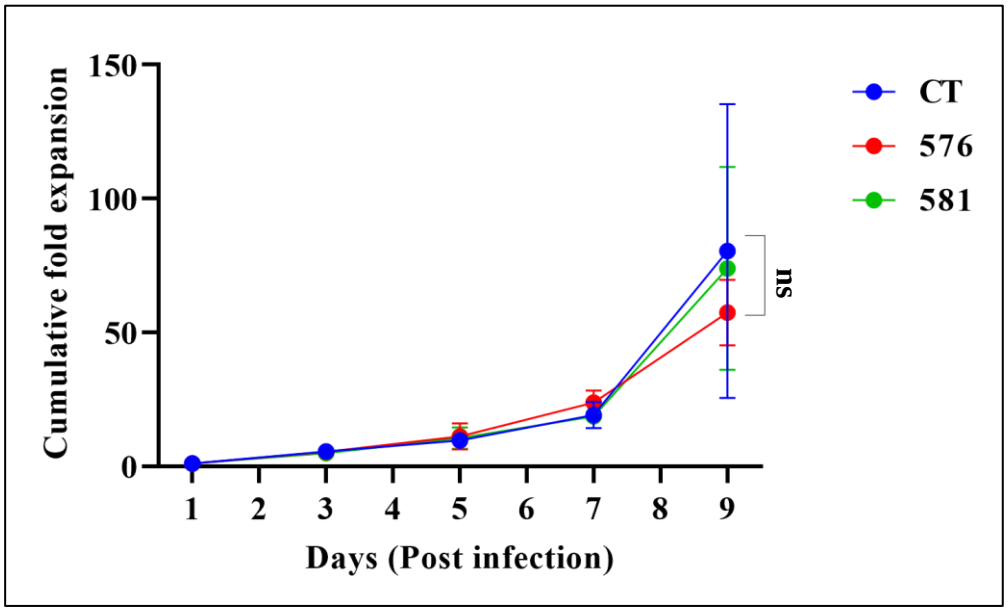

Figure 4-12: hnRNPA3 is knocked down in cell line TF-1 showed no effect on the growth

A Western blot analysis of hnRNPA3 protein expression in TF-1 cells transduced with shRNA constructs (576 and 581). HeLa was used as a positive control (PC). CT refers to construct 497. GAPDH (37 kDa) was used as a loading control. **B** Growth curves of TF-1 cells monitored for 9 days following transduction with control or hnRNPA3 shRNA constructs. Data represent mean ±1 SD from three independent biological replicates (N = 3). Statistical significance was assessed using two-way ANOVA (time × growth) with Bonferroni's multiple-comparison test across all time points; ns = not significant.

THP-1 (**Figure 4-13A**) and OCI-AML2 (**Figure 4-14A**) cells were transduced with two sgRNA constructs referenced (610 and 611) targeting hnRNPA3, followed by puromycin selection for four days. WB confirmed that construct 610 produced a substantial reduction in hnRNPA3 protein (~70% decrease relative to control), whereas construct 611 was less efficient and only achieved partial depletion. GAPDH was used as a loading control (**Figure 4-13B**) (**Figure 4-14B**).

Cell growth was then monitored over a nine-day period. In both THP-1 and OCI-AML2, growth of KO cells were indistinguishable from control, regardless of the construct used; two-way ANOVA analysis confirmed no significant differences in fold expansion between KO and control populations.

Together, these data show that CRISPR-Cas9 mediated depletion of hnRNPA3 does not affect the growth of AML cell lines. This finding supports the use of shRNA and indicates that hnRNPA3 is dispensable for AML growth under standard culture conditions. It is likely shRNA (Ref 581) is an off-target effect (see Discussion).

4.2.3 Overexpression of hnRNPA3 does not alter proliferation of AML cells

To further examine the function of hnRNPA3, overexpression studies were carried out to determine if raising protein levels had any measurable impact on growth given that RNA binding proteins are known to influence RNA stability, processing, and translation, all of which can feed into growth regulation. WB analysis confirmed modest elevation of hnRNPA3 expression in U937 and NOMO-1 cells transduced with the overexpression construct Ref.(613) compared with controls (**Figure 4-15A and B**) (**Figure 4-16A and B**). However, the magnitude of overexpression achieved was limited, and did not represent a strong gain of function perturbation. Consistent with this, growth curves showed that both U937 and NOMO-1 cells expanded at rates indistinguishable from control populations across the 7-day monitoring period (**Figure 4-15C**) (**Figure 4-16C**).

Given the absence of robust hnRNPA3 overexpression, these data do not support strong conclusions regarding gain of function effects on AML cell growth. Nevertheless, when interpreted alongside the knockdown experiments, which demonstrated that substantial hnRNPA3 depletion does not impair proliferation, the overall data indicate that hnRNPA3 levels are not rate-limiting for AML cell growth under basal culture conditions.

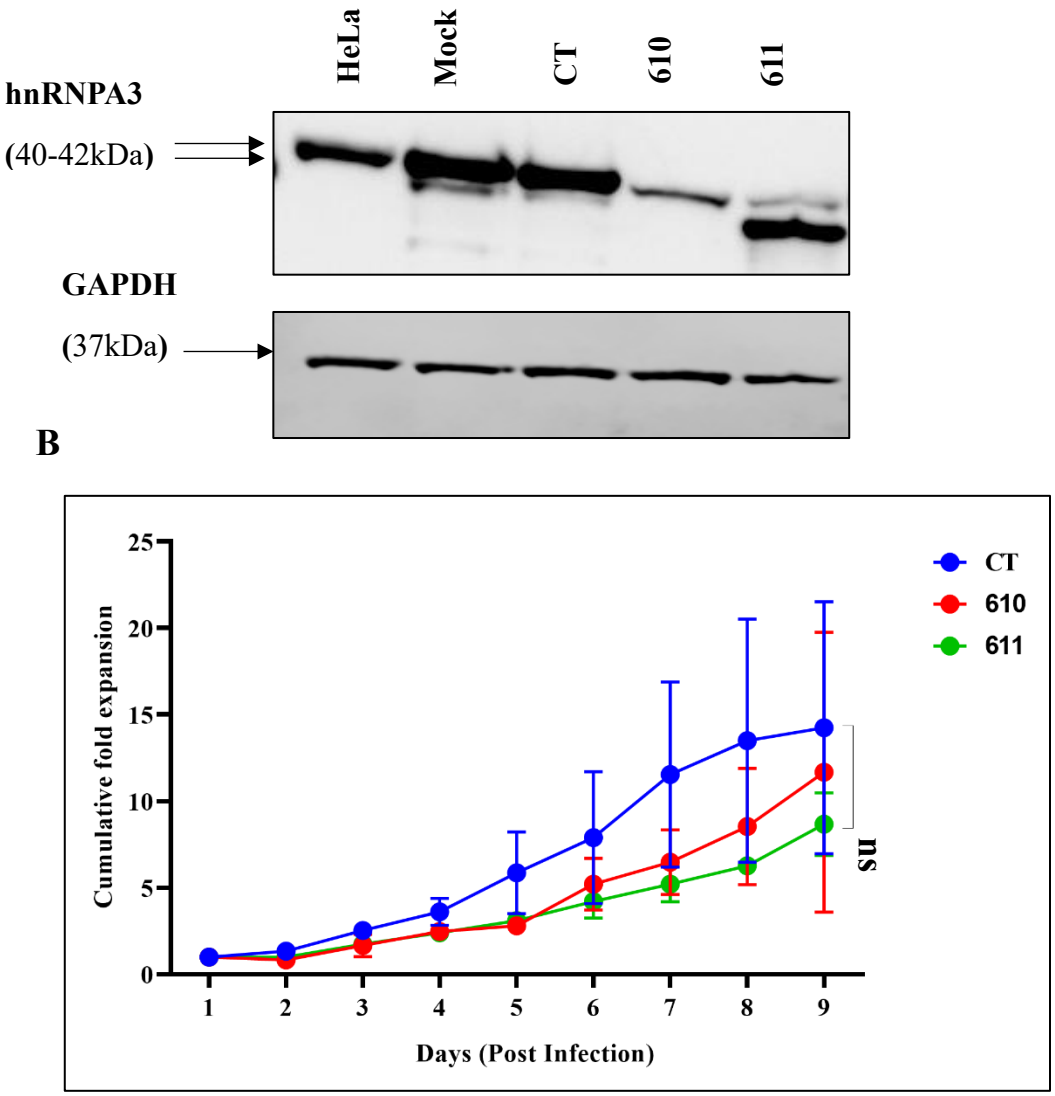

Figure 4-13: CRISPR CAS-9 mediated knockout of hnRNPA3 in THP-1 cells has no significant effect on growth

A WB analysis of hnRNPA3 protein expression in THP-1 cells transduced with CRISPR Cas-9 sgRNA constructs 610 and 611. GAPDH (37 kDa) was used as a loading control. HeLa was included as a positive control (PC). CT refers to control construct (407). B Growth curves of THP-1 cells monitored for 9 days following transduction with control or hnRNPA3 knockout constructs (610 and 611). Data represent mean ± 1SD from three independent biological replicates (N = 3). Statistical analysis was performed using two-way ANOVA (time × growth) followed by Bonferroni's multiple-comparison test across all time points; ns = not significant.

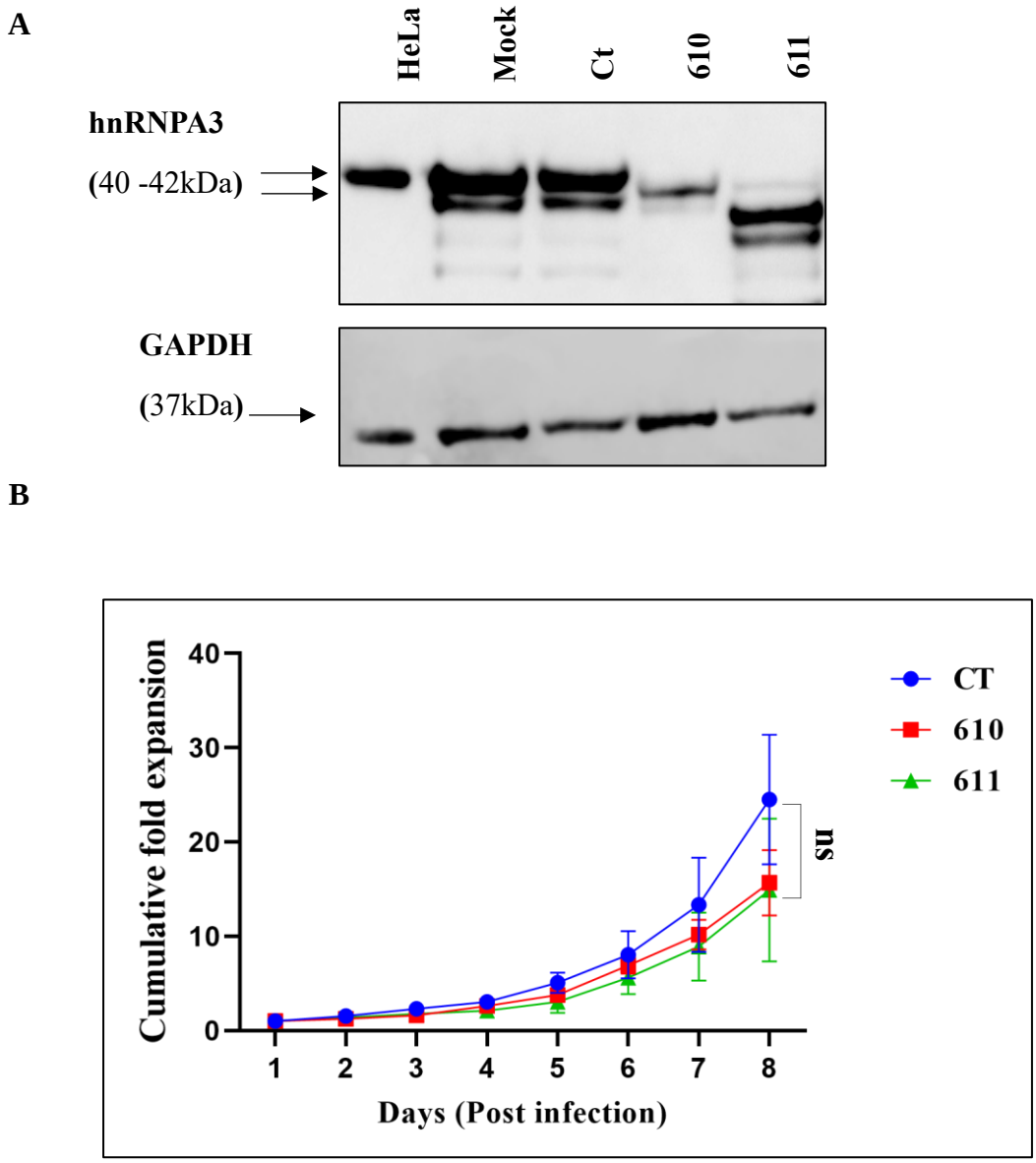

Figure 4-14: CRISPR CAS-9 mediated knockout of hnRNPA3 shows no significance in OCIAML2

A WB analysis of hnRNPA3 protein expression in OCI-AML2 cells transduced with CRISPR-Cas9 knockout constructs Ref. 610 and 611. GAPDH (37 kDa) was used as a loading control. HeLa was included as a positive control (PC). CT refers to control construct (407). **B** Growth curves of OCI-AML2 cells monitored for 8 days following transduction with control or hnRNPA3 KO constructs (610 and 611). Data represent mean ± 1SD from three independent biological replicates (N = 3). Statistical analysis was performed using two-way ANOVA (time × growth) followed by Bonferroni's multiple-comparison test across all time points; ns = not significant.

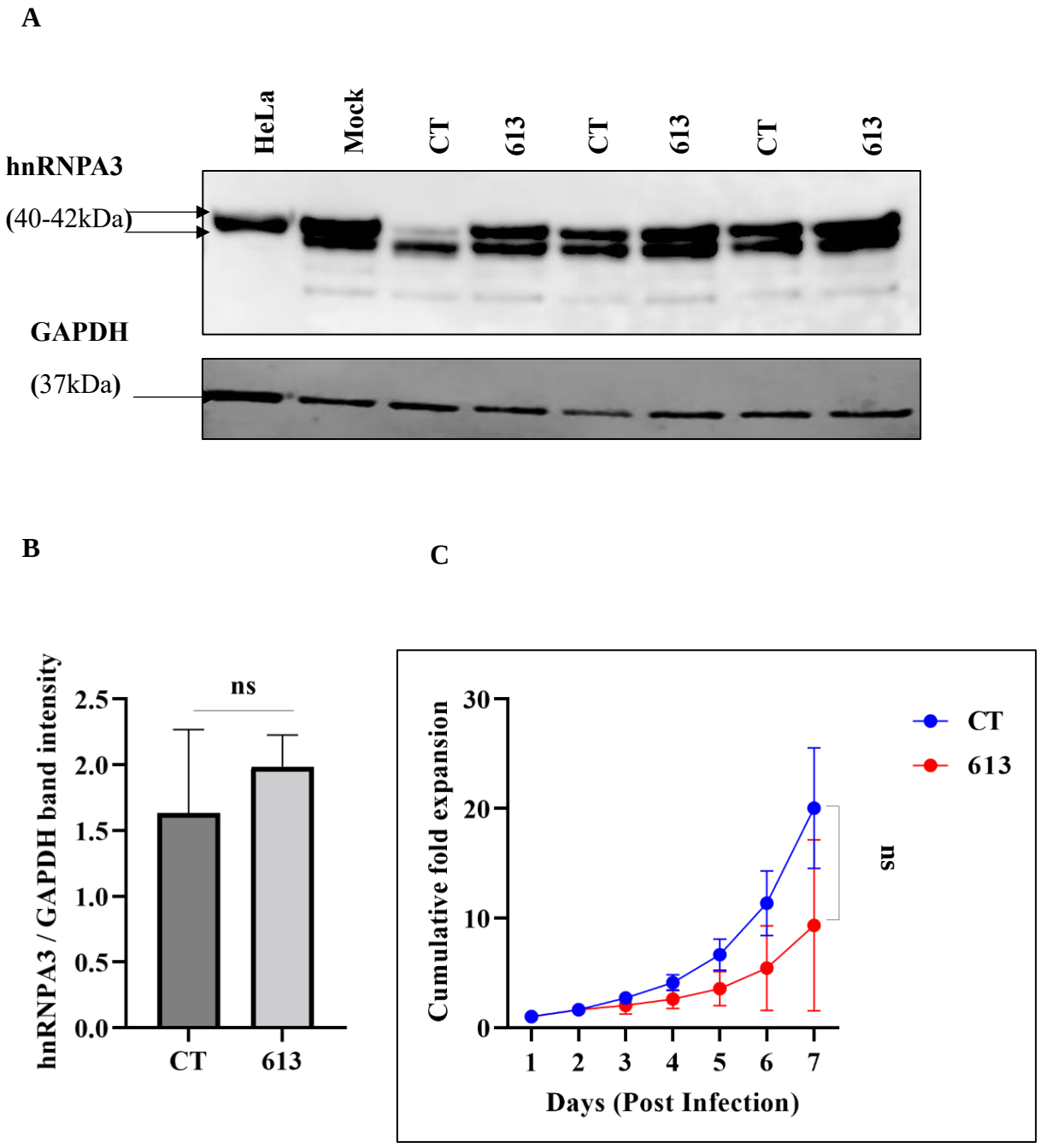

Figure 4-15: Overexpression of U937 shows no significance on growth

A WB analysis assessing hnRNPA3 in U937 cells following transduction. **A** distinct band was detected at 40-42 kDa in hnRNPA3-OE cells. HeLa cell line was used as a positive control (PC). CT refers to construct 407 and hnRNPA3 OE refers to construct 613.**B** Densitometric quantification of hnRNPA3analysis using ImageJ normalised to GAPDH. Bars show mean with + 1SD (N = 3 biological replicates). Statistics by one-way ANOVA with Dunnett's post-hoc vs CT; no statistically significant increase was observed. **C** Growth curves of U937 cells monitored for 7 days after transduction with control or hnRNPA3-OE constructs. Data represent mean ± 1SD from three independent biological replicates (N = 3). Statistical significance was assessed using two-way ANOVA (time × growth) with Bonferroni's multiple-comparison test; no statistically significant increase was observed.

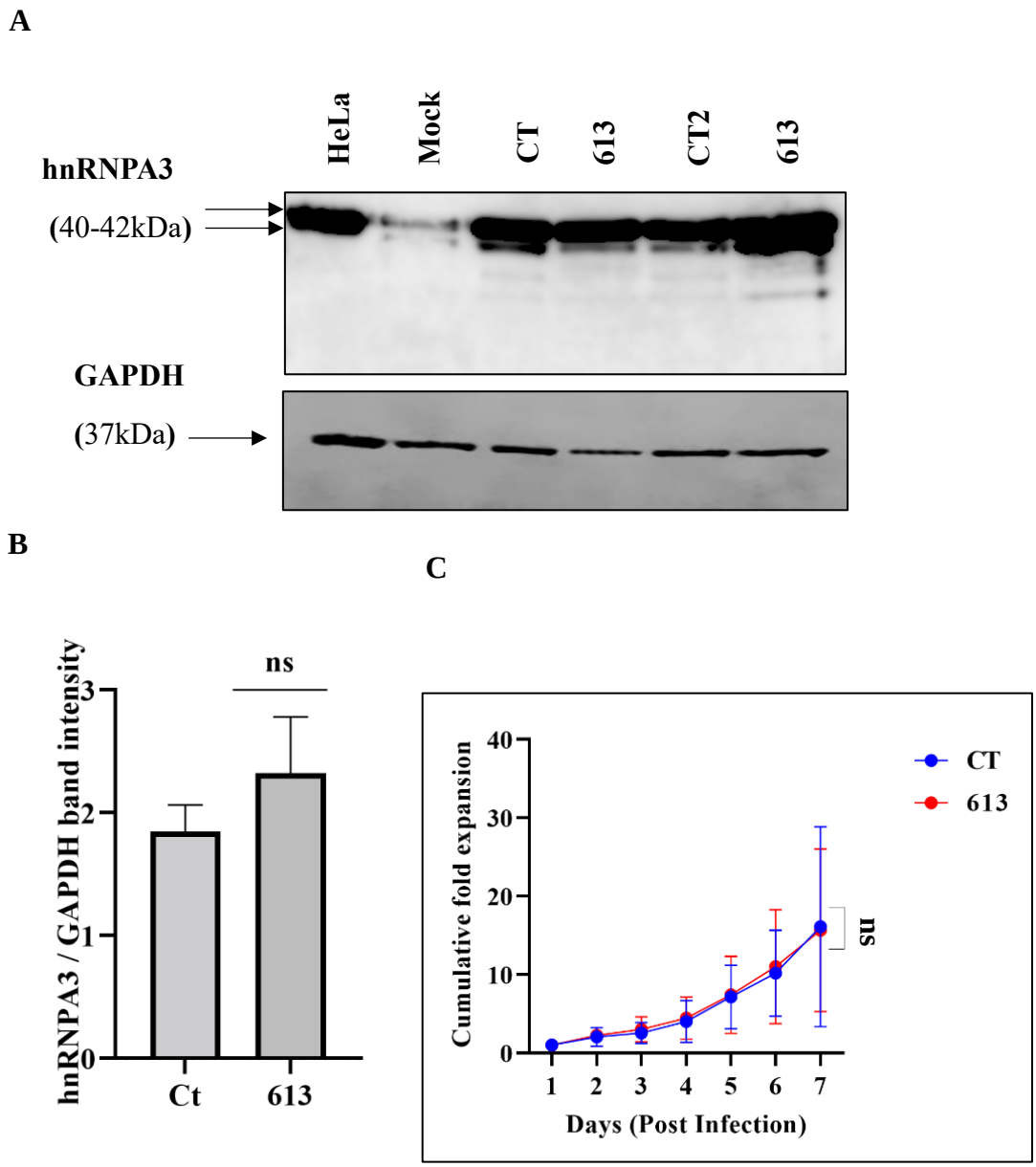

Figure 4-16: Overexpression of hnRNPA3 in NOMO-1

A WB assessing hnRNPA3 in NOMO-1 cells following transduction. **A** protein band at ~42 kDa was detected in hnRNPA3-OE cells. HeLa cell line was included as a positive control (PC). CT refers to construct 407, and hnRNPA3 OE corresponds to construct 613.**B** Densitometry analysis performed using ImageJ. Relative hnRNPA3 expression was determined by normalising band intensity to GAPDH. Data represent mean + 1SD (N=3) Statistics by one-way ANOVA with Dunnett's post-hoc vs CT; * $p < 0.05$. **C** The growth curve of NOMO-1 cells stably transduced with hnRNPA3 (construct Ref. 613) compared with the control (CT). Cell counts were recorded daily for 7 days. Data are presented as mean ± 1SD from (N=3) independent experiments. A two-way ANOVA with Bonferroni's multiple comparisons was performed; no significant differences were observed in proliferation (ns).

Taken together, these findings suggest that hnRNPA3 is unlikely to function as a primary regulator of AML cell proliferation. Instead, its biological role may be context dependent and confined to specialised cellular processes, such as RNA metabolism or stress-response pathways, rather than day to day growth control (see Discussion).

4.2.4 hnRNPA0 protein exhibits limited expression across AML cell lines

WB was used to examine hnRNPA0 expression across a panel of AML cell lines, with HeLa included as a positive control. Expression was highly restricted. A protein band at ~32 kDa was detected only in KG1a and HEL, while the other lines (THP-1, OCI-AML2, TF-1, U937, SKNO-1, and MV4-11) showed little to no detectable protein **(Figure 4-17A)**. KG1a was selected for KD experiments, since it expresses hnRNPA0 endogenously, while THP-1 and U937, which showed no detectable expression, were used for overexpression studies.

4.2.5 hnRNPA0 KD in AML cell line reduced cell growth

Two shRNA constructs (Refs 600 and 605) were used to suppress hnRNPA0 expression. Both were chosen after small-scale optimisation during this work, which confirmed that they effectively reduced hnRNPA0 mRNA and protein. Lentiviral transduction in KG1a cells gave high GFP positivity, showing good infection efficiency. Western blotting confirmed a strong loss of hnRNPA0 protein in both knockdowns compared with the control (**Figure 4-18A**), with construct 605 giving a slightly deeper reduction.

Across seven days of monitoring, cell counts showed a steady drop in viable cells in both knock-downs relative to control (**Figure 4-18B**). The pattern points to slower proliferation when hnRNPA0 is reduced, suggesting that the protein is needed to maintain normal growth in A0 positive AML cells. To examine why hnRNPA0 knock-down reduced KG1a cell growth, cell-cycle profiles were analysed. Both shRNA constructs caused a marked accumulation of cells in the G2/M phase, while the proportions in G1 and S phases remained largely unchanged (**Figure 4-19A**).This pattern indicates a delay at the G2/M transition in hnRNPA0-depleted cells. Apoptosis was then measured using the ApoTracker assay. Both knock-down groups showed higher proportions of apoptotic cells than the control, with shRNA 605 producing the stronger effect (**Figure 4-19A, Figure 4-19B**). Together, these results show that loss of hnRNPA0 leads to G2/M accumulation and enhanced apoptosis, providing a cellular explanation for the reduced proliferation observed in KG1a cells.

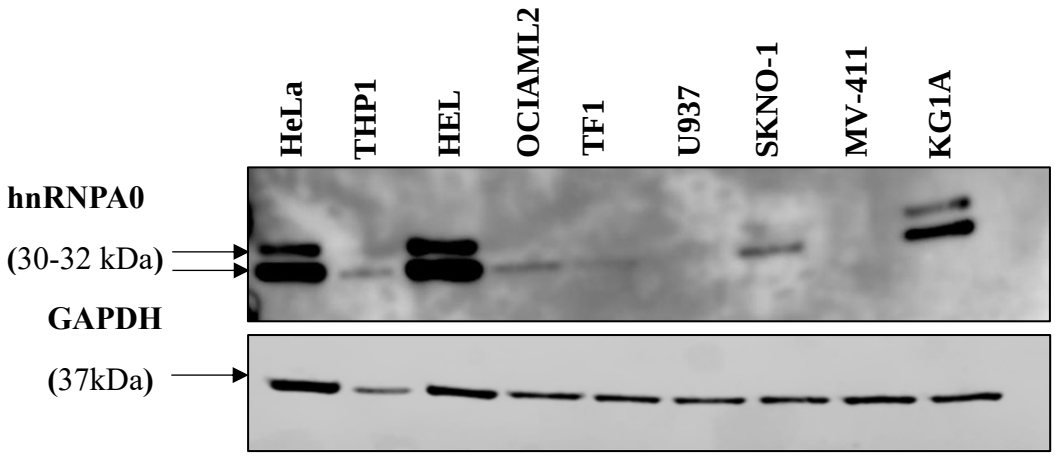

Figure 4-17: hnRNPA0 shows variable protein expression across AML cell lines

WB analysis showing hnRNPA0 protein levels in a panel of AML cell lines (THP-1, HEL, OCI-AML2, TF-1, U937, SKNO-1, MV-4-11, and KG1a). HeLa cells were included as a positive control (PC). hnRNPA0 was detected as a doublet band around 30–32 kDa. GAPDH (37 kDa) was used as a loading control. Data are representative of N = 3 independent experiments.

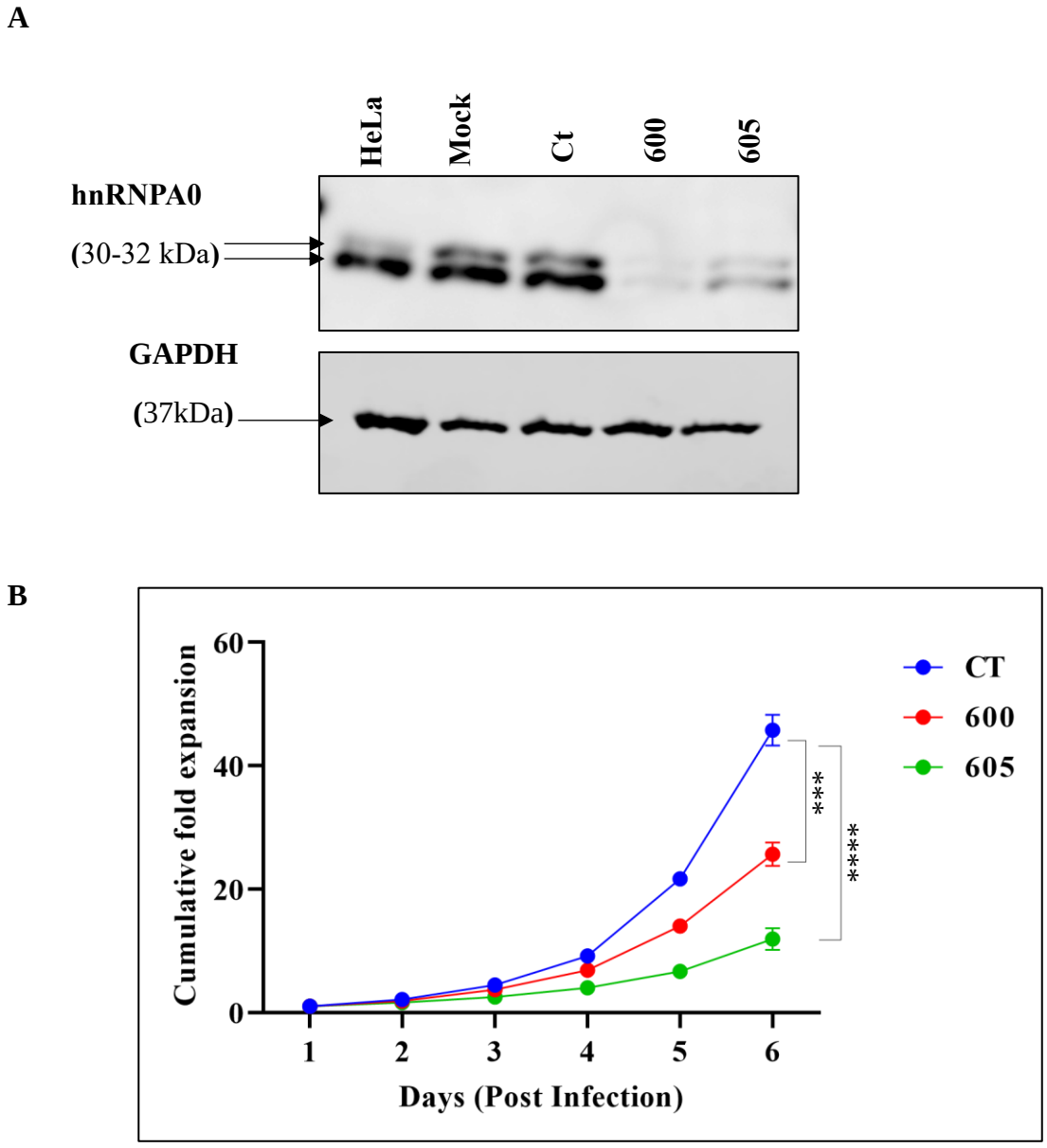

Figure 4-18:hnRNPA0 knockdown impairs KG1a cell growth

A WB showing hnRNPA0 protein expression in KG1a cells transduced with control (CT; construct 497) and hnRNPA0 shRNA constructs (Ref. 600 and 605). HeLa cells served as a positive control (PC). A protein band at 30-32 kDa confirmed hnRNPA0 detection, and GAPDH (37 kDa) was used as a loading control. **B** Growth curves of KG1a cells monitored for 6 days following lentiviral transduction with control or hnRNPA0 knockdown constructs. Data represent mean ± 1SD from four independent biological replicates (N = 4). Statistical significance was assessed using two-way ANOVA (time × growth) with Bonferroni's multiple-comparison test; *** $p < 0.001$, **** $p < 0.0001$.

A

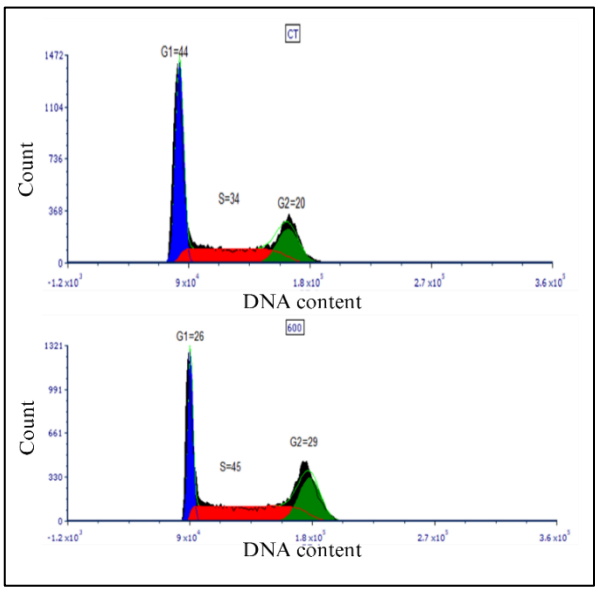

B

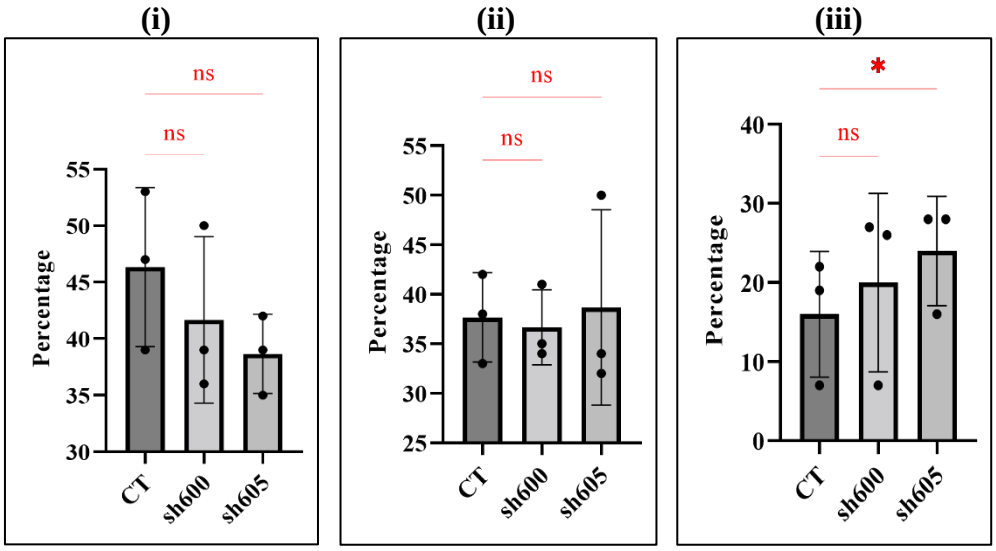

Figure 4-19: Effects of hnRNPA0 knockdown on cell cycle on KG1a

Example of quantification of cell-cycle phase distribution **A** Representative DNA-content histograms illustrating G1, S, and G2/M phases in control (CT) and hnRNPA0 knockdown (shRNA600) KG1a cells.. **B** Quantification of cell-cycle phase distribution (G1 (i), S (ii), G2/M (iii) ratios) showing accumulation of cells in G2/M following hnRNPA0 depletion. Bars represent mean + 1 SD from three biological replicates (N = 3). Data were analysed by repeated-measures one-way ANOVA (Tukey's multiple-comparison test); p * < 0.01 for G2 vs C.

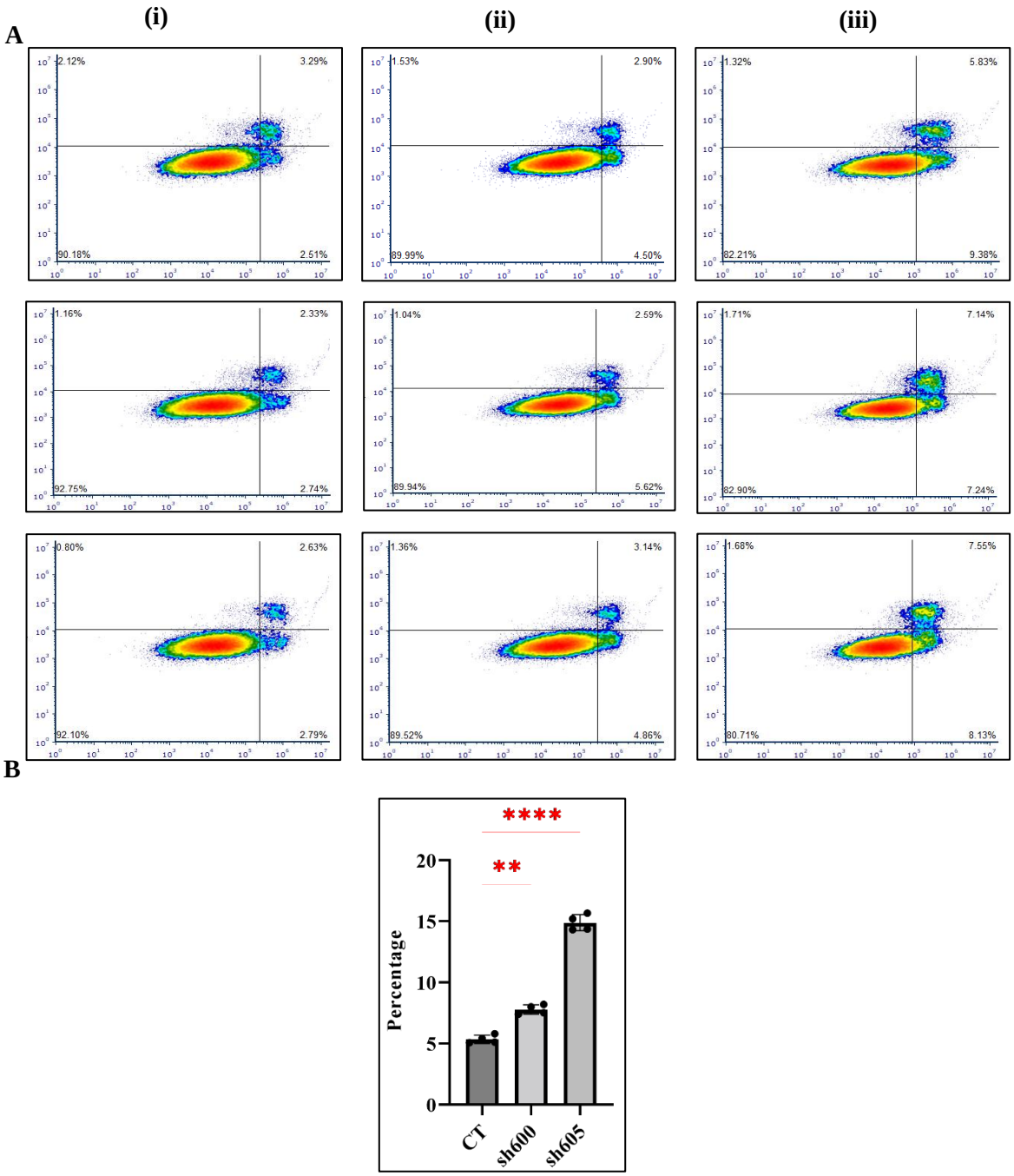

Figure 4-20: Effects of hnRNPA0 knockdown on apoptosis on KG1a

A Apoptosis analysis using ApoTracker / Viability-dye propidium iodide staining. Two-parameter density plots display apoptosis-marker fluorescence (ApoTracker, x-axis) versus viability-dye fluorescence PI (y-axis). Quadrants denote viable (ApoTracker$^-$/PI$^-$), early apoptotic (ApoTracker$^+$/PI$^-$), and late apoptotic/necrotic (ApoTracker$^+$/PI$^+$) populations. Representative plots are shown for (i) control, (ii) shRNA1 (600), and (iii) shRNA2 (605), quadrant percentages are displayed. **B** Quantification of total apoptosis (early + late apoptotic following hnRNPA0 KD. Bars represent mean +1SD from four replicates (N = 4). Statistical analysis was performed using one-way ANOVA with Dunnett's multiple-comparison test comparing each knockdown to control. A significant increase was observed in sh600 (**p < 0.01) and was more pronounced in sh605 (****p < 0.0001) relative to control.

.

4.2.6 hnRNPA0 overexpression is efficiently achieved in AML cell lines but does not alter proliferation

Stable overexpression hnRNPA0 was performed using the PincoGFP-hnRNPA0 construct (Ref. 490), which had been previously sequence-verified. Retrovirus generated from Phoenix producer cells was used to transduce THP-1 and U937 cells. Efficient viral transduction was confirmed by flow cytometric detection of GFP expression, with a high proportion of GFP^+ cells observed across replicates (≈45–61%)(**Figure 4-20A**).

Despite efficient transduction, enforced hnRNPA0 overexpression at the protein level was modest and variable, limiting the extent of gain-of-function achieved in these models. Growth assays were therefore conducted to determine whether enforced hnRNPA0 expression under these conditions altered AML cell proliferation. THP-1 cells were monitored daily for eight days, and U937 cells every second day up to day 9. In both models, growth kinetics of hnRNPA0-expressing cells were indistinguishable from GFP controls throughout the observation period (**Figure 4-21B**) (**Figure 4-22B**).

Given the absence of robust hnRNPA0 overexpression, these data do not support strong conclusions regarding gain of function effects on AML cell growth. However, when interpreted alongside knockdown experiments in hnRNPA0 positive models, where depletion significantly impaired proliferation and survival, the findings reinforce the context dependent requirement for hnRNPA0 in AML rather than a universal growth-promoting role.

4.3 Discussion

4.3.1 Overview

AML frequently exploits RNA binding protein pathways to sustain blast survival, yet which RBPs are truly required for cellular fitness, as opposed to merely reflecting disease state, remains unclear. Understanding these dependencies helps distinguish context specific survival factors from incidental expression markers. In this chapter, two A/B family candidates prioritised in Chapter 3, hnRNPA3 and hnRNPA0, were interrogated under baseline in vitro culture conditions using three orthogonal approaches (shRNA, CRISPR-Cas9, and overexpression). Across assays, hnRNPA3 perturbation (shRNA knockdown or CRISPR editing) showed no significant change in cumulative viable cell counts over a nine day growth period relative to control **(Figure 4-10**) and (**Figure 4-11**).

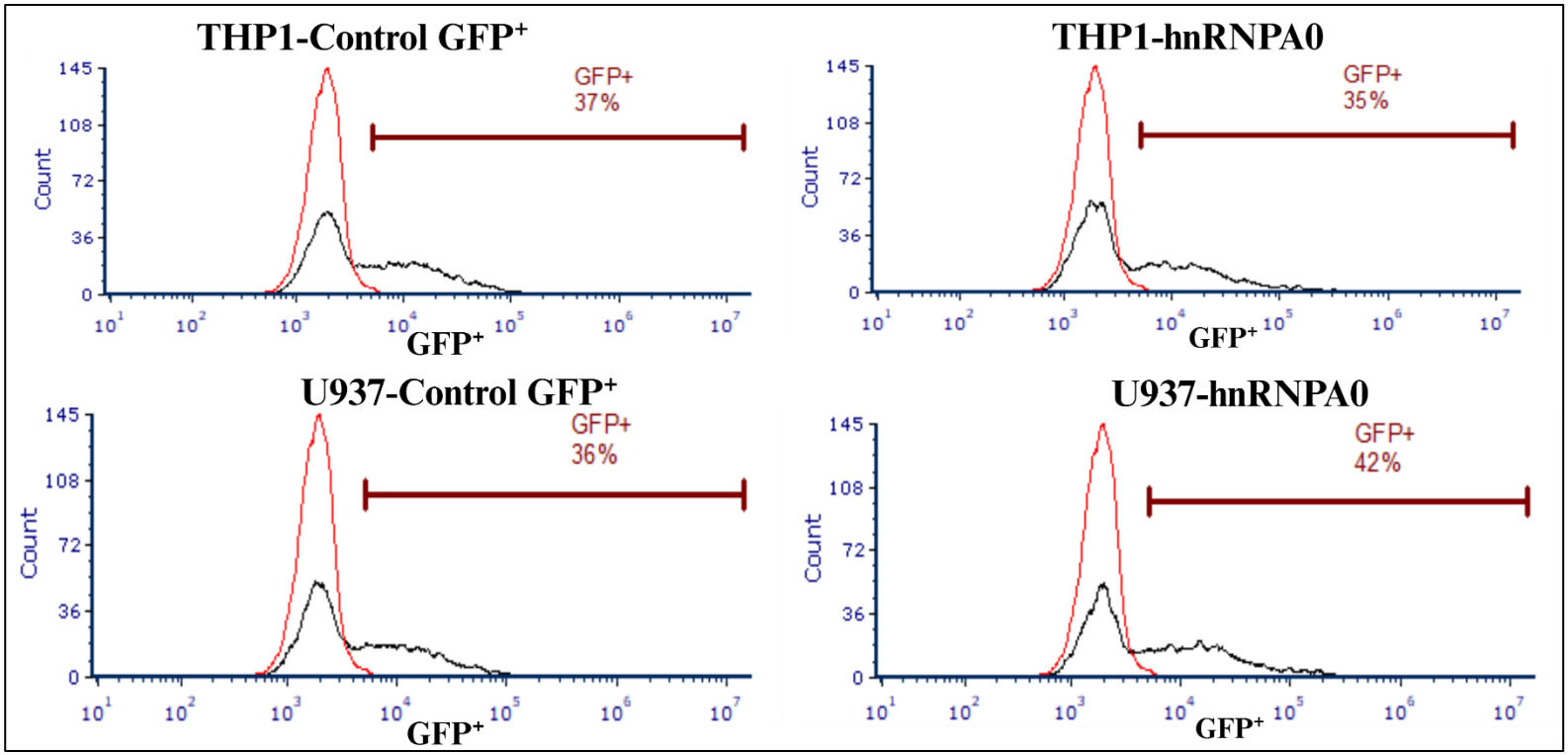

Figure 4-21: Flow cytometric verification of hnRNPA0 overexpression in THP-1 and U-937 cells

THP1 and U937 cells were transduced CT GFP$^+$ vector and an hnRNPA0 expression vector carrying a GFP. Histograms show GFP fluorescence intensity from viable single-cell populations. The red trace represents GFP fluorescence from transduced cells, while the black trace indicates background autofluorescence from untraduced (mock) cells. The GFP$^+$ gate is marked by the bracket, and the percentage of GFP$^+$ events is annotated on each plot. Data are representative of N = 3 independent experiments.

A

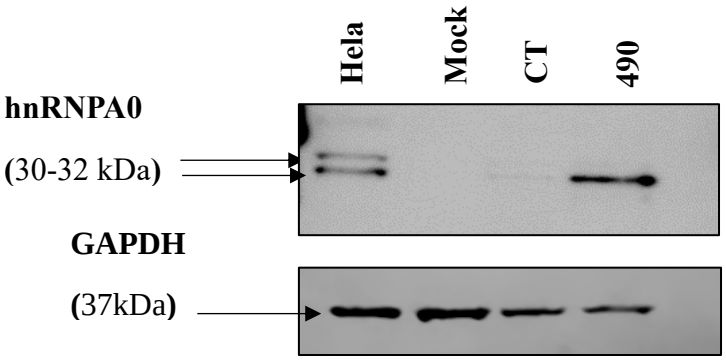

B

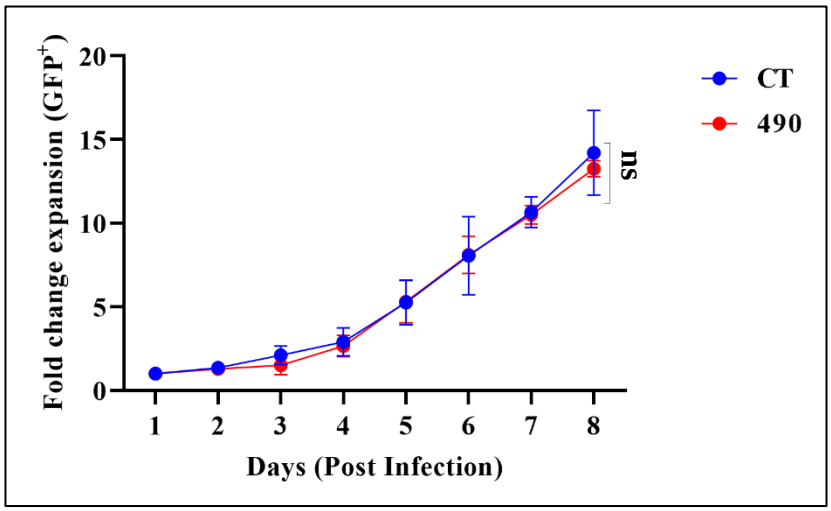

Figure 4-22: Enhanced expression of hnRNPA0 in THP-1 cells does not effect growth

A WB confirming hnRNPA0 overexpression in THP-1 cells transduced with the overexpression construct (Ref. 490). HeLa cells served as a positive control (PC). Control (CT) refers to construct 99 (vector-only). A band at ~30–32 kDa was detected in hnRNPA0-OE cells. GAPDH (37 kDa) was used as a loading control. **B** Growth curves of THP-1 cells monitored for 8 days following transduction with control or hnRNPA0 overexpression constructs. Data represent mean ± 1SD from three independent biological replicates (N = 3). Statistical analysis was performed using two-way ANOVA (time × growth) with Bonferroni's multiple-comparison test across all time points; ns = not significant.

A

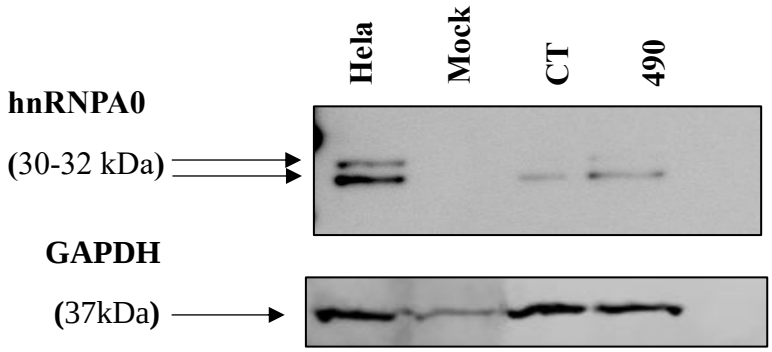

B

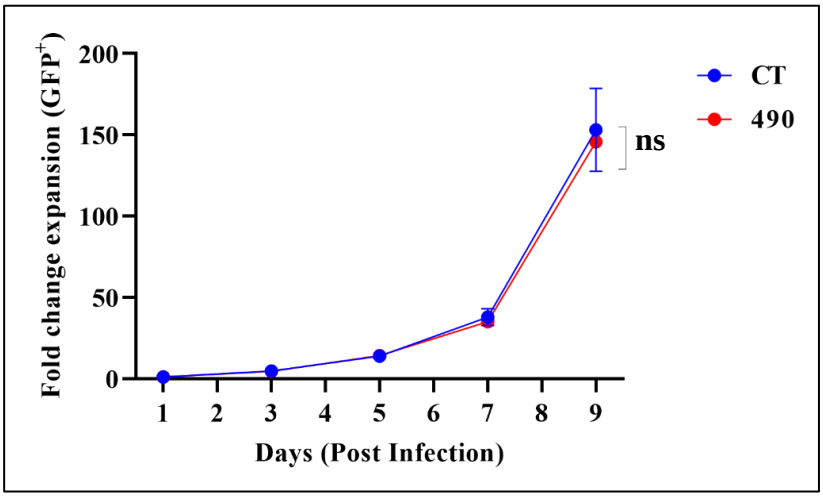

Figure 4-23: Enhanced expression of hnRNPA0 in U937 cells does not effect on growth

A WB analysis confirming hnRNPA0 overexpression in U937 cells transduced with the overexpression construct (Ref. 490). HeLa cells served as a positive control (PC). Control (CT) refers to construct 99 (vector-only). GAPDH (37 kDa) was used as a loading control. A distinct band at ~30–32 kDa was detected in the hnRNPA0-OE condition. **B** Growth curves of U937 cells monitored for 9 days following transduction with control and hnRNPA0 overexpression constructs. Data represent mean ± 1SD from three independent biological replicates (N = 3). Statistical analysis was performed using two-way ANOVA (time × growth) with Bonferroni's multiple-comparison test across all time points; ns = not significant.

Overexpression of hnRNPA3 similarly failed to enhance short term proliferation. Taken together, these data indicate that hnRNPA3 is dispensable for baseline AML proliferation and short term survival under the experimental conditions tested. Any association between elevated hnRNPA3 expression and poor clinical outcome is therefore more likely to reflect disease context or stress dependent functions rather than a direct growth dependency.

By contrast, hnRNPA0 displayed restricted expression across AML models but showed clear functional importance in hnRNPA0 positive cells. Reducing hnRNPA0 consistently resulted in impaired proliferation, accumulation at the G2/M phase, and increased apoptotic markers, in line with its established role in stabilising checkpoint-associated transcripts such as GADD45α (Lal et al. 2004). Importantly, ectopic re-expression of hnRNPA0 in hnRNPA0 negative cell lines did not confer a proliferative advantage, indicating a context dependent requirement rather than a universal growth promoting role.

Overall, this chapter highlights a clear functional divergence between the two RBPs studied: hnRNPA3 appears largely neutral with respect to baseline proliferation in standard culture conditions, whereas hnRNPA0 supports normal growth and survival specifically in hnRNPA0 expressing AML cells. This distinction provides the rationale for the transcriptomic dissection of hnRNPA0 loss presented in Chapter **5** (**Figure 4-23)** summarises the hnRNPA3/hnRNPA0 experimental workflow employed in Chapter **4**.

4.3.2 hnRNPA3 is dispensable for baseline AML growth

Large patient cohorts consistently associate higher hnRNPA3 expression with adverse clinical outcome (Cancer Genome Atlas Research et al. 2013). However, in this study, no conclusive evidence was found that modulation of hnRNPA3 levels alters baseline proliferation of AML cell lines. Across three orthogonal perturbation strategies shRNA mediated knockdown, CRISPR-Cas9 editing, and the overexpression hnRNPA3 perturbation did not produce a reproducible growth phenotype under standard culture conditions.

Knockdown results were discordant. shRNA 576 achieved robust protein KD (~90%) without affecting proliferation, whereas shRNA 581 caused growth inhibition despite weaker knockdown. This pattern is characteristic of sequence dependent off target toxicity rather than true on target dependency, a well recognised limitation of RNAi based approaches (Bartoszewski and Sikorski 2019; Chen et al. 2021; Goel and Ploski 2022). Consistent with this interpretation, neither construct significantly altered viable cell expansion in TF-1 cells.

CRISPR-Cas9 editing using guides 610 and 611 reduced hnRNPA3 protein levels by approximately 70% in THP-1 and OCI AML2 cells (**Figure 4-13, Figure 4-14**) without impacting growth. While incomplete knockout or the generation of hypomorphic or escape alleles cannot be excluded through mechanisms such as exon skipping or alternative translation initiation (Yuen et al. 2017; Wang et al. 2024)

The concordance between CRISPR editing and strong shRNA mediated depletion without a growth phenotype strengthens the inference that hnRNPA3 is not required for baseline AML proliferation.

Ectopic overexpression of hnRNPA3 in U937 and NOMO-1 cells (**Figure 4-15, Figure 4-16**) did not result in a measurable increase in short term growth. However, the modest impact on overall protein abundance limits the strength of gain of function conclusions and suggests that overexpression approaches may not fully capture isoform-specific or post translationally regulated functions (Prelich 2012).

Taken together, these independent perturbation approaches indicate that hnRNPA3 is dispensable for AML cell growth under basal in vitro conditions. Importantly, this finding does not exclude context dependent roles for hnRNPA3 under conditions of genotoxic stress, differentiation pressure, or specific genetic backgrounds, which may better reflect its association with poor clinical outcome (Schuschel et al. 2020; Amano et al. 2021; Ren et al. 2021).

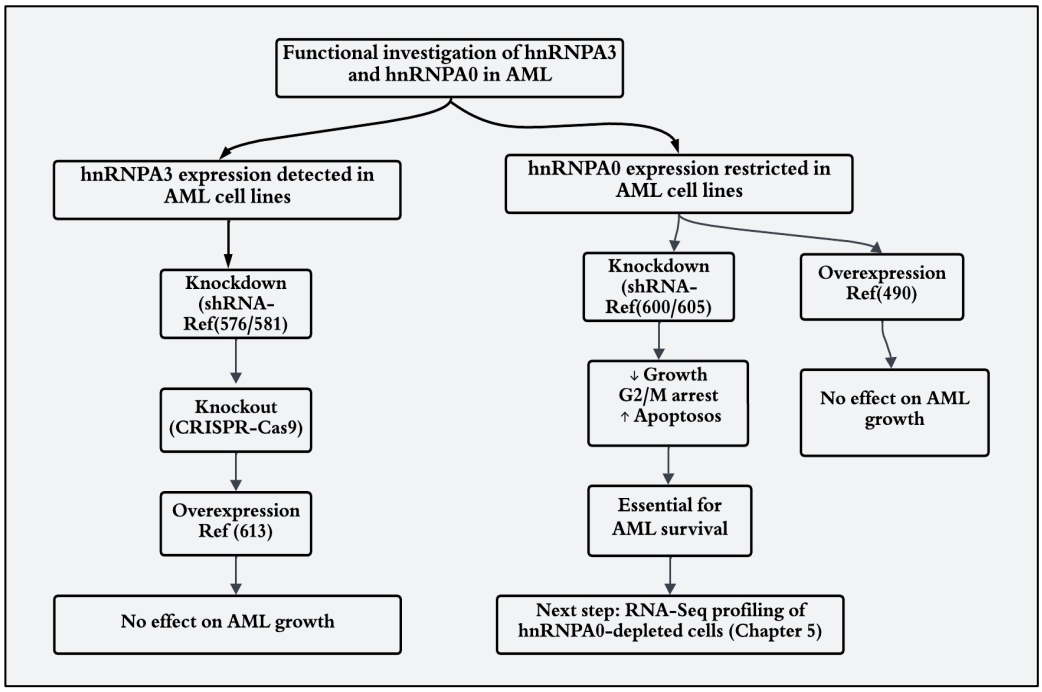

Figure 4-24 Functional workflow of hnRNPA3 and hnRNPA0 analysis in AML cell lines

Based on multi criteria ranking, hnRNPA3 and hnRNPA0 were selected for experimental study. To assess their roles in AML biology, I applied a systematic workflow combining expression screening, knockdown, knockout, and overexpression approaches across a panel of AML cell lines. The data demonstrated that hnRNPA3, despite variable expression and prognostic association, was dispensable for AML growth. In contrast, hnRNPA0, although restricted in its expression to a subset of AML models, showed a reproducible impact on cellular fitness, with knockdown impairing proliferation and cell survival, accompanied by G2/M accumulation and increased apoptotic signalling. These findings identify hnRNPA0 as a context dependent regulator of AML cell growth and survival and establish the rationale for transcriptomic profiling of hnRNPA0 depleted cells presented in Chapter 5.

4.3.3 Reconciling the hnRNPA3 paradox: biomarker versus conditional effector (and isoforms)

Across AML models, hnRNPA3 often appeared as two closely migrating protein bands at ~40-42 kDa, most clearly in U937 cells. This pattern suggests that the protein exists in several isoforms or carries post-translational modifications that alter its electrophoretic mobility, stability, or subcellular localisation. However, the present knockdown and overexpression approaches did not distinguish between these potential isoforms. The shRNA constructs were designed against shared coding regions and therefore are likely to reduce total hnRNPA3 levels rather than selectively targeting individual variants. Likewise, the overexpression construct represents a single annotated transcript and may not fully recapitulate the endogenous isoform spectrum. If only one of these forms is linked to the poor-prognosis signal seen in patients, then standard knockdown or over-expression methods may have masked the relevant species. Future work should therefore separate these forms more precisely for example, by treating samples with phosphatase to identify modified bands, designing CRISPR guides that remove one isoform at a time, or using cell fractionation and proteomic mapping to determine which pool (nuclear or cytoplasmic) carries the key function.

Although altering hnRNPA3 levels had no measurable effect on cell proliferation in the models tested, this does not exclude isoform specific or context dependent functions that were not captured in the assays performed**.** I did not examine its influence on differentiation, drug response, or tolerance to stress. It is therefore possible that hnRNPA3 acts primarily as a regulator of RNA-processing networks rather than as a direct driver of proliferation (Schuschel et al. 2020). This interpretation is consistent with observations in other cancers where elevated hnRNPA3 expression correlates with aggressive disease yet does not establish a clear survival dependency in vitro (Amano et al. 2021; Ren et al. 2021).

Mechanistic evidence from t (8;21) AML supports this view. Liu et al. (2024) showed that hnRNPA3 recognises the m⁶A methylation mark on *RUNX1::RUNX1T1* pre mRNA and helps control its splicing and differentiation. Because m⁶A is a reversible RNA modification that shapes transcript stability, this finding connects hnRNPA3's poor outcome association to altered splicing within specific fusion contexts, rather than to a universal growth effect. Notably, none of the AML cell lines used in this study harbour the t(8;21) translocation, which may explain why hnRNPA3-associated phenotypes linked to *RUNX1:RUNX1T1* splicing were not detectable under the experimental conditions tested.

More generally, many RNA binding proteins shape how cells handle genotoxic or metabolic stress instead of controlling day-to-day proliferation. If hnRNPA3 contributes to RNA surveillance or DNA-damage responses, its impact is likely to appear only when cells face chemotherapy or bone marrow stress, where stromal and metabolic cues remodel AML behaviour (Goulard et al. 2018; Wang et al. 2019; Menter and Tzankov 2022; Cai et al. 2025). This framework reconciles the apparent discrepancy between its association with poor patient survival and the absence of a growth phenotype in vitro, supporting the interpretation that hnRNPA3 may function as a conditional rather than constitutive effector.

4.3.4 hnRNPA0 defines a checkpoint dependent survival requirement in the A0 positive AML model tested

Across our models, loss of hnRNPA0 reduced proliferation, increased G_2/M accumulation, and elevated apoptosis in the KG1a model, indicating a checkpoint-linked survival phenotype under the baseline conditions tested (**Figure 4-18 Figure 4-19**). These findings are consistent with prior evidence placing hnRNP proteins at the centre of apoptotic and checkpoint regulation in cancer biology (Kedzierska and Piekielko-Witkowska 2017).

Mechanistically, hnRNPA0 may promote MYB expression through direct interaction with the enhancer long non-coding RNA MY34UE-AS, thereby supporting proliferation and survival of leukaemic cells (Liu et al. 2024). This provides a plausible transcriptional route by which A0 sustains growth and survival in A0-positive AML, complementing its established role in stabilising AU-rich element (ARE) mRNAs such as GADD45α and $p27^{Kip1}$ within the p38/MK2 → hnRNPA0 signalling axis (Lal et al. 2004; Young et al. 2014; Cannell et al. 2015b).

Notably, overexpression of hnRNPA0 in A0 negative lines did not enhance growth, suggesting that its function is context dependent requiring an appropriate transcriptomic and/or stress background rather than universally growth-promoting. Taken together, the restricted expression, knockdown vulnerability, and overexpression neutrality support the view that hnRNPA0 acts as a context specific dependency. This conclusion underpins the mechanistic focus of Chapter 5, which applies transcriptomic profiling to define the ARE-centred regulatory programme downstream of hnRNPA0 loss and to test whether disrupting this network compromises AML cell viability.

4.3.5 Limitations

Several features of my experimental design define how far these conclusions can be generalised. RNAi off targets, the divergent outcomes with shRNA 576 (stronger protein knockdown, no growth effect) versus shRNA 581 (weaker knockdown, growth inhibition) are characteristic of sequence-dependent off-target toxicity rather than true on-target dependency. This behaviour is well documented for RNAi and can yield apparent fitness phenotypes unrelated to the intended transcript (Jackson et al. 2003; Bartoszewski and Sikorski 2019; Chen et al. 2021; Goel and Ploski 2022). I mitigated this by (i) using multiple hairpins, (ii) confirming protein depletion by immunoblot, and (iii) validating with CRISPR Cas9; nonetheless, RNAi artefacts remain a caveat for the hnRNPA3 KD dataset.

Partial CRISPR effects and protein rescue, our CRISPR guides (610/611) reduced hnRNPA3 protein by ~70 % without altering proliferation. While this aligns with the shRNA-576 result, CRISPR edits can yield hypomorphic or escape alleles via in-frame indels, exon skipping, or alternative translation initiation that preserve partial function and blunt subtle phenotypes (Yuen et al. 2017; Wang et al. 2024). Thus, a strict “no-effect” interpretation should be limited to baseline conditions; small conditional roles for hnRNPA3 could be missed if residual proteoforms remain.

Limited overexpression efficiency represents an important technical limitation of the hnRNPA3 gain-of-function experiments. Despite successful viral delivery of hnRNPA3 cDNA, no robust or statistically significant increase in hnRNPA3 protein levels was achieved across the tested models. As a result, the absence of a detectable phenotype under overexpression conditions cannot be interpreted as evidence that hnRNPA3 is functionally inert. Rather, these data indicate that the overexpression system was insufficient to meaningfully perturb hnRNPA3 dosage, limiting conclusions that can be drawn from these assays.

Model constraints (monoculture vs niche), all functional assays were conducted in established AML lines outside the bone-marrow microenvironment. Stromal contact, cytokine gradients, hypoxia, and metabolic competition remodel AML signalling and can reveal context-dependent dependencies (Goulard et al. 2018; Menter and Tzankov 2022). Consequently, our findings describe baseline, cell-autonomous requirements and may under estimate roles that emerge under genotoxic stress, metabolic pressure, or niche signalling.

Sampling and analytics analyses focused on a defined panel of AML lines with documented protein expression; although effect sizes were consistent within models and statistics were applied where appropriate (e.g., two-way ANOVA for growth curves), broader validation in primary AML samples and in vivo models is needed. All in-vitro assays were performed in triplicate and confirmed by independent repeats, ensuring internal consistency. Finally, figure-level constraints (e.g., limited time courses, immunoblot densitometry variability) mean that negative results should be interpreted as the absence of a detectable effect under the tested conditions, not proof of absence.

Taken together, these guard rails justify our cautious interpretation: hnRNPA3 is dispensable for baseline growth across models tested, whereas hnRNPA0 defines a context-specific survival requirement in A0-positive cells. The next sections translate these patterns into testable mechanistic and therapeutic hypotheses.

4.3.6 Conclusion

Taken together, the data from this chapter deliver a split verdict. Under standard culture conditions, hnRNPA3 is dispensable for baseline AML growth in the models tested, despite its association with poorer survival in patient cohorts. This supports a potential role as a contextual marker or conditional modulator rather than a constitutive driver of proliferation.

By contrast, hnRNPA0 demonstrated a reproducible functional dependency in the KG1a model where it is endogenously expressed. Its depletion reduced proliferation, increased G2/M accumulation, and elevated apoptosis under baseline culture conditions, supporting a checkpoint-linked survival phenotype. This behaviour is consistent with disruption of ARE-mRNA stabilisation within the p38/MK2 → hnRNPA0 → GADD45α/$p27^{Kip1}$ axis (Lal et al. ; Wong et al. ; Cannell et al. ; Sheikh). Collectively, these findings suggest that hnRNPA0 functions as a context-dependent survival regulator in the A0-positive model examined, in contrast to the baseline dispensability of hnRNPA3.

These contrasts validate the prioritisation established in Chapter 3 and provide the conceptual basis for the next phase of investigation. Chapter 5 therefore focuses on transcriptome-wide characterisation of hnRNPA0 depletion to define its downstream regulatory programme, while recognising that hnRNPA3 may warrant future evaluation under stress, therapy-mimicking, or microenvironmental conditions rather than in baseline monoculture.

5 hnRNPA0 knockdown increases BCL2L11 (BIM) in AML cells

5.1 Introduction

hnRNPA0 was identified in Chapter **4** as a context dependent regulator of survival in the KG1a AML model examined. Functional studies demonstrated that knockdown of hnRNPA0 significantly reduced AML cell viability and proliferative capacity, accompanied by accumulation of cells in the G2/M phase of the cell cycle and activation of apoptotic signalling pathways. These findings established hnRNPA0 as a key determinant of AML cell growth and survival but did not define the molecular mechanisms through which these effects were mediated. hnRNPA0 is a member of the heterogeneous nuclear ribonucleoprotein (hnRNP) family of RNA binding proteins, which coordinate post transcriptional gene regulation by controlling mRNA stability, processing and translation. hnRNPA0 has been shown to bind AU-rich elements within target transcripts, thereby influencing mRNA half-life and enabling rapid adaptation of gene expression in response to cellular stress and signalling cues (Young et al. 2014). Through this mode of regulation, hnRNPA0 is positioned to exert broad effects on pathways governing cell cycle control, survival and differentiation. Evidence linking hnRNPA0 to myeloid malignancy remains limited and is largely confined to therapy related myeloid neoplasms harbouring del(5q) chromosomal abnormalities. In this context, hnRNPA0 haploinsufficiency disrupts AU-rich element-mediated mRNA stability and alters myeloid differentiation programmes, implicating hnRNPA0 as a regulator of haematopoietic cell fate (Young et al. 2014). However, beyond this genetically defined subset, the transcriptional programmes governed by hnRNPA0 in AML cells remain poorly characterised, and its contribution to leukaemic cell growth and survival has not been systematically explored. Functional studies in Chapter **4** demonstrated that hnRNPA0 knockdown disrupts AML cell viability with a concomitant reduction in cell growth. This was mediated by accumulation of cells in G2/M of cell cycle and activation of apoptotic signalling. However, the downstream transcriptional programmes governed by hnRNPA0 remain undefined. To resolve this, an unbiased, transcriptome wide approach is required. RNA sequencing (RNAseq) enables systematic identification of genes and pathways that are ‘swtiched on’ or ‘off’ (Mortazavi et al. 2008), (Wang et al. 2009). RNAseq can therefore provide gene expression data implicating changes in the transcriptome as a conseqeunce of hnRNPA0 KD; providing the molecular context for the phenotypes observed in Chapter **4**.

5.1.1 Aims and Objectives

The overall aim of this chapter is to define the transcriptional consequences of hnRNPA0 knockdown in AML cells and to identify molecular pathways regulated by hnRNPA0 that influence AML cell state and stress responses. To achieve this goal, I have the following objectives.

- **Isolate high quality RNA from AML cells to determine the transcriptomic changes associated with hnRNPA0 knockdown**

  Total RNA will be extracted from KG1a cells transduced hnRNPA0 shRNA and scrambled control constructs (expressing GFP alone). Following QC assessment of RNA integrity, samples will be shipped to Novogene for library preparation and RNA seq.

- **Identify genes and pathways affected by hnRNPA0 KD**

  Sequencing data will be analysed to establish differential gene expression between control and hnRNPA0 KD cultures generated above. Enrichment analyses will be used to identify potential biological processes that are associated with apoptosis, stress responses, and cell cycle checkpoint regulation. These Then integrate the findings with resources including TCGA, BloodSpot, DepMap, and BeatAML to relate these molecular changes to patient data and therapeutic context.

5.2 Results

The overall experimental workflow is shown in (**Figure 5-1)**.

5.2.1 Generation of hnRNPA0 knockdown cells for RNA seq

To examine the molecular consequences of reducing hnRNPA0 expression, the KG1a AML cell line was selected as the experimental model. KG1a was chosen because it endogenously expresses detectable hnRNPA0 protein and demonstrated a reproducible survival associated phenotype following hnRNPA0 knockdown in Chapter **4**, including reduced proliferation, G_2/M accumulation, and increased apoptosis. In contrast, A0 negative models did not exhibit growth enhancement upon overexpression, supporting the view that functional dependency is restricted to A0 positive contexts. This made KG1a the most appropriate system in which to characterise downstream transcriptional consequences of hnRNPA0 depletion

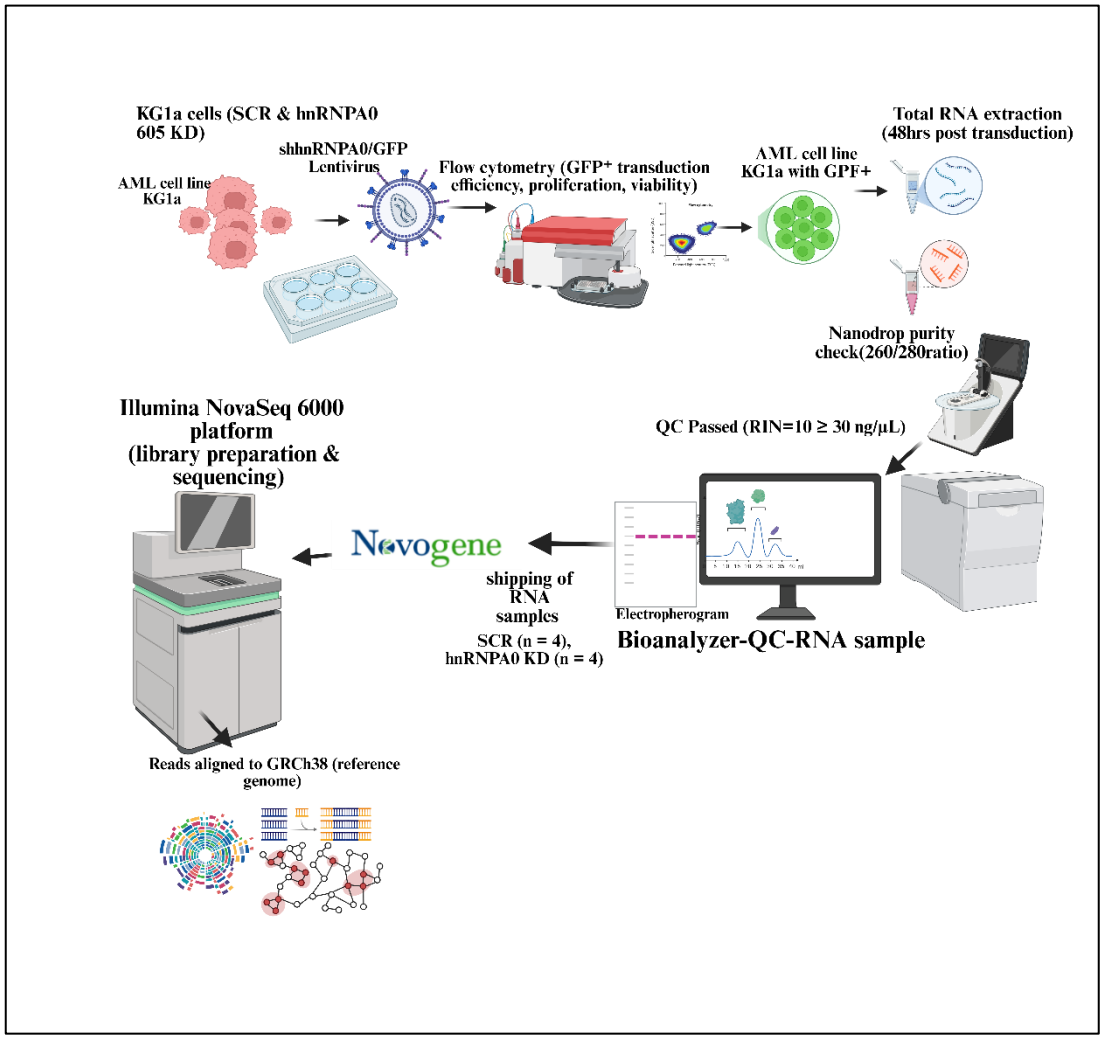

Figure 5-1 Workflow of RNA seq analysis following hnRNPA0 KD in AML cells

Overview of the experimental design. KG1a AML cells were transduced with shRNA targeting hnRNPA0 (construct 605) and a scrambled control (construct 497). GFP expression was used to confirm high transduction efficiency, and reduced hnRNPA0 protein expression was confirmed by WB. RNA was extracted and purity analysed with a NanoDrop spectrophotometer and Agilent Bioanalyzer. High quality RNA was processed for library preparation and sequenced on the Illumina NovaSeq 6000 platform. Sequencing reads were aligned to the GRCh38 human reference genome, and differential expression was determined. Subsequent analyses included gene ontology, KEGG, and Reactome pathway enrichment, as well as Hallmark GSEA. Candidate genes were explored experimentally by WB,(**Figure 5-20**, **Figure 5-21**, **Figure 5-22**) enabling construction of a mechanistic framework for the role of hnRNPA0 in AML(N=4).

KG1a cells were transduced with a previously validated hnRNPA0 shRNA construct (Ref. 605), alongside a scrambled control, as described and validated in Chapter **4**. Transduction efficiency, assessed by GFP fluorescence, exceeded 95%, indicating near complete infection of the cell population. Western blot analysis confirmed effective reduction of hnRNPA0 protein levels following transduction with shRNA 605 compared with the scrambled control (see Chapter **4**)

Based on this efficient knockdown, shRNA 605 was selected for all subsequent RNA seq experiments. Total RNA was extracted from knockdown and control cultures two days following transduction for downstream transcriptomic analysis.

5.2.2 RNA extraction, sequencing, and data quality control

Total RNA was extracted from KG1a cells transduced with shRNA construct 605 and from scrambled control cells using the RNeasy Plus Mini Kit (Qiagen 2019). Each RNA preparation was assessed for concentration and purity using a NanoDrop spectrophotometer (Scientific 2022), and integrity was evaluated using an Agilent Bioanalyzer assay (Technologies 2016). RNA yields ranged from approximately 64 to 371 ng/µL, with absorbance ratios close to expected values (260/280 ≈ 2.0 and 260/230 within acceptable range). All samples exceeded 30 ng/µL, meeting the concentration threshold required for downstream library preparation (**Table 5-1**). The Bioanalyzer electropherograms showed the characteristic 18S and 28S rRNA peaks with no evidence of degradation. Each replicate both control and KD recorded a RNA Integrity Number (RIN) of 10 (**Figure 5-3; Table 5-1**). Although RNA integrity and purity were confirmed across all samples, technical variability arising from library preparation, sequencing depth, and batch effects cannot be entirely excluded. Nevertheless, the high RIN values and consistency between biological replicates support the overall robustness and reliability of the dataset for downstream transcriptomic analysis.

5.2.3 Alignment to the reference genome

RNA-seq libraries were prepared by Novogene and sequenced on the Illumina NovaSeq 6000 platform. Each sample generated 40–55 million paired-end 150 bp reads. After adapter trimming, over 94 % of bases achieved Q30 or higher, indicating high sequencing accuracy. The GC content and base quality distribution plots (**Figure 5-4)** were consistent with typical human RNAseq datasets and showed no evidence of library construction bias. Sequencing

reads were aligned to the GRCh38 human reference genome using HISAT2. Alignment metrics were strong, with 94–96% of reads mapping to the genome, ~87% mapping uniquely, and <5% aligning to multiple loci. These values demonstrate that the libraries were high quality, balanced across conditions, and suitable for downstream data analyses. For both KD and SCR samples, mapping quality was consistent across replicates. Properly paired reads accounted for ~86–89% of the data, confirming robust library preparation. Approximately 45–48% of mapped reads spanned splice junctions, as expected for poly(A) selected RNA seq.

Table 5-1 RNA sample quality control summary

RNA extracted from hnRNPA0 KD and SCR KG1a cells was assessed for concentration and purity using a NanoDrop spectrophotometer. RNA integrity was confirmed on an Agilent 2100 Bioanalyzer.

Abbreviations: SCR: scrambled control, **KD:** hnRNPA0 knockdown**, S:** sample identifier**, No:** replicate number**, ng/µL:** RNA concentration**, 260/280:** absorbance ratio at 260 nm and 280 nm**, 260/230:** absorbance ratio at 260 nm and 230 nm**, RIN:** RNA integrity number.

S	Condition	No	ng/µL	260/280	260/230	RIN
1	**SCR1**	**1**	154.2	2.02	2.03	10
2	**hnRNPA0_KD1**		152.4	2.03	1.95	10
3	**SCR2**	**2**	221.9	2.04	2.08	10
4	**hnRNPA0_KD2**		108.2	1.99	1.94	10
5	**SCR3**	**3**	370.6	2.01	2.17	10
6	**hnRNPA0_KD3**		64.1	2.01	1.71	10
7	**SCR4**	**4**	219.3	2.04	1.53	10
8	**hnRNPA0_KD4**		163.2	2.01	1.70	10

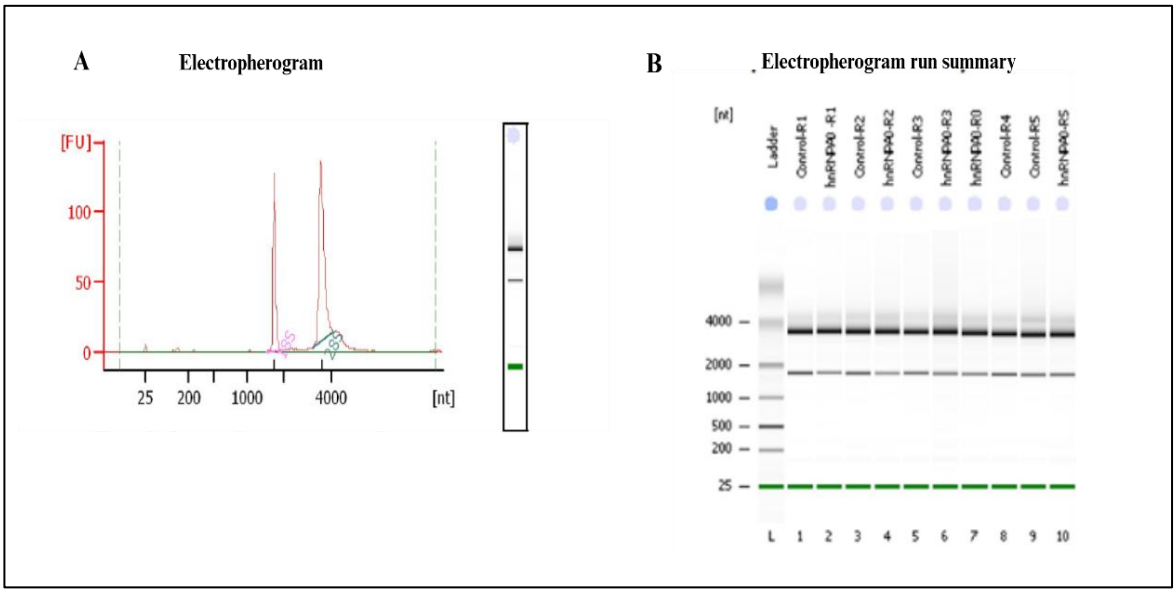

Figure 5-2 RNA sample preparation and quality control following hnRNPA0 KD in AML cells

A Electropherogram illustrating RNA integrity from a single KG1a sample, and the x-axis shows nucleotide length (nt), while the y-axis represents fluorescence units (FU). Distinct 18S and 28S rRNA peaks are visible, indicating intact RNA. **B** Gel run summary image showing RNA profiles across all samples processed on the same Bioanalyzer chip. Lane L indicates the RNA ladder, with fragment sizes shown in nucleotides (nt). Consistent banding patterns across samples confirm comparable RNA quality between conditions.

.

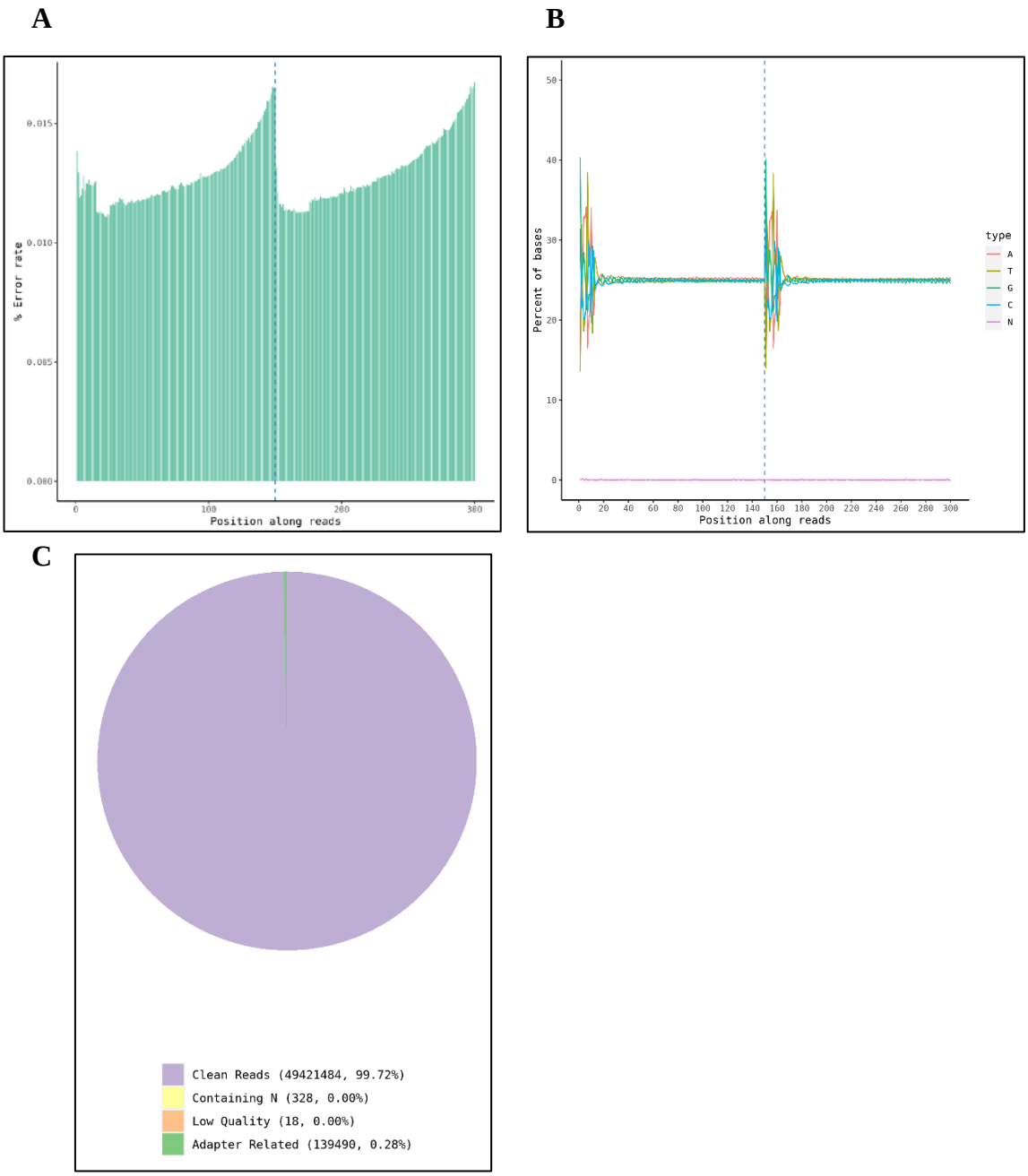

Figure 5-3 Sequencing quality control metrics for RNA seq libraries

Quality control plots generated from KG1a hnRNPA0 KD and SCR RNA seq libraries and this a SCR sample in this figure. **A** Distribution of base quality scores across sequencing cycles for all samples. **B** GC content profiles of sequencing reads, showing the proportion of reads across GC percentages. **C** Filtering summary generated by the sequencing provider, indicating the proportions of clean reads, adaptor related reads, low quality reads, and N containing reads.

Most reads mapped to exonic regions, with only small fractions assigned to intronic or intergenic areas (**Figure 5-4**; **Table 5-2**). Manual inspection of representative genes in Integrative Genomics Viewer (IGV), showed clean alignment across annotated exons with no obvious mismatches. Together, these metrics demonstrate strong alignment quality, uniform read distribution across gene features, and a reliable dataset for downstream expression analyses.

5.2.4 Global gene expression profiles

Global transcriptome profiles were quantified as fragments per kilobase per million mapped reads (FPKM)(Trapnell et al. 2010). The distribution of FPKM values spanned several orders of magnitude, as expected for poly(A)-selected RNA (Wang et al. 2009). Log_2 (FPKM + 1) distributions were highly similar across libraries, with boxplots showing nearly identical medians and interquartile ranges (**Figure 5-5**). Pairwise sample correlations were uniformly high ($r > 0.97$), indicating strong reproducibility among biological replicates (**Figure 5-6**)(Conesa et al. 2016). Principal component analysis (PCA) separated hnRNPA0 KD and SCR samples along the first component, while replicates within each group clustered tightly (**Figure 5-7**)(Ringner 2008). This pattern reflects consistent within-group profiles and clear differences between conditions. Together, these metrics demonstrate high technical consistency across samples and provide a robust foundation for subsequent differential-expression and pathway analyses.

5.2.5 Differential gene expression analysis

Differential gene expression analysis was performed using DESeq2 to compare hnRNPA0 KD and SCR samples. Genes were considered significantly differentially expressed at an adjusted p-value < 0.05 and an absolute log_2 fold-change ≥ 1. Under these criteria, 1,179 genes were identified, including 606 upregulated and 573 downregulated transcripts in the KD group A volcano plot (**Figure 5-8**), displays the distribution of log_2 fold changes and adjusted p-values for all genes, with upregulated and downregulated transcripts highlighted. A heatmap of the differentially expressed genes (**Figure 5-9**), shows clustering of samples by condition, with KD replicates grouping together and SCR replicates forming a separate cluster. A bar plot summarising the numbers of up and downregulated genes is shown in (**Figure 5-10**). Together, these analyses outline the set of transcripts altered following hnRNPA0 KD.

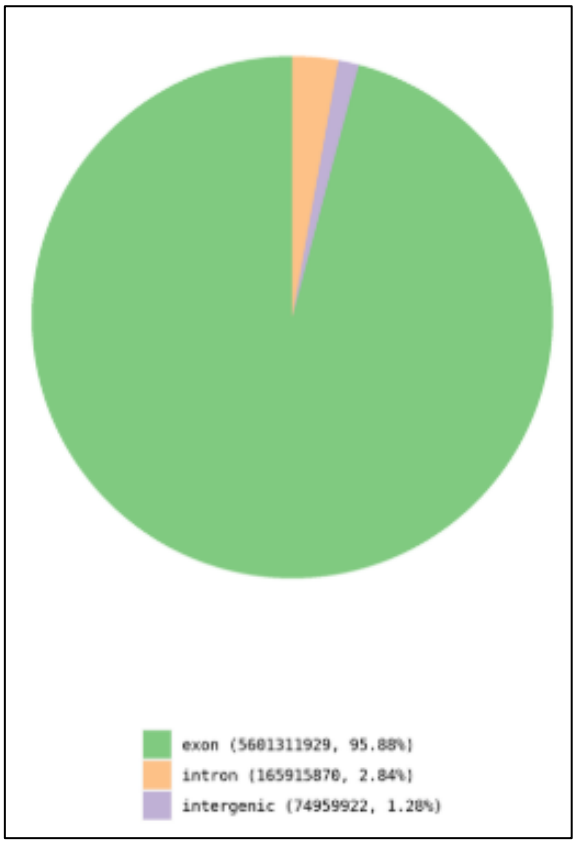

Figure 5-4 Alignment metrics for RNA seq libraries

Pie chart showing the proportions of sequencing reads aligning to exonic, intronic, and intergenic genomic regions in the SCR1 KG1a RNA seq library. This distribution demonstrates predominant exonic alignment, consistent with high quality RNA seq data suitable for downstream transcriptomic analyses.

Table 5-2 Alignment statistics for RNA seq libraries

Summary of mapping results for hnRNPA0 KD and SCR KG1a cells aligned to the GRCh38 reference genome using HISAT2. Values indicate the proportion of reads that were successfully mapped and aligned to specific categories.

Total Reads: Total number of sequenced reads per sample, **Total Map (%):** Percentage of reads that aligned to the reference genome, **Unique Map (%):** Reads that aligned to a single genomic location, **Multi Map (%):** Reads that aligned to more than one genomic location, **Proper Pair (%):** Percentage of read pairs that aligned in correct orientation and distance, **Splice Map (%):** Percentage of mapped reads spanning exon–exon junctions.

Condition	Total Reads	Total Map (%)	Unique Map (%)	Multi Map (%)	Proper Pair (%)	Splice Map (%)
SCR1	41,264,924	94.50	90.86	3.65	45.47	45.66
hnRNPA0_KD1	49,421,484	94.16	89.81	4.36	44.95	44.17
SCR2	45,769,772	93.69	89.62	4.07	44.87	41.90
hnRNPA0_KD2	40,774,486	94.16	89.87	4.27	44.98	42.49
hnRNPA0_KD3	52,715,224	94.14	89.75	4.39	44.93	42.48
SCR4	53,810,844	94.63	90.20	4.43	45.14	42.16
SCR3	38,303,364	95.60	91.51	4.09	45.76	43.96
hnRNPA0_KD4	40,520,998	95.87	91.91	3.97	45.96	46.21

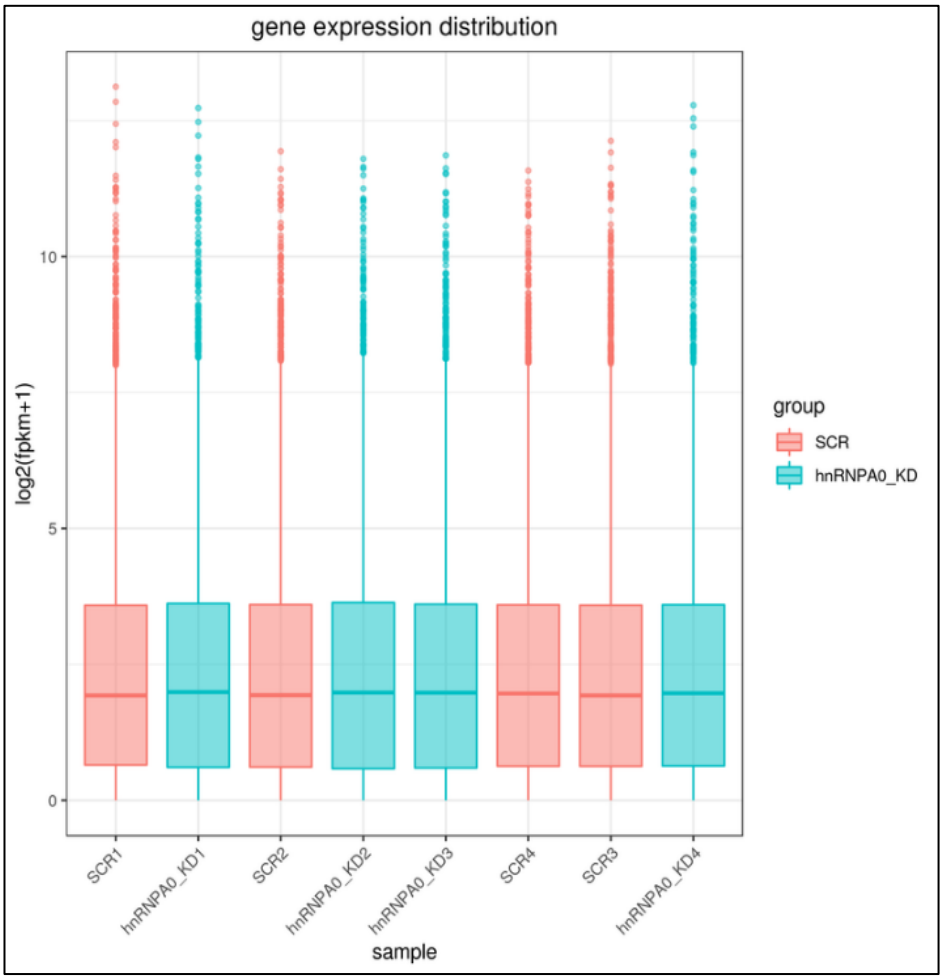

Figure 5-5 Boxplot of gene expression distributions across hnRNPA0 KD and SCR replicates

Boxplots of $\log_2$(FPKM+1) values showing comparable expression distribution ranges across all KD and SCR libraries.

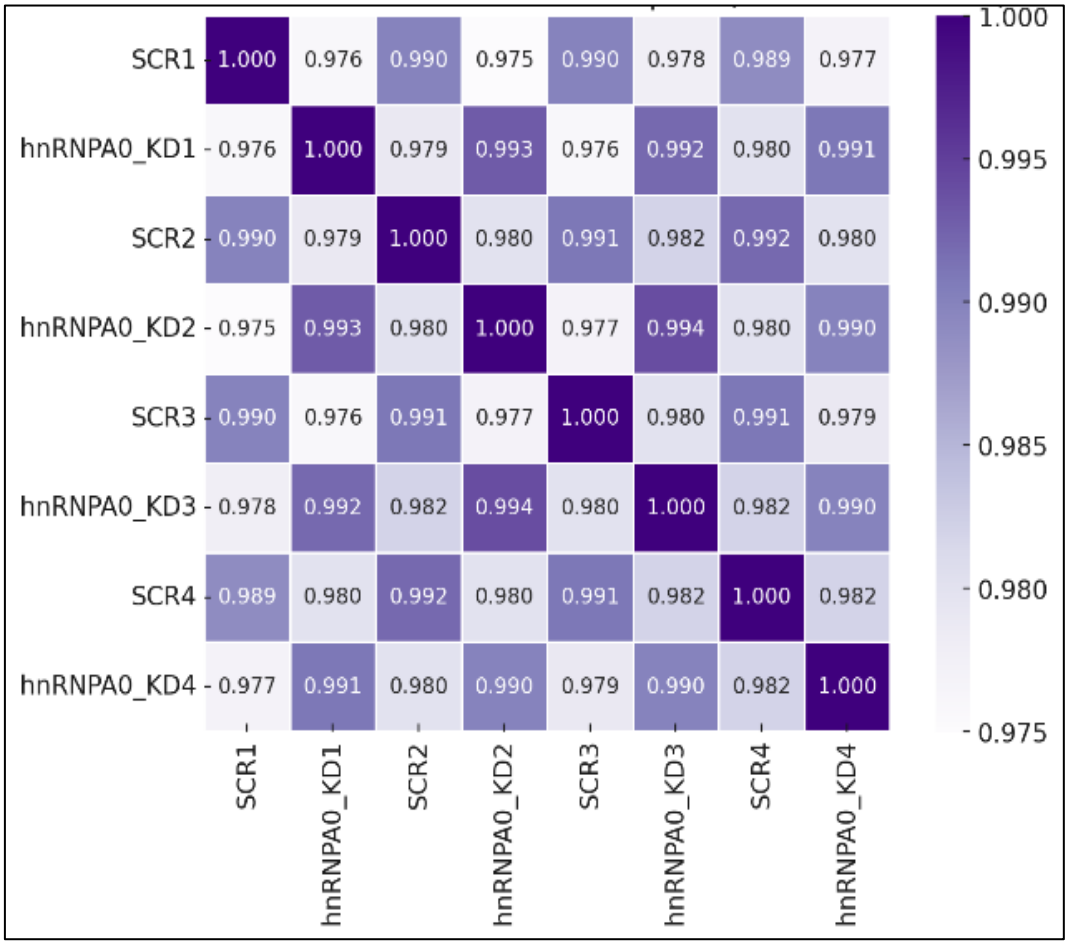

Figure 5-6 Correlation heatmap of hnRNPA0 KD and SCR replicates

Heatmap showing pairwise Pearson correlation coefficients among all KD and SCR RNA seq libraries. Colour intensity represents the strength of correlation, with darker shades indicating higher correlation values and lighter shades indicating lower correlation values. The colour bar denotes the range of Pearson correlation coefficients observed across samples ($r \approx 0.975$–1.000), demonstrating high reproducibility between biological replicates.

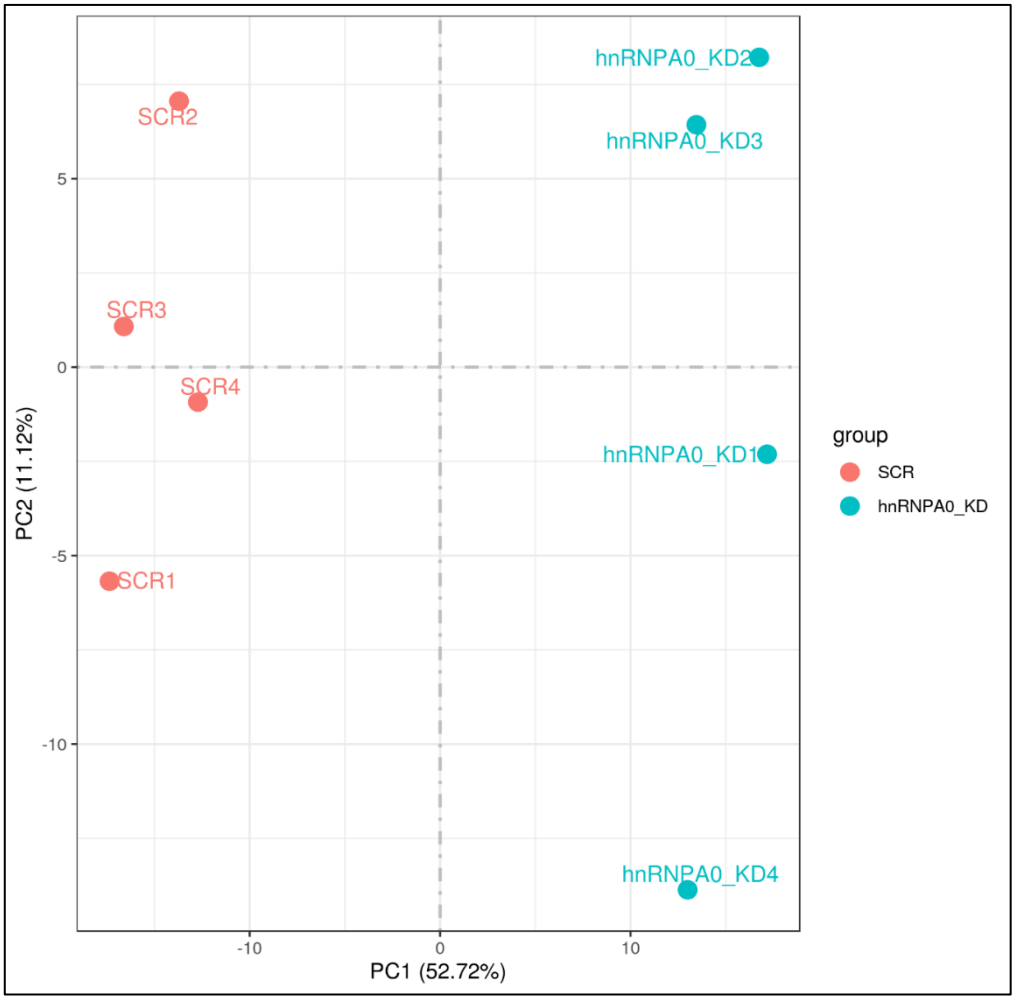

Figure 5-7 Principal component analysis of RNAseq samples

PCA of RNAseq expression profiles from hnRNPA0 KD and SCR samples. Replicates grouped by condition, and KD and SCR samples were resolved along the first principal component. PC1 and PC2 values are shown as percentages of the total variance captured.

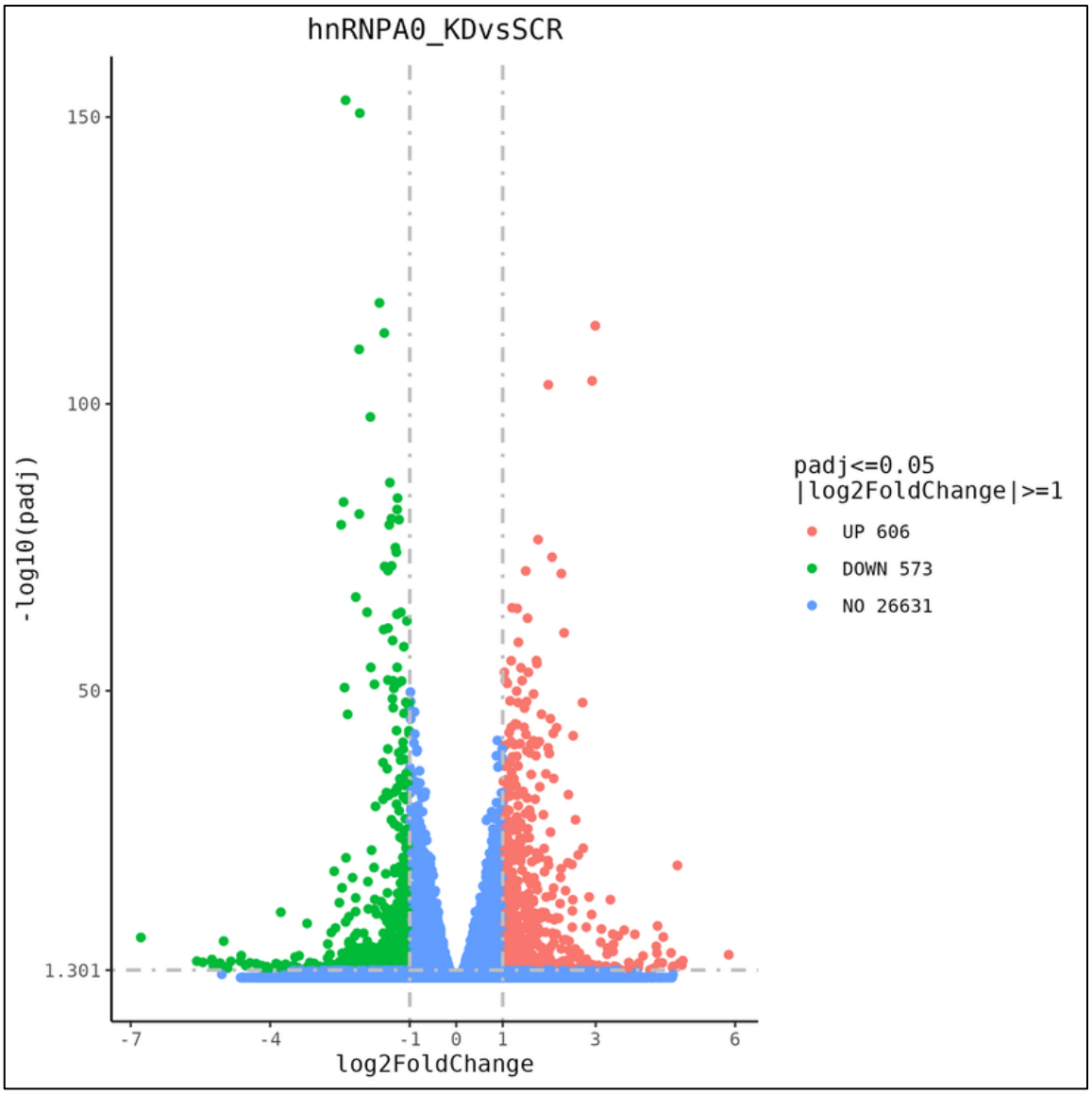

Figure 5-8 Volcano plot of differentially expressed genes following hnRNPA0 KD in KG1a cells

Volcano plot showing $\log_2$ fold change and $\log_{10}$ adjusted p-values for all analysed genes. Red data points represent genes meeting the significance thresholds for upregulation (padj < 0.05 and $|\log_2 FC| \geq 1$), green data points represent significantly downregulated genes using the same criteria, and blue data points correspond to genes that did not meet significance or fold change thresholds.

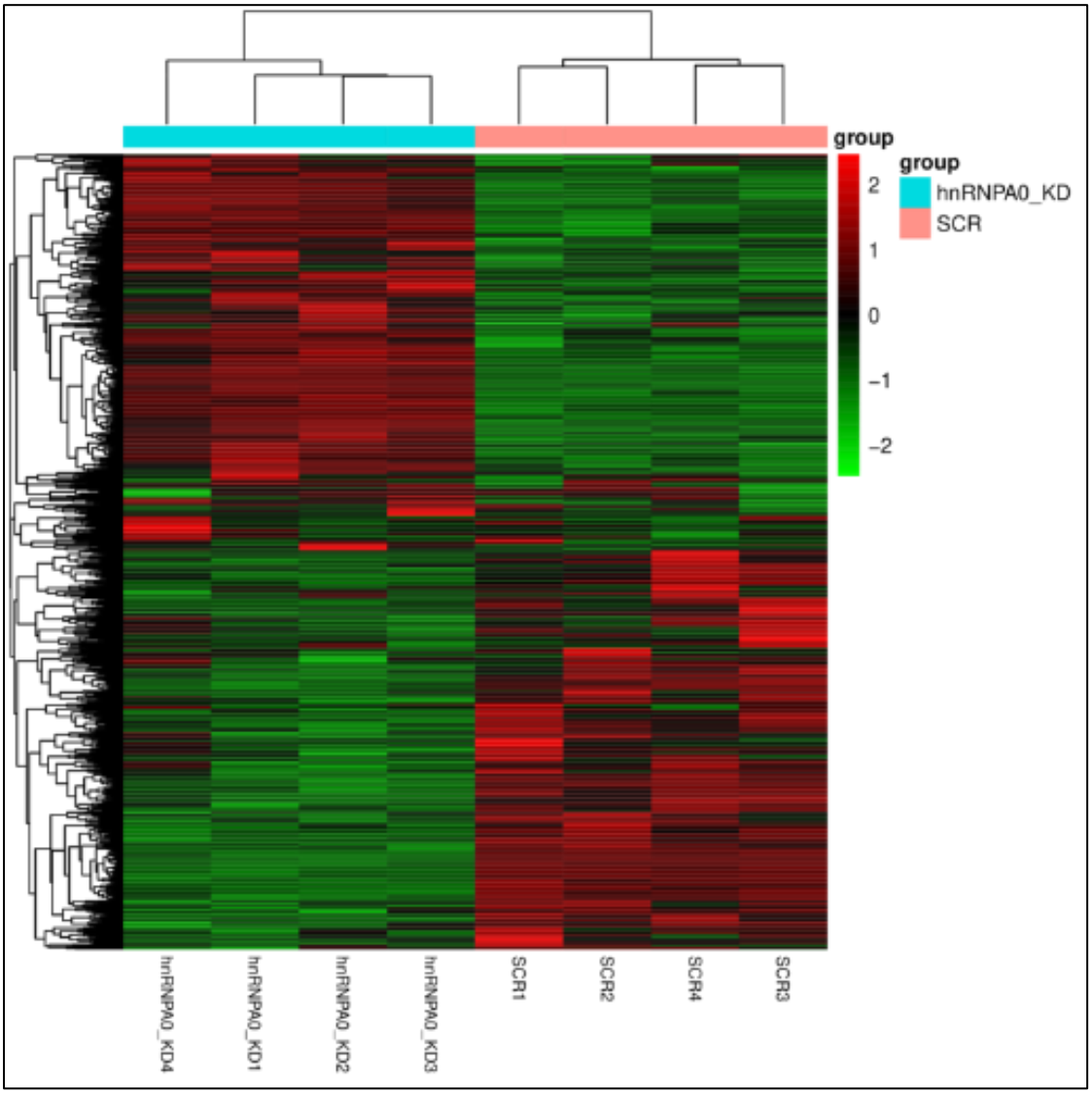

Figure 5-9 Heatmap of differentially expressed genes in hnRNPA0 KD and SCR cells

Heatmap displaying the z-scored expression values of significantly differentially expressed genes across all samples. Rows represent genes and columns represent biological replicates. Colours indicate relative expression levels (red = higher expression, green = lower expression). Hierarchical clustering was applied to both genes and samples.

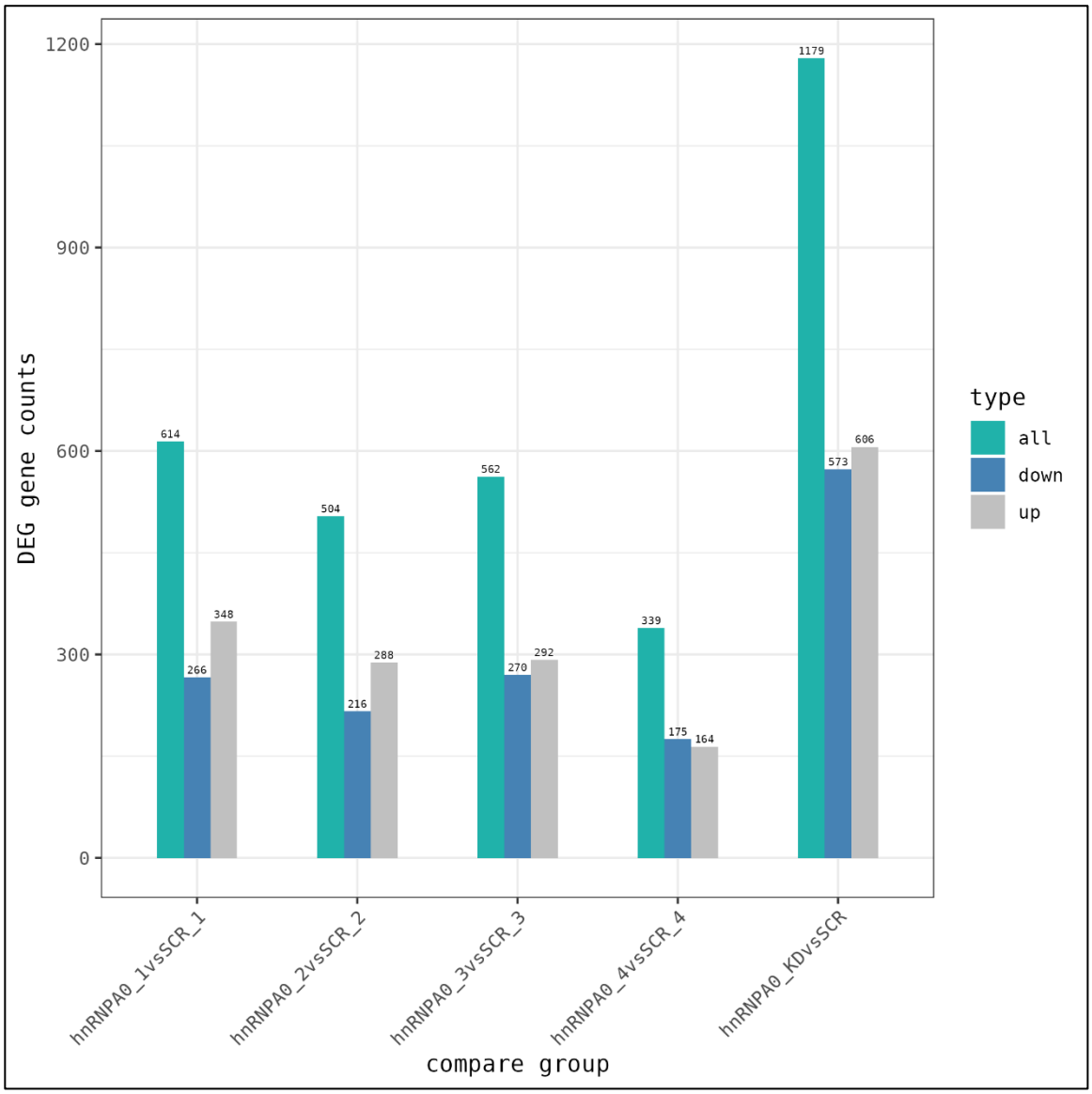

Figure 5-10 Histogram of DEG distribution

Histogram showing the number of differentially expressed genes (DEGs) across comparison groups. Bars represent total DEGs as well as upregulated and downregulated subsets for each KD versus SCR comparison.

5.2.6 Functional enrichment analysis

GO enrichment analysis revealed significant over-representation of terms related to signal transduction, receptor activity, immune response, and protein phosphorylation. Enriched biological process terms included immune-related processes and regulation of cellular signalling, while molecular function terms were dominated by receptor binding and enzyme regulatory activity. Cellular component terms were primarily associated with membrane-related compartments and protein complexes (**Figure 5-11**). KEGG pathway analysis showed significant enrichment of multiple signalling and regulatory pathways following hnRNPA0 knockdown. Enriched pathways included cytokine–cytokine receptor interaction, TNF signalling, TGF-β signalling, FOXO signalling, Hippo signalling, and pathways associated with hematopoietic cell lineage and cell adhesion (**Figure 5-12).** These KEGG enrichment results are summarised in Figure 1-13, which illustrates the breadth of signalling and immune-associated pathways deregulated in response to hnRNPA0 depletion. Gene Set Enrichment Analysis (GSEA) was used to assess coordinated changes across predefined Hallmark gene sets. All transcripts were ranked according to their expression differences between hnRNPA0 KD and SCR samples, and enrichment scores were calculated to determine whether specific gene sets accumulated at the top or bottom of the ranked list. Several Hallmark pathways showed positive enrichment in the KD condition (**Figure 5-13 and Figure 5-15**). These included Apoptosis (NES = 1.76, FDR q = 0.15), TNF-α signalling via NF-κB (NES = 1.59, FDR q = 0.09), and Mitotic spindle (NES = 1.68, FDR q = 0.12), each meeting the predefined enrichment threshold (FDR q < 0.25). Conversely, multiple gene sets showed negative enrichment (**Figure 5-13 and Figure 5-14**), including E2F targets (NES = –2.16, FDR q = 0.01), G2/M checkpoint (NES = –1.90, FDR q = 0.02), Oxidative phosphorylation (NES = –1.68, FDR q = 0.05), and mTORC1 signalling (NES = –1.31, FDR q = 0.19), also satisfying the same enrichment criterion. In summary, integrated functional enrichment analyses revealed a coordinated suppression of cell cycle associated programmes alongside nominal enrichment of stress-responsive and apoptotic signalling pathways following hnRNPA0 knockdown. GO and KEGG analyses consistently highlighted deregulation of pathways linked to cell-cycle progression, signal transduction, and immune-associated processes, supporting a transcriptional landscape consistent with the survival-associated phenotype observed in Chapter 4.

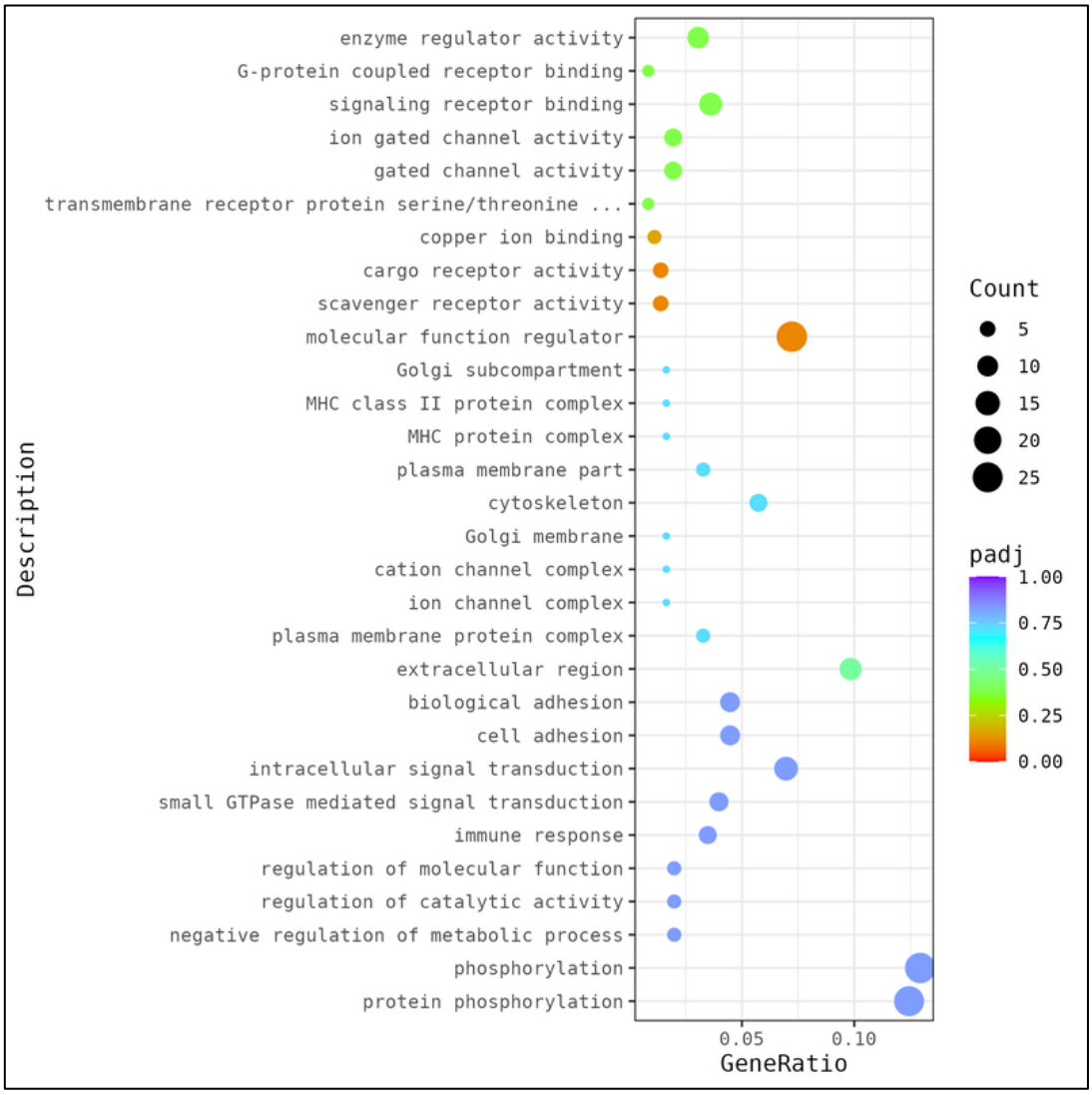

Figure 5-11 Gene Ontology (GO) enrichment analysis of differentially expressed genes following hnRNPA0 KD in KG1a cells.

Scatterplot showing enriched GO categories identified from significantly altered transcripts. Each circle represents an individual GO term, with circle size indicating the number of genes annotated to the term (count) and colour representing the adjusted p-value (padj). The x-axis shows the gene ratio, denoting the proportion of differentially expressed genes associated with each category. Enriched terms span biological process, molecular function, and cellular component categories.

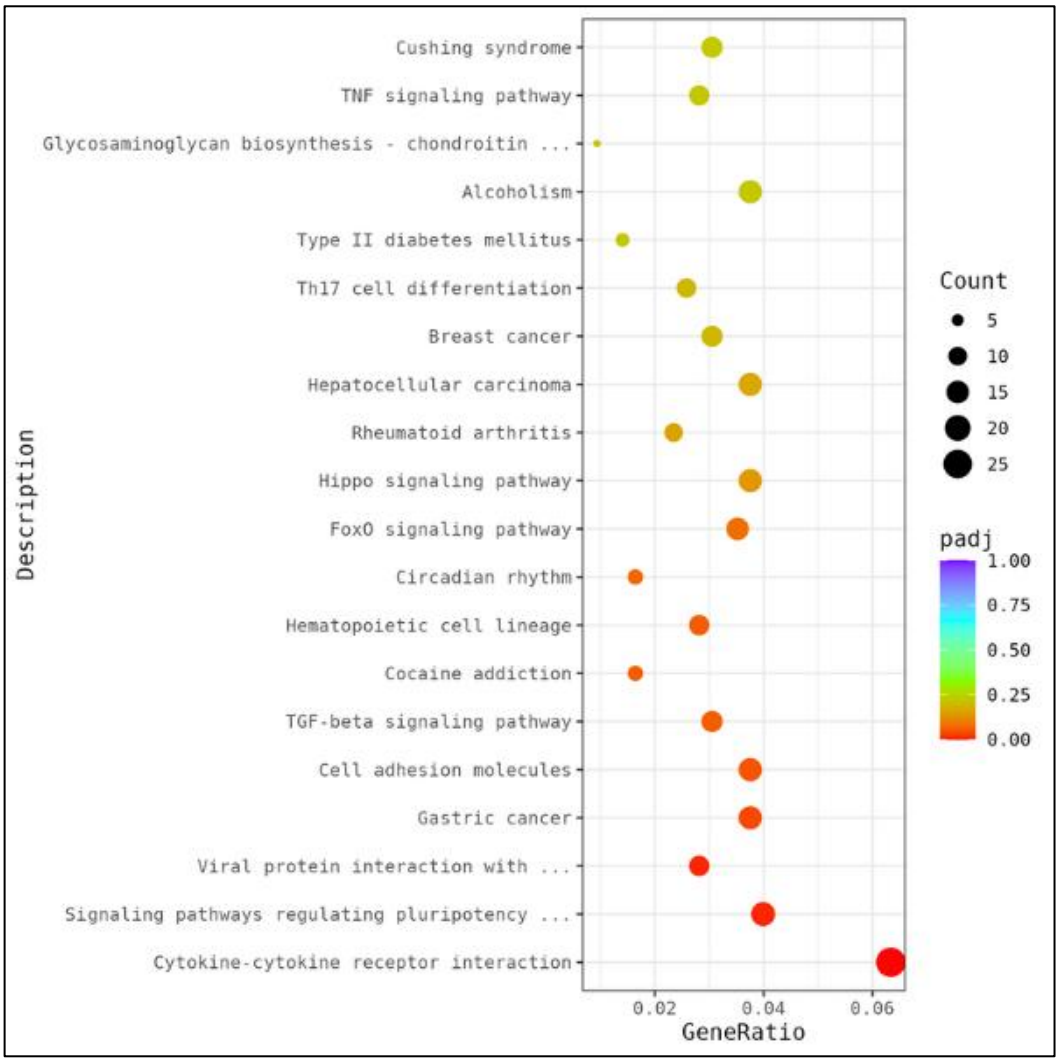

Figure 5-12 KEGG pathway enrichment analysis of differentially expressed genes following hnRNPA0 knockdown in KG1a cells

Scatterplot of enriched KEGG pathways, where dot size indicates the number of differentially expressed genes associated with each pathway (Count) and colour represents the adjusted p-value (padj). The x-axis shows the Gene ratio, reflecting the proportion of differentially expressed genes assigned to each pathway. Enriched pathways span multiple signalling, metabolic, and cellular processes identified from the dataset.

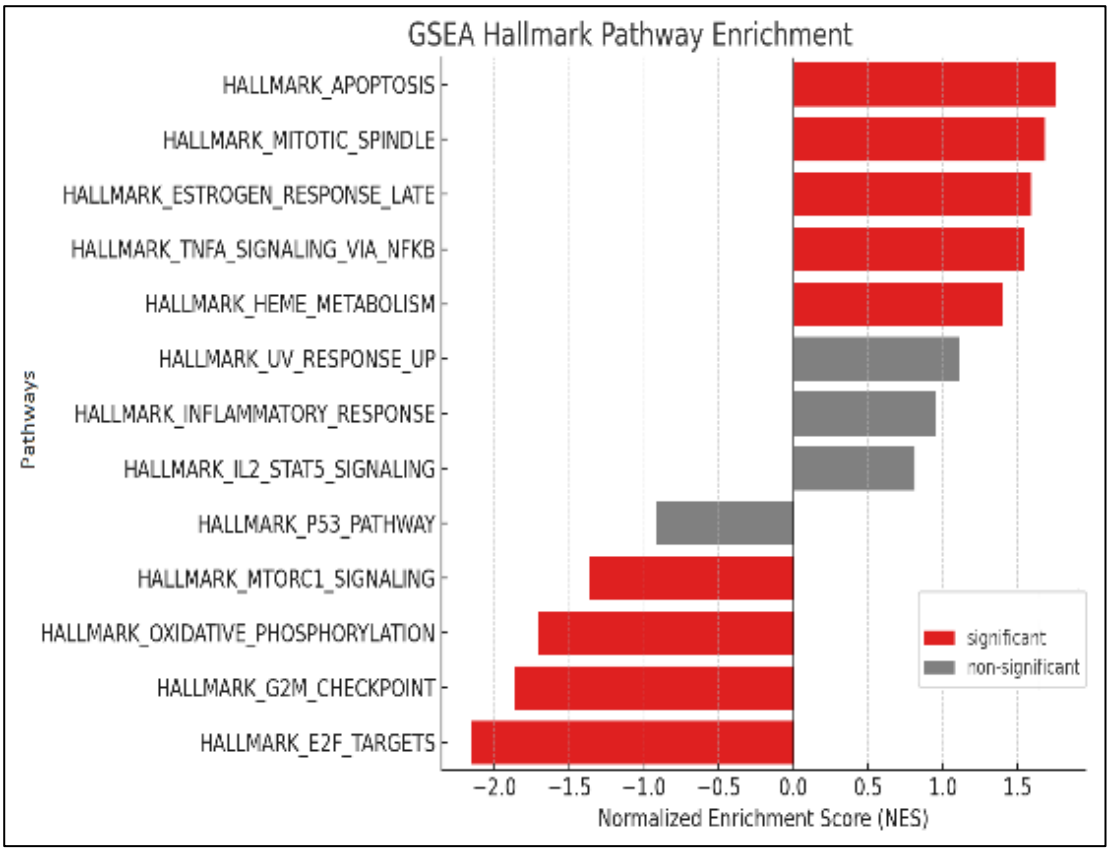

Figure 5-13 Hallmark gene set enrichment analysis (GSEA) of differentially expressed genes following hnRNPA0 KD in KG1a cells ranked by NES

Bar plot showing normalised enrichment scores (NES) for Hallmark pathways derived from GSEA. Pathways with positive NES values are displayed on the right and pathways with negative NES values on the left. Red bars indicate gene sets meeting significance thresholds (padj < 0.05), while grey bars denote non-significant gene sets.

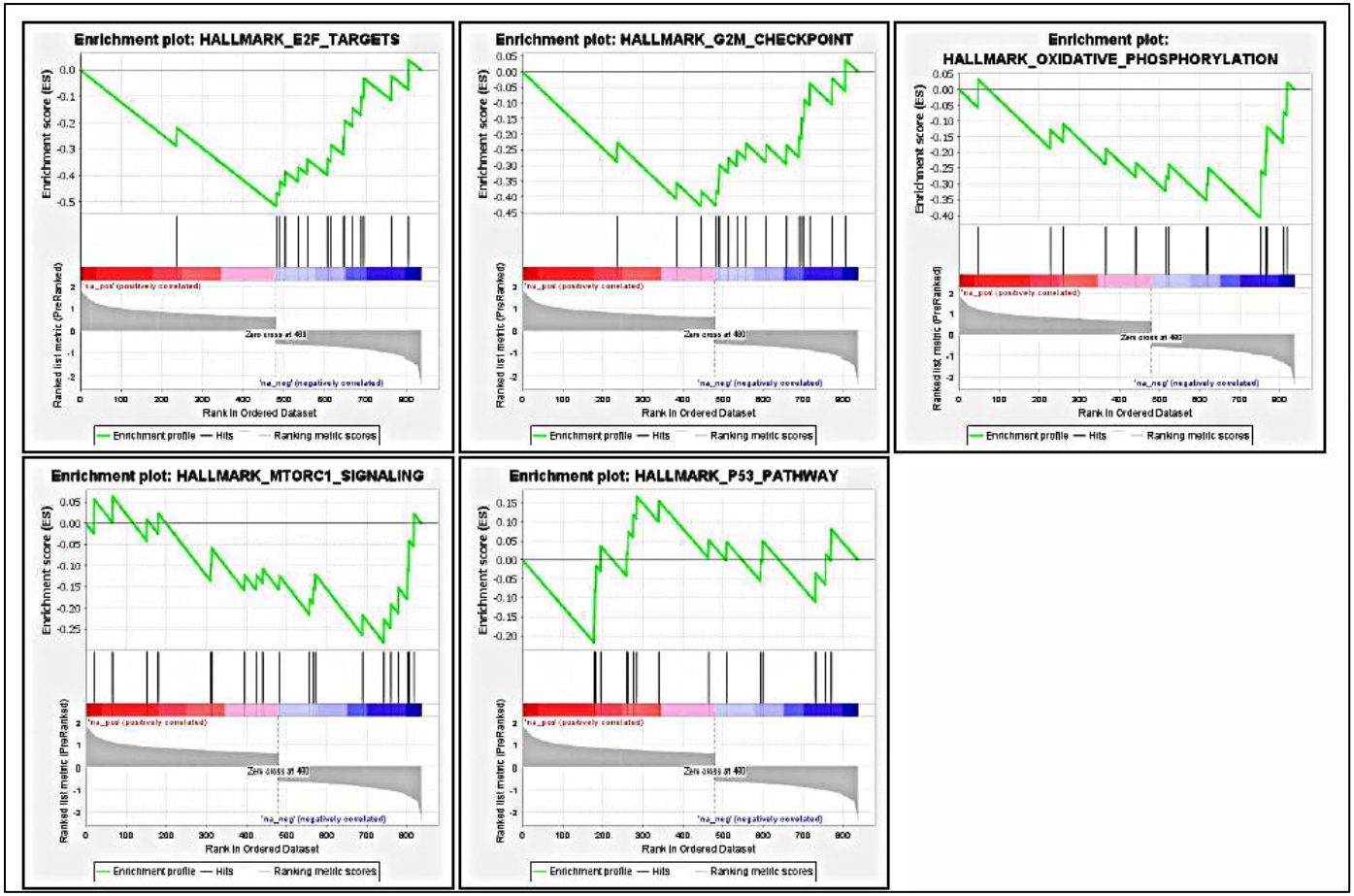

Figure 5-14 Representative GSEA enrichment plots for hallmark pathways with negative NES in hnRNPA0 KD cells

Each plot displays the running enrichment score (green line), the positions of genes belonging to the pathway within the ranked gene list (black vertical lines), and the ranked metric distribution (grey). Shown are representative negatively enriched Hallmark pathways including E2F targets, G2/M checkpoint, oxidative phosphorylation, mTORC1 signalling, and the p53 pathway.

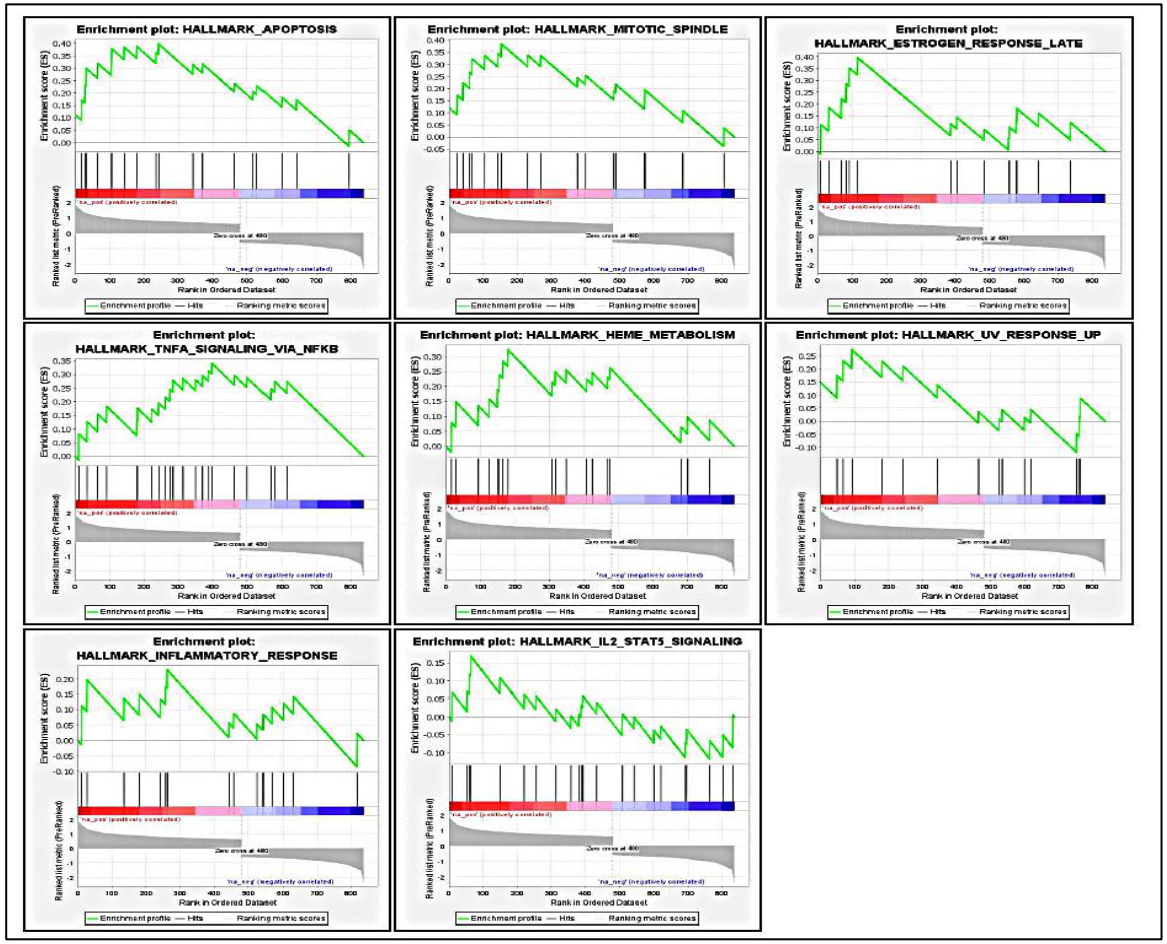

Figure 5-15 Representative positively enriched Hallmark pathways in hnRNPA0 KD cells

Representative GSEA enrichment plots of Hallmark pathways with positive normalised enrichment scores (NES). Shown are example plots including Apoptosis, Mitotic spindle, Oestrogen response (late), TNFα signalling via NF-κB, Haem metabolism, UV response (up), Inflammatory response, and IL2/STAT5 signalling. Each plot displays the running enrichment score (green line), the distribution of pathway genes within the ranked gene list (black vertical lines), and the ranked metric (grey).

While GSEA demonstrated negative enrichment of proliferative signatures, including E2F targets and the G2/M checkpoint, together with relative enrichment of apoptotic and inflammatory Hallmark gene sets, apoptosis associated transcripts emerged as a coherent functional theme across multiple analytical layers. To further interrogate this pattern, differentially expressed genes within curated apoptotic pathways were examined individually. Among canonical pro-apoptotic mediators, *BCL2L11* (BIM) demonstrated one of the strongest and most consistent fold increases across biological replicates following hnRNPA0 knockdown. In contrast, other established apoptotic regulators, including BAX, BBC3 (PUMA), and anti-apoptotic BCL2 family members, showed either modest, inconsistent, or non-significant changes in expression. This selective upregulation positioned BIM as a leading candidate within the apoptotic transcriptional response.

These findings suggested a potential link between hnRNPA0 depletion and transcriptional priming of mitochondrial apoptotic pathways, rather than establishing a direct causal mechanism. On this basis, BIM was prioritised for further validation. In summary, RNA seq analysis of hnRNPA0-depleted KG1a cells revealed coordinated suppression of proliferative gene programmes alongside enrichment of stress-responsive and apoptosis related transcripts. Although 1,179 genes were differentially expressed, *BCL2L11* was selected for focused analysis due to both the magnitude and reproducibility of its transcriptional induction and its established biological role in regulating mitochondrial apoptosis.

At the protein level, however, it was not possible to conclusively demonstrate increased BIM abundance following hnRNPA0 knockdown, as comparable increases were also observed in scrambled (SCR) control cells. These findings should therefore be interpreted cautiously, particularly given that the analysis represents a single experimental determination and may be influenced by viral transduction effects or technical variability in protein isolation. Further optimisation and replication will be required to confirm protein-level regulation. Nevertheless, BCL2L11 mRNA expression was elevated following hnRNPA0 depletion and demonstrated an inverse correlation with hnRNPA0 mRNA levels in independent AML datasets. Collectively, these data indicate that hnRNPA0 knockdown is associated with transcriptional enrichment of apoptotic programmes, although definitive execution-phase apoptosis was not established under the conditions tested.

5.2.7 Integration of RNA seq findings with public AML datasets

5.2.7.1 BCL2L11 expression increases with myeloid maturation and remains elevated across AML subtypes

To confirm the transcriptional upregulation of *BCL2L11* identified in the RNA seq dataset, I assessed its expression across AML subtypes using the BloodSpot database (Bagger et al. 2019). Expression data were derived from the human datasets GSE42519, GSE13159, and GSE24006, which together cover both normal haematopoietic compartments and patient derived AML blasts. In normal haematopoiesis, *BCL2L11* mRNA expression increased sixteen-fold myeloid maturation (**Figure 5-16A**). Levels were lowest in HSCs and MPPs, then increased through CMPs and GMPs, reaching their highest expression in mature polymorphonuclear cells and monocytes. This supports the known pro apoptotic role of BIM, which becomes more active in differentiated myeloid cells where survival signals are weaker (O'Connor et al. 1998). Across AML samples, *BCL2L11* mRNA levels were significantly higher than in normal human HSC (**Figure 5-16B**). Among cytogenetic groups, the highest expression appeared in cases with complex karyotypes and in those carrying the *t(11q23)/MLL* rearrangement. Samples with *t(15;17)* or *t(8;21)* showed comparatively lower levels, although still above those seen in normal controls.

Using the HSC expression level as a baseline, roughly eight out of ten AML samples were above the ± 2 SD threshold, while only about 0.1 % fell below it. Further, *hnRNPA0* mRNA levels inversely correlate with *BCL2L11* mRNA expression in AML (**Figure 5-19**), using the OHSU AML dataset in cBioPortal (n = 200) (Cerami et al. 2012; Gao et al. 2013). This suggests an association between BIM and hnRNPA0; consistent with BIM behaving as a stress responsive, pro-apoptotic gene that becomes more active when hnRNPA0 levels are reduced.

5.2.7.2 BCL2L11 is not required for basal AML cell line survival

To determine whether AML cells depend on BIM for viability, I analysed CRISPR Cas9 gene effect (Chronos) scores for *BCL2L11* across 30 AML cell lines from DepMap. Scores centred around 0 with a minority < –0.5, indicating that BIM is non-essential for survival under steady state conditions (**Figure 5-17**).

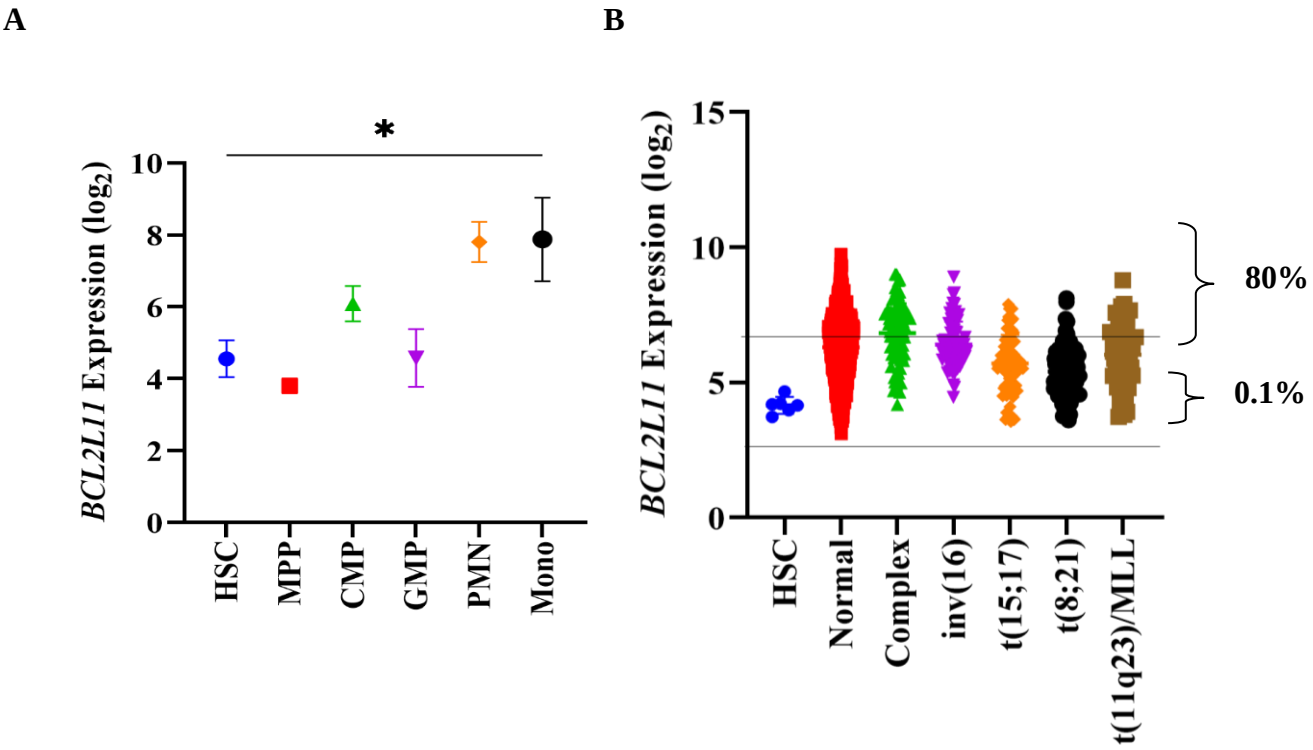

Figure 5-16 *BCL2L11* (BIM) expression increases with myeloid maturation and remains elevated across AML subtypes (BloodSpot datasets)

A Microarray data (log_2) showing *BCL2L11* mRNA expression in normal human haematopoietic cells. Probeset (1558143_a_at) from **GSE42519** (Rapin et al. 2014) (Svendsen et al. 2016) was used (n=252) (Rapin et al. 2014). Data represents mean ± 1SD. Statistical analysis was performed using one-way ANOVA with Tukey's multiple comparisons tests; * denotes $p<0.01$ vs HSC. **B** Expression of *BCL2L11* mRNA in AML subtypes compared to normal human HSC. Probeset (1558143_a_at) was used for analysis from Human Normal Haematopoiesis (**GSE42519**) and AML blasts (**GSE13159**) (Kohlmann et al. 2008; Haferlach et al. 2010), (**GSE15434**) (Klein et al. 2009), (**GSE61804**) (Metzelder et al. 2015), GSE14468 (Wouters et al. 2009; Taskesen et al. 2011), The Cancer Genome Atlas (TCGA) (Bagger et al. 2019)(**n=251**) (Kohlmann et al. 2008). Data represents mean ± 2 SD. Statistical analysis was performed using one-way ANOVA with Tukey's multiple comparisons test to HSC. he horizontal lines indicate the mean ± 2 standard deviations (SD) of normal HSC expression. The percentage of patients down or upregulated in AML compared to HSC is shown.

HSC-haematopoietic stem cell, **MPP**-Multipotential progenitors, **CMP**-Common myeloid progenitor cell, **GMP**-Granulocyte monocyte progenitors, **Mono**-Monocytes, **PMN** Polymorphonuclear cells

HSC - haematopoietic stem cell, **Normal** -AML with normal karyotype, **Complex** - AML with complex karyotype, **inv (16)** - AML with inv (16), **t (15;17)** - AML with t (15;17), **t (8;21)** AML with t (8;21), **t(11q23)/MLL (aka KMT2A)** - AML with t(11q23)/MLL.

5.2.7.3 Higher BCL2L11 expression shows a slight but non-significant association with improved patient survival

To evaluate the prognostic impact of *BCL2L11* (BIM) in AML, TCGA mRNA patient data were analysed using cBioPortal (Cerami et al. 2012). Comparing upper and lower quartiles of *BIM* mRNA expression, AML patients in the high expression quartile displayed longer median overall survival (30.6 months) and disease free survival (30.6 months) compared with the low expression group (16.4 and 24.6 months, respectively). However, these differences did not reach statistical significance (OS Log-rank p = 0.18; DFS Log-rank p = 0.29) (**Figure 5-18A** and **Figure 5-18B**).

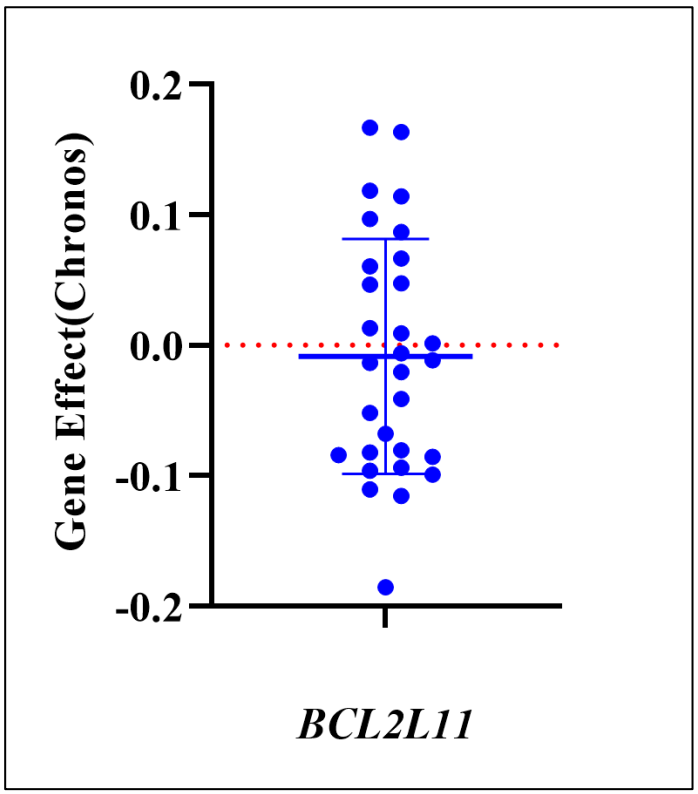

Figure 5-17 *BCL2L11* is non-essential for basal cell survival (DepMap, Chronos dataset)

CRISPR Cas9 gene-effect data showing dependency scores for *BCL2L11* across AML cell lines obtained from the DepMap https://depmap.org/portal/. (Chronos) dataset, each blue dot represents an individual AML cell line. The red dotted line marks the non-essential reference threshold (Chronos = 0). Most scores cluster near 0, indicating that *BCL2L11* knockout does not significantly impair cell viability under steady state conditions. Negative scores would reflect reduced survival following gene loss.

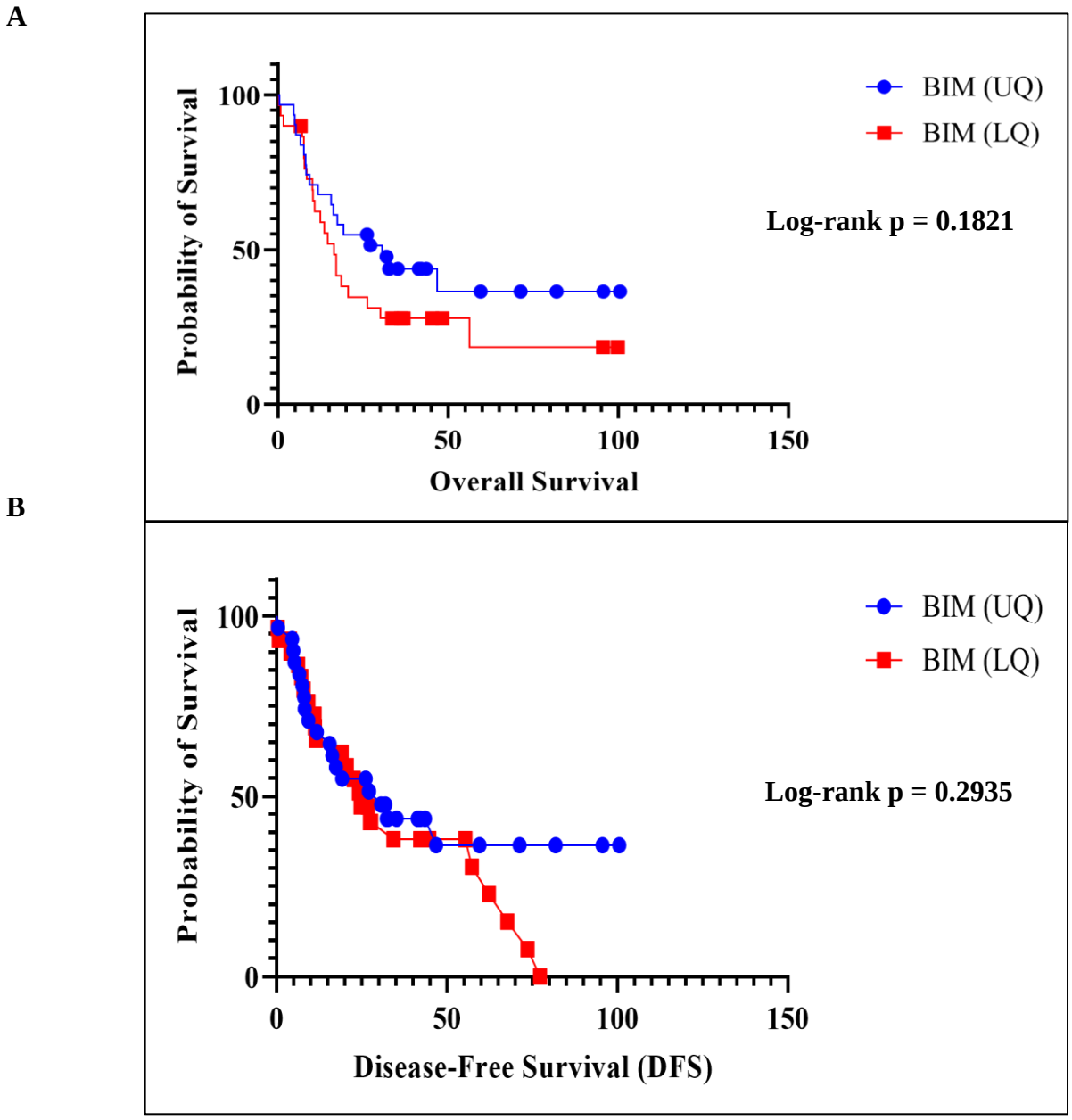

Figure 5-18 Higher *BCL2L11* expression shows a non-significant trend toward improved survival in AML patient samples (TCGA, cBioPortal)

Kaplan–Meier survival curves for AML patients stratified by upper-quartile (UQ) and lower-quartile (LQ) expression of *BCL2L11 mRNA* (BIM). Data were obtained from the TCGA cohort (Cancer Genome Atlas Research et al. 2013) via cBioPortal (www.cbioportal.org). Each group contained 62 patients (UQ = 62; LQ = 62). **A** Overall Survival (OS), log-rank p = 0.1821 **B** Disease-Free Survival (DFS) , log-rank p = 0.2935, Blue = UQ; Red = LQ.

.

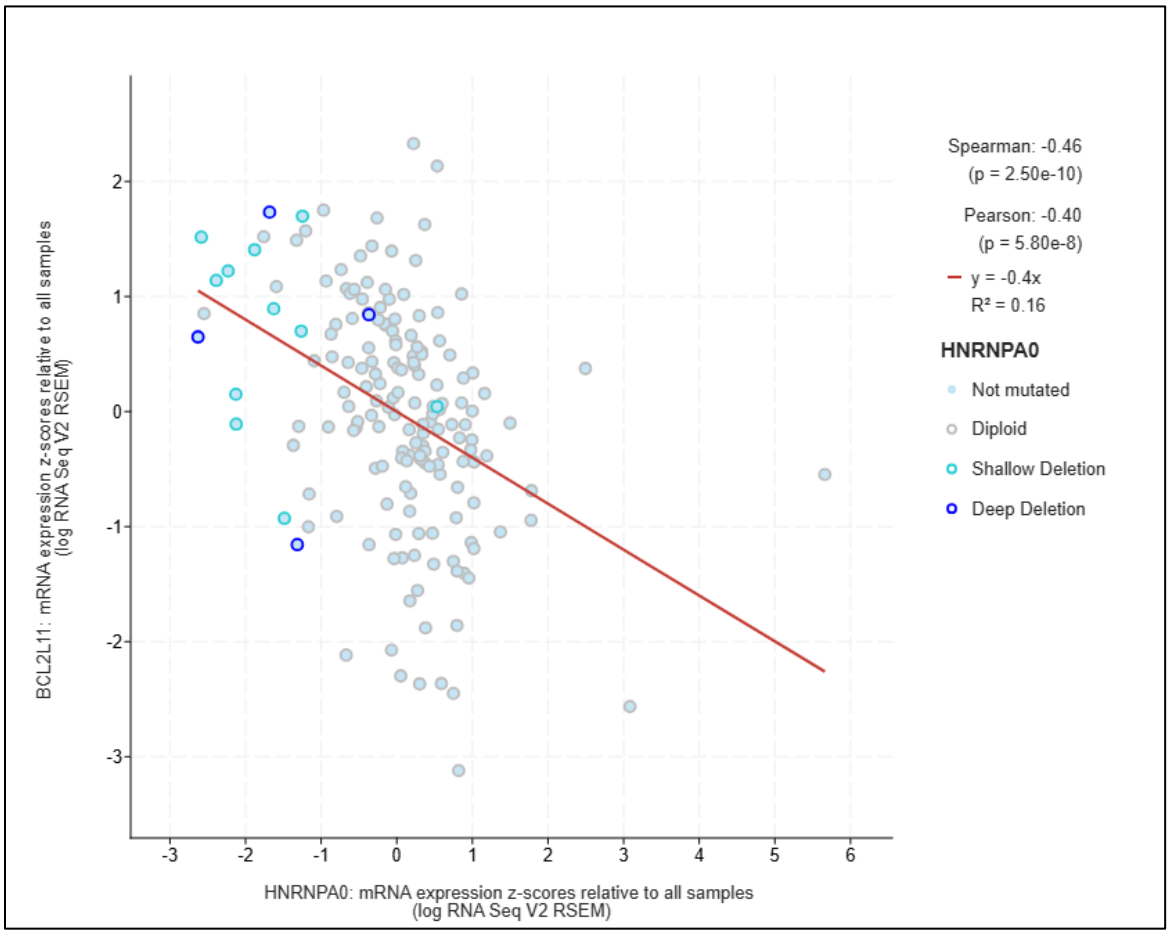

Figure 5-19 Lower *hnRNPA0* expression correlates with higher *BCL2L11* expression in AML patient samples (TCGA, cBioPortal)

Scatterplot showing *hnRNPA0* mRNA expression (x-axis) plotted against *BCL2L11* mRNA expression (y-axis) across AML patient samples from the TCGA cohort (N=173). Each dot represents an individual sample, coloured according to copy-number status: diploid (grey), shallow deletion (light blue), deep deletion (dark blue), or not profiled. The fitted regression line illustrates the moderate negative correlation between the two genes, consistent with the Pearson and Spearman coefficients displayed on the plot. Spearman and Pearson correlation coefficients with corresponding *p*-values are shown on the plot. Data were obtained from cBioPortal (www.cbioportal.org) (Cerami et al. 2012; Gao et al. 2013)

5.2.8 Candidate gene validation

The transcriptomic analyses described above indicated that hnRNPA0 knockdown is associated with enrichment of apoptosis-related gene expression programmes, consistent with the cellular phenotypes observed in Chapter 4. Among the differentially expressed genes, BCL2L11 (BIM) was selected as a candidate for further investigation due to its marked transcriptional upregulation following hnRNPA0 depletion and its well-established role in regulating mitochondrial apoptosis (O'Connor et al. 1998), (Bouillet et al. 1999). BIM is a pro apoptotic, BH3 only member of the BCL-2 family that promotes cell death through activation of BAX/BAK and inhibition of anti-apoptotic BCL-2 proteins (Willis and Adams 2005), (Youle and Strasser 2008). Based on these transcriptomic findings, BIM was taken forward for exploratory validation at the protein level.

RNAseq data showed a significant 4.2-fold increase in *BCL2L11* (BIM) mRNA gene expression upon hnRNPA0 KD (**Figure 5-8**). To confirm these changes at a protein level, WB was performed. As shown in **Figure 5-20,** BIM was detected in the positive control line (OCI-AML2). In Mock KG1a cells (**Figure 5-20**), little no expression of BIM isoforms was observed as expected. However, in SCR treated KG1a cells, three bands were observed; consistent with the known isoforms: BIM-EL (~23 kDa), BIM-L (~19 kDa), and BIM-S (~15 kDa) (Willis and Adams 2005). This suggests that the apoptotic pathway is also activated in the control cells (see discussion). In comparison to hnRNPA0 KD, a similar level of BIM expression was observed which did not support the mRNA expression data. The caveat to these data is that they only represent one determination and would need to be repeated in order to be sure of the consistency of this observation.

Since BIM activity can be enhanced by Caspase 8 activity (Luo et al. 1998). I next analysed Caspase 8 protein expression. To confirm Caspase-8 activation and validate the WB, HeLa cells were treated with apoptotic inducer staurosporine for 1, 3, and 6 hours and were used as a positive control. Caspase 8 expression was induced in a time dependent manner. When analysing KG1a cells, neither SCR or hnRNPA0 KD induced Caspase 8 expression (**Figure 5-21**), suggesting that the extrinsic apoptotic pathway was not triggered under these conditions. However, Caspase-9 showed induction of expression of this protein in SCR and hnRNPA0 KD (**Figure 5-22**), indicating that the intrinsic caspase cascade was active at the time of protein isolation but again there was no evidence of a differential effect of KD in this preliminary set of data.

In conclusion, these data indicate that reduction of hnRNPA0 is associated with increased BCL2L11 (BIM) transcription, consistent with enrichment of apoptosis related gene expression programmes observed at the transcriptomic level. However, based on this single experimental assessments, this transcriptional change was not accompanied by clear activation of downstream caspase pathways under the conditions examined. Collectively, these observations suggest that hnRNPA0 knockdown is linked to transcriptional priming of apoptotic signalling, without definitive evidence of execution phase apoptosis at the protein level, in line with the RNA seq and GSEA analyses.

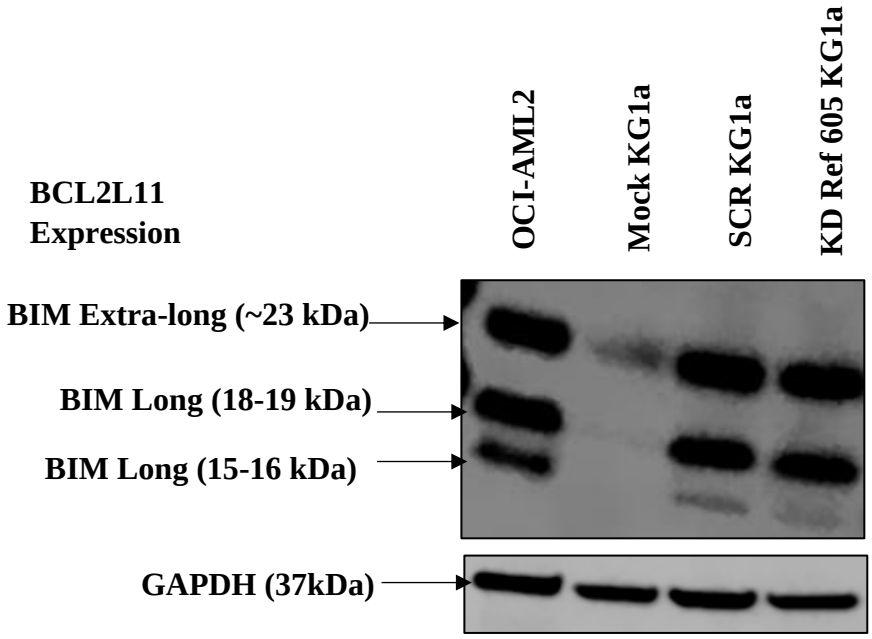

Figure 5-20 BIM (BCL2L11) protein expression in hnRNPA0 KD in KG1a cells

WB showing BIM protein isoforms in hnRNPA0 KD and SCR KG1a cells, alongside OCI-AML2 as a positive cell line. Multiple BIM isoforms are detected, including BIM extra-long (~23 kDa), long (~18–19 kDa), and short (~15–16 kDa). GAPDH (37 kDa) was used as a loading control. (N=1)

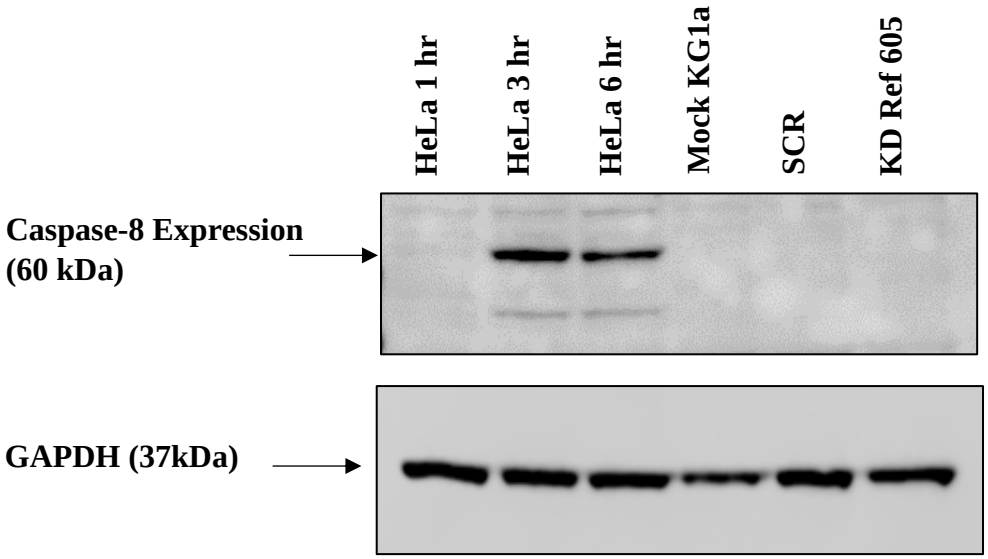

Figure 5-21 Caspase-8 protein levels remain unchanged following hnRNPA0 KD in KG1a cells

WB analysis of Caspase-8 in hnRNPA0 KD and SCR KG1a cells. HeLa cells treated with staurosporine for 1, 3, and 6 hours were included as a positive control to induce apoptotic caspase activation. The blot shows the ~60-kDa procaspase-8 band. GAPDH (37 kDa) was used as a loading control. No detectable change in Caspase-8 levels was observed following hnRNPA0 KD (N=1).

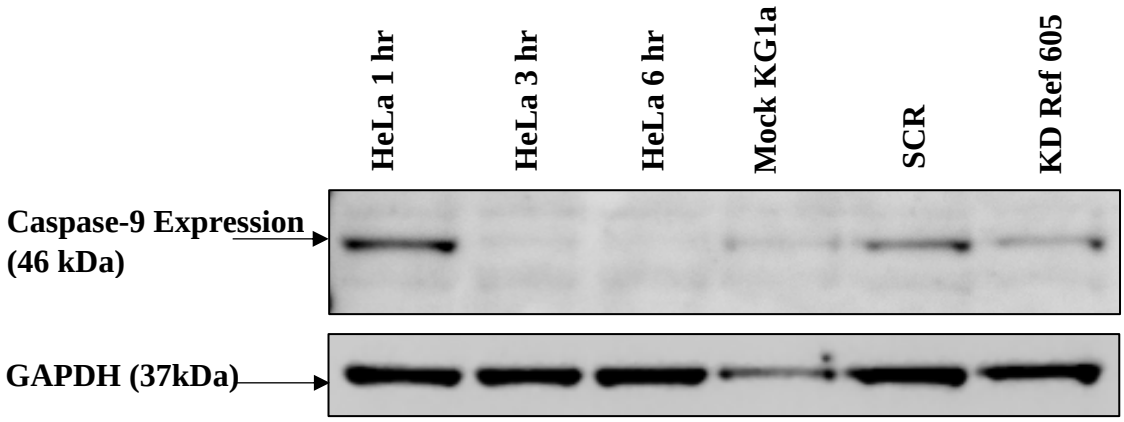

Figure 5-22 Caspase-9 protein levels are unchanged following hnRNPA0 KD in KG1a cells

WB analysis of Caspase-9 in hnRNPA0 KD and SCR KG1a cells. HeLa cells treated with staurosporine for 1, 3, and 6 hours were included as a positive control to induce apoptotic caspase activation. The blot shows detection of the ~46 kDa procaspase-9 band. GAPDH (37 kDa) was used as a loading control(N=1).

5.3 Discussion

5.3.1 Overview of key findings

This chapter demonstrates that reduced levels of hnRNPA0 in AML cells causes a transcriptional reprogramming of gene expression, suppressing proliferative networks and activating apoptotic and stress response pathways. RNA sequencing of hnRNPA0 KD KG1a cells produced high quality data, with over 94 % of reads aligning to the human genome, confirming that observed differences were biological rather than technical. In total**,** 1,179 transcripts were significantly altered (606 up and 573 downregulated), indicating that hnRNPA0 regulates a wide span of genes in AML. Pathway level analysis revealed a coherent pattern: cell cycle and DNA replication programmes were strongly suppressed, while stress responsive and apoptotic signatures were consistently enriched. Both GO and KEGG analyses highlighted reduced activity in E2F driven and G2/M checkpoint genes, whereas GSEA confirmed the enrichment of apoptosis and p53 related pathways, consistent with a cellular shift from proliferation toward a stress-adaptive, death prone state.

Among the genes most strongly affected was the pro apoptotic effector BCL2L11 (BIM), which increased markedly following reduction in hnRNPA0 levels. Further *hnRNPA0* and *BCL2L11* levels are inversely related across AML cohorts. Together, these observations indicate that reducing hnRNPA0 expression dampens cell cycle activity and is associated with transcriptional enrichment of apoptotic signalling pathways.

5.3.2 Mechanistic interpretation

The transcriptomic data indicate that loss of hnRNPA0 disrupts the balance between growth and stress adaptation in AML cells. This was evident from coordinated downregulation of E2F regulated and G2/M checkpoint genes, together with enrichment of apoptotic and p53 associated transcriptional pathways. These observations are consistent with the established role of hnRNPA0 as a post transcriptional regulator that stabilises damage response transcripts.

Earlier studies first described hnRNPA0 as a small nuclear component that binds RNA (Myer and Steitz 1995). Later, it was shown that the kinase MK2 can phosphorylate it on serine 84 during cellular stress (Rousseau et al. 2002). That phosphorylation appears to influence subcellular localisation and RNA binding affinity. When this signal is active, hnRNPA0 protects certain mRNAs from degradation especially those involved in cell cycle recovery and inflammatory signalling. When p53 is missing or defective, cells appear to rely on this MK2

hnRNPA0 branch as a substitute checkpoint system. In p53 defective non small cell lung cancer (NSCLC) models exposed to DNA damaging chemotherapy Cannell et al. (Cannell et al. 2015a) described how hnRNPA0 takes over part of p53's role by stabilising $p27^{Kip1}$ and GADD45A transcripts, which together hold the cycle at the G1/S and G2/M borders. This safeguard helps damaged cells pause long enough to repair DNA but also makes them more tolerant to chemotherapy.

In the AML model presented here, reduction of hnRNPA0 was associated with decreased expression of E2F and G2/M related transcriptional programmes, together with relative enrichment of apoptotic gene signatures. These findings are consistent with disruption of checkpoint-associated regulatory networks and increased transcriptional susceptibility to stress-responsive pathways.

The induction of BCL2L11 (BIM) following hnRNPA0 knockdown further supports the presence of an apoptosis-related transcriptional shift. However, given the limited protein-level validation and absence of strong caspase activation, these findings are best interpreted as evidence of apoptotic priming at the transcriptional level rather than definitive execution-phase apoptosis. Similar regulatory switching behaviour has been reported for other RNA binding proteins such as HuR (ELAVL1), whose localisation is controlled by Cdk1-dependent phosphorylation (Kim et al. 2008). In both cases, post-translational modification and nuclear–cytoplasmic shuttling influence whether protective or stress-associated transcripts are preferentially stabilised.

Altogether, these findings suggest that in AML cells hnRNPA0 functions as a post-transcriptional regulator of checkpoint associated gene expression. When present and phosphorylated, it contributes to maintenance of stress-adaptive transcriptional programmes; when reduced, checkpoint control may be compromised, accompanied by enrichment of apoptotic transcriptional signatures. This context dependent behaviour may help explain how hnRNPA0 supports tumour cell fitness under stress while creating transcriptional vulnerability when suppressed.

5.3.3 Comparison with existing literature

Several studies have investigated how RNA binding proteins influence cellular stress responses and survival in malignant cells (Cannell et al. 2015a), although relatively few have examined hnRNPA0 in the context of AML. Previous work has largely focused on solid tumours,

particularly lung and colorectal cancers, where hnRNPA0 supports cell survival following DNA damage by maintaining cell-cycle checkpoint integrity (Konishi et al. 2020).

My findings in AML are consistent with this conceptual framework but highlight a context dependent outcome. In contrast to solid tumours, loss of hnRNPA0 in AML is associated with suppression of proliferative programmes and relative enrichment of apoptotic transcriptional signatures, as reflected by downregulation of E2F- and G2/M associated gene networks and transcriptional evidence of increased apoptotic pathway activity following hnRNPA0 knockdown. This divergence likely reflects lineage-specific transcriptional dependencies and a reduced capacity of myeloid cells to compensate for disruption of post transcriptional regulation.

5.3.4 Limitations of the Study

The RNA seq experiments presented in this chapter were performed in a single AML cell line (KG1a), providing a controlled system in which to interrogate the transcriptional consequences of hnRNPA0 knockdown. While this approach enabled robust identification of hnRNPA0 associated transcriptional programmes, it does not capture the genetic heterogeneity or microenvironmental influences present in primary AML. Validation across additional AML cell lines and, ideally, ex vivo patient material will therefore be required to assess the broader generalisability of these findings (Domcke et al. 2013; Gillet et al. 2013).

A key limitation of this study is the lack of comprehensive protein level validation for the transcriptional changes identified by RNA-seq. Although RNA-level alterations provide important mechanistic insight, mRNA abundance does not always correlate directly with protein expression, particularly in the context of RNA binding proteins that regulate translation and mRNA stability. As such, the transcriptional signatures reported here should be interpreted as indicative of pathway-level disruption rather than definitive evidence of altered protein activity. Future studies incorporating systematic protein level analyses will be necessary to confirm the functional consequences of hnRNPA0 depletion.

This chapter primarily focused on transcriptional outputs following hnRNPA0 loss. RNA binding proteins frequently exert multi-layered regulatory effects, influencing not only transcript abundance but also mRNA splicing, export, localisation, and translation. These additional layers of post transcriptional regulation were beyond the scope of the present analysis but may contribute substantially to the observed phenotypes (Keene 2007; Kang et al. 2020).

It also remains unclear whether hnRNPA0 directly binds BCL2L11 (BIM) mRNA or whether BIM upregulation occurs indirectly through upstream stress responsive signalling pathways. Future experiments such as RIP seq or CLIP seq would enable direct identification of hnRNPA0 RNA targets and determine whether BIM transcripts are physically associated with hnRNPA0 (Ule et al. 2003; Keene 2007). In addition, targeted rescue experiments or reporter assays interrogating BIM 3′-UTR regions would help distinguish direct from indirect regulatory mechanisms.

An additional experimental limitation relates to the use of viral shRNA mediated knockdown approaches. Viral transduction can induce non-specific cellular stress responses, including interferon signalling and low level apoptotic priming, which may contribute to basal BIM expression observed in control cells (Bridge et al. 2003; Grimm et al. 2006). These effects complicate interpretation of downstream protein analyses and emphasise the value of complementary genetic strategies, such as CRISPR-Cas9 mediated gene editing, to confirm hnRNPA0 specific effects (Shalem et al. 2014).

Overall, while these limitations do not undermine the central transcriptional observations of this chapter, they define important boundaries for interpretation and highlight clear directions for future work aimed at resolving the mechanistic and protein-level consequences of hnRNPA0 dysregulation in AML.

5.3.5 Conclusion

Taken together, the findings presented in this chapter demonstrate that reduction of hnRNPA0 in AML cells is associated with extensive transcriptional reprogramming characterised by suppression of proliferative and cell cycle associated pathways and enrichment of stress responsive and apoptotic gene expression programmes. These transcriptional changes are consistent with the reduced cell growth and increased apoptotic susceptibility at the transcriptional level observed following hnRNPA0 knockdown in Chapter **4**.

Among the differentially expressed genes, BCL2L11 (BIM) emerged as a prominent stress responsive pro apoptotic factor whose expression increased following hnRNPA0 depletion and showed an inverse relationship with hnRNPA0 across AML cohorts. While protein level validation was limited, the combined transcriptomic, pathway level, and patient derived expression analyses support an association between hnRNPA0 reduction and apoptotic priming, rather than definitive activation of execution-phase apoptosis.

Protein level validation and functional follow up experiments were limited by time constraints associated with completion of this study; however, the transcriptomic datasets generated here provide a robust framework for future mechanistic investigations aimed at defining direct hnRNPA0 RNA targets and clarifying its role in apoptotic regulation in AML.

6 Discussion

AML is a biologically heterogeneous malignancy characterised by genetic, transcriptional and clinical diversity, which contributes to variable treatment responses and high relapse rates (Cancer Genome Atlas Research et al. 2013; Dohner et al. 2015; Dohner et al. 2022). Despite advances in molecular classification and targeted therapies, AML remains a disease with significant unmet clinical need, driven by high rates of primary treatment failure, frequent relapse, and the emergence of therapy resistance, particularly in older or unfit patients who are unable to tolerate intensive chemotherapy (Cancer Genome Atlas Research et al. 2013; Dohner et al. 2015; Short et al. 2020). Historically, much of AML research has focused on transcription factors and oncogenic signalling pathways as primary drivers of leukaemogenesis (Dohner et al. 2022). For example, recurrent alterations in transcription factors such as *RUNX1* and CEBPA, alongside aberrant activation of oncogenic signalling pathways including FLT3, have been shown to play central roles in AML initiation and maintenance (Cancer Genome Atlas Research et al. 2013; Dohner et al. 2022). While these approaches have provided important insights, they do not fully account for the dynamic regulation of gene expression required for cellular adaptation to stress, therapy, and microenvironmental cues (Hanahan and Weinberg 2011). To understand the changes in the proteome and transcriptome of AML blasts, a recent study analysed the nuclear proteome of AML blasts and compared it to normal human stem / progenitor cells ($CD34^+$) (Alanazi et al. 2020). This study showed widespread disruption of protein expression levels likely influencing nuclear regulatory networks important in the pathophysiology of AML (Alanazi et al. 2020). Within these dysregulated nuclear protein networks, multiple RNA binding proteins, including members of the hnRNP family, emerged as candidates of interest. RNA binding proteins (RBPs) play essential roles in determining mRNA splicing, stability, localisation and translation, thereby coordinating gene expression programmes in a context dependent manner (Keene 2007; Hentze et al. 2018). Through these mechanisms, RBPs enable rapid cellular responses to stress and contribute to phenotypic plasticity, a hallmark of malignant cells (Castello et al. 2012; Gebauer et al. 2021). Among RBPs, the hnRNP family constitutes a large and functionally diverse group of proteins with established roles in RNA metabolism and stress responses. Dysregulation of hnRNP family members has been implicated in multiple human diseases, including cancer, yet their roles in haematological malignancies such as AML remain incompletely defined (Gebauer et al. 2021).

6.1 Expression profiling of hnRNP family members in AML

Chapter 3 defined the expression landscape of many hnRNP family members across normal haematopoiesis and AML. Rather than establishing functional causality, this chapter aimed to identify patterns of hnRNP expression that are associated with AML and would therefore warrant deeper mechanistic investigation. Analysis of publicly available transcriptomic datasets revealed that many *hnRNP* mRNA expression is not uniform across haematopoietic differentiation but instead shows dynamic regulation as cells progress from stem and progenitor compartments toward mature myeloid lineages. This observation aligns with the established role of RBP as regulators of cellular plasticity, enabling rapid post transcriptional adaptation during differentiation and stress responses (Keene 2007; Hentze et al. 2018; Gebauer et al. 2021). Within AML cohorts, several hnRNPs displayed downregulated expression relative to normal haematopoietic counterparts, supporting the concept that post transcriptional regulatory networks are frequently disrupted in malignant cells (Castello et al. 2012; Hentze et al. 2018). Such dysregulation is increasingly recognised as a hallmark of cancer, contributing to phenotypic heterogeneity, stress tolerance, and therapy resistance beyond what can be explained by genetic lesions alone (Hanahan and Weinberg 2011; Castello et al. 2012). Importantly, Chapter 3 highlighted *hnRNPA0* and *hnRNPA3* as candidates of particular interest based on expression patterns that were consistently dysregulated in AML compared with normal haematopoietic cells and maintained across independent datasets.

Both *hnRNPA0* and *hnRNPA3* showed expression levels consistent with enrichment in malignant myeloid contexts and relative divergence from normal differentiation associated expression trajectories, suggesting potential relevance to leukaemic cell state rather than normal lineage maturation. These expression patterns are biologically plausible in light of prior literature implicating hnRNP family members in the regulation of stress responsive RNA programmes, cell cycle control, and checkpoint regulation. hnRNPs have been shown to modulate post-transcriptional networks that support cellular adaptation to genotoxic stress and proliferative pressure, processes that are central to AML pathobiology (Keene 2007; Castello et al. 2012; Hentze et al. 2018; Gebauer et al. 2021). However, expression (proteomic and transcriptomic) profiling alone cannot determine whether these proteins actively sustain leukaemic phenotypes or merely reflect broader transcriptional states.

It is important to acknowledge the limitations inherent to the analyses presented in Chapter 3. The expression profiling analyses were based on transcriptomic datasets which reflects mRNA abundance rather than protein levels or functional activity. Whilst some association with

protein levels was attempted, this dataset was limited to fifteen AML samples. As post-transcriptional regulation and protein stability are frequently altered in AML, mRNA expression alone may not accurately predict biological function. In addition, the analyses did not incorporate mutational status, longitudinal disease progression, or relapse-specific datasets, limiting the ability to assess whether hnRNPA0 or hnRNPA3 expression is associated with genetic drivers, disease evolution, or treatment resistance. Accordingly, while Chapter 3 identified hnRNPA0 and hnRNPA3 as biologically plausible candidates based on expression patterns, it could not determine causality or functional relevance. These limitations underscore the hypothesis-generating nature of the chapter and provided the rationale for subsequent functional perturbation studies and transcriptomic interrogation undertaken in Chapters 4 and 5.

6.2 Functional impact of hnRNPA0 and hnRNPA3 knockdown in AML cell lines

Chapter 4 moved beyond descriptive expression patterns to directly test whether altered hnRNP A0 or A3 expression had functional consequences for AML cells. Using targeted knockdown approaches (shRNA and CRISPR-Cas9), this chapter examined how perturbation of hnRNPA0 and hnRNPA3 expression influenced key cellular phenotypes relevant to leukaemia development, including cell growth, viability, and cell cycle progression. Knockdown of hnRNPA0 impaired AML cell fitness, leading to reduced proliferative capacity and compromised viability across multiple AML cell line models. These effects were accompanied by alterations in cell cycle distribution and increased apoptosis, supporting a role for hnRNPA0 as an active regulator of survival**.** This interpretation is consistent with prior studies implicating hnRNPA0 in stress-responsive RNA regulation, checkpoint control, and maintenance of cell survival under conditions of genotoxic or proliferative stress (Rousseau et al. 2002; Cannell et al. 2015a). In contrast, KD of hnRNPA3 resulted in a weaker and more variable phenotypic effect, suggesting that hnRNPA3 may play a more context dependent or supportive role within broader RNA regulatory networks rather than functioning as a dominant regulatory node. This distinction is in line with emerging literature indicating that hnRNP family members exhibit functional heterogeneity, with some proteins exerting central regulatory control while others contribute redundantly or in a context-specific manner (Keene 2007; Castello et al. 2012; Hentze et al. 2018; Gebauer et al. 2021).

Importantly, these functional studies were performed in a small number of AML cell line models, and whilst represent a tractable system for mechanistic studies do not fully capture the genetic, epigenetic, and microenvironmental complexity of primary AML (Gillet et al. 2013; Klco et al. 2014). As such, the observed differential dependency on hnRNPA0 versus hnRNPA3 should be interpreted with caution in the context of *in vitro* models. Extension of these findings into primary AML blasts, patient-derived xenograft (PDX) systems, or *in vivo* models will be required to establish translational relevance and determine whether hnRNPA0 dependency is maintained in more physiologically representative settings (Townsend et al. 2016; Brown and Carmichael 2024). Taken together, the data presented in Chapter 4 identify hnRNPA0 as a dominant post transcriptional regulator supporting AML cell survival, while suggesting a more limited or context dependent contribution for hnRNPA3.

6.3 Transcriptomic effects of hnRNPA0 knockdown in AML cells

Building on the functional findings of Chapter 4, which identified hnRNPA0 as a regulator of AML cell survival, Chapter 5 used RNA sequencing to investigate the global molecular consequences of hnRNPA0 KD in AML cells. This approach enabled unbiased analysis of transcriptome wide gene expression changes (Mortazavi et al. 2008; Wang et al. 2009). This strategy was particularly appropriate given the established role of hnRNPA0 as a post transcriptional regulator, whose effects are expected to manifest across coordinated gene networks rather than through isolated targets. RNAseq analysis revealed extensive transcriptional reprogramming following hnRNPA0 KD, with over one thousand transcripts significantly altered. Rather than focusing solely on individual genes, pathway level analyses were used to contextualise these changes. Functional enrichment approaches, including GO, KEGG and GSEA, are widely recognised as essential tools for interpreting large scale expression datasets by identifying coherent biological programmes affected by experimental perturbation (Subramanian et al. 2005; Liberzon et al. 2015; Conesa et al. 2016). Across these complementary analyses, a consistent pattern emerged. Transcripts associated with cell cycle progression, DNA replication, and E2F regulated programmes were broadly suppressed, while stress responsive and apoptotic pathways were enriched. This transcriptional signature aligns with previous descriptions of hnRNPA0 as a stress regulated RNA binding protein that supports checkpoint integrity and cell survival under conditions of genotoxic stress (Rousseau et al. 2002; Cannell et al. 2015a).

In the context of AML cells, reduction of hnRNPA0 appears to dismantle these protective networks, shifting the balance away from proliferation toward stress adaptation and apoptotic

priming. One of the most prominent transcriptional changes observed was the marked upregulation of BCL2L11 (BIM), a BH3 only pro apoptotic member of the BCL-2 family(see Chapter **5**). BIM is a well established mediator of mitochondrial apoptosis, acting through activation of BAX/BAK and antagonism of anti apoptotic BCL-2 proteins (O'Connor et al. 1998). Importantly, the transcriptomic findings were further supported by analysis of AML mRNA patient datasets, which demonstrated an inverse correlation between *hnRNPA0* and *BCL2L11* mRNA expression across patient cohorts (Cerami et al. 2012; Gao et al. 2013). While these associations do not establish direct regulation, they strengthen the relevance of the RNAseq findings beyond the cell line model and suggest that hnRNPA0 dependent transcriptional programmes may also operate in clinical AML.

Several limitations should be considered when interpreting the transcriptomic findings presented in Chapter 5. First, RNAseq captures changes in mRNA abundance but does not directly assess protein levels, post translational modifications, or functional protein activity. Given that RBP such as hnRNPA0 exert regulatory control at multiple post-transcriptional levels, including mRNA stability, localisation, and translation, important regulatory effects may not be fully reflected at the transcript level alone (Keene 2007; Kang et al. 2020). Second, the transcriptomic analyses were performed in AML cell line models, which provide a controlled and tractable system for mechanistic investigation but do not fully recapitulate the genetic heterogeneity, clonal architecture, or microenvironmental influences present in primary AML. Consequently, the transcriptional programmes identified here may not fully represent hnRNPA0 dependent regulation in patient blasts *in vivo.* Finally, the RNA sequencing analysis was conducted at a single experimental time point following hnRNPA0 KD and therefore does not capture dynamic or temporal changes in gene expression, nor does it distinguish primary hnRNPA0 dependent regulatory events from secondary stress responses. This is in addition to be studied in one cell line. Future studies incorporating proteomic profiling, temporal analyses, and validation in primary AML samples or *in vivo* models will be required to refine the mechanistic framework proposed here and to establish the translational relevance of hnRNPA0 dependent transcriptional programmes.

6.4 Clinical implications of hnRNPA0 dysregulation in AML

The findings presented in this thesis highlight the importance of hnRNPA0 contributing to leukaemic cell survival through coordinated control of apoptotic pathways. While transcription factors and signalling cascades have traditionally dominated therapeutic strategies in AML, increasing evidence indicates that dysregulation of RNA metabolism represents an additional

layer of vulnerability in malignant cells (Hentze et al. 2018; Gebauer et al. 2021). From a clinical perspective, the identification of hnRNPA0-dependent transcriptional programmes raises the possibility that hnRNPA0 expression or activity could serve as a biomarker of cellular stress tolerance or apoptotic priming in AML. Rather than acting as a direct therapeutic target, hnRNPA0 status may reflect the capacity of leukaemic cells to buffer genotoxic or metabolic stress, thereby influencing treatment response. In this context, reduced hnRNPA0 expression may reflect diminished stress tolerance in leukaemic cells, potentially predisposing them to enhanced apoptotic priming and altered sensitivity to apoptosis inducing therapies (Hanahan and Weinberg 2011; Hentze et al. 2018). Notably, transcriptomic analysis following hnRNPA0 KD revealed consistent upregulation of pro apoptotic signalling, including induction of BCL2L11, a key mediator of mitochondrial apoptosis.

BCL2L11 is a critical determinant of apoptotic priming and functions through activation of BAX - BAK and antagonism of anti apoptotic BCL-2 family proteins (O'Connor et al. 1998). This observation is of particular relevance given the established clinical use of the BCL-2 inhibitor venetoclax in AML. Venetoclax based therapies exploit mitochondrial apoptotic dependency and have demonstrated significant clinical benefit, particularly in older or unfit AML patients, where treatment responses are closely linked to apoptotic priming and BCL2L11 dependent signalling (Tyner et al. 2018; Short et al. 2020; Dohner et al. 2022). Although the present study does not directly assess drug sensitivity, the hnRNPA0 dependent induction of BCL2L11 provides a mechanistic rationale for future investigation into whether hnRNPA0 expression modulates responsiveness to venetoclax based regimens.

Importantly, direct therapeutic targeting of hnRNPA0 itself presents substantial challenges. As a multifunctional RBP lacking intrinsic enzymatic activity, hnRNPA0 is not readily amenable to conventional small-molecule inhibition. Moreover, hnRNPA0 participates in broad RNA regulatory networks, raising concerns regarding on-target toxicity in normal cells (Keene 2007; Castello et al. 2012). These considerations suggest that hnRNPA0 is more plausibly positioned as a contextual regulator or biomarker of therapeutic vulnerability rather than a standalone drug target. Taken together, the clinical relevance of hnRNPA0 dysregulation may lie in its capacity to shape apoptotic competence and stress adaptation in AML cells. By influencing the balance between survival and apoptotic priming, hnRNPA0 dependent regulatory programmes could contribute to differential treatment responses and may inform future strategies aimed at patient stratification or rational combination therapies, particularly in the context of venetoclax based treatment approaches.

6.5 Future directions

Although beyond the mechanistic framework proposed in this thesis, the findings also situate hnRNPA0 within a broader and rapidly evolving field of RNA regulatory therapeutics in AML. Increasingly, RNA metabolism is recognised not merely as a downstream reflection of oncogenic signalling, but as an active determinant of leukemic cell survival and stress adaptation (Hentze et al. 2018; Gebauer et al. 2021). Epitranscriptomic modifiers, particularly components of the m6A machinery, microRNAs, spliceosome factors, and RNA-binding proteins have all emerged as regulators of leukemic stem cell maintenance and treatment response (Hyde and Liu 2010; Zhou et al. 2017; Yankova et al. 2021; Zhou et al. 2021).

Preclinical studies targeting m6A regulators have demonstrated impaired AML propagation with relatively limited impact on normal haematopoiesis, suggesting a potential therapeutic window (Yankova et al. 2021; Zhou et al. 2021). In this context, disruption of post-transcriptional stabilisers such as hnRNPA0 may represent a complementary strategy, particularly if such proteins contribute to sustaining pro-survival transcriptional programmes or buffering apoptotic stress (Rousseau et al. 2002; Cannell et al. 2015a). While hnRNPA0 itself is not currently druggable using conventional small-molecule approaches, its position within RNA regulatory networks highlights a broader vulnerability at the level of post-transcriptional control (Keene 2007; Hentze et al. 2018).

Despite this promise, significant translational barriers remain. RNA-directed therapies face challenges including delivery to the bone marrow niche, endosomal escape, stability in circulation, and off-target effects (Hyde and Liu 2010; Garbayo et al. 2024). In addition, AML heterogeneity suggests that RNA regulatory dependencies are unlikely to be uniform across all patients (Cancer Genome Atlas Research et al. 2013; Dohner et al. 2022), reinforcing the need for biomarker-driven stratification strategies. It is therefore plausible that targeting RNA regulatory pathways will prove most effective in defined molecular subgroups or resistance settings rather than as universally applicable therapies.

In the near term, the most realistic therapeutic trajectory lies in rational combination approaches. RNA-directed interventions may function as resistance-modifying platforms that enhance sensitivity to established agents, including BCL-2 inhibition or stress-inducing therapies (Tyner et al. 2018; Short et al. 2020; Dohner et al. 2022). Within this framework, modulation of hnRNPA0-dependent transcriptional programmes could potentially influence

apoptotic priming and therapeutic responsiveness, although this requires direct functional validation.

Taken together, these considerations position RNA regulation not as an immediate replacement for current AML therapies, but as an emerging layer of therapeutic opportunity. Continued integration of transcriptomic profiling, mechanistic interrogation of RNA-binding proteins, and biomarker-guided clinical investigation will determine whether post-transcriptional vulnerabilities such as hnRNPA0 dependency can be translated into clinically meaningful strategies in AML.

.

6.6 Conclusion

hnRNPA0 is a context dependent regulator of AML cell survival, whose loss disrupts proliferative programmes and promotes apoptotic priming at the transcriptional level. More broadly, this work underscores the importance of RBP as integral components of leukaemic regulatory networks. This vulnerability may be exploitable through therapies that engage hnRNPA0 mediated apoptotic mechanisms, reinforcing the relevance of post transcriptional regulation as a critical but underexplored dimension of AML biology.

Refrenceses

Acar, M. et al. 2015. Deep imaging of bone marrow shows non-dividing stem cells are mainly perisinusoidal. *Nature* 526(7571), pp. 126-130. Available at: https://www.ncbi.nlm.nih.gov/pubmed/26416744doi: 10.1038/nature15250

Aguilar-Garrido, P., Otero-Sobrino, Á., Navarro-Aguadero, M., Velasco-Estévez, M. and Gallardo, M. 2022. The Role of RNA-Binding Proteins in Hematological Malignancies. *Int J Mol Sci* 23(17). doi: 10.3390/ijms23179552

Aitken, M. J. et al. 2022. Heterogeneous nuclear ribonucleoprotein K is overexpressed in acute myeloid leukemia and causes myeloproliferation in mice via altered Runx1 splicing. *NAR cancer* 4(4), p. zcac039.

Akashi, K., Traver, D., Miyamoto, T. and Weissman, I. L. 2000. A clonogenic common myeloid progenitor that gives rise to all myeloid lineages. *Nature* 404(6774), pp. 193-197. Available at: https://www.ncbi.nlm.nih.gov/pubmed/10724173doi: 10.1038/35004599

Alaggio, R. et al. 2022. The 5th edition of the World Health Organization Classification of Haematolymphoid Tumours: Lymphoid Neoplasms. *Leukemia* 36(7), pp. 1720-1748. Available at: https://doi.org/10.1038/s41375-022-01620-2doi: 10.1038/s41375-022-01620-2

Alanazi, B. et al. 2020. Integrated nuclear proteomics and transcriptomics identifies S100A4 as a therapeutic target in acute myeloid leukemia. *Leukemia* 34(2), pp. 427-440. Available at: https://www.ncbi.nlm.nih.gov/pubmed/31611628doi: 10.1038/s41375-019-0596-4

Alarcón, C. R., Goodarzi, H., Lee, H., Liu, X., Tavazoie, S. and Tavazoie, S. F. 2015. HNRNPA2B1 is a mediator of m6A-dependent nuclear RNA processing events. *Cell* 162(6), pp. 1299-1308.

Alberti, S., Gladfelter, A. and Mittag, T. 2019. Considerations and Challenges in Studying Liquid-Liquid Phase Separation and Biomolecular Condensates. *Cell* 176(3), pp. 419-434. Available at: https://www.ncbi.nlm.nih.gov/pubmed/30682370doi: 10.1016/j.cell.2018.12.035

Alpert, J. S. and Chen, Q. M. 2017. Stem Cell Therapy: The Phoenix in Clinical Medicine? *Am J Med* 130(9), pp. 1003-1004. doi: 10.1016/j.amjmed.2017.04.045

Amano, N. et al. 2021. High HNRNPA3 expression is associated with lymph node metastasis and poor prognosis in patients treated with radical cystectomy. *Urol Oncol* 39(3), pp. 196 e191-196 e197. Available at: https://www.ncbi.nlm.nih.gov/pubmed/33160845doi: 10.1016/j.urolonc.2020.10.072

Arai, F. et al. 2004. Tie2/angiopoietin-1 signaling regulates hematopoietic stem cell quiescence in the bone marrow niche. *Cell* 118(2), pp. 149-161. doi: 10.1016/j.cell.2004.07.004

Arber, D. A. et al. 2016. The 2016 revision to the World Health Organization classification of myeloid neoplasms and acute leukemia. *Blood* 127(20), pp. 2391-2405. doi: 10.1182/blood-2016-03-643544

Bagger, F. O., Kinalis, S. and Rapin, N. 2019. BloodSpot: a database of healthy and malignant haematopoiesis updated with purified and single cell mRNA sequencing profiles. *Nucleic Acids Res* 47(D1), pp. D881-D885. Available at: https://www.ncbi.nlm.nih.gov/pubmed/30395307doi: 10.1093/nar/gky1076

Baldridge, M. T., King, K. Y. and Goodell, M. A. 2011. Inflammatory signals regulate hematopoietic stem cells. *Trends Immunol* 32(2), pp. 57-65. doi: 10.1016/j.it.2010.12.003

Banani, S. F., Lee, H. O., Hyman, A. A. and Rosen, M. K. 2017. Biomolecular condensates: organizers of cellular biochemistry. *Nat Rev Mol Cell Biol* 18(5), pp. 285-298. Available at: https://www.ncbi.nlm.nih.gov/pubmed/28225081doi: 10.1038/nrm.2017.7

Barretina, J. et al. 2012. The Cancer Cell Line Encyclopedia enables predictive modelling of anticancer drug sensitivity. *Nature* 483(7391), pp. 603-607. Available at: https://www.ncbi.nlm.nih.gov/pubmed/22460905doi: 10.1038/nature11003

Bartoszewski, R. and Sikorski, A. F. 2019. Editorial focus: understanding off-target effects as the key to successful RNAi therapy. *Cell Mol Biol Lett* 24, p. 69. doi: 10.1186/s11658-019-0196-3

Batra, A., Sparks, A., Singh, R., Zakai, N. A. and Herrera, D. A. 2025. Characteristics and Survival of Secondary Acute Myeloid Leukemia From Myelodysplastic Syndromes in Older Adults: A Population Analysis. *Clin Lymphoma Myeloma Leuk* 25(6), pp. e417-e423. Available at: https://www.ncbi.nlm.nih.gov/pubmed/39952850doi: 10.1016/j.clml.2025.01.012

Baum, C. M., Weissman, I. L., Tsukamoto, A. S., Buckle, A. M. and Peault, B. 1992. Isolation of a candidate human hematopoietic stem-cell population. *Proc Natl Acad Sci U S A* 89(7), pp. 2804-2808. Available at: https://www.ncbi.nlm.nih.gov/pubmed/1372992doi: 10.1073/pnas.89.7.2804

Bazinet, A. et al. 2022. Azacitidine plus venetoclax in patients with high-risk myelodysplastic syndromes or chronic myelomonocytic leukaemia: phase 1 results of a single-centre, dose-escalation, dose-expansion, phase 1–2 study. *The Lancet Haematology* 9(10), pp. e756-e765. Available at: https://doi.org/10.1016/S2352-3026(22)00216-2doi: 10.1016/S2352-3026(22)00216-2 [Accessed: 2025/11/17].

Beijer, D. et al. 2021. Characterization of HNRNPA1 mutations defines diversity in pathogenic mechanisms and clinical presentation. *JCI Insight* 6(14). Available at: https://www.ncbi.nlm.nih.gov/pubmed/34291734doi: 10.1172/jci.insight.148363

Belhadj, S., Terradas, M., Munoz-Torres, P. M., Aiza, G., Navarro, M., Capella, G. and Valle, L. 2020. Candidate genes for hereditary colorectal cancer: Mutational screening and systematic review. *Human Mutation* 41(9), pp. 1563-1576.

Berg, J. S. et al. 2011. Imprinted genes that regulate early mammalian growth are coexpressed in somatic stem cells. *PLoS One* 6(10), p. e26410. Available at: https://www.ncbi.nlm.nih.gov/pubmed/22039481doi: 10.1371/journal.pone.0026410

Bick, A. G. et al. 2020. Inherited causes of clonal haematopoiesis in 97,691 whole genomes. *Nature* 586(7831), pp. 763-768. doi: 10.1038/s41586-020-2819-2

Boisset, J. C., van Cappellen, W., Andrieu-Soler, C., Galjart, N., Dzierzak, E. and Robin, C. 2010. In vivo imaging of haematopoietic cells emerging from the mouse aortic endothelium. *Nature* 464(7285), pp. 116-120. Available at: https://www.ncbi.nlm.nih.gov/pubmed/20154729doi: 10.1038/nature08764

Bomsztyk, K., Denisenko, O. and Ostrowski, J. 2004. hnRNP K: one protein multiple processes. *Bioessays* 26(6), pp. 629-638. Available at: https://www.ncbi.nlm.nih.gov/pubmed/15170860doi: 10.1002/bies.20048

Bouillet, P. et al. 1999. Proapoptotic Bcl-2 relative Bim required for certain apoptotic responses, leukocyte homeostasis, and to preclude autoimmunity. *Science* 286(5445), pp. 1735-1738. Available at: https://www.ncbi.nlm.nih.gov/pubmed/10576740doi: 10.1126/science.286.5445.1735

Bridge, A. J., Pebernard, S., Ducraux, A., Nicoulaz, A.-L. and Iggo, R. 2003. Induction of an interferon response by RNAi vectors in mammalian cells. *Nature Genetics* 34(3), pp. 263-264. Available at: https://doi.org/10.1038/ng1173doi: 10.1038/ng1173

Broughton, S. E. et al. 2012. The GM-CSF/IL-3/IL-5 cytokine receptor family: from ligand recognition to initiation of signaling. *Immunol Rev* 250(1), pp. 277-302. doi: 10.1111/j.1600-065X.2012.01164.x

Brown, F. C. and Carmichael, C. L. 2024. Patient-Derived Xenograft Models for Leukemias. *Methods Mol Biol* 2806, pp. 31-40. doi: 10.1007/978-1-0716-3858-3_4

Cai, X. et al. 2025. Epigenetic-modification associated hnRNPA3 acts as a prognostic biomarker and promotes malignant progression of HCC. *BMC Cancer* 25(1), p. 661. Available at: https://www.ncbi.nlm.nih.gov/pubmed/40211173doi: 10.1186/s12885-025-14028-9

Calvi, L. M. et al. 2003. Osteoblastic cells regulate the haematopoietic stem cell niche. *Nature* 425(6960), pp. 841-846. doi: 10.1038/nature02040

Camacho, V., McClearn, V., Patel, S. and Welner, R. S. 2017. Regulation of normal and leukemic stem cells through cytokine signaling and the microenvironment. *Int J Hematol* 105(5), pp. 566-577. Available at: https://www.ncbi.nlm.nih.gov/pubmed/28176225doi: 10.1007/s12185-017-2184-6

Cancer Genome Atlas Research, N. et al. 2013. Genomic and epigenomic landscapes of adult de novo acute myeloid leukemia. *N Engl J Med* 368(22), pp. 2059-2074. Available at: https://www.ncbi.nlm.nih.gov/pubmed/23634996doi: 10.1056/NEJMoa1301689

Cannell, I. G. et al. 2015a. A Pleiotropic RNA-Binding Protein Controls Distinct Cell Cycle Checkpoints to Drive Resistance of p53-Defective Tumors to Chemotherapy. *Cancer Cell* 28(5), pp. 623-637. Available at: https://www.ncbi.nlm.nih.gov/pubmed/26602816doi: 10.1016/j.ccell.2015.09.009

Cannell, I. G. et al. 2015b. A Pleiotropic RNA-Binding Protein Controls Distinct Cell Cycle Checkpoints to Drive Resistance of p53-Defective Tumors to Chemotherapy. *Cancer Cell* 28(6), p. 831. Available at: https://www.ncbi.nlm.nih.gov/pubmed/28843280doi: 10.1016/j.ccell.2015.11.003

Cao, Z., Guan, L., Yu, R., Yang, F. and Chen, J. 2023. High Expression of Heterogeneous Nuclear Ribonucleoprotein A1 Facilitates Hepatocellular Carcinoma Growth. *J Hepatocell Carcinoma* 10, pp. 517-530. Available at: https://www.ncbi.nlm.nih.gov/pubmed/37034304doi: 10.2147/JHC.S402247

Castello, A. et al. 2012. Insights into RNA biology from an atlas of mammalian mRNA-binding proteins. *Cell* 149(6), pp. 1393-1406. doi: 10.1016/j.cell.2012.04.031

Cerami, E. et al. 2012. The cBio cancer genomics portal: an open platform for exploring multidimensional cancer genomics data. *Cancer Discov* 2(5), pp. 401-404. Available at: https://www.ncbi.nlm.nih.gov/pubmed/22588877doi: 10.1158/2159-8290.CD-12-0095

Chambers, S. M. et al. 2007. Hematopoietic fingerprints: an expression database of stem cells and their progeny. *Cell Stem Cell* 1(5), pp. 578-591. Available at: https://www.ncbi.nlm.nih.gov/pubmed/18371395doi: 10.1016/j.stem.2007.10.003

Chen, C., Huang, L., Sun, Q., Yu, Z., Wang, X. and Bu, L. 2022. HNRNPA2B1 Demonstrates Diagnostic and Prognostic Values Based on Pan-Cancer Analyses. *Comput Math Methods Med* 2022, p. 9867660. Available at: https://www.ncbi.nlm.nih.gov/pubmed/35529270doi: 10.1155/2022/9867660

Chen, F., Li, G., Fu, S. and Zhang, J. 2025. Functional Landscape of hnRNPA3 in Disease Pathogenesis. *Wiley Interdiscip Rev RNA* 16(2), p. e70010. Available at: https://www.ncbi.nlm.nih.gov/pubmed/40130711doi: 10.1002/wrna.70010

Chen, J. et al. 2021. Off-target effects of RNAi correlate with the mismatch rate between dsRNA and non-target mRNA. *RNA Biol* 18(11), pp. 1747-1759. Available at: https://www.ncbi.nlm.nih.gov/pubmed/33397184doi: 10.1080/15476286.2020.1868680

Chi, E. Y., Weickmann, J., Carpenter, J. F., Manning, M. C. and Randolph, T. W. 2005. Heterogeneous nucleation-controlled particulate formation of recombinant human platelet-activating factor acetylhydrolase in pharmaceutical formulation. *J Pharm Sci* 94(2), pp. 256-274. Available at: https://www.ncbi.nlm.nih.gov/pubmed/15570600doi: 10.1002/jps.20237

Chow, A. et al. 2011. Bone marrow CD169+ macrophages promote the retention of hematopoietic stem and progenitor cells in the mesenchymal stem cell niche. *J Exp Med* 208(2), pp. 261-271. Available at: https://www.ncbi.nlm.nih.gov/pubmed/21282381doi: 10.1084/jem.20101688

Clarke, J. P., Thibault, P. A., Salapa, H. E. and Levin, M. C. 2021. A Comprehensive Analysis of the Role of hnRNP A1 Function and Dysfunction in the Pathogenesis of Neurodegenerative Disease. *Front Mol Biosci* 8, p. 659610. Available at: https://www.ncbi.nlm.nih.gov/pubmed/33912591doi: 10.3389/fmolb.2021.659610

Clery, A., Blatter, M. and Allain, F. H. 2008. RNA recognition motifs: boring? Not quite. *Curr Opin Struct Biol* 18(3), pp. 290-298. Available at: https://www.ncbi.nlm.nih.gov/pubmed/18515081doi: 10.1016/j.sbi.2008.04.002

Collonnier, C. et al. 2017. CRISPR-Cas9-mediated efficient directed mutagenesis and RAD51-dependent and RAD51-independent gene targeting in the moss Physcomitrella patens. *Plant Biotechnol J* 15(1), pp. 122-131. Available at: https://www.ncbi.nlm.nih.gov/pubmed/27368642doi: 10.1111/pbi.12596

Comazzetto, S., Shen, B. and Morrison, S. J. 2021a. Niches that regulate stem cells and hematopoiesis in adult bone marrow. *Dev Cell* 56(13), pp. 1848-1860. doi: 10.1016/j.devcel.2021.05.018

Comazzetto, S., Shen, B. and Morrison, S. J. 2021b. Niches that regulate stem cells and hematopoiesis in adult bone marrow. *Developmental Cell* 56(13), pp. 1848-1860. Available at: https://doi.org/10.1016/j.devcel.2021.05.018doi: 10.1016/j.devcel.2021.05.018 [Accessed: 2025/11/08].

Conesa, A. et al. 2016. A survey of best practices for RNA-seq data analysis. *Genome Biol* 17, p. 13. Available at: https://www.ncbi.nlm.nih.gov/pubmed/26813401doi: 10.1186/s13059-016-0881-8

David, C. J., Chen, M., Assanah, M., Canoll, P. and Manley, J. L. 2010. HnRNP proteins controlled by c-Myc deregulate pyruvate kinase mRNA splicing in cancer. *Nature* 463(7279), pp. 364-368. Available at: https://www.ncbi.nlm.nih.gov/pubmed/20010808doi: 10.1038/nature08697

Dempster, J. M. et al. 2021. Chronos: a cell population dynamics model of CRISPR experiments that improves inference of gene fitness effects. *Genome Biol* 22(1), p. 343. Available at: https://www.ncbi.nlm.nih.gov/pubmed/34930405doi: 10.1186/s13059-021-02540-7

Desai, P. et al. 2018. Somatic mutations precede acute myeloid leukemia years before diagnosis. *Nature Medicine* 24(7), pp. 1015-1023. Available at: https://doi.org/10.1038/s41591-018-0081-zdoi: 10.1038/s41591-018-0081-z

Di Tullio, A., Vu Manh, T. P., Schubert, A., Castellano, G., Mansson, R. and Graf, T. 2011. CCAAT/enhancer binding protein alpha (C/EBP(alpha))-induced transdifferentiation of pre-B cells into macrophages involves no overt retrodifferentiation. *Proc Natl Acad Sci U S A* 108(41), pp. 17016-17021. Available at: https://www.ncbi.nlm.nih.gov/pubmed/21969581doi: 10.1073/pnas.1112169108

Dias, S., Månsson, R., Gurbuxani, S., Sigvardsson, M. and Kee, B. L. 2008. E2A proteins promote development of lymphoid-primed multipotent progenitors. *Immunity* 29(2), pp. 217-227. doi: 10.1016/j.immuni.2008.05.015

DiNardo, C. D. et al. 2020. Azacitidine and Venetoclax in Previously Untreated Acute Myeloid Leukemia. *N Engl J Med* 383(7), pp. 617-629. doi: 10.1056/NEJMoa2012971

Dlamini, Z., Shoba, B. and Hull, R. 2020. Splicing machinery genomics events in acute myeloid leukaemia (AML): in search for therapeutic targets, diagnostic and prognostic biomarkers. *Am J Cancer Res* 10(9), pp. 2690-2704. Available at: https://www.ncbi.nlm.nih.gov/pubmed/33042611

Döhner, H. et al. 2024. Genetic risk classification for adults with AML receiving less-intensive therapies: the 2024 ELN recommendations. *Blood* 144(21), pp. 2169-2173. doi: 10.1182/blood.2024025409

Dohner, H. et al. 2022. Diagnosis and management of AML in adults: 2022 recommendations from an international expert panel on behalf of the ELN. *Blood* 140(12), pp. 1345-1377. Available at: https://www.ncbi.nlm.nih.gov/pubmed/35797463doi: 10.1182/blood.2022016867

Dohner, H., Weisdorf, D. J. and Bloomfield, C. D. 2015. Acute Myeloid Leukemia. *N Engl J Med* 373(12), pp. 1136-1152. Available at: https://www.ncbi.nlm.nih.gov/pubmed/26376137doi: 10.1056/NEJMra1406184

Domcke, S., Sinha, R., Levine, D. A., Sander, C. and Schultz, N. 2013. Evaluating cell lines as tumour models by comparison of genomic profiles. *Nature Communications* 4(1), p. 2126. Available at: https://doi.org/10.1038/ncomms3126doi: 10.1038/ncomms3126

Dreyfuss, G., Kim, V. N. and Kataoka, N. 2002. Messenger-RNA-binding proteins and the messages they carry. *Nat Rev Mol Cell Biol* 3(3), pp. 195-205. doi: 10.1038/nrm760

Dreyfuss, G., Matunis, M. J., Pinol-Roma, S. and Burd, C. G. 1993. hnRNP proteins and the biogenesis of mRNA. *Annu Rev Biochem* 62, pp. 289-321. Available at: https://www.ncbi.nlm.nih.gov/pubmed/8352591doi: 10.1146/annurev.bi.62.070193.001445

Dzierzak, E. and Speck, N. A. 2008. Of lineage and legacy: the development of mammalian hematopoietic stem cells. *Nat Immunol* 9(2), pp. 129-136. doi: 10.1038/ni1560

Essers, M. A., Offner, S., Blanco-Bose, W. E., Waibler, Z., Kalinke, U., Duchosal, M. A. and Trumpp, A. 2009. IFNalpha activates dormant haematopoietic stem cells in vivo. *Nature* 458(7240), pp. 904-908. doi: 10.1038/nature07815

Fuster, J. J. et al. 2017. Clonal hematopoiesis associated with TET2 deficiency accelerates atherosclerosis development in mice. *Science* 355(6327), pp. 842-847. doi: 10.1126/science.aag1381

Gallardo, M., Hornbaker, M. J., Zhang, X., Hu, P., Bueso-Ramos, C. and Post, S. M. 2016. Aberrant hnRNP K expression: All roads lead to cancer. *Cell Cycle* 15(12), pp. 1552-1557. Available at: https://www.ncbi.nlm.nih.gov/pubmed/27049467doi: 10.1080/15384101.2016.1164372

Gallardo, M. et al. 2015. hnRNP K Is a Haploinsufficient Tumor Suppressor that Regulates Proliferation and Differentiation Programs in Hematologic Malignancies. *Cancer Cell* 28(4), pp. 486-499. Available at: https://www.ncbi.nlm.nih.gov/pubmed/26412324doi: 10.1016/j.ccell.2015.09.001

Gao, R., Yu, Y., Inoue, A., Widodo, N., Kaul, S. C. and Wadhwa, R. 2013. Heterogeneous nuclear ribonucleoprotein K (hnRNP-K) promotes tumor metastasis by induction of genes involved in extracellular matrix, cell movement, and angiogenesis. *J Biol Chem* 288(21), pp. 15046-15056. Available at: https://www.ncbi.nlm.nih.gov/pubmed/23564449doi: 10.1074/jbc.M113.466136

Garbayo, E. et al. 2024. RNA-loaded nanoparticles for the treatment of hematological cancers. *Adv Drug Deliv Rev* 214, p. 115448. Available at: https://www.ncbi.nlm.nih.gov/pubmed/39303823doi: 10.1016/j.addr.2024.115448

Gebauer, F., Schwarzl, T., Valcarcel, J. and Hentze, M. W. 2021. RNA-binding proteins in human genetic disease. *Nat Rev Genet* 22(3), pp. 185-198. Available at: https://www.ncbi.nlm.nih.gov/pubmed/33235359doi: 10.1038/s41576-020-00302-y

Genovese, G. et al. 2014. Clonal hematopoiesis and blood-cancer risk inferred from blood DNA sequence. *N Engl J Med* 371(26), pp. 2477-2487. Available at: https://www.ncbi.nlm.nih.gov/pubmed/25426838doi: 10.1056/NEJMoa1409405

Geuens, T., Bouhy, D. and Timmerman, V. 2016. The hnRNP family: insights into their role in health and disease. *Human genetics* 135(8), pp. 851-867.

Gillet, J. P., Varma, S. and Gottesman, M. M. 2013. The clinical relevance of cancer cell lines. *J Natl Cancer Inst* 105(7), pp. 452-458. Available at: https://www.ncbi.nlm.nih.gov/pubmed/23434901doi: 10.1093/jnci/djt007

Goel, K. and Ploski, J. E. 2022. RISC-y Business: Limitations of Short Hairpin RNA-Mediated Gene Silencing in the Brain and a Discussion of CRISPR/Cas-Based Alternatives. *Front Mol Neurosci* 15, p. 914430. doi: 10.3389/fnmol.2022.914430

Goulard, M., Dosquet, C. and Bonnet, D. 2018. Role of the microenvironment in myeloid malignancies. *Cell Mol Life Sci* 75(8), pp. 1377-1391. Available at: https://www.ncbi.nlm.nih.gov/pubmed/29222645doi: 10.1007/s00018-017-2725-4

Grimm, D. et al. 2006. Fatality in mice due to oversaturation of cellular microRNA/short hairpin RNA pathways. *Nature* 441(7092), pp. 537-541. doi: 10.1038/nature04791

Guidugli, L. et al. 2017. Clinical utility of gene panel-based testing for hereditary myelodysplastic syndrome/acute leukemia predisposition syndromes. *Leukemia* 31(5), pp. 1226-1229. Available at: https://www.ncbi.nlm.nih.gov/pubmed/28104920doi: 10.1038/leu.2017.28

Haferlach, T. et al. 2010. Clinical utility of microarray-based gene expression profiling in the diagnosis and subclassification of leukemia: report from the International Microarray Innovations in Leukemia Study Group. *J Clin Oncol* 28(15), pp. 2529-2537. Available at: https://www.ncbi.nlm.nih.gov/pubmed/20406941doi: 10.1200/JCO.2009.23.4732

Han, S. P., Tang, Y. H. and Smith, R. 2010a. Functional diversity of the hnRNPs: past, present and perspectives. *Biochem J* 430(3), pp. 379-392. doi: 10.1042/bj20100396

Han, Siew P., Tang, Yue H. and Smith, R. 2010b. Functional diversity of the hnRNPs: past, present and perspectives. *Biochemical Journal* 430(3), pp. 379-392. Available at: https://doi.org/10.1042/BJ20100396doi: 10.1042/bj20100396 [Accessed: 11/20/2025].

Hanahan, D. and Weinberg, R. A. 2011. Hallmarks of cancer: the next generation. *Cell* 144(5), pp. 646-674. Available at: https://www.ncbi.nlm.nih.gov/pubmed/21376230doi: 10.1016/j.cell.2011.02.013

Hennig, S. et al. 2015. Prion-like domains in RNA binding proteins are essential for building subnuclear paraspeckles. *J Cell Biol* 210(4), pp. 529-539. doi: 10.1083/jcb.201504117

Hentze, M. W., Castello, A., Schwarzl, T. and Preiss, T. 2018. A brave new world of RNA-binding proteins. *Nat Rev Mol Cell Biol* 19(5), pp. 327-341. Available at: https://www.ncbi.nlm.nih.gov/pubmed/29339797doi: 10.1038/nrm.2017.130

Hercus, T. R., Thomas, D., Guthridge, M. A., Ekert, P. G., King-Scott, J., Parker, M. W. and Lopez, A. F. 2009. The granulocyte-macrophage colony-stimulating factor receptor: linking its structure to cell signaling and its role in disease. *Blood* 114(7), pp. 1289-1298. doi: 10.1182/blood-2008-12-164004

Higuchi, M., O'Brien, D., Kumaravelu, P., Lenny, N., Yeoh, E. J. and Downing, J. R. 2002. Expression of a conditional AML1-ETO oncogene bypasses embryonic lethality and establishes a murine model of human t(8;21) acute myeloid leukemia. *Cancer Cell* 1(1), pp. 63-74. Available at: https://www.ncbi.nlm.nih.gov/pubmed/12086889doi: 10.1016/s1535-6108(02)00016-8

Ho, J. S. et al. 2021. HNRNPM controls circRNA biogenesis and splicing fidelity to sustain cancer cell fitness. *Elife* 10. doi: 10.7554/eLife.59654

Hodson, D. J., Screen, M. and Turner, M. 2019. RNA-binding proteins in hematopoiesis and hematological malignancy. *Blood* 133(22), pp. 2365-2373. doi: 10.1182/blood-2018-10-839985

Hormaechea-Agulla, D. et al. 2021. Chronic infection drives Dnmt3a-loss-of-function clonal hematopoiesis via IFNγ signaling. *Cell Stem Cell* 28(8), pp. 1428-1442.e1426. doi: 10.1016/j.stem.2021.03.002

Hyde, R. K. and Liu, P. P. 2010. The role of microRNAs in acute myeloid leukemia. *F1000 Biol Rep* 2, p. 81. Available at: https://www.ncbi.nlm.nih.gov/pubmed/21170374doi: 10.3410/B2-81

Ikizler, T. A. et al. 2020. KDOQI Clinical Practice Guideline for Nutrition in CKD: 2020 Update. *American Journal of Kidney Diseases* 76(3, Supplement 1), pp. S1-S107. Available at: https://www.sciencedirect.com/science/article/pii/S0272638620307265doi: https://doi.org/10.1053/j.ajkd.2020.05.006

Iwasaki, H. and Akashi, K. 2007. Myeloid lineage commitment from the hematopoietic stem cell. *Immunity* 26(6), pp. 726-740. doi: 10.1016/j.immuni.2007.06.004

Jackson, A. L. et al. 2003. Expression profiling reveals off-target gene regulation by RNAi. *Nat Biotechnol* 21(6), pp. 635-637. Available at: https://www.ncbi.nlm.nih.gov/pubmed/12754523doi: 10.1038/nbt831

Jain, S., Wheeler, J. R., Walters, R. W., Agrawal, A., Barsic, A. and Parker, R. 2016. ATPase-Modulated Stress Granules Contain a Diverse Proteome and Substructure. *Cell* 164(3), pp. 487-498. Available at: https://www.ncbi.nlm.nih.gov/pubmed/26777405doi: 10.1016/j.cell.2015.12.038

Jaiswal, S. et al. 2014. Age-related clonal hematopoiesis associated with adverse outcomes. *N Engl J Med* 371(26), pp. 2488-2498. Available at: https://www.ncbi.nlm.nih.gov/pubmed/25426837doi: 10.1056/NEJMoa1408617

Jean-Philippe, J., Paz, S. and Caputi, M. 2013. hnRNP A1: the Swiss army knife of gene expression. *Int J Mol Sci* 14(9), pp. 18999-19024. Available at: https://www.ncbi.nlm.nih.gov/pubmed/24065100doi: 10.3390/ijms140918999

Jin, Z., Liang, F., Yang, J. and Mei, W. 2017. hnRNP I regulates neonatal immune adaptation and prevents colitis and colorectal cancer. *PLoS Genet* 13(3), p. e1006672. Available at: https://www.ncbi.nlm.nih.gov/pubmed/28296893doi: 10.1371/journal.pgen.1006672

Jungfleisch, J. and Gebauer, F. 2025. RNA-binding proteins as therapeutic targets in cancer. *RNA Biol* 22(1), pp. 1-8. doi: 10.1080/15476286.2025.2470511

Kang, D., Lee, Y. and Lee, J. S. 2020. RNA-Binding Proteins in Cancer: Functional and Therapeutic Perspectives. *Cancers (Basel)* 12(9). doi: 10.3390/cancers12092699

Kedzierska, H. and Piekielko-Witkowska, A. 2017. Splicing factors of SR and hnRNP families as regulators of apoptosis in cancer. *Cancer Lett* 396, pp. 53-65. Available at: https://www.ncbi.nlm.nih.gov/pubmed/28315432doi: 10.1016/j.canlet.2017.03.013

Keene, J. D. 2007. RNA regulons: coordination of post-transcriptional events. *Nat Rev Genet* 8(7), pp. 533-543. Available at: https://www.ncbi.nlm.nih.gov/pubmed/17572691doi: 10.1038/nrg2111

Keeshan, K., Santilli, G., Corradini, F., Perrotti, D. and Calabretta, B. 2003. Transcription activation function of C/EBPalpha is required for induction of granulocytic differentiation. *Blood* 102(4), pp. 1267-1275. Available at: https://www.ncbi.nlm.nih.gov/pubmed/12702500doi: 10.1182/blood-2003-02-0477

Kim, H. H. et al. 2008. Nuclear HuR accumulation through phosphorylation by Cdk1. *Genes Dev* 22(13), pp. 1804-1815. doi: 10.1101/gad.1645808

King, K. Y. and Goodell, M. A. 2011. Inflammatory modulation of HSCs: viewing the HSC as a foundation for the immune response. *Nature Reviews Immunology* 11(10), pp. 685-692. Available at: https://doi.org/10.1038/nri3062doi: 10.1038/nri3062

Klco, J. M. et al. 2014. Functional heterogeneity of genetically defined subclones in acute myeloid leukemia. *Cancer Cell* 25(3), pp. 379-392. Available at: https://www.ncbi.nlm.nih.gov/pubmed/24613412doi: 10.1016/j.ccr.2014.01.031

Klein, H. U., Ruckert, C., Kohlmann, A., Bullinger, L., Thiede, C., Haferlach, T. and Dugas, M. 2009. Quantitative comparison of microarray experiments with published leukemia related gene expression signatures. *BMC Bioinformatics* 10, p. 422. Available at: https://www.ncbi.nlm.nih.gov/pubmed/20003504doi: 10.1186/1471-2105-10-422

Kobayashi, H. et al. 2010. Angiocrine factors from Akt-activated endothelial cells balance self-renewal and differentiation of haematopoietic stem cells. *Nat Cell Biol* 12(11), pp. 1046-1056. doi: 10.1038/ncb2108

Kohlmann, A. et al. 2008. An international standardization programme towards the application of gene expression profiling in routine leukaemia diagnostics: the Microarray Innovations in LEukemia study prephase. *Br J Haematol* 142(5), pp. 802-807. Available at: https://www.ncbi.nlm.nih.gov/pubmed/18573112doi: 10.1111/j.1365-2141.2008.07261.x

Konig, M. F., Giles, J. T., Nigrovic, P. A. and Andrade, F. 2016. Antibodies to native and citrullinated RA33 (hnRNP A2/B1) challenge citrullination as the inciting principle underlying loss of tolerance in rheumatoid arthritis. *Ann Rheum Dis* 75(11), pp. 2022-2028. Available at: https://www.ncbi.nlm.nih.gov/pubmed/26865600doi: 10.1136/annrheumdis-2015-208529

Konishi, H. et al. 2020. A tumor-specific modulation of heterogeneous ribonucleoprotein A0 promotes excessive mitosis and growth in colorectal cancer cells. *Cell Death Dis* 11(4), p. 245. Available at: https://www.ncbi.nlm.nih.gov/pubmed/32303675doi: 10.1038/s41419-020-2439-7

Koury, M. J. and Ponka, P. 2004. New insights into erythropoiesis: the roles of folate, vitamin B12, and iron. *Annu Rev Nutr* 24, pp. 105-131. doi: 10.1146/annurev.nutr.24.012003.132306

Kwon, I. et al. 2013. Phosphorylation-regulated binding of RNA polymerase II to fibrous polymers of low-complexity domains. *Cell* 155(5), pp. 1049-1060. Available at: https://www.ncbi.nlm.nih.gov/pubmed/24267890doi: 10.1016/j.cell.2013.10.033

Lachowiez, C. A., DiNardo, C. D. and Loghavi, S. 2023. Molecularly Targeted Therapy in Acute Myeloid Leukemia: Current Treatment Landscape and Mechanisms of Response and Resistance. *Cancers (Basel)* 15(5). doi: 10.3390/cancers15051617

Lal, A., Mazan-Mamczarz, K., Kawai, T., Yang, X., Martindale, J. L. and Gorospe, M. 2004. Concurrent versus individual binding of HuR and AUF1 to common labile target mRNAs. *EMBO J* 23(15), pp. 3092-3102. doi: 10.1038/sj.emboj.7600305

Laslo, P. et al. 2006. Multilineage transcriptional priming and determination of alternate hematopoietic cell fates. *Cell* 126(4), pp. 755-766. doi: 10.1016/j.cell.2006.06.052

Laurenti, E. and Göttgens, B. 2018. From haematopoietic stem cells to complex differentiation landscapes. *Nature* 553(7689), pp. 418-426. doi: 10.1038/nature25022

Lee, B. P., Pilling, L. C., Bandinelli, S., Ferrucci, L., Melzer, D. and Harries, L. W. 2019. The transcript expression levels of HNRNPM, HNRNPA0 and AKAP17A splicing factors may be predictively associated with ageing phenotypes in human peripheral blood. *Biogerontology* 20(5), pp. 649-663. Available at: https://www.ncbi.nlm.nih.gov/pubmed/31292793doi: 10.1007/s10522-019-09819-0

Lennartsson, J. and Ronnstrand, L. 2012. Stem cell factor receptor/c-Kit: from basic science to clinical implications. *Physiol Rev* 92(4), pp. 1619-1649. Available at: https://www.ncbi.nlm.nih.gov/pubmed/23073628doi: 10.1152/physrev.00046.2011

Li, Z. et al. 2023. Research Progress on the Structural and Functional Roles of hnRNPs in Muscle Development. *Biomolecules* 13(10). doi: 10.3390/biom13101434

Liberzon, A., Birger, C., Thorvaldsdottir, H., Ghandi, M., Mesirov, J. P. and Tamayo, P. 2015. The Molecular Signatures Database (MSigDB) hallmark gene set collection. *Cell Syst* 1(6), pp. 417-425. Available at: https://www.ncbi.nlm.nih.gov/pubmed/26771021doi: 10.1016/j.cels.2015.12.004

Lindsley, R. C. et al. 2015. Acute myeloid leukemia ontogeny is defined by distinct somatic mutations. *Blood* 125(9), pp. 1367-1376. Available at: https://www.ncbi.nlm.nih.gov/pubmed/25550361doi: 10.1182/blood-2014-11-610543

Linet, M. S. et al. 2019. Benzene Exposure Response and Risk of Myeloid Neoplasms in Chinese Workers: A Multicenter Case-Cohort Study. *J Natl Cancer Inst* 111(5), pp. 465-474. doi: 10.1093/jnci/djy143

Liu, C., Wang, Y., Shi, M., Tao, X., Man, D., Zhang, J. and Han, B. 2024. hnRNPA0 promotes MYB expression by interacting with enhancer lncRNA MY34UE-AS in human leukemia cells. *Biochem Biophys Res Commun* 724, p. 150221. Available at: https://www.ncbi.nlm.nih.gov/pubmed/38865811doi: 10.1016/j.bbrc.2024.150221

Liu, J. et al. 2012. Aberrant expression of splicing factors in newly diagnosed acute myeloid leukemia. *Onkologie* 35(6), pp. 335-340. Available at: https://www.ncbi.nlm.nih.gov/pubmed/22722453doi: 10.1159/000338941

Liu, M. et al. 2021. HNRNPH1 Is a Novel Regulator Of Cellular Proliferation and Disease Progression in Chronic Myeloid Leukemia. *Front Oncol* 11, p. 682859. Available at: https://www.ncbi.nlm.nih.gov/pubmed/34295818doi: 10.3389/fonc.2021.682859

Liu, Y. and Shi, S. L. 2021. The roles of hnRNP A2/B1 in RNA biology and disease. *Wiley Interdiscip Rev RNA* 12(2), p. e1612. Available at: https://www.ncbi.nlm.nih.gov/pubmed/32588964doi: 10.1002/wrna.1612

Luo, X., Budihardjo, I., Zou, H., Slaughter, C. and Wang, X. 1998. Bid, a Bcl2 interacting protein, mediates cytochrome c release from mitochondria in response to activation of cell surface death receptors. *Cell* 94(4), pp. 481-490. Available at: https://www.ncbi.nlm.nih.gov/pubmed/9727491doi: 10.1016/s0092-8674(00)81589-5

Ma, A. S., Moran-Jones, K., Shan, J., Munro, T. P., Snee, M. J., Hoek, K. S. and Smith, R. 2002. Heterogeneous nuclear ribonucleoprotein A3, a novel RNA trafficking response element-binding protein. *J Biol Chem* 277(20), pp. 18010-18020. doi: 10.1074/jbc.M200050200

Maher, K. R. 2025. Toward a Deeper Understanding of Clonal Evolution in Acute Myeloid Leukemia: Translational and Clinical Impacts. *Scientific Archives* 1(1), pp. 1-14. Available at: https://www.scientificarchives.com/article/toward-a-deeper-understanding-of-clonal-evolution-in-acute-myeloid-leukemia-translational-and-clinical-impacts?utm_source=chatgpt.com

Majeti, R., Park, C. Y. and Weissman, I. L. 2007. Identification of a hierarchy of multipotent hematopoietic progenitors in human cord blood. *Cell Stem Cell* 1(6), pp. 635-645. doi: 10.1016/j.stem.2007.10.001

Mancarella, C., Bley, N. and Penalva, L. O. F. 2024. Editorial: RNA-binding proteins in cancer: advances in translational research. *Front Cell Dev Biol* 12, p. 1390044. doi: 10.3389/fcell.2024.1390044

Mann, Z., Sengar, M., Verma, Y. K., Rajalingam, R. and Raghav, P. K. 2022. Hematopoietic Stem Cell Factors: Their Functional Role in Self-Renewal and Clinical Aspects. *Front Cell Dev Biol* 10, p. 664261. Available at: https://www.ncbi.nlm.nih.gov/pubmed/35399522doi: 10.3389/fcell.2022.664261

Marenda, M., Lazarova, E. and Gilbert, N. 2022. The role of SAF-A/hnRNP U in regulating chromatin structure. *Curr Opin Genet Dev* 72, pp. 38-44. doi: 10.1016/j.gde.2021.10.008

Maris, C., Dominguez, C. and Allain, F. H. 2005. The RNA recognition motif, a plastic RNA-binding platform to regulate post-transcriptional gene expression. *FEBS J* 272(9), pp. 2118-2131. Available at: https://www.ncbi.nlm.nih.gov/pubmed/15853797doi: 10.1111/j.1742-4658.2005.04653.x

Martínez-Cuadrón, D. et al. 2024. Outcomes after intensive chemotherapy for secondary and myeloid-related changes acute myeloid leukemia patients aged 60 to 75 years old: a retrospective analysis from the PETHEMA registry. *Haematologica* 109(1), pp. 115-128.

Available at: https://haematologica.org/article/view/haematol.2022.282506doi: 10.3324/haematol.2022.282506 [Accessed: 2025/11/19].

McFarland, J. M. et al. 2018. Improved estimation of cancer dependencies from large-scale RNAi screens using model-based normalization and data integration. *Nat Commun* 9(1), p. 4610. Available at: https://www.ncbi.nlm.nih.gov/pubmed/30389920doi: 10.1038/s41467-018-06916-5

McHale, C. M., Zhang, L. and Smith, M. T. 2011. Current understanding of the mechanism of benzene-induced leukemia in humans: implications for risk assessment. *Carcinogenesis* 33(2), pp. 240-252. Available at: https://doi.org/10.1093/carcin/bgr297doi: 10.1093/carcin/bgr297 [Accessed: 11/15/2025].

Medvinsky, A. and Dzierzak, E. 1996. Definitive hematopoiesis is autonomously initiated by the AGM region. *Cell* 86(6), pp. 897-906. Available at: https://www.ncbi.nlm.nih.gov/pubmed/8808625doi: 10.1016/s0092-8674(00)80165-8

Méndez-Ferrer, S., Lucas, D., Battista, M. and Frenette, P. S. 2008. Haematopoietic stem cell release is regulated by circadian oscillations. *Nature* 452(7186), pp. 442-447. Available at: https://doi.org/10.1038/nature06685doi: 10.1038/nature06685

Menter, T. and Tzankov, A. 2022. Tumor Microenvironment in Acute Myeloid Leukemia: Adjusting Niches. *Front Immunol* 13, p. 811144. Available at: https://www.ncbi.nlm.nih.gov/pubmed/35273598doi: 10.3389/fimmu.2022.811144

Metcalf, D. 2008. Hematopoietic cytokines. *Blood* 111(2), pp. 485-491. Available at: https://www.ncbi.nlm.nih.gov/pubmed/18182579doi: 10.1182/blood-2007-03-079681

Metzelder, S. K. et al. 2015. NFATc1 as a therapeutic target in FLT3-ITD-positive AML. *Leukemia* 29(7), pp. 1470-1477. Available at: https://www.ncbi.nlm.nih.gov/pubmed/25976987doi: 10.1038/leu.2015.95

Meyers, R. M. et al. 2017. Computational correction of copy number effect improves specificity of CRISPR-Cas9 essentiality screens in cancer cells. *Nat Genet* 49(12), pp. 1779-1784. Available at: https://www.ncbi.nlm.nih.gov/pubmed/29083409doi: 10.1038/ng.3984

Mikkola, H. K. and Orkin, S. H. 2006. The journey of developing hematopoietic stem cells. *Development* 133(19), pp. 3733-3744. doi: 10.1242/dev.02568

Mori, Y., Chen, J. Y., Pluvinage, J. V., Seita, J. and Weissman, I. L. 2015. Prospective isolation of human erythroid lineage-committed progenitors. *Proc Natl Acad Sci U S A* 112(31), pp. 9638-9643. Available at: https://www.ncbi.nlm.nih.gov/pubmed/26195758doi: 10.1073/pnas.1512076112

Morrison, S. J. and Scadden, D. T. 2014. The bone marrow niche for haematopoietic stem cells. *Nature* 505(7483), pp. 327-334. Available at: https://doi.org/10.1038/nature12984doi: 10.1038/nature12984

Mortazavi, A., Williams, B. A., McCue, K., Schaeffer, L. and Wold, B. 2008. Mapping and quantifying mammalian transcriptomes by RNA-Seq. *Nature Methods* 5(7), pp. 621-628. Available at: https://doi.org/10.1038/nmeth.1226doi: 10.1038/nmeth.1226

Mossadegh-Keller, N. et al. 2013. M-CSF instructs myeloid lineage fate in single haematopoietic stem cells. *Nature* 497(7448), pp. 239-243. Available at: https://www.ncbi.nlm.nih.gov/pubmed/23575636doi: 10.1038/nature12026

Moumen, A., Magill, C., Dry, K. and Jackson, S. P. 2013. ATM-dependent phosphorylation of heterogeneous nuclear ribonucleoprotein K promotes p53 transcriptional activation in response to DNA damage. *Cell Cycle* 12(4), pp. 698-704. Available at: https://doi.org/10.4161/cc.23592doi: 10.4161/cc.23592

Myer, V. E. and Steitz, J. A. 1995. Isolation and characterization of a novel, low abundance hnRNP protein: A0. *RNA* 1(2), pp. 171-182. Available at: https://www.ncbi.nlm.nih.gov/pubmed/7585247

Novershtern, N. et al. 2011. Densely interconnected transcriptional circuits control cell states in human hematopoiesis. *Cell* 144(2), pp. 296-309. Available at: https://www.ncbi.nlm.nih.gov/pubmed/21241896doi: 10.1016/j.cell.2011.01.004

O'Connor, L., Strasser, A., O'Reilly, L. A., Hausmann, G., Adams, J. M., Cory, S. and Huang, D. C. 1998. Bim: a novel member of the Bcl-2 family that promotes apoptosis. *EMBO J* 17(2), pp. 384-395. Available at: https://www.ncbi.nlm.nih.gov/pubmed/9430630doi: 10.1093/emboj/17.2.384

Orkin, S. H. and Zon, L. I. 2008. Hematopoiesis: an evolving paradigm for stem cell biology. *Cell* 132(4), pp. 631-644. doi: 10.1016/j.cell.2008.01.025

Ottersbach, K. and Dzierzak, E. 2005. The murine placenta contains hematopoietic stem cells within the vascular labyrinth region. *Dev Cell* 8(3), pp. 377-387. doi: 10.1016/j.devcel.2005.02.001

Pabst, T. and Mueller, B. U. 2007. Transcriptional dysregulation during myeloid transformation in AML. *Oncogene* 26(47), pp. 6829-6837. doi: 10.1038/sj.onc.1210765

Palis, J., Robertson, S., Kennedy, M., Wall, C. and Keller, G. 1999. Development of erythroid and myeloid progenitors in the yolk sac and embryo proper of the mouse. *Development* 126(22), pp. 5073-5084. Available at: https://www.ncbi.nlm.nih.gov/pubmed/10529424doi: 10.1242/dev.126.22.5073

Papaemmanuil, E. et al. 2016. Genomic Classification and Prognosis in Acute Myeloid Leukemia. *N Engl J Med* 374(23), pp. 2209-2221. Available at: https://www.ncbi.nlm.nih.gov/pubmed/27276561doi: 10.1056/NEJMoa1516192

Perl, A. E. et al. 2019. Gilteritinib or Chemotherapy for Relapsed or Refractory FLT3-Mutated AML. *N Engl J Med* 381(18), pp. 1728-1740. Available at: https://www.ncbi.nlm.nih.gov/pubmed/31665578doi: 10.1056/NEJMoa1902688

Pietras, E. M. 2017. Inflammation: a key regulator of hematopoietic stem cell fate in health and disease. *Blood* 130(15), pp. 1693-1698. doi: 10.1182/blood-2017-06-780882

Pietras, E. M. et al. 2016. Chronic interleukin-1 exposure drives haematopoietic stem cells towards precocious myeloid differentiation at the expense of self-renewal. *Nat Cell Biol* 18(6), pp. 607-618. doi: 10.1038/ncb3346

Prelich, G. 2012. Gene overexpression: uses, mechanisms, and interpretation. *Genetics* 190(3), pp. 841-854. Available at: https://www.ncbi.nlm.nih.gov/pubmed/22419077doi: 10.1534/genetics.111.136911

Pronk, C. J., Veiby, O. P., Bryder, D. and Jacobsen, S. E. 2011. Tumor necrosis factor restricts hematopoietic stem cell activity in mice: involvement of two distinct receptors. *J Exp Med* 208(8), pp. 1563-1570. Available at: https://www.ncbi.nlm.nih.gov/pubmed/21768269doi: 10.1084/jem.20110752

Qiagen. 2019. *RNeasy Plus Mini Handbook*. Hilden, Germany: Qiagen. Available at: https://www.qiagen.com/us/resources/resourcedetail?id=16b8f578-d192-4613-ae32-8e02e0b0fa77&lang=en [Accessed: 08/12/2025].

Qian, H. et al. 2007. Critical role of thrombopoietin in maintaining adult quiescent hematopoietic stem cells. *Cell Stem Cell* 1(6), pp. 671-684. Available at: https://www.ncbi.nlm.nih.gov/pubmed/18371408doi: 10.1016/j.stem.2007.10.008

Qin, Y. Z. et al. 2018. Outcome and Minimal Residual Disease Monitoring in Patients with t(16;21) Acute Myelogenous Leukemia Undergoing Allogeneic Hematopoietic Stem Cell Transplantation. *Biol Blood Marrow Transplant* 24(1), pp. 163-168. Available at: https://www.ncbi.nlm.nih.gov/pubmed/28939454doi: 10.1016/j.bbmt.2017.09.002

Qureshi, W., Jamal, A., Gohar, A., Mansuri, M. I., Irfan, M., Khan, I. A. and Shakeel, M. 2025. Relapse-specific genetic patterns in the exomic mutational landscape in acute myeloid leukemia. *Egyptian Journal of Medical Human Genetics* 26(1), p. 57. Available at: https://doi.org/10.1186/s43042-025-00688-6doi: 10.1186/s43042-025-00688-6

Rapin, N. et al. 2014. Comparing cancer vs normal gene expression profiles identifies new disease entities and common transcriptional programs in AML patients. *Blood* 123(6), pp. 894-904. Available at: https://www.ncbi.nlm.nih.gov/pubmed/24363398doi: 10.1182/blood-2013-02-485771

Ren, X., Dong, Y., Duan, M., Zhang, H. and Gao, P. 2021. Abnormal expression of HNRNPA3 in multistep hepatocarcinogenesis. *Oncol Lett* 21(1), p. 46. Available at: https://www.ncbi.nlm.nih.gov/pubmed/33281957doi: 10.3892/ol.2020.12307

Richmond, T. D., Chohan, M. and Barber, D. L. 2005. Turning cells red: signal transduction mediated by erythropoietin. *Trends Cell Biol* 15(3), pp. 146-155. doi: 10.1016/j.tcb.2005.01.007

Rieger, M. A., Hoppe, P. S., Smejkal, B. M., Eitelhuber, A. C. and Schroeder, T. 2009. Hematopoietic cytokines can instruct lineage choice. *Science* 325(5937), pp. 217-218. doi: 10.1126/science.1171461

Ringner, M. 2008. What is principal component analysis? *Nat Biotechnol* 26(3), pp. 303-304. Available at: https://www.ncbi.nlm.nih.gov/pubmed/18327243doi: 10.1038/nbt0308-303

Rosenbauer, F. and Tenen, D. G. 2007. Transcription factors in myeloid development: balancing differentiation with transformation. *Nat Rev Immunol* 7(2), pp. 105-117. doi: 10.1038/nri2024

Rousseau, S., Morrice, N., Peggie, M., Campbell, D. G., Gaestel, M. and Cohen, P. 2002. Inhibition of SAPK2a/p38 prevents hnRNP A0 phosphorylation by MAPKAP-K2 and its interaction with cytokine mRNAs. *EMBO J* 21(23), pp. 6505-6514. Available at: https://www.ncbi.nlm.nih.gov/pubmed/12456657doi: 10.1093/emboj/cdf639

Ryu, H. G. et al. 2021. HNRNP A1 Promotes Lung Cancer Cell Proliferation by Modulating VRK1 Translation. *Int J Mol Sci* 22(11). Available at: https://www.ncbi.nlm.nih.gov/pubmed/34071140doi: 10.3390/ijms22115506

Schuschel, K., Helwig, M., Hüttelmaier, S., Heckl, D., Klusmann, J. H. and Hoell, J. I. 2020. RNA-Binding Proteins in Acute Leukemias. *Int J Mol Sci* 21(10). doi: 10.3390/ijms21103409

Scientific, T. F. 2022. *NanoDrop One Microvolume UV-Vis Spectrophotometers User Guide*. Wilmington, DE, USA: Thermo Fisher Scientific. Available at: https://documents.thermofisher.com/TFS-Assets/MSD/brochures/BR52720-NanoDrop-One.pdf [Accessed: 08/12/2025].

Sezaki, M., Hayashi, Y., Wang, Y., Johansson, A., Umemoto, T. and Takizawa, H. 2020. Immuno-Modulation of Hematopoietic Stem and Progenitor Cells in Inflammation. *Front*

Immunol 11, p. 585367. Available at: https://www.ncbi.nlm.nih.gov/pubmed/33329562doi: 10.3389/fimmu.2020.585367

Shalem, O. et al. 2014. Genome-scale CRISPR-Cas9 knockout screening in human cells. *Science* 343(6166), pp. 84-87. doi: 10.1126/science.1247005

Sheikh, M. S. 2015. RNA-binding Protein, GADD45-alpha, p27(Kip1), p53 and Genotoxic Stress Response in Relation to Chemoresistance in Cancer. *Mol Cell Pharmacol* 7(3), pp. 41-45. Available at: https://www.ncbi.nlm.nih.gov/pubmed/27066162

Shlush, L. I. et al. 2014. Identification of pre-leukaemic haematopoietic stem cells in acute leukaemia. *Nature* 506(7488), pp. 328-333. doi: 10.1038/nature13038

Short, N. J., Konopleva, M., Kadia, T. M., Borthakur, G., Ravandi, F., DiNardo, C. D. and Daver, N. 2020. Advances in the Treatment of Acute Myeloid Leukemia: New Drugs and New Challenges. *Cancer Discov* 10(4), pp. 506-525. Available at: https://www.ncbi.nlm.nih.gov/pubmed/32014868doi: 10.1158/2159-8290.CD-19-1011

Subramanian, A. et al. 2005. Gene set enrichment analysis: a knowledge-based approach for interpreting genome-wide expression profiles. *Proc Natl Acad Sci U S A* 102(43), pp. 15545-15550. Available at: https://www.ncbi.nlm.nih.gov/pubmed/16199517doi: 10.1073/pnas.0506580102

Sugiyama, T., Kohara, H., Noda, M. and Nagasawa, T. 2006. Maintenance of the Hematopoietic Stem Cell Pool by CXCL12-CXCR4 Chemokine Signaling in Bone Marrow Stromal Cell Niches. *Immunity* 25(6), pp. 977-988. Available at: https://doi.org/10.1016/j.immuni.2006.10.016doi: 10.1016/j.immuni.2006.10.016 [Accessed: 2025/11/08].

Svendsen, J. B., Baslund, B., Cramer, E. P., Rapin, N., Borregaard, N. and Cowland, J. B. 2016. MicroRNA-941 Expression in Polymorphonuclear Granulocytes Is Not Related to Granulomatosis with Polyangiitis. *PLoS One* 11(10), p. e0164985. Available at: https://www.ncbi.nlm.nih.gov/pubmed/27755585doi: 10.1371/journal.pone.0164985

Swanson, M. S. and Dreyfuss, G. 1988. RNA binding specificity of hnRNP proteins: a subset bind to the 3' end of introns. *EMBO J* 7(11), pp. 3519-3529. Available at: https://www.ncbi.nlm.nih.gov/pubmed/3208740

Tallman, M. S., Nabhan, C., Feusner, J. H. and Rowe, J. M. 2002. Acute promyelocytic leukemia: evolving therapeutic strategies. *Blood* 99(3), pp. 759-767. Available at: https://www.ncbi.nlm.nih.gov/pubmed/11806975doi: 10.1182/blood.v99.3.759

Taoudi, S., Morrison, A. M., Inoue, H., Gribi, R., Ure, J. and Medvinsky, A. 2005. Progressive divergence of definitive haematopoietic stem cells from the endothelial compartment does not

depend on contact with the foetal liver. *Development* 132(18), pp. 4179-4191. Available at: https://www.ncbi.nlm.nih.gov/pubmed/16107475doi: 10.1242/dev.01974

Taskesen, E. et al. 2011. Prognostic impact, concurrent genetic mutations, and gene expression features of AML with CEBPA mutations in a cohort of 1182 cytogenetically normal AML patients: further evidence for CEBPA double mutant AML as a distinctive disease entity. *Blood* 117(8), pp. 2469-2475. Available at: https://www.ncbi.nlm.nih.gov/pubmed/21177436doi: 10.1182/blood-2010-09-307280

Tawana, K., Brown, A. L. and Churpek, J. E. 2022. Integrating germline variant assessment into routine clinical practice for myelodysplastic syndrome and acute myeloid leukaemia: current strategies and challenges. *Br J Haematol* 196(6), pp. 1293-1310. Available at: https://www.ncbi.nlm.nih.gov/pubmed/34658019doi: 10.1111/bjh.17855

Technologies, A. 2016. *Agilent 2100 Bioanalyzer System User Guide*. Santa Clara, CA, USA: Agilent Technologies. Available at: https://www.agilent.com/cs/library/usermanuals/Public/Copy%20of%20G3430-94038.pdf [Accessed: 8/12/2025].

Testa, U., Castelli, G. and Pelosi, E. 2023. TP53-Mutated Myelodysplasia and Acute Myeloid Leukemia. *Mediterr J Hematol Infect Dis* 15(1), p. e2023038. doi: 10.4084/mjhid.2023.038

Thandapani, P., O'Connor, T. R., Bailey, T. L. and Richard, S. 2013. Defining the RGG/RG motif. *Mol Cell* 50(5), pp. 613-623. Available at: https://www.ncbi.nlm.nih.gov/pubmed/23746349doi: 10.1016/j.molcel.2013.05.021

Thiele, J. et al. 2023. The international consensus classification of myeloid neoplasms and acute Leukemias: myeloproliferative neoplasms. *Am J Hematol* 98(1), pp. 166-179. Available at: https://www.ncbi.nlm.nih.gov/pubmed/36200127doi: 10.1002/ajh.26751

Till, J. E. 1961. A direct measurement of the radiation sensitivity of normal mouse bone marrow cells. *Radiat Res* 14, pp. 213-222. Available at: https://www.ncbi.nlm.nih.gov/pubmed/13776896

Tilliole, P., Fix, S. and Godin, J. D. 2024. hnRNPs: roles in neurodevelopment and implication for brain disorders. *Front Mol Neurosci* 17, p. 1411639. doi: 10.3389/fnmol.2024.1411639

Townsend, E. C. et al. 2016. The Public Repository of Xenografts Enables Discovery and Randomized Phase II-like Trials in Mice. *Cancer Cell* 30(1), p. 183. Available at: https://www.ncbi.nlm.nih.gov/pubmed/27479034doi: 10.1016/j.ccell.2016.06.008

Trapnell, C. et al. 2010. Transcript assembly and quantification by RNA-Seq reveals unannotated transcripts and isoform switching during cell differentiation. *Nat Biotechnol* 28(5),

pp. 511-515. Available at: https://www.ncbi.nlm.nih.gov/pubmed/20436464doi: 10.1038/nbt.1621

Tusi, B. K. et al. 2018. Population snapshots predict early haematopoietic and erythroid hierarchies. *Nature* 555(7694), pp. 54-60. doi: 10.1038/nature25741

Tyner, J. W. et al. 2018. Functional genomic landscape of acute myeloid leukaemia. *Nature* 562(7728), pp. 526-531. Available at: https://www.ncbi.nlm.nih.gov/pubmed/30333627doi: 10.1038/s41586-018-0623-z

UK, C. R. 2019. *Acute myeloid leukaemia (AML) statistics: incidence, mortality and survival in the UK*. Available at:

https://www.cancerresearchuk.org/health-professional/cancer-statistics/statistics-by-cancer-type/leukaemia-aml

Ule, J., Jensen, K. B., Ruggiu, M., Mele, A., Ule, A. and Darnell, R. B. 2003. CLIP identifies Nova-regulated RNA networks in the brain. *Science* 302(5648), pp. 1212-1215. Available at: https://www.ncbi.nlm.nih.gov/pubmed/14615540doi: 10.1126/science.1090095

Valverde, R., Edwards, L. and Regan, L. 2008. Structure and function of KH domains. *FEBS J* 275(11), pp. 2712-2726. Available at: https://www.ncbi.nlm.nih.gov/pubmed/18422648doi: 10.1111/j.1742-4658.2008.06411.x

Van Hooijdonk, C. A., Glade, C. P. and Van Erp, P. E. 1994. TO-PRO-3 iodide: a novel HeNe laser-excitable DNA stain as an alternative for propidium iodide in multiparameter flow cytometry. *Cytometry* 17(2), pp. 185-189. doi: 10.1002/cyto.990170212

Vembuli, H., Gor, R., Ramalingam, S., Perales, S. and Rajasingh, J. 2024. RNA binding proteins in cancer chemotherapeutic drug resistance. *Front Cell Dev Biol* 12, p. 1308102. doi: 10.3389/fcell.2024.1308102

Wang, E. et al. 2019. Targeting an RNA-Binding Protein Network in Acute Myeloid Leukemia. *Cancer Cell* 35(3), pp. 369-384.e367. Available at: https://doi.org/10.1016/j.ccell.2019.01.010doi: 10.1016/j.ccell.2019.01.010 [Accessed: 2025/08/23].

Wang, Y. et al. 2020. MiR-CLIP reveals iso-miR selective regulation in the miR-124 targetome. *Nucleic Acids Research* 49(1), pp. 25-37. Available at: https://doi.org/10.1093/nar/gkaa1117doi: 10.1093/nar/gkaa1117 [Accessed: 11/20/2025].

Wang, Y., Zhai, Y., Zhang, M., Song, C., Zhang, Y. and Zhang, G. 2024. Escaping from CRISPR-Cas-mediated knockout: the facts, mechanisms, and applications. *Cell Mol Biol Lett* 29(1), p. 48. Available at: https://www.ncbi.nlm.nih.gov/pubmed/38589794doi: 10.1186/s11658-024-00565-x

Wang, Z., Gerstein, M. and Snyder, M. 2009. RNA-Seq: a revolutionary tool for transcriptomics. *Nature Reviews Genetics* 10(1), pp. 57-63. Available at: https://doi.org/10.1038/nrg2484doi: 10.1038/nrg2484

Wei, Q. and Frenette, P. S. 2018. Niches for Hematopoietic Stem Cells and Their Progeny. *Immunity* 48(4), pp. 632-648. Available at: https://www.ncbi.nlm.nih.gov/pubmed/29669248doi: 10.1016/j.immuni.2018.03.024

Wienecke, C. P. et al. 2024. Clonal relapse dynamics in acute myeloid leukemia following allogeneic hematopoietic cell transplantation. *Blood* 144(3), pp. 296-307. Available at: https://www.ncbi.nlm.nih.gov/pubmed/38669617doi: 10.1182/blood.2023022697

Willis, S. N. and Adams, J. M. 2005. Life in the balance: how BH3-only proteins induce apoptosis. *Curr Opin Cell Biol* 17(6), pp. 617-625. Available at: https://www.ncbi.nlm.nih.gov/pubmed/16243507doi: 10.1016/j.ceb.2005.10.001

Wilson, N. K. et al. 2015. Combined Single-Cell Functional and Gene Expression Analysis Resolves Heterogeneity within Stem Cell Populations. *Cell Stem Cell* 16(6), pp. 712-724. doi: 10.1016/j.stem.2015.04.004

Wong, J. J., Lau, K. A., Pinello, N. and Rasko, J. E. 2014. Epigenetic modifications of splicing factor genes in myelodysplastic syndromes and acute myeloid leukemia. *Cancer Sci* 105(11), pp. 1457-1463. Available at: https://www.ncbi.nlm.nih.gov/pubmed/25220401doi: 10.1111/cas.12532

Wouters, B. J., Lowenberg, B., Erpelinck-Verschueren, C. A., van Putten, W. L., Valk, P. J. and Delwel, R. 2009. Double CEBPA mutations, but not single CEBPA mutations, define a subgroup of acute myeloid leukemia with a distinctive gene expression profile that is uniquely associated with a favorable outcome. *Blood* 113(13), pp. 3088-3091. Available at: https://www.ncbi.nlm.nih.gov/pubmed/19171880doi: 10.1182/blood-2008-09-179895

Xie, W. et al. 2021. Crucial roles of different RNA-binding hnRNP proteins in Stem Cells. *International Journal of Biological Sciences* 17(3), pp. 807-817. Available at: https://www.ijbs.com/v17p0807.htmdoi: 10.7150/ijbs.55120

Yamashita, M., Nitta, E. and Suda, T. 2016. Regulation of hematopoietic stem cell integrity through p53 and its related factors. *Ann N Y Acad Sci* 1370(1), pp. 45-54. doi: 10.1111/nyas.12986

Yankova, E. et al. 2021. Small-molecule inhibition of METTL3 as a strategy against myeloid leukaemia. *Nature* 593(7860), pp. 597-601. Available at: https://www.ncbi.nlm.nih.gov/pubmed/33902106doi: 10.1038/s41586-021-03536-w

Yoshihara, H. et al. 2007. Thrombopoietin/MPL signaling regulates hematopoietic stem cell quiescence and interaction with the osteoblastic niche. *Cell Stem Cell* 1(6), pp. 685-697. Available at: https://www.ncbi.nlm.nih.gov/pubmed/18371409doi: 10.1016/j.stem.2007.10.020

Youle, R. J. and Strasser, A. 2008. The BCL-2 protein family: opposing activities that mediate cell death. *Nat Rev Mol Cell Biol* 9(1), pp. 47-59. Available at: https://www.ncbi.nlm.nih.gov/pubmed/18097445doi: 10.1038/nrm2308

Young, D. J., Stoddart, A., Nakitandwe, J., Chen, S. C., Qian, Z., Downing, J. R. and Le Beau, M. M. 2014. Knockdown of Hnrnpa0, a del(5q) gene, alters myeloid cell fate in murine cells through regulation of AU-rich transcripts. *Haematologica* 99(6), pp. 1032-1040. Available at: https://www.ncbi.nlm.nih.gov/pubmed/24532040doi: 10.3324/haematol.2013.098657

Yuen, G., Khan, F. J., Gao, S., Stommel, J. M., Batchelor, E., Wu, X. and Luo, J. 2017. CRISPR/Cas9-mediated gene knockout is insensitive to target copy number but is dependent on guide RNA potency and Cas9/sgRNA threshold expression level. *Nucleic Acids Res* 45(20), pp. 12039-12053. doi: 10.1093/nar/gkx843

Zhang, J. F., Liu, X. L., Lin, Y. D., Li, Y. L., Pan, J. W., Zong, S. and Zhou, Y. 2016. [hnRNP K Contributes to Adriamycin Resistance in Acute Myeloid Leukemia through Regulating Autophagy]. *Zhongguo Shi Yan Xue Ye Xue Za Zhi* 24(6), pp. 1665-1669. Available at: https://www.ncbi.nlm.nih.gov/pubmed/28024474doi: 10.7534/j.issn.1009-2137.2016.06.010

Zhou, J. et al. 2021. Identification of therapeutic targets and prognostic biomarkers from the hnRNP family in invasive breast carcinoma. *Aging (Albany NY)* 13(3), pp. 4503-4521. Available at: https://www.ncbi.nlm.nih.gov/pubmed/33495416doi: 10.18632/aging.202411

Zhou, X. et al. 2017. HnRNP-L promotes prostate cancer progression by enhancing cell cycling and inhibiting apoptosis. *Oncotarget* 8(12), pp. 19342-19353. Available at: https://www.ncbi.nlm.nih.gov/pubmed/28038443doi: 10.18632/oncotarget.14258

Zovein, A. C. et al. 2008. Fate tracing reveals the endothelial origin of hematopoietic stem cells. *Cell Stem Cell* 3(6), pp. 625-636. doi: 10.1016/j.stem.2008.09.018

7 Appendix

A

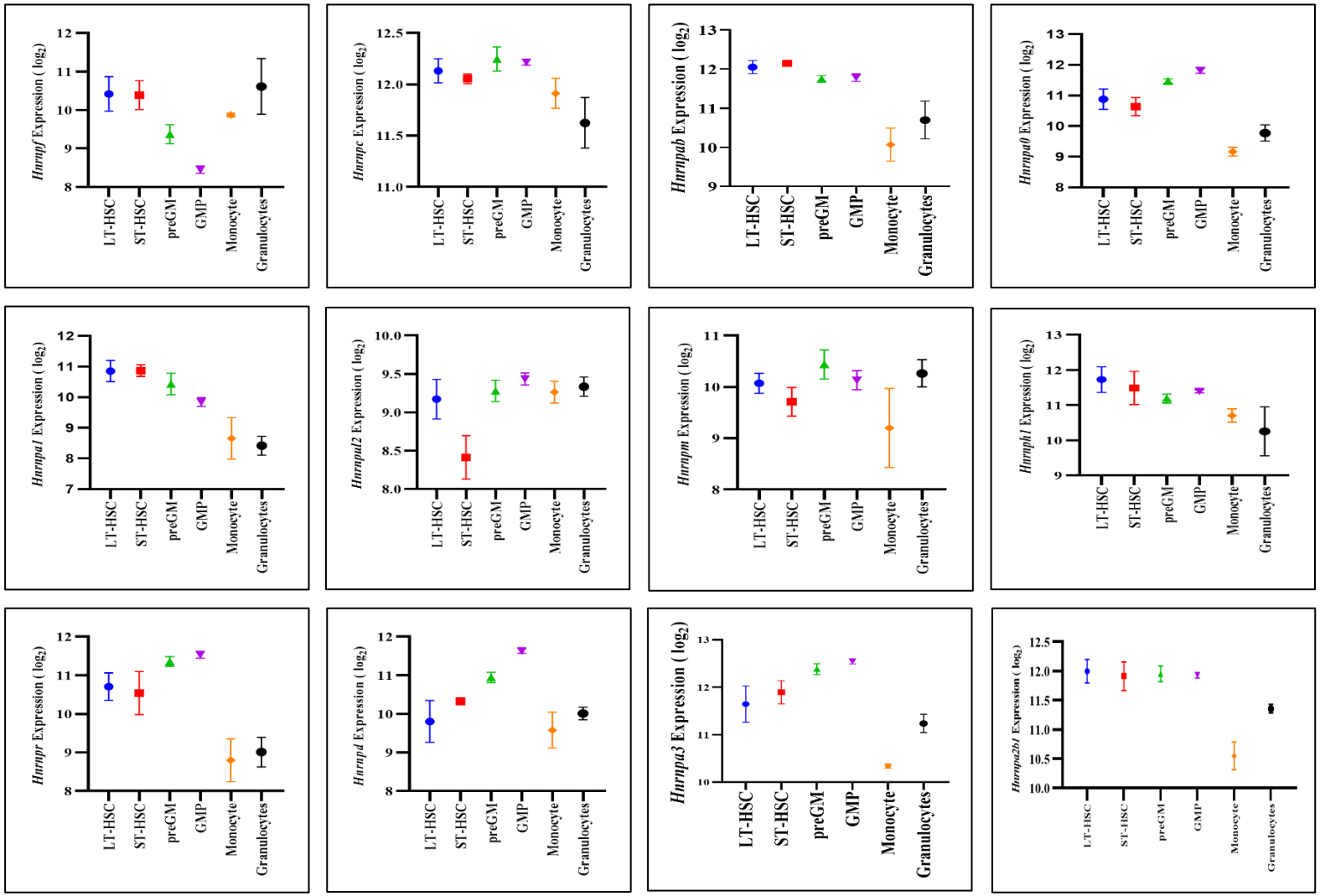
Hnrnpf Expression (log2)
Hnrnpc Expression (log2)
Hnrnpab Expression (log2)
Hnrnpa0 Expression (log2)
Hnrnpa1 Expression (log2)
Hnrnpdl2 Expression (log2)
Hnrnpm Expression (log2)
Hnrnph1 Expression (log2)
Hnrnpr Expression (log2)
Hnrnpd Expression (log2)
Hnrnpa3 Expression (log2)
Hnrnpa2b1 Expression (log2)
LT-HSC
ST-HSC
preGM
GMP
Monocyte
Granulocytes

B

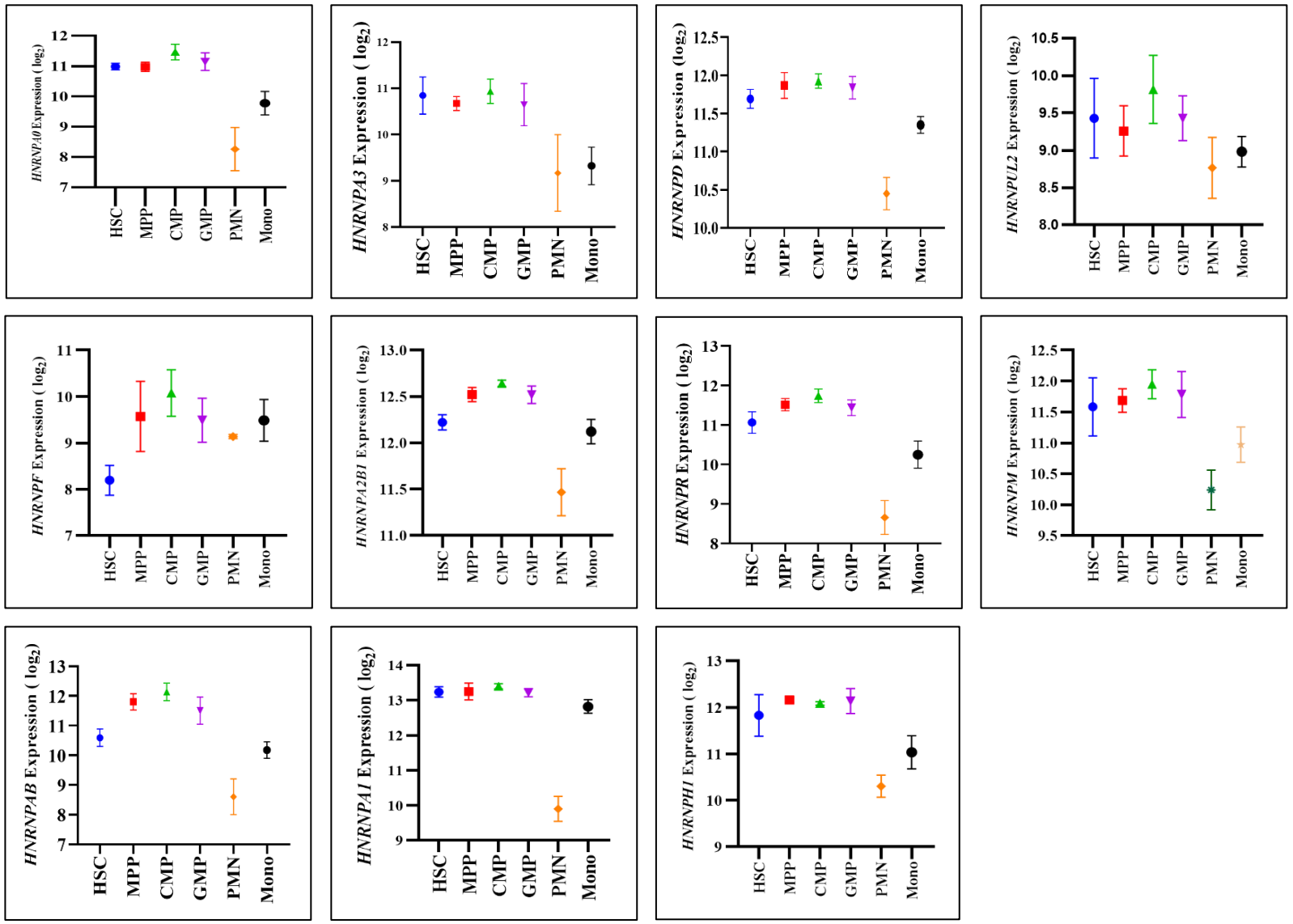
HNRNPA0 Expression (log2)
HNRNPA3 Expression (log2)
HNRNPD Expression (log2)
HNRNPUL2 Expression (log2)
HNRNPF Expression (log2)
HNRNPA2B1 Expression (log2)
HNRNPR Expression (log2)
HNRNPM Expression (log2)
HNRNPAB Expression (log2)
HNRNPA1 Expression (log2)
HNRNPH1 Expression (log2)
HSC
MPP
CMP
GMP
PMN
Mono

C

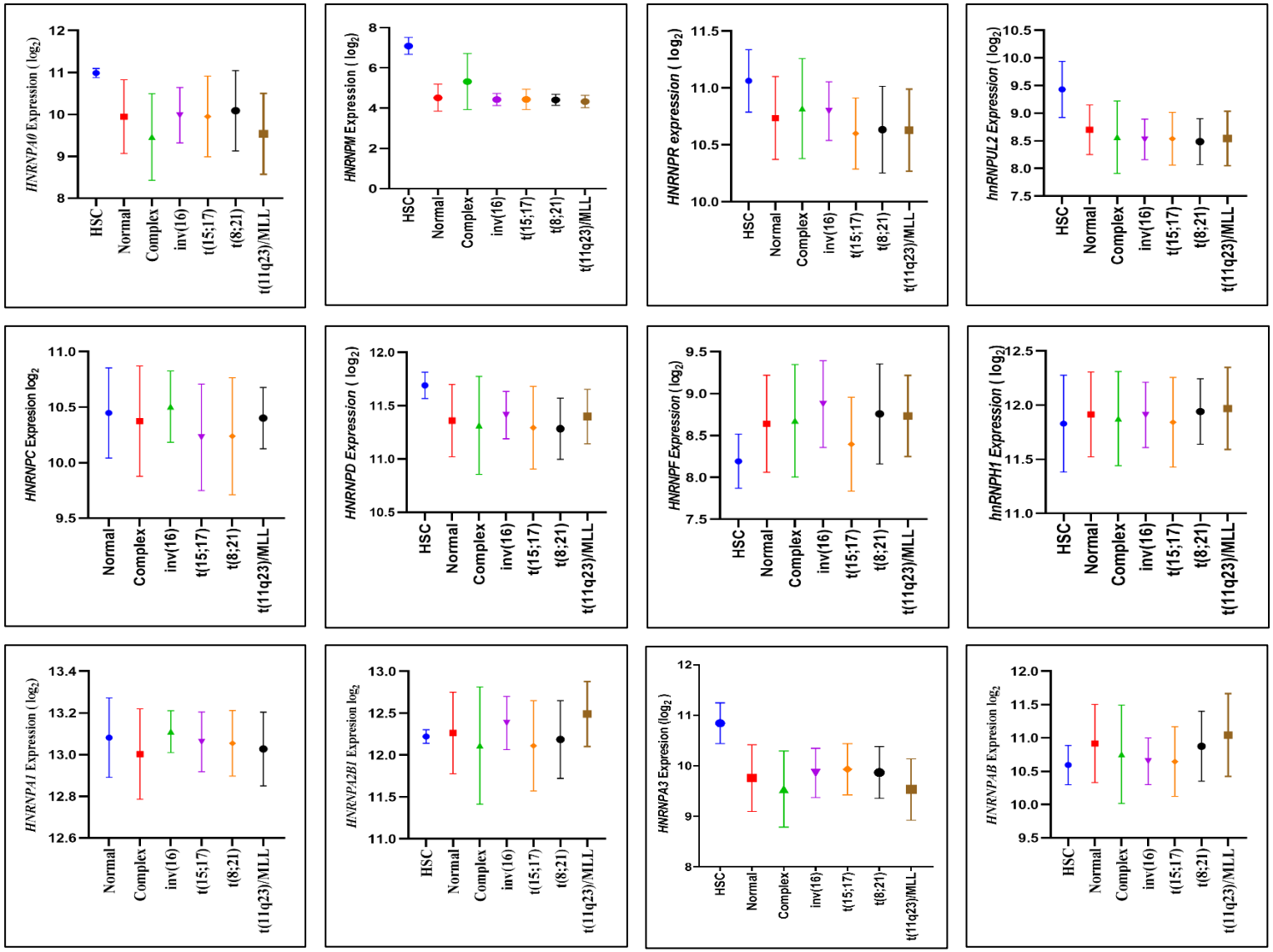
HNRNPA0 Expression (log2)
HNRNPM Expression (log2)
HNRNPR expression (log2)
hnRNPUL2 Expression (log2)
HNRNPC Expresion log2
HNRNPD Expression (log2)
HNRNPF Expression (log2)
hnRNPH1 Expression (log2)
HNRNPA1 Expression (log2)
HNRNPA2B1 Expresion log2
HNRNPA3 Expresion (log2)
HNRNPA4B Expresion log2
HSC
Normal
Complex
inv(16)
t(15;17)
t(8;21)
t(11q23)/MLL

Figure 7-1 Comprehensive expression profiling of *HNRNPs* family members across murine haematopoiesis, normal human HSCs, and AML patients samples

A Murine haematopoietic populations representing progressive stages of differentiation. Cell populations include long term haematopoietic stem cells (LT-HSC), short term haematopoietic stem cells (ST-HSC), multipotent progenitors (MPP), granulocyte macrophage progenitors (GMP), monocytes, and granulocytes. Expression values are presented as $\log_2$ transformed transcript levels, illustrating lineage associated regulation of hnRNP family members during normal murine haematopoiesis.

B Normal human haematopoietic stem and progenitor cell populations, including haematopoietic stem cells (HSC), multipotent progenitors (MPP), common myeloid progenitors (CMP), granulocyte macrophage progenitors (GMP), megakaryocyte erythroid progenitors (MEP), and mature monocytes. Data are shown as $\log_2$ transformed expression values.

C *HNRNPs* family member expression between normal human haematopoietic stem cells (HSCs) and acute myeloid leukaemia (AML) patient samples**.** Data are shown as $\log_2$ transformed expression values.